AD-757 768

ESTIMATION OF THE MECHANICAL PROPERTIES
OF ROCK MASSES

Charles Fairhurst

Minnesota University
Minneapolis, Minnesota

January 1973

3200.8 (Att 1 to Encl 1)
Mar 7, 66

DOCUMENT CONTROL DATA - R & D

(Security classification of title, body of abstract and indexing annotation must be entered when the overall report is classified)

1. ORIGINATING ACTIVITY (Corporate author)	2a. REPORT SECURITY CLASSIFICATION
Civil and Mineral Engineering University of Minnesota, Minneapolis	Unclassified
	2b. GROUP

3. REPORT TITLE

THE MECHANICAL PROPERTIES OF ROCK MASSES

4. DESCRIPTIVE NOTES (Type of report and inclusive dates)

Final Report   15 January 1972 – 14 January 1973

5. AUTHOR(S) (First name, middle initial, last name)

Charles Fairhurst

6. REPORT DATE	7a. TOTAL NO. OF PAGES	7b. NO. OF REFS
January 1973	212	205

8a. CONTRACT OR GRANT NO.	9a. ORIGINATOR'S REPORT NUMBER(S)
H0220011	
b. PROJECT NO. ARPA Order No. 1579	
c.	9b. OTHER REPORT NO(S) (Any other numbers that may be assigned this report)
Amendment No. 2	
d. Program Code 2F10	

10. DISTRIBUTION STATEMENT

Distribution of this report is unlimited

11. SUPPLEMENTARY NOTES	12. SPONSORING MILITARY ACTIVITY
	Advanced Research Projects Agency

13. ABSTRACT

This report describes research activities in three separate areas related to the overall aim of improving the estimation of the mechanical properties of rock masses. These three fields are broadly classified as; the intrinsic properties of rock fracture, the mechanical failure of block jointed models of rock masses and the continuum characterization of rock masses for deformation calculations.

The fracture of brittle rock is considered as an energy absorbing process where the 'work of fracture' is the dominent material property. An associated material property 'the effective crack length' is defined as a through-the-structure crack which develops after the application of load but controls the maximum load carrying capacity at the structure. Numerical analytical procedures are outlined to predict the complete force deformation response of a structure failing due to an extending through-the-structure crack. These predicted force deformation curves are compared with experimentally derived results for three commonly used tensile strength tests. The ambiguities often referred to in tensile testing of rock as the shape and size effect are successfully explained using the two material properties of 'work of fracture' and the effective crack length.

DD FORM 1473
1 NOV 65

The mechanical failure of block jointed model were studied using
a servo-controlled loading system such that the progressive col-
lapse of these models under uniaxial compressive loading could
be studied in detail. The mechanism of collapse at these block
jointed models were recorded photographically and indicate that
several mechanisms are operative in this process. These include;
fracture of individual blocks, rotation of individual blocks,
collapse of columns of blocks by rotation or buckling, slip along
joint planes and by shear deformation of individual blocks. No
single simple theory of failure appears capable at this time of pre-
dicting the collapse loads of such systems.

The dilatant nature of the collapse of these block jointed models
was studied under two different confinement pressures. Failure of
the specimens was again controlled using a servo-controlled testing
machine. These tests illustrate that the volumetric strain behavior
of jointed specimens can be vastly different from that of comparable
unjointed specimens.

The continuum characterization of a jointed rock mass is briefly
reported in this report. The research results of this work have
been reported in readily available journals so is only briefly re-
viewed here. The low shear stiffness of joints in general results
in an anisotropic continuum characterization of the rock mass with
a low shear stiffness. The practical significance of the anisotropic
characterization, in that the pressure 'bulb' from any applied load
on a boundary is distorted from that of the isotropic case, is dis-
cussed. The effect of joint spacing and thickness upon the reliability
as a function of the number of dilatometer tests in a jointed rock mass
is also discussed and presented in detail in one of the published
papers.

14. KEY WORDS	LINK A		LINK B		LINK C	
	ROLE	WT	ROLE	WT	ROLE	WT
ROCK MECHANICS						
ROCK FRACTURE						
BLOCK JOINTED MODELS						
CONTINUUM CHARACTERIZATION						
JOINTS						
ROCK MASS						
CONTROLLED FAILURE						
FATIGUE BLOCK MODELS						
BEAM TEST						
RING TEST						
WORK OF FRACTURE						
EFFECTIVE CRACK LENGTH						

ic

ESTIMATION OF THE MECHANICAL

PROPERTIES OF ROCK MASSES

Final Report on ARPA Contract No. H0220C11

ERRATA SHEET

Page	Line	
iv	4	replace <u>ABSTRACT</u> with <u>TECHNICAL REPORT SUMMARY</u>
	12	insert <u>stress</u> after tensile
7	29	...elliptical flaw that would cause the flaw to extend unstably...
8	34	scopic and the macroscopic domains.
14	4	replace $\nu'-\nu'$ with $U'-U$
	6	...can be <u>determined</u> using a
	7	curve fitting procedure,...
19	2up	delete <u>material constants</u> ... <u>distributors</u>
	1up	
23	last line	add "motion can result from these stresses at a considerable distance away from the crack tip. In this discussion, permanent deformation is defined as the permanent defor-"
35	11	to read "...large hole is 0.430 times the..."
	13	3,400 lbs
	14	3,020 lbs
51	Figure 2.11	b, c, d replace vertical axis scale with <u>0 to 20,000 lbs</u> instead of 0-20 lbs.
74	Figure 2.39	a, b replace vertical axes scale with <u>0 to 14,000 lbs</u> and label <u>Force</u>

FINAL REPORT

ARPA–USBM CONTRACT H0220011 New.

ESTIMATION OF THE MECHANICAL PROPERTIES OF ROCK MASSES

Principal Investigator - Professor Charles Fairhurst

Tel.: (612) 373-3135

Department of Civil and Mineral Engineering

University of Minnesota

Contract Duration: 15 January 1972-3 December 1972 (January 14 including
Final Report)

Contract Amount: $50,000

Sponsored by

Advanced Research Projects Agency

ARPA Order No. 1579, Amend. No. 3

Program Code 2F10
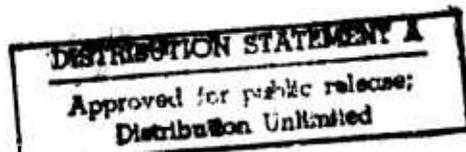
PREFACE

This work covers work conducted in the calendar year of 1972 on the research task entitled "The Mechanical Properties of Rock Masses". This research task was originally planned as a three year program but was prematurely curtailed after this, the second year. The material contained in this report thus relies upon the work completed in the first year of the contract but primarily reports that work completed in 1972. Several individuals have worked on this contract, these are:

> E. T. Brown*
> J. A. Hudson**
> B. Singh***
> M. P. Hardy***
> C. Fairhurst***   (Principal Investigator)

Dr. E. T. Brown acted as a consultant in this work and performed many of the tests on the block jointed models herein recorded. He also provided the literature survey on joints and block jointed models at no cost to the contract. Dr. J. A. Hudson was instrumental in procurement of the contract and in many aspects of the experimental work reported in the section on the intrinsic properties of rock and the tests of block jointed models. Dr. B. Singh completed the work on the "continuum characterization of rock masses" in the contract period. This work was initiated in the first year of the contract and is now fully reported in three published papers, hence, only a brief summmar of this work is given in this report. The section on the intrinsic properties of rock represents some of the material generated by M. P. Hardy for his doctorate dissertation. Professor C. Fairhurst (Principal Investigator) directed the research and played an active part in all aspects of it.

This report was prepared by M. P. Hardy.

*Currently Associate Professor of Civil Engineering, James Cook University of Northern Queensland, Townsville, Queensland, Australia.
**Currently Senior Research Scientist, Tunnels Division, Transport and Road Research Laboratory, Crowthrone, Berkshire, England.
***Post Doctoral Research Associate, Research Fellow, Professor and Head respectively, Civil and Mineral Engineering Department, University of Minneapolis, Minneapolis, Minnesota 55455 U.S.A.

This report describes research activities in three separate areas related to the overall aim of improving the estimation of the mechanical properties of rock masses. These three fields are broadly classified as; the intrinsic properties of rock failure, the mechanical failure of block jointed models of rock masses and the continuum characterization of rock masses for deformation calculations

The fracture of brittle rock is considered as an energy absorbing process where the 'work of fracture' is the dominent material property. An associated material property 'the effective crack length' is defined as a through-the-structure crack which develops after the application of load but controls the maximum load carrying capacity at the structure. Numerical analytical procedures are outlined to predict the complete force deformation response of a structure failing due to an extending through-the-structure crack. These predicted force deformation curves are compared with experimentally derived results for three commonly used tensile strength tests. The ambiquities often referred to in tensile testing of rock as the shape and size effect are successfully explained using the two material properties of 'work of fracture' and the effective crack length.

The mechanical failure of block jointed model were studied using a servo-controlled loading system such that the progressive collapse of these models under uniaxial compressive loading could be studied in detail. The mechanism of collapse at these block jointed models were recorded photographically and indicate that several mechanisms are operative in this process. These include; fracture of individual blocks, rotation of individual blocks, collapse of columns of blocks of rotation or buckling, slip along joint planes and by shear deformation of individual blocks. No single simple theory of failure appears capable at this time of predicting the collapse loads of such systems.

The dilatant nature of the collapse of these block jointed models was studied under two different confinement pressures. Failure of the specimens was again controlled using a servo-controlled testing machine. These tests illustrate that the volumetric strain behavior of jointed specimens can be vastly different from that of comparable unjointed specimens.

The continuum characterization of a jointed rock mass is briefly reported in this report. The research results of this work have been reported in readily available journals so is only briefly reviewed here. The low shear stiffness of joints in general results in an anisotropic continuum characterization of the rock mass with a low shear stiffness. The practical significance of the anisotropic characterization, in that the pressure 'bulb' from any applied load on a boundary is distorted from that of the isotropic case, is discussed. The effect of joint spacing and thickness upon the reliability as a function of the number of dilatometer tests in a jointed rock mass is also discussed and presented in detail in one of the published papers.

TABLE OF CONTENTS

Chapter

CHAPTER 1

INTRODUCTION AND OBJECTIVES

The need for a better understanding of the mechanical behavior of rock masses is a main reason why rock mechanics has emerged, over the past two decades, as a specific subject for study. Unfortunately, much of the current research appears to be academic scientific inquiry in the laboratory with little or no detectable aim towards practical utility. On the other hand, many field studies, supposedly directed towards the determination of practically useful information, are found to be of limited value because of an inadequate theoretical framework on which to plan experiments or interpret the results.

Development of a rational approach to the problem of estimating the mechanical behavior of a rock mass was the aim of the research initiated under the general title "Estimation of the Mechanical Properties of Rock Masses." This research effort was originally planned to cover a three year period. The work reported in this report represents the results of the second year of this effort and hence relies somewhat on work that was initiated within the first year of this contract (ARPA Contract H0101610).

Methods of determining the mechanical behavior of a structure fall into two general categories, the analytic method and the synthetic method. In the analytic method, the response of the structure to the applied loads is predicted from experimentally determined properties, representative of the material. To be representative, the specimens used in the experiments must be large enough to contain a statistically adequate number of all structural elements (i.e. those components which significantly influence the deformational response of the structure). Comparison of the predicted response with that observed gives a measure of the validity of the analysis. The analytical method is the one that has been most extensively and successfully used in mechanics.

In the synthetic method, the deformational behavior of the structure is computed by considering the interaction between the various significant structural components, based on a knowledge of the deformational behavior of each individual component.

In attempting to determine the mechanical behavior of a rock mass it appears that a combined analytic-synthetic approach is required. The structural elements frequently include joints, etc., spaced several feet apart, so that it is impractical to test samples large enough to be considered representative. The overall structure may be several thousands of feet in dimension so that it is equally impracticable to determine and take individually into account all structural elements.

It does seem possible to sample each significant structural element, determine representative values of the necessary properties, and use these in the analysis of the overall structural behavior.

6

Many rock masses consist of two main structural elements, viz.,
(1) relatively intact blocks, divided by (2) essentially planar dis-
continuities. Following the method of study outlined above, it
should be possible to deduce the mechanical behavior of the rock
mass from separate study of the mechanical behavior of the intact
blocks and the discontinuities. This behavior can be most thorough-
ly investigated in the laboratory, (assuming that the field environ-
ment can be maintained or reproduced in the laboratory).

The mechanical properties can be conveniently considered in the
two groups: (a) Deformation properties, (b) Strength properties.
The relative importance of the two gruops will change with the prac-
tical problem. Thus, foundations, and mine subsidence problems may
be influenced most by the deformation properties of the rocks; where-
as, tunnel lining, and mine pillar support designs will be determined
more by the strength properties.

For an overall study of rock mass behavior, therefore, one
can define several inter-related research tasks:

Study of the deformability and strength of intact rock.
Study of the deformability and strength of discontinuities.
Study of the deformability and strength of 'jointed' rock masses.

As already mentioned, laboratory tests are preferable to field
tests since a much broader range of test conditions can be imposed
at much lower cost. Against this, however, is the important fact
that force capabilities of laboratory equipment limit the size of
the specimens that can be tested. This is particularly true when
testing specimens from intact rock. Correlation between laboratory
and field must, therefore, include consideration of the influence of
size of specimen on measured properties.

Review of the literature indicates that numerous investigations
are in progress on the subject of deformability and strength of dis-
continuities. It also appears that reasonably consistent values
are obtained, so that it should be possible to rationally derive
field values from laboratory studies.

Although much attention has been paid to the problems of lab-
oratory testing of intact rock specimens, there is considerable uncer-
tainty as to how laboratory values can be interpreted for field
situations. Different laboratory testing procedures have given
widely differing results indicating that the truly representative
material properties (which do not vary with test method) are not be-
ing computed from the results. No valid extrapolation to field
scale parameters can be made until such 'intrinsic' material proper-
ties have been determined.

Studies of the deformability and strength of rock masses have been very limited in view of the expensive nature of full scale studies. To overcome this, two main approaches can be used: viz.

(1) "Back calculation", in which examples of rock mass collapses are analyzed to determine the conditions that existed at the instant of collapse. The need to specify the applied loads with some accuracy has generally limited such calculations to cases involving rock-slope collapses.

The second approach.

(2) Model studies of rock masses, in which simulated rock masses can be deformed to collapse in the laboratory, should provide very useful information on the full-scale behavior, if the corresponding properties of the discontinuities and the intact rock are known.

Considering past and present research by other investigators, it was decided that the following studies would contribute most towards a better understanding of the overall problem:

1. Theoretical and experimental determination of intrinsic material properties for intact rock.

2. Laboratory study of the deformation and strength behavior of models jointed rock masses.

3. Analytical study of the response of jointed rock masses to applied loads. This should include a theoretical examination of the validity of procedures now used to determine the in-situ deformability of rock masses.

These research tasks are reported in the following chapters in the order listed above.

Chapter 2 considers the intrinsic properties of intact rock but specifically rock fracture. The subject of rock fracture is probably the most studied aspect of the mechanical properties of rock yet is still not well understood. The compressive failure of rock has only recently been studied in a controlled means such that the mechanism of failure can be individually studied. These studies have shown that tensile splitting is a dominant mode of failure controlling the peak load carrying capacity of the material. Studies of the tensile strength of rock result in paradoxical results. The observed tensile strength is not a constant and, hence, cannot be considered an intrinsic property of the material as once thought.

This chapter considers tensile fracture of rock in some detail with specific emphasis on five commonly used tensile testing configuration. Tensile fracture is considered as a process involving

growth of a through-the-structure crack surface. An energy balance criterion is used to determine the complete force-deformation response of each of the five testing configurations. Experimental results for three of the analysed testing configurations, the beam test, Brazilean test and the ring test are presented with comparison with the predictions. Two intrinsic material properties, the work of fracture and the effective crack length are suggested as being useful in the understanding of the failure of rock in tensile situations.

Chapters 3 and 4 discuss the mechanical behavior of block jointed models. A literature survey on the shear strength of joints and previous work on the collapse of block-jointed systems is contained in Appendicies I and II respectively. Contrary to the experience in intact rock, the mechanisms of failure of composite intact rock and joints has not been fully explored. These experiments were designed to observe the mechanisms of failure of a simulated block jointed model. This was done in both the uniaxial test and triaxial tests. It is not until the mechanisms of failure are understood that failure theories can be developed to predict failure loads in other situations. Nonetheless, many failure theories do exist for jointed materials. The relevance of these theories to the observed failure mechanisms is discussed. (Appendix III contains additional work that was completed on the fatigue characteristics of these models.)

Chapter 5 very briefly reviews a considerable amount of work regarding the continuum characterization of rock. This work has the most direct practical significance. One section of this work reviews the significance of rock mass deformation determinations from the aspect of size of the measuring instrument relative to joint spacings and number of tests required to give reliable modulus measurements. This work is now fully reported in readily available journals and although only briefly mentioned here, is considered a major contribution of this research effort.

Integration of these three research efforts was to be the subject of the third year of this research so only a brief overview and summary is presented in the final chapter.

9

CHAPTER 2

THE INTRINSIC PROPERTIES OF ROCK - THE FRACTURE OF ROCK

Introduction

The understanding of the failure characteristics of a material are fundamental to the correct use of that material in any engineering design. At this stage man is far from properly using rock as an engineering material both because of its inherent variability as found naturally and because of an inability to forecast the behavior of the rock under a given loading situation. The potential benefits from a detailed understanding of rock behavior are enormous both in improved efficiency of rock excavation and improved stability of underground openings such as tunnels and mining excavation.

Existing theories of rock failure are generally emperical in nature, with very little fundamental theoretical background. Because of the basic weakness of rock in tension and the preponderance of compressive stress fields in problems concerning rock most attention has been given to compressive strength theories, with such names as Coulomb, Mohr, Griffith, McClintock and Walsh being associated with various failure theories. However, with these emperical or semi-emperical failure theories, it is difficult to extrapolate laboratory results to field situations, or into stress conditions which have not previously been explored. The possibility of other parameters such as stress gradient, intermediate principal stress, lateral stiffness, pore fluid, time, temperature, dilatancy and even geometry have to be studied experimentally.

The distinction between tensile criteria and compressive criteria has always been maintained, although the Griffith compressive stress criteria assumes failure to begin by tensile failure around a pre-existing crack. Detailed observation of compressive failure of rock (see for example WAWERSIK 1968) reveal that failure is complex as many structural changes take place within the rock before the compressive peak is reached, and in the post peak region coalescence of cracks and macroscopic shear deformation result in the reduction of the load carrying capacity of the specimen to, or near to, zero. The attempt of a continuum characterization of this process is open to question. However, it is apparent that tensile splitting is a dominant mechanism in the compressive failure of rock.

Tensile strength criteria have been implied to be much simpler than that for compression failure, but tensile failure of rock is quite complex. Simple theories of maximum tensile stress produce many paradoxes and appear to be unsatisfactory.

This chapter proposes that the tensile strength of rock be characterized by two parameters; the 'work of fracture' of the material, which has dimensions of energy per unit area, and a length, which will be termed an "effective crack length". Both these parameters can be uniquely determined, and help to explain many of the observed paradoxes in the conventional stress criterion. These two properties have to be used in conjunction with analysis of a body or structure in the 'cracked' state. Discussion is presented as to the relevance of this analysis to compressive failure of rock and rock masses. Experimental results are presented to support this characterization of the tensile failure of

brittle rock for the beam test, Brazilian test and the ring test.

THE THEORY OF ROCK FAILURE

The Failure Mechanisms in Rock

The term "rock" encompasses a great variety of solids which on the macroscopic scale can be considered to possess some cohesion. In general rock is not a continuum as it contains voids in the form of pore space or elongated cavities induced by the rocks past (unknown) thermal and mechanical history. Rock, in most instances, is an aggregate of more than one mineral type; these minerals are often distinguishable to the naked eye as individual crystals and may be arranged such that the rock is anisotropic. From such a brief description of the nature of rock it is not surprising to find that the complete understanding of the failure process in rock is not yet fully understood.

Discussion and analysis of materials must start from simplified ideal materials with eventual incorporation of peculiarities inherent in the particular material of interest. One assumption often made is that the ideal material is isotropic, homogeneous and to have no memory. For this type of material two fundamental mechanisms of failure can be discussed based upon the possible motion of atoms and molecules. They are generally referred to as shear and cleavage. Shear is associated with a row of molecules or atoms translating relative to its neighboring atoms as shown in Fig. 2.1a. This is traditionally the dominant mechanism in plastic or ductile behavior of metals such as mild steel. The other fundamental mechanism, cleavage, is characterized by separation of the atoms or molecules to such a distance that no interatomic forces act to reunite the atoms, Fig. 2.1b. All other mechanisms observable in failure such as grinding and curshing of material can be reduced to an interaction of these two mechanisms. However, the integration of these two fundamental mechanisms to give a useful overall macroscopic behavior of the material is possible only in a few materials and then over only a very limited range of deformation.

The reduction of observed phenomena to the two fundamental mechanisms outlined above presents some difficulty and has necessitated the phenomenological description of other observed modes of deformation. Friction is a good example of this. Fundamentally, friction is due to either the shearing of welded points of two surfaces in contact as in a metal, brittle cracking of asperities as in some rocks, or 'ploughing' which involves chip formation in brittle materials or plastic flow in ductile materials. A detailed description of each contact area of the sliding surface is impractical so the observed phenomena is described in terms of the overall response of the surface; the coefficient of friction for metals, or coefficient of friction and the cohesion for rock. Slip of two surfaces relative to each other and the associated factors, friction and cohesion are very important in rock, both on the microscopic scale and the macroscopic scale, (see for example, JAEGER and COOK 1969 and Appendix I of this report) but is fundamentally different from shear dislocation as described earlier. In a shear dislocation within a crystal the tensile strength perpendicular to the dislocation is not changed relative to the ideal material whereas when slip takes place with the associated frictional resistance between two surfaces, the normal tensile strength is very low to zero.

A non-linear response of strain to an applied stress can result from either of the two fundamental mechanisms. In ductile material the onset of non-linear behaviour is characterized by the development of Leuder's Lines, these lines representing thin planes on which dislocation movement takes place. In extremely brittle materials such as glass the non-linear response is due to cleavage or crack growth. Methods of analysis have developed separately for the two fundamental mechanisms; shear movement is generally studied from the theory of dislocations, while analysis of cleavage and crack growth has its origins in the energy balance method introduced by GRIFFITH (1921).

For most rocks studies under low confining pressures and at low temperatures very little evidence of dislocation growth has been found. At high confining pressures and at high temperatures dislocation movement, or twinning and gliding of crystals, is observed (RALEIGH 1965). Most rock which are encountered in engineering practice are found in relatively low stress state and at low temperatures. Under these conditions most rocks fail in a brittle manner (this being defined as failure due predominantly to crack growth and coalescence of cracks.)

Considerable attention has been focused on the Griffith Criterion and its application to rock in the past decade, with the orginal theory being modified to account for closing of cracks under compressive stress field, the pore fluid pressures present in the cracks, and the three dimensional aspect of cracks. Here we attempt to highlight the important aspects of the Griffith Theory as it is applied to rock.

Rock as a Griffith Material in Tension

Griffith's fundamental and extremely important contributions to material science was to recognize that in extending a crack energy is abosrbed, or lost, to the material. This energy was likened by Griffith to the surface energy of a fluid and hence termed 'surface energy'. Using this energy in the analysis of eliptical cracks Griffith determined the stress in a uniaxial or biaxial tension test of a plate containing an elliptical flaw would extend unstably. Griffith originally applied this analysis to glass where there appears to be good agreement between theory and practice (e.g. flawless glass has been produced having a strength near the theoretically obtainable strength of approximately E/10). The hypothesis by Griffith that materials contained flaws, which he characterized as elliptical cavities, was at the time a bold and new approach to material science particularly when the original hypothesis was applied to glass, an apparently homogeneous, isotropic material. For rock this hypothesis becomes much less daring as it is obvious that most rocks contain flaws and imperfections from an ideal homogeneous and isotropic body.

In study of the energy absorbed by crack growth in metals it was realized that the energy absorbed was much higher than that required to separate a plane of atoms. OROWAN (1952) and IRWIN(1948) recognized that although this energy was absorbed by plastic movement near the crack tip the original Griffith energy balance method was still applicable if the surface energy term in the Griffith expressions was replaced by the 'work of fracture', this being the total energy absorbed by the material for a crack to grow a unit of area, thus including the plastic work and the surface energy. The plastic work is abosrbed by the material in the formation of shear dislocations near the crack tip. [it has been suggested see COTTERELL (1963), that even in glass some dislocation movements take place at the tip of an advancing crack.]

More detailed analysis of crack tip stress fields by BARENBLATT (1959-1962) and DUGALE (1960) using idealized models for the plastic yield at the crack tip arrive at essentially the same energy balance criterion at the onset of unstable crack propagation as originally proposed by Griffith and modified by Orowan and Irwin. However, it must be remembered that any non-linear material response must be localized to the crack tip region.

Rock, being in general an assemblage of crystals and discontinuities, could not be expected to satisfy the implications inherent in Griffith's original theory. However, the principles proposed by Griffith have been shown to be a useful guide in understanding rock behavior. Experimental observation of the surface energy or the work of fracture in rock reveals that it is several orders of magnitude higher than that observed in pure crystals of the same materials as those in the rock (see for example PERKINS and KRECH 1966). This has been explained as being due to:

a) plastic deformations
b) inaccurate estimates of the true surface area created
c) release of residual stresses within the rock (FRIEDMAN et al 1972)
d) microcracking near the crack tip(HOAGLAND et al 1972)

Plastic deformations have been eliminated by testing at low temperatures which normally reduces the tendency for dislocation movement and by electron microscopic observation of the crack tip region by HOADLAND et al (1972). Accurate measurements of the true surface have been able to account for a factor of ten in the discrepancy of single crystal works of fracture and that of rock, but this is still not sufficient. It appears that both c) and d) can account for a significant portion of the absorbed energy along with energy absorbed by slippage along favorably inclined cracks ahead of the crack tip. However, these mechanisms of energy absorption are all localized to the area of the crack tip, so depending upon the scale of the observed crack tip, linear elastic analysis can be used for the overall response with the appropriate "work of fracture" being used in a very similar manner as that of OROWAN and IRWIN. On the microscopic scale individual mechanisms can be isolated and studied.

This discussion logically leads to considering two distinct size domains in crack growth in rock. These can be conveniently referred to as the microscopic domains. The characteristic size of these two regions depends upon the structure of the rock but a useful guideline of the microscopic domain is that area of the tip of a crack in which the overall continuum representation would have to be non-linear. This is generally of the same magnitude as the grain size of the rock. The remainder of the body can be considered in the macrodomain. In fracture mechanics IRWIN (1960) has developed a procedure for estimating the size of the plastic deformed zone, r_y, at the tip of the crack with:

$$r_y = E\gamma/2\Pi\sigma_{ys}^2 \qquad \qquad ...(1)$$

where σys is the 0.2 percent offset tensile yield strength. In the study of fracture in metals this might be used to delineate the micro and macrodomains. The quantity r_y could be used for rocks as an index number to compare different rock types, with this number being interpreted as the minimum effective crack length size for which linear elasticity could be applied.

In the microscopic domain the crack path is a result of the interaction of crystals of different minerals, pore volume and pre-existing cracks. If this volume were considered as a linear isotropic homogeneous continuum, the maximum tensile stress would be at the crack tip, but because of the inhomogenieties of the rock structure and the variation of local surface energies, slip can occur across pre-existing weaknesses, micro-cracks can extend away from the major crack tip, and bridges of material between pores can fail. All these mechanisms absorb energy, contributing to the ' croscopic 'work of fracture'.

In the macroscopic domain the crack path is determined by large scale variations in material properties, anisotropy of the material and by the overall stress field. The detailed mechanisms occurring at the crack tip need not be considered as these determine the crack path variability and in general are accounted for in the work of fracture property. To determine the conditions necessary for crack growth the energy equilibrium method has been suggested, but before describing the usefulness of this method on the macro scale discussion is presented on two other concepts often used in tensile testing literature; the tensile strength, and the critical stress intensity method.

Maximum Tensile Stress as a Strength Criterion

The tensile strength of brittle materials is not often referred to as a material property since the realization by GRIFFITH (1921) of the dependence of the strength of a brittle material on the maximum flaw size within the material. From the energy balance analysis of a plate containing an elliptical flaw Griffith found the observed tensile strength σ_g to be

$$\sigma_g = (2E\alpha/\pi Co)^{1/2} \qquad \qquad ...(2)$$

where
  E = Modulus of Elasticity
  α = Surface Energy
  Co = Initial flaw length or crack length

Griffith also determined that the stress at the crack tip, σ_t, to be

$$\sigma_t = 2\sigma_g (Co/\rho)^{1/2} \qquad \qquad ...(3)$$

where
  ρ = Radius of the crack tip.

The crack tip stress, σ_t, was later assumed by GRIFFITH (1924) to be a material property, but the obvious question arose of how to define the crack tip radius ρ. It is impossible to define the crack tip radius in rock without becoming involved in a very detailed description of the micro cracking and material variations at the crack tip.

However, in rock mechanics many attempts have been made to measure the "tensile strength" of rocks, primarily as an index property to aid in comparing different rocks. The approach was to assume that there is a given distribution of flaws or cracks within the rock and the largest flaw would control the tensile strength of the rock. This effect could explain an apparent size effect. As the test sample size was increased, and hence the strength would decrease with size. For all tensile tests there is a large variability from test to test, but it was

soon found that the mean strength of a group of tests of the same geometry and test conditions is not consistent from groups of different test geometries. Typical test geometries include the direct tension test, the beam test and the diametral compression of discs or rings commonly known as the "Brazilian test". In each of these tests different stress gradients exist and differing volumes of rock are subject to tensile stresses, so these effects should be considered in comparing the tests. Attempts have been made to consider these effects and the statistical distribution of cracks in applying WEIBULL's (1939) statistical theory of failure to these different tests. These methods are summarized by JAEGER and COOK (1969) and are considered in detail by HUDSON (1971). As is often found, (see FREUDENTHAL (1968)), in applying statistical theories to failure, the problem of determining material properties degenerates to curve fitting exercises with very little physical insight to the mechanisms involved. HUDSON (1971) found that, even using statistical theories based upon the probability of there being a crack at critical dimensions within the stressed volume the 'material constants' defined by Weibull varied with different test geometries and different sizes. However, this theory is a useful start in understanding the variations in tensile strength, but it appears that further understanding of the failure process is required to fully explain tensile failure of rock.

The Stress Intensity Criterion of Strength

The Stress Intensity Factor approach to tensile failure of materials has its origin in the representation of the crack in an otherwise continuous material. WESTERGAARD (1939) characterized a crack as a planar discontinuity at zero thickness. For this type of crack the crack tip radius is zero, and hence, the stresses are infinite. No material can physically withstand infinite stresses and, in reality, they do not exist. The predicted infinite stresses are a result of the mathematical analysis based upon certain assumtions both in the constitutive equations, linearity, and the formulation of compatibility, infinitesimal strain. However, is is obvious that the constitutive relationship and the geometric characterization of the material near the crack tip is more crude than the general analytical assumption of infinitesimal strain. To overcome these problems while still being able to utilize existing mathematical expertise IRWIN (1957) introduced the concept of the stress intensity factor.

The Stress Intensity Factor is defined and illustrated with reference to Fig. 2.2. This is defined for a slit type crack where the tensile stress is singular but because the stress intensity factor is the limit of $\sigma_{yy}\sqrt{r}$ as r approaches zero, its value is finite and dependent upon the far field stresses or forces. Figure 2.2 shows the stress intensity factor for cleavage opening of the crack, corresponding stress intensity factors are defined for longitudinal and transverse shear deformation, (see PARIS and SIH 1965).

The critical Stress Intensity Factor is the value of the Stress Intensity Factor at initiation of unstable crack growth and was originally proposed by Irwin to be the material property controlling crack growth. Subsequent experimental work has shown the critical Stress Intensity Factor to be effected by size and shape of the test specimen (see for example BROWN and SRAWLEY 1965) but most of these effects can be explained in terms of the plastic deformations occurring at the tip of the crack.

The equivalence of the stress-intensity approach and the energy release hypothesis has been illustrated by IRWIN (1957) for the case of opening mode deformations with

$$K_I^2 = E\gamma \text{ for plane stress}$$

$$K_I^2 = E\gamma/(1-\nu^2) \text{ for plane stress} \qquad \ldots(4)$$

This equivalence is based upon the assumption that the crack will extend in the plane of the crack. For more complex crack paths involving curvature of the crack path the equivalence of the energy release and the stress intensity method is difficult to establish and the interaction the various deformation modes is not fully established.

This simplified characterization of the crack, as a slit of zero thickness allows for greater use of existing mathematical expertise to solve problems involving cracks under various loading conditions and within non infinite bodies, PARIS and SIH (1965) and SNEDDON and LOWENGRUB (1969) present good reviews of available solutions. With bodies of finite dimensions the analytical techniques are often complex and applicable for only a small range of crack lengths. Numerical techniques often have to be used to solve the complex differential and integral equations.

The finite element method (F.E.M.) of stress analysis has been used to determine the Stress Intensity Factors for cracked loaded bodies. CHAN et al (1970) and WEBER (1971) have used conventional finite elements to determine the stress intensity at the crack tip, while ROA et al (1971) and BYSKOV (1970) have used a hybrid and special cracked elements respectively to overcome the high density of elements required at the crack tip when conventional elements are used. ANDERSON et al (1971), HARDY (1971) and HAYES (1972) have found alternative methods of utilizing conventional finite elements in fracture mechanics by considering the energy changes in a body for different crack lengths.

The Finite Element Analysis of Cracked Structures

The Finite Element Method is now widely used in most fields of engineering so no further discussion will be presented here. A body under external surface tractions or internal body forces is divided into a finite number of triangular or rectangular elements. The displacements of the nodal points of the elements are determined by inversion of the global stiffness matrix [K], which is made up from the individual stiffness matrix of each element and the multiplication by the load vector. All loads are assumed to act through the nodal points. The strain energy of the body can be found directly from the displacement distribution and the stiffness matrix. In matrix notation this can be represented as

$$U = \delta^T [K] \delta \qquad \ldots(5)$$

where U is the total strain energy of the body and δ is the displacement vector for the nodes in the body.

It can be shown that the strain energy calculated in this manner is a lower bound solution. The accuracy of this solution can be improved by reducing the element size in regions of high stress gradient; thus in fracture mechanics pro-

blems this implies small elements at the crack tip.

In studies of crack growth using the finite element method U the strain energy is calculated for two bodies, are with crack length 1, the other with crack length 1+dl, dl represents a small change in the crack length resulting in an increase of crack area ΔA. The strain energy release rate γ is then

$$\gamma = \frac{dU}{dA} \doteq \frac{U^+ - U}{\Delta A} \qquad \qquad \ldots(6)$$

where U_+ strain energy of body with crack length 1
     U^+ strain energy of body with crack length 1 + dl

If F represents the external forces on the body, then the crack will extend from 1 to 1+dl when the strain energy release rate equals or exceeds the critical strain energy release rate γ_c, or "the work of fracture". This is a restatement of the original Griffith criterion, that fracture will occur when all the energy available from the change in strain energy is absorbed by forming the new crack length. The strain energy can be represented in terms of the external forces, if no body forces are acting,

$$U = \frac{F^2}{2M} \qquad \qquad \ldots(7)$$

where M is the modulus for the particular body being studied, then by substitution into equation 6 and replacing γ by γ_c, the work of fracture, we find the force F_c required to cause crack extension

$$F_c = (2\gamma_c \Delta A/(\frac{1}{M} - \frac{1}{M}))^{1/2} \qquad \qquad \ldots(8)$$

This method is similar to that suggested by IRWIN and KIES (1952) as the 'compliance method'. Previously, the compliance ($\frac{1}{M}$) was determined experimentally for bodies of different crack lengths and then differentiated to find the change in compliance with crack length for substitution into the equation

$$\gamma_c = 1/2 \ F^2 \ \frac{d}{dA} \ (\frac{1}{M}) \qquad \qquad \ldots(9)$$

which is in effect the same as equation 8.

For many situations the variation of the compliance with crack length is so low that large errors can result from the experimental method. With the F.E.M. this is not a problem as the strain energy can be determined to many significant figures, and hence the modulus.

The Stress Intensity Factor can also be determined from equation 8 using the relationship expressed earlier between K_I and γ in equation 4, if simple crack opening displacement is the only mode of crack displacement

$$K_I = (E\gamma)^{1/2}$$
$$K_I = (E \ \frac{U^1 - U}{dA}))^{1/2} \qquad \qquad \ldots(10)$$

Similarly, the crack will extend when $K_I c$ the critical Stress Intensity Factor is exceeded.

This method of determining K_I for complex geometries has been shown by ANDERSON et al (1971) to be more economical than attempting to determine K_I from either the stresses near the crack tip or the displacement of the crack surfaces.

In many rock mechanic situations, the experimental output is a force versus displacement response of the structure or a test specimen indicating the failure locus of the failing specimen. If the test specimen is one for which failure is due to the extension of a crack, the predicted forece-displacement response can be constructed using the theory outlined above. Equation 8 can be used to incrementally construct the force displacement response; the force F_c at initiation of crack extension is found for a particular crack length, then the displacement δ at the crack length is determined from

$$\delta = 2\frac{U}{F_c}$$

...(11)

On a typical force-displacemetn specimen response the energy balance criterion can easily be visualized. Figure 2.3a, b, c show a typical test, the modulus as a function of crack length and the predicted force versus displacement structural response. The slope of line OB represents the modulus of the structure when the crack length is $C + \delta C$. If the loading system were such that controlled failure of the structure can be achieved, then the shaded area OBC represents the energy that is absorbed by the structure as the crack length extends from C to δC. Fig. 2.4a and b diagramatically demonstrate the derivation of equation 8, fig. 2.4a, for a 'soft' loading system and 2.4b for a 'stiff' loading system. As the end result is independent of the loading system this tends to suggest that this criterion is independent of the loading characteristics. This can be formally proved in many ways, for a simple structure with one applied force PARIS and SIH (1965) gives an elegant proof of this independence and BUEKNER (1958) has formally proved that this criterion is independent of the stiffness of the loading system for an arbitrarily loaded structure.

Analysis of Structures Containing Multiple Cracks and/or Curved Cracks

In many rock mechanic problems curved cracks are developed and many cracks may propagate; chip formation in "cutting" brittle rock is a result of a curved crack initiating near the cutter and progressing to a free face. (HARDY and FAIRHURST 1973.) In blasting where gas pressures are considered by some to be most important in the ultimate shape of the crater (see PORTER 1971) many cracks have the option of extending. Analytical methods of predicting crack trajectories are in general based upon stress conditions of the uncracked state and as such are not particularly reliable. In problems of fragmentation either by mechanical or thermal means understanding of crack initiation criterion and direction of propagation are fundamental to improved research and ultimately design.

The above energy balance method of crack extension can be applied to the problem of crack direction and multiple crack growth irrespective of the means of inducing the internal stresses, thermal or mechanically. [However, at this stage the method that will be outlined is considered expensive.]

To investigate the most probable crack path through a loaded structure alternative crack paths must be considered and as the crack path that maximizes the energy release will form at lower external loads than other crack directions

then this crack direction will be most probable. For example, consider figure 2.5(a) which represents a ledged rock about to be chipped off by the action of the forces F. Three or four probable crack direction increments are selected and analysed with the function $v^1- v$, the energy release, plotted as a function at crack direction, figure 2.5(b). The direction which maximizes the energy release can be determined. a curve fitting fracture, and from equation 8 the force, F, required to stabaly propogate that section of the crack can be determined. At each step in the crack growth sequence several possible crack paths are again considered to determine the most probable crack path. In this fashion a curved crack path can be developed. At each step of this analysis a new (a modified) finite element mesh has to be prepared, and for each increment of crack growth several finite element solutions have to be considered, thus this method is relatively expensive.

When there is a possibility of two or more cracks growing, a similar procedure is adopted, trial and observation. If, in a given structure, we have two cracks C_1 and C_2, the strain energy, U, is determined for the body with crack lengths C_1 and C_2 and the imposed boundary conditions. U_1 is then determined for a body with crack lengths $C_1 + \delta C$ and C_2 and then U_2 is determined for a body with crack lengths C_1 and $C_2 + \delta C$. If U_2-U^2 is greater than U_1-U, then C_2 will extend at a ...over applied load than C_1 and visa versa. An application of this will be discussed in a later section in the investigation of the ring test. For certain internal to external diameter ratios there exists the possibility of a crack growing from the inside diameter to the outside diameter, as for a crack to grow from the outside diameter to the inside diameter, this is shown diagramatically in figure 2.5b.

THE FINITE ELEMENT ANALYSIS OF SPECIFIC TEST GEOMETRIES.

Analytical Predictions

In this study, the growth of cracks in five common laboratory tests were analyzed. These were:

> Beam Test
> Direct Tension Test
> Brazilian Test
> Ring Test
> Hydraulic Fracturing Test

These tests were chosen as they represent the most common methods of determining the tensile strength.

The beam test has been analyzed more intensively than the other tests and this work has been reported in a paper entitled THE FAILURE OF ROCK BEAMS. PART I THEORETICAL STUDIES by M.P. Hardy, J.A. Hudson and C. Fairhurst which will appear in the January edition of the International Journal of Rock Mechanics and Mining Science of 1973. Part II of this paper reports the Experimental Studies which will be mentioned later in this report.

Figure 2.6 shows a summary of the shapes used to study these five tests with a summary of the number of elements and the number of modal points in each finite element mesh. The crack is modeled in these studies as a slit, and can easily be

varied in length by changing the boundary conditions along the vertical axis of symmetry in each case. This is acceptable in these cases as this is the line along which fracture is likely to occur if the material being studied is homogeneous and isotropic.

The number of different crack lengths analyzed for each structure is shown in Fig. 2.6. Sufficient crack lengths were taken to get a realistic estimate of the variation of strain energy and modulus as a functional crack length. Attention was focused on the initial crack lengths as in most cases this is where the change in strain energy is smallest, and the region of most interest in the failure of the structure because the initial crack length will control the load carrying capacity of the structure.

Figure 2.7 shows in more detail the finite element mesh for each test. These meshes were selected such that the mesh near the tip of the crack would be independent of the crack length. This minimizes the effect of the mesh on the estimate of the strain energy of the system, and as the difference between the strain energy of each structure with increasing crack length is used in the analysis, any error in the strain energy will not affect the estimate of the force required for failure.

The output for each of these tests is presented in Fig. 2.8 through Fig. 2.12. Each of these figures shows the modulus versus crack length, the force versus crack length and the force versus displacement. This later curve is the conventional experimental output. For the hydraulic fracturing test, which is only for the case of pressure restricted to the hole and not inside the crack, the modulus is a little different than that for the other tests, where the applied loads are unidirectional. The modulus in this case can be defined with reference to the slope at the pressure, P, versus internal volume charge, ΔV, response of the structure, which would automatically show the energy as the area under the P-ΔV curve, or for dimensional similarity with the previous tests, the modulus can be defined with reference to a fictitious force, F, and fictitious displacement δ. F can be defined as the pressure multipled by the surface area over which it acts, and the displacement can then be calculated from equation 11

$$\delta = \frac{2U}{F}$$

...(11)

then the modulus is defined as before

$$M = \frac{F}{\delta} = \frac{P}{\Delta V}$$

...(12)

The response force versus displacement is generally represented as the vertical force, such that the area under the force-displacement curve reflects the external strain energy. However, any displacement between two points within the specimen can be plotted versus force. This may be required to compare the exact experimental output with the predicted curve. For example, often a transverse displacement relative to the crack path is measured as a control parameter in the experimental procedure. Several such transverse or generally horizontal displacements are shown in Figures 2.8 to 2.12. Fig. 2.12 shows the pressure versus internal diameter for the hydraulic fracturing test.

BERRY (1960) has constructed a stress-strain locus for a plate under uniaxial tension containing a crack from Griffith's analysis. This assumes the plate is infinite, but the similarity between the results of Berry's curve on Fig. 2,9c can be seen. Direct application of Griffith's results (with σ_g as the assumed tensile strength) to each of these tests would predict that the applied force, F, to initiate crack growth would be inversely proportional to the square root of the crack length. This can easily be seen from the direct tension test where

$$F = \sigma_g A \qquad \qquad \ldots(13)$$

where A is the total cross-sectional area of the test piece, but in general for the other tests A will be a function of the geometry of the test, then by substitution for σ_g from equation 2

$$F = (2E\gamma/\pi C_o)^{1/2} A \qquad \qquad \ldots(14)$$

$$= k/C_o^{1/2} \qquad \qquad \ldots(15)$$

k will be different for each test reflecting the factor A. Using the value of the force at crack length of 0.1 inches to calculate the constant of proportionality, k, in equation 15 for each of the test geometries studied the expected force at a crack length of $(C_o=)$ 0.2 inches was calculated. These results are shown in Table I along with forces predicted from the energy balance method for a crack length of 0.2 inches. Notice that for the direct tensile test the agreement is excellent as would be expected because this test is closest to the original Griffith analysis. The agreement is good for the beam test and acceptable for the Brazilian test, but for the ring test the agreement is very poor. This illustrates the possible error of using the Griffith value of tensile strength rather than the original energy balance basis of a failure.

	Direct Tension	Beam Test	Brazilian Test	Ring Test	Hydraulic Fracturing
load at crack length=.1"	2810	1212	19,497	4,200	6,200
load at crack length=.2"	1970	854	12,772	4,200	4,300
load at crack length=.2" if $F = k/c^{1/2}$	1980	857	13,750	592	4,400

Table I: Comparison of the forces required to cause crack growth at a crack length of 0.2" calculated from either the energy balance method or the direct application of the tensile stress criterion.

The Brazilian and ring tests figures 2.10 and 2.11 respectively are interesting because the load carrying capacity does not reduce to zero as with the other tests. After the vertical crack is fully developed, the load is

carried by the two remaining "Dees". This phenomena occurs in many compressive testing situations particularly in the failure of jointed block models as will be discussed in chapter 3. In non-uniform rock high modules inclusion are subject to high diametral stresses and vertical splitting is an available mechanism to relieve the high stress build ups. This is a possible mechanism for the formation of small vertical cracks in uniaxial testing of rock.

Size Effect

The problem of the effect of a specimen size effort the observed strength of unjointed rock is of basic importance to the extrapolation of laboratory experimental results to engineering applications. BROWN (1971) has reviewed existing experimental and theoretical considerations and concludes that the literature contains a body of conflicting and generally inconclusive data. PRATT et al (1972) have recently shown an apparently dramatic dependence of strength on size for Cedar City quartz deorite under uniaxial compression. HUCK (1972) shows a much reduced size effect for charcoal diorite granite and no significant size effect for Indiana limestone for samples from two inches to 36 inches in diameter. These experiments were all conducted on samples of apparently unjointed rock. The effect of major discontinuities on the strength of the rock mass in considered in later chapters.

The above mentioned review and experimental results have been conducted on rock in compressive stress fields while very little research has been conducted on the size effect of rock in tension [HIENS (1972) has recently shown a slight size effect in brazilian tests on samples of dacite Valders limestone and St. Cloud gray granodiorite]. Griffith's theory can be used to illustrate two possible extremes in the discussion of size effect.

If the distribution of cracks throughout a body is ideally random with all crack lengths equal, and such that no carck interfered with an adjacent crack, then the crack length C could be a material property. The tensile strength

$$\sigma_g = \sqrt{\frac{2E\gamma}{\Pi C}} \qquad \ldots (2)$$

is independent of specimen size. On the other extreme if the crack length distribution is completely random, the maximum crack length C, encountered in a rock specimen would be proportional to the specimen length l. Thus for two testing situations of the same material and similar shape, but different length l_1 and l_2 the strength ratios σ_1 to σ_2 would be

$$\frac{\sigma_1}{\sigma_2} = \left(\frac{l_2}{l_1}\right)^{1/2} = \left(\frac{V_2}{V_1}\right)^{1/6} \qquad (16)$$

where V_1 and V_2 are the volumes of the two test specimens.

WEIBULL's (1939) statistical theory of failure predicts

$$\frac{\sigma_1}{\sigma_2} = \left(\frac{V_2}{V_1}\right)^{1/m} \tag{17}$$

[provided σ_m the minimum strength of an elemental material is taken as zero] where m is a material constant depending upon the strength distribution within the material.

The effect of size can be considered using the Finite Element analysis outlined above to investigate the expected size effect for different testing method. It can be very easily shown that for an energy criterion as has been used in this analysis that if the energy absorbed is proportional to length squared (new surface created) and that the energy available is proportional to length cubed, strain energy changes, then for two geometrically similar structures the failure stresses will be related in an inverse square root of length, i.e.

$$\frac{\sigma_1}{\sigma_2} = \left(\frac{l_2}{l_1}\right)^{1/2} \tag{18}$$

which is, in fact, identical to equation 16.

Now is when we consider that for a given rock the effective crack length is a material property, then for two structures of different size the geometric similarity is not maintained. Fig. 2.13 shows two geometrically similar bodies with length ratio χ. If we normalize the applied force by a length squared we have, in effect, a stress comparison. Curve R S T shows the 'stress' versus normalized crack length, for the body of length L, and curve P Q T shows the 'stress' versus normalized crack length for the body with length χL. If geometric similarity were maintained, then the respective stresses at failure would be as shown at points A and B in accordance with equation 18. If the effective crack length remains the same in both cases, the ratio crack length to body dimension, C/L, will reduce to C/χL and the strength of the larger body will move along curve P Q T to C. Now if there is to be no apparent size effect, the reduction in stress due to the size increase for constant geometry must equal the increase in strength for the reduction in the C/L ratio or

$$\left(\Delta\ \sigma\right)^{L \to \chi}_{C/L\ \text{constant}} = \left(\Delta\ \sigma\right)^{C/L \to 1/\chi\ C/L}_{L\ \text{constant}} \tag{19}$$

we know the dependence of σ on χ. This is tiven by equation 18, so if stress has a similar dependence in the change in crack length, then there will be no apparent size effect. Table 1 shows that for the five tests conducted all

but one, the ring test, show a very near dependence on crack length to the expression

$$\sigma \text{ failure } \alpha \frac{1}{\sqrt{C/L}} \tag{15a}$$

so we could expect very little dependence of strength of size for the test geometries studied. However, the ring test should show a very marked size effect. This has not been experimentally investigated, but does suggest some interesting tests which could be very simply conducted. For the beam test three different shapes were analysed to investigate this size effect. These results are summarized in Table II. No clear trend is established which seems to agree with the results of HIENS (1972) and HUDSON (1971), and BROWN (1971) although Brown reports on compressive failures.

Beam Volume	Span: Depth Ratio 5:3	5:2	5:1
1	100	100	100
8	96	106	103

Table II – Variation in tensile strength, in Beam Tests

Shape Effect

The shape effect is expressed simply as the variation of the apparent tensile strength with shape of the test geometry, with care to eliminate the size effect. Beam tests show a considerable shape effect, this can again be partly explained by the Weibull's theory, see HUDSON (1971) but again the material constants are not independent of test (shape or volume). Fig. 2.14 shows observed results on three beam shapes (from HUDSON (1971)). From the results of tests on a beam 12" x 4" material constants were found by curve fitting, these constants were used to predict the failure dis ributors for beam tests of 12" x 2" material constants were found by curve fitting; these constants were used to predict the failure distributors

for beam tests of 12" x 2" x 2" and 23" x 1" x 1". The predicted and actual results are shown in Fig. 2.14.

Three beam shapes were analysed in this study using the energy balance method outlined earlier, to investigate the effect of shape on the observed tensile strength. Fig. 2.15 shows the three shapes considered; the span was held constant. The results are summarized in Table 3.

Span: Depth Ratio	Max Load (Simple Beam Theory)	Max Load (Finite Element Analysis)	Max Load for CL=H/20	Max Load for CL=Constant
5:3	9	9.06	5.23	7.56
5:2	4	4.14	2.96	3.51
5:1	1	1	1	1

Table 3. Predicted maximum beam loads for different beam shapes and analysis procedures.

Simple beam theory with a maximum tensile stress criterion suggest a maximum load carrying capacity for the three beams in the ratio 9 : 4 : 1, the finite element stress analysis of uncracked beams agrees with these results. The maximum load for a crack length a fixed ratio of the beam height, in this case H/20 produces load ratios of 5.23 : 2.96 : 1 which suggest that the 5 : 3 beam is very weak relative to the 5 : 1 beam. For the case of a constant crack length the load ratio is 7.56 : 3.51 : 1 which again indicates that the strength decreases as the span to depth ratio decreases. This agrees with the trend of the experimental results obtained by HUDSON (1971), and also with the results predicted by the Weibull's analysis. However, this effect is not considered in the Weibull's analysis, as the strength distribution is independent of the specimen geometry. This may account for some of the discrepancy between the Weibull's theory and the observed results, as previously noted and illustrated in fig. 2.14.

A shape effect can also be theoretically observed in the ring test. Two ring tests were analysed, one with external diameter to external diameter ID/OD ratio of 1 to 10 and the other with ID/OD 1 to 4. These results are compared in fig. 2.16.

It is of interest to define an apparent tensile strength as the maximum tensile stress that exists in an uncreacked body calculated from the force or pressure required to cause crack growth. As the force to cause crack growth is a function of crack length for all tests the apparent tensile strength is then a function of crack length. The apparent tensile strength has been calculated for all the test grometries analysed for a crack length c=0.1

inches. These results are summarized in table 4. The crack length of 0.1
inches is not identical with the total crack length for all the test geometries
as plotted in figures 2.8 to 2.12. For the tests where symmetrical cracks
develop the ring tests and the hydraulic fracturing test, the crack length
is half of the total crack length so the forces shown in table 4 for these
tests are the forces at a total crack length of 0.2 inches. The stresses
for the ring tests were calculated from some results listed in JAEGER and
COOK (1969).

The large variation in apparent tensile strength indicated in table 4
is not uncommon in tests on rock. HAWKES and MELLOR (1972) suggest that the
Brazilian test should be used to measure the tensile strength of rock rather
than a ring test because the Brazilian test results closer to the strength
indicated by the direct tension test, without questioning if in fact the
tensile stress criterion of failure is appropriate.

	Beam Test	Direct Tension	Brazilian Test	Ring Test OD/ID=10	Ring Test OD/ID=4	Hydraulic Fracturing
Maximum load F max. at crack length of o.1 inches	1,220	5,500	19,400	4,220	2,000	2,800*
Tensile stress in uncracked body at F = F max.	2,280	2,750	3,090	4,220	2,720	2,960

* in this case this number refers to the pressure within the hole to cause crack
propagation.

Table 4.   Comparisons of Apparent Tensile Strength for
Different Tests

Influence of Rock Microstructure

The method of generating complete force-displacement curve for a test
by incrementally constructing the curve from considerations of the absorbed
energy is unrealistic unless modifications are made to account for inhomogeneity.
In fact, the analysis up to this point is only valid for an isotropic,
homogeneous continuum with a constant 'work of fracture'.

The nature of rock.

Rock is a complex material. It was formed hundreds of thousands of years ago and has subsequently been subjected to an unknown history of thermal and mechanical trauma. In general, rock can be described as a material system consisting of many constituent minerals aggregated in a complex non-continuum; voids exist in the form of pores between grains and cracks generated by thermal and mechanical processes; residual stresses may exist and pore fluid may be present. It is little consolation that synthetic materials can be equally complex - BRADSTREET (1958) describes ceramic production as "minerals of inconstant composition and doubtful purity exposed to immeasurable heat long enough to carry unknown reactions partly to completion, forming the hetero-geneous nonstochiometric materials known as ceramics".

To model precisely the structure of a specific rock specimen, containing discrete grains and grain boundaries, would require considerable computer storage, be extremely time consuming and always incomplete. In addition, the analysis becomes more complicated because determination of the fracture path (by considerations of a minimum potential energy condition) will involve two factors: the change in strain energy (as for the ideal material) and the work of fracture - both of which are function of the fracture path.

Although fracture paths often appear to be very irregular when viewed on a plane surace, the third dimension of a crack must not be ignored. If a very thin section of rock were to be tested, the individual grains on inhomo-genieties will greatly affect the experimental output, but in most engineering applications larger bodies of rock are stressed where the third dimension must be considered. In this case, the advancing crack tip will not be uniform in length throughout the body; some weak sections will allow the crack tip to advance further than in other areas, but when considered as a whole these variations will tend to balance out, so that the observed work of fracture may be much more uniform than that for a very thin section of rock.

However, three aspects of the microstructural inhomogeneity are con-sidered as they are of fundamental siganificance and important in the context of experimental data interpretation:

1. The 'work of fracture' can be a function of the crack length. This could be caused either by a random or progressive variation in the 'work of fracture' through the specimen or by a progressive change in the failure mechanism.
2. A Pre-existing crack could exist in the path of fracture. This is a special case of the first aspect (with the 'work of fracture' equal to zero over the pre-existing crack length) but with an additional influence on the modulus of the structure before the crack is reached.
3. Permanent deformations occur during the failure process. When the beam is unloaded the axial displacement does not return to zero.

Variation in the 'Work of Fracture'

The possible types of variation in the 'work of fracture' are shown in Fig. 2.17. A constant 'work of fracture' is represented by the dotted line AB. If the 'work of fracture' oscillated about a fixed value with no bias, the complete force-displacement curve would similarly oscillate about the smooth theoretical curve. The depth of the crack front will effectively smooth out these oscillations in the observed 'work of fracture'.

Alternatively, the 'work of fracture' might increase or decrease with crack length (AC or AD in Fig. 2.17) and then the complete force-displacement curve would progressively diverge from that for the ideal material. The modified curve could be constructed, however, from the ideal curve (using equation 8 if the relationship between 'work of fracture' and crack length were known.

The presence of a pre-existing crack.

The effect of a pre-existing crack on the modulus of a failing structure is shown in Fig. 2.18. A comparison of the modulus reduction curves for the two cases shown in Fig. 2.18 shows that the beam modulus is noticeably affected just before the fracture reaches the pre-existing crack. The complete force-displacement curve for this test is represented by the heavy line in Fig. 2.19a. The area LPM represents the surface energy that does not have to be supplied because of the pre-existing crack. In rock it is likely that a distribution of such cracks will cause many minor perturbations in the descending portion of the curve, but it is unlikely that a pre-existing crack would traverse the whole rock structure so this effect may be masked by the depth of the crack. This effect should be very noticeable in very thin specimens.

In a conventional testing machine these local perturbations will be masked by the elastic unloading stiffness of the testing machine. The heavy line in Fig. 2.19b shows the complete force-displacement curve that would be obtained for a beam containing an initial crack (such that the loading path is OR) and a pre-existing crack (causing the perturbation LPM). When the point R is reached, the initial crack propagates but the elastic unloading of the testing machine (along XX') dominates the force-displacement curve. At N, the failure locus is intercepted but excess energy given by area RPN has been supplied by the testing machine and the crack continues to propagate until point S is reached; the extra energy is absorbed as surface energy such that area RPN is equal to area NSTM. Failure is then reinitiated by loading along the local modulus line from S to T. In a closed-loop testing machine, the actual curve ORPMU may be observed if an appropriate control feedback displacement is chosen (see HUDSON et al 1972).

Permanent Deformations

The theoretical analysis has been based on the assumption that the material is elastic-brittle. This assumption is reasonable for only a small proportion of fine grained rock types; most rocks exhibit significant permanent deformations when stressed in tension or compression. This factor must be included in the analysis because the complete force-displacement curve for the beam failure process will be affected by the additional absorbed energy. This additional energy is different from that discussed early in the discussion of the energy within the term 'work of fracture'. In most of the rock tensile tests discussed the load is applied as a compressive force over a very small area, as in the Brazilian and Beam test. Within the test specimen there are high compressive and shear stresses throughout the structure. Permanent defor-

mation that occurs at the loading point when the load is returned to zero at some stage in the failure process.

Observations of the complete force-displacement curve will not enable the energy associated with the creation of new surfaces to be separated from the energy associated with permanent deformations unless the beam is unloaded. Assuming that the dimensions of the beam have not been significantly altered by permanent deformations, the elastic unloading process will indicate a local modulus at various stages in the structural breakdown of the specimen - the same modulus that would be exhibited by a purely elastic-brittle specimen.

This suggests a simple experimental procedure to separate the two types of absorbed energy and hence enable a valid comparison of the theoretical and experimental results to be made. The diagram in Fig. 2.20a indicates the geometric separation of the two energies during an increment of crack growth and Fig. 2.20b shows how the experimentally observed curve can be 'corrected' to the curve for an ideal material.

In Fig. 2.20a the heavy line shows loading of the structure to S, an increment of crack growth to T and unloading back to P with a permanent deformation of PO. To isolate the surface energy from "plastic" energy, the point Q is located such that QT is parallel and equal to PO. The path)SQO is the force-displacement characteristic for loading, a small increase in crack length and unloading with no permanent deformation. The area OSQ corresponds to the surface energy of the newly created crack surfaces. The remaining shaded area OQSTP corresponds to the energy absorbed during permanent deformation.

Fig. 2.20b shows how the observed curve (represented by the heavy line) can be incrementally corrected to a continuous curve for an ideal material. At any point on the force axis, the unloading moduli lines from each curve are parallel.

In rock structures the permanent deformation mechanisms may be complicated by secondary effects. For example, closure of cracks on unloading may be inhibited by grain dislodgement. The unloading moduli should, therefore, be compared at pimilar force levels and the permanent deformation found by extracpolation of the initial unloading modulus.

Discussion of Size Characterization of Rock

The hypothesis of this section has been that the tensile failure of rock can be characterized by two parameters, the work of fracture, and the effective crack length. Analytical predictions have been presented to suggest that this type of characterization can explain some of the discrepancies observed between a maximum tensile stress strength criterion and observed experimental results, while recognizing that some statistical theory should be superimposed on the energy method to account for the inherent variability of rock. Superficially this method and failure criterion is identical to Griffiths failure theory, but now an energy analysis is made of every structure for which failure can occur by crack propagation, and there is a different interpretation of the meaning of the effective crack length.

The effective crack length which characterizes each particular rock type is related to the development of a macroscopic crack through the rock sample, and is not related to classical Griffith flaws which are generally related to grain size and internal crystalline imperfection. The classical, or often discussed, Griffith flaw is now considered as a defect that can occur at the tip of the crack and is not a through-the-structure defect. The effect of individual flaws account for the micro-cracking at the tip of the crack and will contribute to the overall term 'work of fracture'. They may be considered to affect the zone at the tip of the crack with macroscopically has a non-linear stress-strain response because of the relaxation due to micro-cracking.

This characterization of a crack in rock is consistent with that proposed by HOAGLAND et al (1972) and is represented in Fig. 2.21 which is taken from HOAGLAND et al. The effective crack length is developed when the zone of micro-cracking at the crack tip is fully developed. Then this zone progresses with the macroscopic crack. On a typical force-displacement response for a complete test on a rock specimen it is proposed that the development of the microcracking to develop the initial effective crak length takes place before the peak load carrying capacity of the structure is reached.

The stress gradient in the region of crack development is important to the development of cracks. For zones of low stress gradient, that is where the tensile stress is uniformly distributed over a large volume of rock as in the direct tension test, considerable microcracking can occur throughout the whole zone of tension with the final macroscopic crack developing after a considerable deformation. It is not until the macroscopic crack starts to develop that the predicted curves shown in Fig. 2.8 to 2.12 are applicable. For test geometries where a high stress gradient exists the microcracking is limited to a very small zone before the macroscopic crack begins to develop, so a comparison of theoretical and experimental results should be more obvious. For structures with low stress gradient, the most probable position of the macroscopic crack is more variable than for situations of high stress gradient. Fig. 2.22 illustrates this point with reference to a short or long span beam.

The effective initial crack length can be uniquely determined by comparing experimental results for Brazilian tests and the ring test. Notice that in Fig. 2.11b the force to cause crack growth in the ring test is initially independent of the crack length. The value of this force can be used to determine the 'work of fracture'. Then by comparing the ratio of the applied force to a ring test to that of a Brazilian test, the effective crack length can be determined. This method is dependent upon the effective crack length being less than the 1.5 times the diameter of the hole in the ring test, but by suitable choice of ring test dimensions the effective crack length can be determined. Fig. 2.22 shows a comparison of the force required to cause fracture in the Brazilian and ring tests, and Fig. 2.22b shows the ratio of the force for the Brazilian to the force to cause failure in the ring test as a function of crack length. Other methods of determining the effective crack length from a single test require a curve fitting procedure, (which is often subjective); a procedure for estimating the effective crack length and the 'work of fracture' from one test was used in the beam paper by HARDY et al (1973) but this procedure is now not considered satisfactory.

EXPERIMENTAL OBSERVATIONS OF FRACTURE

Introduction

The experimental observations reported in this section were designed to check the validity of the theoretical predictions outlined in the previous section. Time and money has not permitted the complete verification of all implications derived from the theoretical observations so experimental work was limited to verify the basic form of the predictions. Much more work could be done to study possible influence on the general hypothesis and these will be outlined in a later stage of this section.

Experimental observations were limited to the beam test, Brazilian test and the ring test. The materials selected for the study were a typical hard rock, Cold Spring Red Granite and Charcoal Grey Granite, and plexiglass (PMMA) as this material is essentially "brittle" in tension and does not have the confusing properties associated with the micro structure of rock; an additional bonus is that it is transparent, thus allowing direct observation of the crack advance so that comparison of beam modulus as a function of crack length can be made.

Much of the experimental work performed on the beam test has been reported in a paper which has been submitted to the International Journal of Rock Mechanics and Mining Science entitled "The Failure of Rock Beams – Part II. EXPERIMENTAL STUDIES" by J.A. Hudson, M.P. Hardy and C. Fairhurst. Only a brief review of the beam test results will be given here.

General Experimental Procedures.

The form of the predicted force-displacement responses of the failing specimen suggests that control of these tests after the peak load carrying capacity is reached could be difficult. Conventional mechanical or hydraulic machines could not be used as excessive strain energy exists within the loaded body at the peak load to supply the energy required for crack propagation so this energy would be observed as kinetic, uncontrolled energy. Thus, using conventional equipment to investigate the dependence of load upon crack length would require many tests on specimen with artificially induced cracks. BERRY (1961) has used this approach in studying crack growth in plexiglass.

Servo-controlled testing systems have recently become popular in rock testing (see a review by HUDSON et al 1972) and with appropriate choice of the feedback parameter control of almost any test can be achieved. For the beam test and the Brazilian test the feedback parameter is chosen as a displacement transverse to the crack path. With rock there is a certain uncertainty of the location of the final crack path so the displacement transducers have to be placed to encompass any possible crack path. For the plexiglas the crack initiation point is known as an initial crack has to be artificially induced. In this case the displacement transducers can be placed as close to the crack faces as practical. This is illustrated in Fig. 2.24 with reference to the beam test. This transverse horizontal displacement is programed to monotonically increase with time. The closed loop

system insures that this condition is met by varying the applied force. The vertical displacement is independently monitored. The force-versus vertical displacement and the force-versus horizontal displacement is continuously recorded on an X-Y-Z recorder.

Beam Tests

Fig. 2.25 shows the experimental arrangement used for testing the beam samples. The load was measured by a load-cell located just above the steel cylinder in Fig. 2.25; the displacement at the loading point or the 'vertical' displacement, δv, was measured by another cantilever transducer that was connected to a steel cylinder just above the loading point and activated by rods connected to the base of the beam bending apparatus.

The plexiglas beams were 11 in. long (loaded over a 10 in. span), 3 in. deep and 1 in. wide with all faces accurately machined and polished. The beams were notched to a depth of 0.5 in. with a diamond saw blade and a fine crack 0.1 in. deep was additionally introduced by striking the base of the notch a sharp blow with a utility knife blade.

Unnotched plexiglas beams could not be controlled with the present system. Further refinements such as a faster servo-valve (with a response time of 1/2 milliseconds), an improved feedback transducer and computerized feedback conditioning (allowing any function of any number of experimental variables to be the independent variable) would enable the failure of unnotched plexiglas beams to be controlled. These refinements were not considered necessary, however, because the notching technique for plexiglas was successful and the failure of unnotched rock beams was controlled.

The rock beams (Cold Spring Red Granite, Minnesota) were 11 in. long (loaded over a 10 in. span), 3 in. or 2 in. deep and 1 in. wide. All the faces were surface ground and the front face was highly polished so that photographs of the propagating crack could be taken.

Controlled Failure of Plexiglas Beams

The initial series of experiments was carried out on plexiglas in order to obtain complete force-displacement curves that were not affected by microstructural inhomogeneity. In addition, the exact crack length at any stage can be determined from photographs or from direct measurements, because of the material transparency.

Experimental Results

The results presented in Fig. 2.26 show the force - 'vertical' displacement curve and the corresponding force - 'horizontal' displacement curve for a selected test.

The 'horizontal' displacement was programmed to linearly increase with time at a rate of $.464 \times 10^{-3}$ in./min. and was constrained to monotonically increase at this rate. The force and 'vertical' displacement were dependent variables and it should be noted that the curve in Fig. 2.26b does not monotonically increase in displacement.

Various stages of crack development were photographically recorded throughout the controlled collapse process, as in Fig. 2.27. The '8' in the photographs is a specimen identification number o.125 in. high. The force and displacements at which these photographs were taken and the area of the beam shown in the photographs are indicated in Fig. 2.26.

The crack propagated in a straight line free from the microstructural irregularities that influence the crack path in rock specimen. The curved shape of the crack tip is in agreement with the observed shape of crack tips in all materials. This is caused by the three dimensional nature of the crack tip stresses which changes from plane stress near the beam surface to a condition more closely related to plane strain in the interior of the beam.

Discussion

In order to compare the experimental results shown in Fig. 2.26 with the complete force-displacement curves predicted by the theoretical technique described earlier, the theoretical curves were derived for this specific testing situation, using the Young's modulus for plexiglas as 4.4×10^5 psi and Poisson's ratio 0.24. These are shown in Fig. 2.29.

Since the 'work of fracture' value for plexiglas is a function of the crack propagation rate, the exact value was unknown and a value was chosen such that the peak loads of the theoretical and experiment curves coincided. This value was 2.68 in.lbs./in.^{2} Independent comparisons of the theoretical and experimental results are the general shape of the curves, the specific displacement values and the force versus crack length.

The shape of the theoretical and experimental force displacement curves and the specific displacement values are in excellent agreement. The experimental 'vertical' displacement values are 0.005 in. more than the theoretical values at corresponding load points on each curve, which is caused by mechanical shakedown and indentation during the initial loading process – when the final portion of pre-peak curve is extrapolated back to the displacement axis, the intercept is at .005 in. The experimental 'horizontal' displacement is not affected by the shakedown and directly agrees with the theoretical curve.

From the photographs in Fig. 2.27, the crack lengths were measured and the theoretical moduli corresponding to these crack lengths are shown in Fig. 2.29a. The crack length measurements were not precise because the crack tip was curved and the curvature changed as the crack propagated. The lengths indicated in Fig. 2.28 represent the average of the lengths at the beam face and in the center of the beam.

The comparison of theoretical and experimental results for all four beams is shown in Fig. 2.29b. The heavy lines are the theoretical prediction for the plexiglas testing geometry and material properties. The location of the curves is a function of the surface energy; these lines correspond to a surface energy value of 2.68 in. lbs./in.^{2} (the value for which the theoretical and experimental peak loads coincided for beam no. 8).

In the earlier theoretical studies it was noted that the energy associated with creating new surfaces could be distinguished from the energy associated with permanent deformations by unloading the beam at various stages. The

force-'vertical' displacement curve in Fig. 2.30 indicate the effect of the 'permanent' displacements upon the observed experimental results. Subsequent experimental work has shown that most of this work is associated with slippage of the beam supports, due to the large deflection of the plexiglas beams. Rollers were used as supports to eliminate this problem in some later tests, and then the observed permanent deformations were, effectively, unnoticeable.

Controlled Failure of Rock Beams.

The main series of experiments was carried out on rock. In this case, the crack length could not be used as an independent experimental observation. The extending crack was visible on the front face of the beam but the geometrical complexity of the microstructural separation precluded precise crack length measurements. Experiments were performed on artificially notched as well as unnotched beams.

Experimental results - Unnotched Beams

Six Cold Spring Red Granite beams were tested in this series, three of dimension 11" x 3" x 1" and three 11" x 2" x 1". Two complete force-displacement curves for the 11 x 3 x 1 beams are shown in fig. 2.31. In these tests, the 'horizontal' displacement was programmed to increase at a rate of .116 in. x 10-3/min. It should be noted that the points P_1 and P_2 were located halfway along each half span. These locations were chosen because the rock beams were unnotched and the crack could develop at a significant distance from the center line.

The curves in Fig. 2.32 illustrate the reduction in beam unloading modulus that occurs throughout the failure process, for a 11" x 2" x 1" beam. The dotted line in Fig. 2.32 is the force - 'vertical' displacement curve after the correction for permanent deformations has been made.

Experimental Results - Notched Beams

Three beams of dimension 11" x 3" x 1" with a diamond cut notch of depth 1/2" below the loading point were tested. Complete force-displacement curves for two of these tests are shown in Fig. 2.33. Unloading moduli were recorded in beam 4 only, but this clearly shows the change in beam modulus as fracture progresses.

Discussion

The curves in Fig. 2.34 are the theoretical curves for the 11 in. span, 2 in. deep beam corresponding to the experimental results shown in Fig. 2.32. Note that the corrected experimental force - 'vertical' displacement curve should be compared with the theoretical results - i.e., the dotted lines in Fig. 2.32. The theoretical curves were calculated such that the peak force in the theoretical and experimental results were identical. This occurred for a work of fracture value of 0.114 in lbs/in2.

In the case of rock beams, it is preferable to compare the force and the estimated crack length for theory and experiment because permanent deformations affect the displacement values. The curve in Fig. 2.35a shows the theoretical relationship between beam modulus and crack length at any stage in the failure process. From this information, the theoretical relationship between load and crack length can be established as shown in Fig. 2.35b. The load versus estimated crack length for the experimental results are shown in Fig. 2.35b. In this figure the theoretical or predicted force load versus crack length is plotted for comparison. [The effective experimental crack length was estimated from the change in unloading moduli shown in Fig. 2.32.] In this case, the agreement between theoretical and experimental results is good. This is because the permanent deformation does not influence the local beam unloading moduli values.

The results from the notched beams give results which are fairly predictable. As the notch represents initiation from a longer effective crack length the peak load is reduced and the "controllability" of the test is increased as the vertical displacement is nearly monotonically increasing with increased fracture. This effect can easily be seen by comparison with the plexiglas theoretical predictions in Fig. 2.26 for this shape beam.

The experimental results of the granite beam tests are summarized in Table 5. Note that the apparent tensile strength of this rock is not consistent but varies with beam shape.

Test	Max. Load F_m Average 3 tests	Max. Variation from F_m	Apparent Tensile Strength
10" x 3" x 1"	902	17.3%	1,500
10 x 2 x 1	663	15.5%	2,480
10" x 3" x 1" with 1/2" notch	628	26%	.

Table 5. Summary of Beam Experiments on Granite

The experimental and theoretical results for plexiglas beam failure were in excellent agreement. For rock, the agreement was not so good. This is because the theoretical model applies to an ideal material but rock does not. The theoretical model must be modified, therefore, to account for the following factors:

1. The difference between the compressive and tensile moduli and non-linearity of the tensile stress-strain curve. This results from micro-cracks opening in tensile regions throughout the body.

2. Permanent deformations. This effect can be partially eliminated by the consideration of forces only and separating the displacements into two components. Both these effects are considered to be more dominant in less competent rock.

Brazilian and Ring Tests

Introduction.

The controlled failure of rock discs has been achieved previously by HUDSON et al (1971) but in those tests the vertical displacement was not recorded. The tests reported in this section relates to the controlled failure of Charcoal Grey Granite and plexiglas discs of outside diameter 4" and internal diameters of zero, as in the case of the Brazilian test, 0.4 inches and one inch. No Brazilian tests were conducted on plexiglas.

Fig. 2.36 summarizes the test geometries and the feedback control displacements. For the granite discs strain gauges had to be used, bonded partially over the disc surface. The central one and half inches of the strain gauge was not bonded to the disc. If this section were bonded then a small crack could cause failure of the strain gauge, and hence premature termination of the test. For the plexiglas discs cantilevers were used to measure the horizontal displacement. This is possible as the displacements are at least one order of magnitude higher in the plexiglas than for rock.

The load was measured by a small 3/4" steel strain gauged load cell. The load was transmitted to the rock through a shaped steel load spreader, with contact over 10° of arc.

The vertical displacement was measured by cantilevers as described in the section of beams. This deflection reflects some 'seating down' of the steel rock contact as load is applied, but does not appear to be significant.

Ring Tests on Plexiglas

Experimental Results

Four ring tests of plexiglas were conducted; two tests with holes of 1" diameter the other two tests with holes of 0.4". All plexiglas tests were pre-cracked with an initial crack length of approximately 0.1 in. by striking a cutting blade and initiating a wedged crack. Some preliminary experiments indicated that a sucessful experiment with slow controlled crack growth was very sensitive to the selection of the feedback parameter. Thus the deformation between points A and B in figures 2-36b was used as the feedback signal, with these points located as close to the crack surface as possible. Before this was done the distance AB was larger and often

unsymmetric cracks would develop with up to a half an inch of uncontrolled crack growth.

Figure 2.37a and b show two curves, one from each shape experiment. These tests were controlled at all times with crack surfaces and crack tip shape very similar to that described for the beam test.

The crack length was continually recorded during these tests by comparison with a scale attached vertically parallel to the expected crack path. Fig. 2.38 shows the load carrying capacity of a disc with a small hole plotted as a function of the crack length for the two experimental tests run for this geometry. The predicted result, modified as described below is also shown for comparison.

Discussion

These tests again agree very well with the predicted force-displacement curves for the ring tests shown in Fig. 2.11. Extrapolation of the unloading moduli indicate that very little "permanent" deformation is associated with these tests. The observed vertical displacement curve is so steep that it is difficult to distinguish individual loading paths.

Figure 2.38 indicates the agreement between the predicted curve, shown as the full line, and the two experimental outputs. Any complete comparison of predicted and experimental is marred by two experimental limitations; the accuracy of the crack length determination and the variability of the initial crack. The crack length was recorded by comparison with a scale attached vertically and parallel to the expected crack path, but the shape of the crack front could sometimes be curved and the two crack paths may not have been equal thereby limiting the accuracy of the crack determination. The natural crack shape is initially very dependant upon the induced initial crack shape. This was introduced by striking a wedge shaped razor into the plexiglas. Control of this crack shape is often difficult and the resulting crack may not be even across the depth of the plexiglas ring.

Equation 8 can be used to modify the predicted values of the ring test for a structure of modulus 10×10^6 psi and work of fracture of 0.114 as used for rock to that of plexiglas, with modulus of $.440 \times 10^6$ psi and work of fracture 2.68 lb-in/in^2 by*

$$\frac{F_1}{F_2} = \sqrt{\frac{\gamma_1}{\gamma_1} \frac{E_2}{E_1}}$$

(20)

---

*Note from equation 8

$$F = \left(2\gamma \; \Lambda A / \left(\frac{1}{M'} - \frac{1}{M} \right) \right)^{1/2}$$

now for identical structures, 1 and 2, with different Young's moduli, E_1 and E_2 respectively.

$$\frac{M_1}{M_2} = \frac{E_1}{E_2}$$

then

$$\frac{F_1}{F_2} = \sqrt{\frac{\gamma_1}{\gamma_2} \times \frac{E_2}{E_1}}$$

where $E_1 = 10.0 \times 10^6$ psi

$E_2 = .440 \times 10^6$ psi

$\gamma_1 = 2.68$ lb in/in^2

$\gamma = .114$

and find that equivalent force to cause fracture for the ring with a 0.1 inch initial crack length as:

$$F_1 = 4,300 \times \sqrt{\frac{2.68}{.114} \cdot \frac{.440}{10}}$$

= 4,380 lbs. This value agrees surprisingly well with the experimentally observed result. The 'work of fracture', 2.68 lb. in/in^2 used in this calcualtion is that found from the beam experiment yet produces excellent agreement with observed results for the ring test. Notice that for the ring test with an applied load of 4,300 lbs. the maximum tensile stress within the uncracked body would be 4,300 psi, whereas for the beam test, with a maximum laod of 600 lbs., the maximum tensile stress in the uncracked beam would be only 1,000 psi. This comparison is not particularly meaningful because of the large (0.6 in) initial crack in the beam test but by extrapolation of Fig. 10b of crack length over beam height of 0.6/3.0 to 0.1/3.0 then the maximum load carrying capacity of a 10" x 3" beam of plexiglas would be 1,300 lbs., thus an apparent tensile strength of 2,170 psi. This indicates again the inconsistency of a simple stress criterion and the possible usefulness of the proposed energy method.

Brazilian and Ring Tests on Charcoal Grey Granite

Experimental Results

Three samples of each shape were tested in this series of experiments. Fig. 2.39 summarizes the observed outputs for each shape test. Both the vertical and horizontal displacements are shown. Notice that in the Brazilian test the peak load is approximately 14,000 lbs., which results in a contact stress between the steel end platen and the rock of 28,000 psi which is high but less than the uniaxial compressive stress for this rock which is between 34,000 and 38,000 psi (see WAWERSIK 1968).

The horizontal displacement which was used as the feedback signal was generated by two strain gauges on opposite sides of the rock disc but was uncalibrated so no attempt has been made to scale these measurements. They are shown only for comparison with the predicted output shown in Fig. 2.10 and 2.11.

Table 6 shows a summary of the results of these 9 tests, listing the maximum load, as a mean of the three tests in each group, the maximum variation from this mean in each group and the maximum tensile stress in the uncracked body at the maximum load. Notice the incredible variation in this "apparent tensile strength".

Figure 2.40 shows three photographs of each test, showing the crack that caused the reduction in load carrying capacity. The discs are still intact although the crack extends very near to the outer boundaries in each case.

After the load carrying capacity was reduced to a minimum by the vertical crack, some tests were continued. As the horizontal displacement was continually increased the load applied to the specimen again began to increase. At this stage no structural changes were occurring within the rock discs. Simply the two "Dee" shaped specimens resulting from the splitting of the discs were being loaded. The load was allowed to increase until above that of the original peak and then unloaded. Had the test continued, total collapse may have resulted by shear failure near the loading points.

In uncontrolled testing of these structures the peak load carrying capacity may result from secondary failure, which occurs at a higher load than the vertical, primary cracking so stress calculations based upon the maximum load could be quite misleading.

Test	Mean Max Load, 3 Tests	Max Variation From Mean %	Apparent Tensile Strength
Brazilian	13,170	7.5%	2,100
Ring Test Small Hole	7,900	7.6%	7,950
Ring Test Large Hole	3,020	7.0%	4,100

Table 6. Experimental Summary of Results from Brazilian and Ring Tests on Charcoal Grey Granite

Discussion

The form of the force-displacement curves agree quite well with the predicted curves shown in Fig. 2.10 and 2.11. The loads at failure are different than those in these figures. This suggests that there is some difference between the charcoal Grey Granite used in these tests and the Cold Spring Red Granite used in the beam tests. This is indeed unfortunate that the same rock type was not used in both tests so that a direct comparison could be made between these tests as in the case of the plexiglas.

If the effective crack length for this Charcoal Grey Granite is less than 0.6 inches, than the maximum load carrying capacity of the ring with the small hole (0.4" diameter) is relatively independent of the effective crack length so this test can be used to determine the 'work of fracture' for Charcoal Grey Granite. For both these granites the Young's modulus is essentially the same (10×10^6 psi) so equation 20 becomes

$$\frac{F_1}{F_2} = \sqrt{\frac{\gamma_1}{\gamma_2}}$$

(20a)

$F_1 = 4,300$ lbs.

$F_2 = 7,900$ lbs.

$\gamma_1 = .114$ lb in/in^2

Thus γ, the work of fracture for Charcoal Grey Granite is approximately .384 lb in/in^2. From Fig. 2.22b the ratio of the strengths F_b and F_r, the maximum load for the Brazilian test and the ring test respectively can be used to determine the effective crack length. The ratio F_b/F_r is 1.67 which is applicable if the total crack length were 0.50 inches, this implying an

effective crack length of 0.25 at either side of the internal hole. This is considerably larger than the effective crack length found for the Cold Spring Red Granite of 0.1 inch, but unfortunately this length was found from a much less satisfactory method, the curve fitting procedure outlined in the beam testing discussion.

The experimental results from the ring test can be used as an independent check of the two material properties, work of fracture and effective crack length derived from the Brazilian test and the ring test with the small hole. From figure 2.16 the ratio of F_{max} for the ring test with the large hole to the F_{max} for the ring test with a small hole at crack length 0.25 can be determined. This ratio is 0.430. Thus, the predicted load carrying capacity of the ring test with the large hole is 0.430 and the experimentally observed maximum load for the ring test with the small hole. This gives 0.430 x 7,900 which is 3.400 lbs. This agrees favorably with the experimentally observed result of 3.020 lbs.

The unloading modulus for these tests is in general very insensitive to changes in crack length. This can be seen from the form of the force-vertical displacement curves. It is very difficult to distinguish the loading and the unloading paths due to the thickness of the ink from the pen recorder. The horizontal displacement is much more sensitive to crack length changes, but the horizontal displacements are uncalibrated. The theoretical method utilizes the change in strain energy or the change in modulus, so for comparison the normalized modulus is shown as a function of horizontal displacement. This can be used to determine the crack length with the body at that particular horizontal displacement by comparison with the theoretical, or F.E. predictions. This has been done and Fig. 2.41 shows the output of one particular Brazilian Test.

Extrapolation of these moduli indicate again that permanent deformations are not significant with this rock under these loading conditions as was found with the plexiglas ring test.

General Discussion of Experimental Results

The experimental results have established the fundamental validity of the theory; complete force-displacement curves should be analysed on the basis of the amount of energy absorbed during an incremental increase in crack length as failure occurs. In the past, the tensile strength has been the (assumed) material property used to characterize the failure of rock in tensile stress fields. When failure is analyzed by energy absorption considerations, however, the material property is the unit 'work of fracture'; the tensile strength, or maximum tensile stress at failure is a function of the type of test and specimen geometry and is not a material property.

Experimental observations have been presented on two commonly used tensile testing methods commonly used on rock to support the hypothesis that hard rock fails by a crack traversing the body. The need for such observation may seem trivial but some had expressed the view that rock fails by a gradual process of micro crack extension throughout the tensile stress zone and that the final crack surface is developed only after considerable load bearing capacity of the structure has been lost. This is supported by the masking of

any unique crack within the structure by the microstructure until such time that very large deformations have occurred and the final crack surfaces have displaced sufficiently for them to be detectable by the naked eye. The fact that microcracking does continue within the rock body is not denied, but the hypothesis is presented that the load carrying capacity of the rock is reduced only after the 'effective crack length' is developed and continues to propagate. The effect of the stress gradient upon this process has been discussed earlier.

The theoretical method has been verified by comparison with experimental results of tests on plexiglas when the crack length can be visually recorded and from the general form of the experimental results on rock and the observed change in modulus (force divided by vertical displacement, or force divided by horizontal displacement whichever applies). As the structure loses its load carrying capacity a crack length can be reduced for all stages of the fracturing process.

The experimental verification of the postulated theory can only be considered preliminary. Extensive testing would be necessary to investigate the effective crack length and the work of fracture for other types of rocks. The possible variation of the 'work of fracture' with different geometries should be investigated. This variation could result from different stress fields at the crack tip. Any variation of this type would be expected to be minor. Testing with many different geometries and with different size specimen could be used to further prove or disprove the theory. The effect of specimen thickness could be studied. For very thin specimen the variation of 'work of fracture' with length should be much more pronounced than for thicker samples where the variations of 'work of fracture' would effectively be averaged out through the thickness of the crack front. Other experimental testing could be carried out to investigate the effect of propagation rate of the 'work of fracture'.

SUMMARY AND CONCLUSIONS

1. A brief review of the mechanisms of tensile failure of materials have been given with particular reference to rock type brittle materials.

2. The hypothesis presented by Griffith that energy is absorbed as cracks extend is adopted as the criterion of fracture with the 'work of fracture' being a material property. The work of fracture includes the energy of all dissipative mechanisms in the region of the crack tip.

3. The "effective crack length" is defined and hypothesized to be a material property. Both the work of fracture and the effective crack length of a rock are required before the load carrying capacity of a particular shape can be determined.

4. The Finite Element stress analysis technique is used to develop complete force versus displacement responses of structures failing due to the extension of a through-the-structure crack.

5. Discussion of the usefulness of this method in predicting crack paths and the development of multiple crack trajectories is presented in light of the energy balance technique.

6. The above mentioned method is used to analyze five commonly used tensile test geometries. These are the beam test, the direct tension test, Brazilian test, the ring test and the hydraulic fracturing test.

7. Discussion is presented upon the variations in the "apparent tensile strength" from specimen size, shape and different tests. These variations are not completely predicted from statistical theories, but become apparent when the energy balance technique is used. The effect of the rock's micro structure upon the predicted force-displacement curves is discussed with particular reference to variations of the work of fracture with crack path, the effect of intersecting a pre-existing crack, and the effects of permanent deformations on the experimentally observed force-displacement curves.

9. A method is proposed for measuring the "effective crack length" and the 'work of fracture' uniquely from comparison of the experimental outputs from the Brazilian and the ring tests.

10. Experimentally observed controlled crack growth in plexiglas beams and rings are described. A closed loop servo-controlled testing machine used with an appropriate across-crack displacement feed-back parameter was used to develop the complete force-displacement curve for each test.

11. The form of the experimentally derived force-displacement curves agreed excellently with the predicted curves.

12. The material property 'work of fracture' experimentally derived from the beam test on plexiglas could be used to predict the lead carrying capacity of the plexiglas ring.

13. Crack growth was controlled in rock beams and discs using the servo-controlled testing system. The appropriate feedback parameter is discussed.

14. Variation of the modulus of the beams and discs were observed as fracture progressed. These variations can be used to estimate the crack length in a failing structure at any point of the test.

15. The Brazilian and ring test indicated a wide range of apparent tensile strength, which was satisfactorily explained using the 'work of fracture' and 'effective crack length' as the relevant material properties.

16. The maximum load carrying capacity of a Brazilian or ring type test may not be that required to cause a splitting crack. Subsequent loading of the structure can exceed that to cause vertical splitting, and could be misinterpreted as being the load related to tensile failure.

17. The finite element technique associated with the correct interpretation of crack growth within a structure can be used to interpret the maximum load carrying capacity of any given structure that will fail by tensile fracture. This apparent tensile stress at which failure occurs is not a natural property but simply a result of the particular geometry being considered and the material properties, 'work of fracture', effective crack length and the elastic constants. The apparent tensile strength could be expected to be different for every geometry.

43

ANDERSON, G.P., RUGGLES, W.L. and STIBOR, G.S., 1971. Use of finite element computer programs in fracture mechanics. Int'l. Journal of Fracture Mech. 7, 1, p 63-76.

BARENBLATT, G.I., 1959. The formation of equilibrium cracks during brittle fracture, general ideas and hypothesis, axially-symatic cracks P.M.M 23, 3 p 434-444.

BARENBLATT, G.I., 1962. "The mathematical theory of equilibrium cracks in brittle fracture". Advance in Appl. Mech., Academic Press, New York, Vol. 7, p 55-129.

BERRY, J.P., 1960. Some kinetic considerations of the Griffith criterion for fracture - I equation of motion at constant force. Journal Mech. Phys. Solids, 8, p 194-206.

BERRY, J.P., 1961. Journal of Polymer Science 50, 107.

BRADSTREET, S.W., 1958. Ceramics - the oldest art and newest science. Bull. Amer. Cer. Soc. 37, 510-512.

BROWN, E.T., 1971. Strength-size effects in rock material. Proc. Symp. Int. Soc. Rock Mech. Paper II-11, Nancy.

BROWN, W.F. and SRAWLEY, J.E., Fracture toughness testing. In Fracture Testing Special Technical Publication ASTM No. 381, p 133-196.

BUEKNER, H.F., 1958. The propagation of cracks and energy of elastic deformation, Trans. ASME, 80 p 1225-1229.

BYSKOV, E., 1970. The calculation of stress intensity factors using the finite element method with cracked elements. Int'l. J. Frac. Mech., Vol. 6.2, p 159-167.

CHAN, S., TUBA, I.S., and WILSON, W.K., 1970. On the finite element method in linear fracture mechanics. Eng. Frac. Mech. 2, 1, 1-18.

COTTRELL, A.H., 1963. Fracture. Roy. Soc. (London) Vol. 276A p1-18.

DUGALE, D.S., 1960. Yielding of steel sheets containing slits, J. Mech. Phy. Sol. Vol. 8, p. 100.

FREUDENTHAL, A.M., 1968. Statistical approach to brittle fracture in Treatise on Fracture, ed. H. Leibowitz. Academic Press, New York.

FRIEDMAN, M., HANDIN, J. and ALANI, G., 1972. Fracture-surface energy of rocks. Int'l. J. Rock Mech. Min. Sc. 9, 6 p 757-766.

GRIFFITH, A.A., 1921. "Phenomenon of rupture and flow of solids" Trans. Roy. Soc. (London) A221, p 163-198.

GRIFFITH, A.A., 1924. Theory of rupture. Proc. 1st. Int'l. Congr. Appl. Mech., Delf, p 55-63.

HARDY, M.P., 1971. Derivation of the "Griffith Locus" for indirect tensile strength tests. Mineral Resources Research Center Program Report No. 24, University of Minnesota, p 123-129.

HARDY, M.P. and FAIRHURST, C., 1973. Chip formation by drag cutters. Presented at the 6th conf. on drilling and rock mechanics. University of Texas, Austin Jan. 22-23.

HARDY, M.P., HUDSON, J.A., FAIRHURST, C., 1973. The failure of rock beams - Part 1 Theoretical Studies, International Journal of Rock Mech. and Min. Sc. Vol. 101, p 53-68.

HAYES, D.J., 1972. A practical application of Buekner's formulation for determining stress intensity factors for cracked bodies. Int'l. Journ. Frac. Mech. 8 (2) p 157-165.

HEINS, R.W., 1972. Aspects of mechanical behavior of rock under static and cyclic loading, Part A: Mechanical behavior of rock under static loading. Semi Annual Tech. Prog. Report. Submitted to USBM Twin Cities Branch, ARPA contract No H0220041

HOAGLAND, R.G., HANN, G.T., ROSENFIELD, A.R., SIMON, R., and NICHOLSON, L.D., 1972. "Influence of microstructure on fracture propagation in rocks". Final report submitted to USBM Twin Cities of ARPA Research Contract No. H0210006, 56 p.

HUCK, P.J., 1972. Effect of specimen size on confined compression testing of rock cores. Final Technical Report ARPA Contract No. H021009 minotired by Twin Cities Bureau of Mines, 80 ps.

HUDSON, J.A., 1971. "A Critical Examination of Indirect Tensile Strength Tests for Brittle Rock", Ph.D. Thesis, unpublished, Univ. of Minnesota, 161 p.

HUDSON, J.A., BROWN, E.T. and RUMMEL, F., 1971. The controlled failure of rock discs and rings loaded in diametral compression. Int'l. Rock Mech. and Min. Sc. 9 (2) p 241-248.

HUDSON, J.A., CROUCH, S.C., FAIRHURST, C., 1972. Soft, stiff and servo-controlled testing machines. A Review with Reference to Rock Failure. Engineering Geology. 6 (3).

HUDSON, J.A., HARDY, M.P., and FAIRHURST, C., 1973. The failure of rock beams, Part II, experimental results. Int'l. J. Rock Mech. and Min. Sc. Vol. 10.1.

IRWIN, G.R., 1948. "Fracture Dynamics". Fracture of Metals, A.S.M., Cleveland, p 147-166.

IRWIN, G.R., 1957. "Analysis of stresses and strains near the end of a crack traversing a plane". Journal Appl. Mech. 24, p 361-364.

IRWIN, G.R., 1960. Plastic zone near a crack and fracture toughness. Proc. Seventh Segamore Ordnance Mats. Res. Conf., August, Syracuse University Press.

IRWIN, G.R., and KIES, J.A., 1952. Fracturing and Fracture Dynamics. Welding, Journal Res. Suppl. 99s-100s.

JAEGER, J.C. and COOK, N.G.W., 1969. The Fundamentals of Rock Mechanics, Methuen & Co. Ltd.

MELLOR, M. and HAWKES, I., 1971. Measurements of tensile strength by diametral compression of discs and annuli. Engineering Geology, 5 (3) p 173-226.

OROWAN, E., 1952. Fundamentals of brittle behavior in metals. Fatigue and Fracture of Metals (MIT Symposium, June, 1950) John Wiley & Sons, Inc., New York, New York p 154.

PARIS, P.C. and SIH, G.C.M., 1965. Stress analysis of cracks in fracture toughness testing. ASTM Special Tech. Pub. 381, p 30-76.

PERKINS, T.M. and KRECKH, W.W., 1966. Effect of cleavage rate and stress level on apparent surface energies for rock, Socl Pet. Eng. J., p 308-314.

PORTER, D.D., 1971. A role of the borehole pressure in blasting: the formation of cracks. Ph.D. Thesis submitted to University of Minnesota.

PRATT, H.R., BLACK, A.D., BROWN, S.W. and BRACE, W.F., 1972. The effect of specimen size on the mechanical properties of enjointed diorite. Int'l. J. Rock Mech. and Min. Sc. 9 (4).

RALEIGH, C.B., 1965. Glide mechanisms in experimentally deformed minerals. Science 150, 739-741.

ROA, A.K., RAJU, I.S. and KRISHNA MURTY, A.V., 1971. A powerful hybrid method in finite element analysis. Int'l. J. Numerical Methods in Eng. 3, p 389-403.

SNEDDON, I.N. and LOWENGRUB, M., 1969. Crack Problems in the Classical Theory of Elasticity. John Wiley and sons, Inc.

WAWERSIK, W., 1968. Detailed analysis of rock failure in laboratory compression tests. Ph.D. Thesis submitted to the Univ. of Minn.

WEBER, P., 1971. The finite element method, applied to fracture mechanics. Rock Fracture, a Symposium of the Int'l. Soc. Rock Mech. Nancy paper II-7.

WESTERGAARD, H.M., 1939. Bearing pressure in cracks. J. Appl. Mech., Vol 61 A-49, A-53.

WEIBULL, W.U. A statistical theory of strength of materials. Ing. Vetenskaps. Akad. Handl. 151, 5-44.

Displaced Position After Shearing

Atomic Centers in
Crystalline Structure —

Applied Shear Force —

(a) Shear

—Applied Tensile Stress

Center Line of Atomic
Centers After Cracking
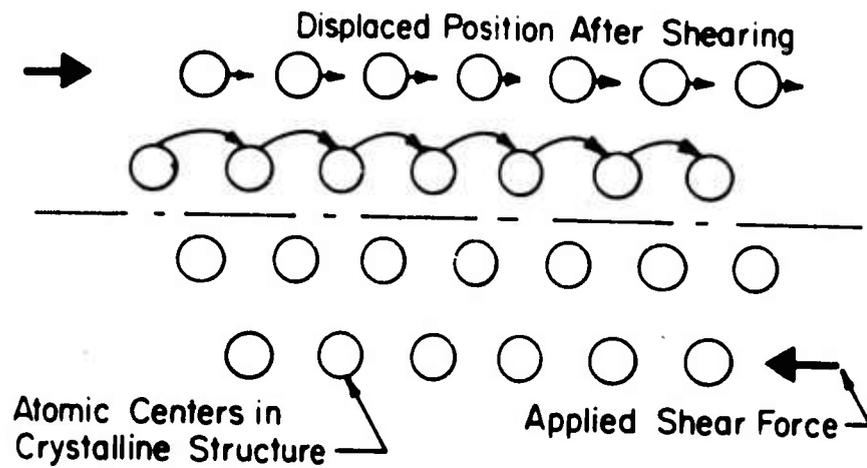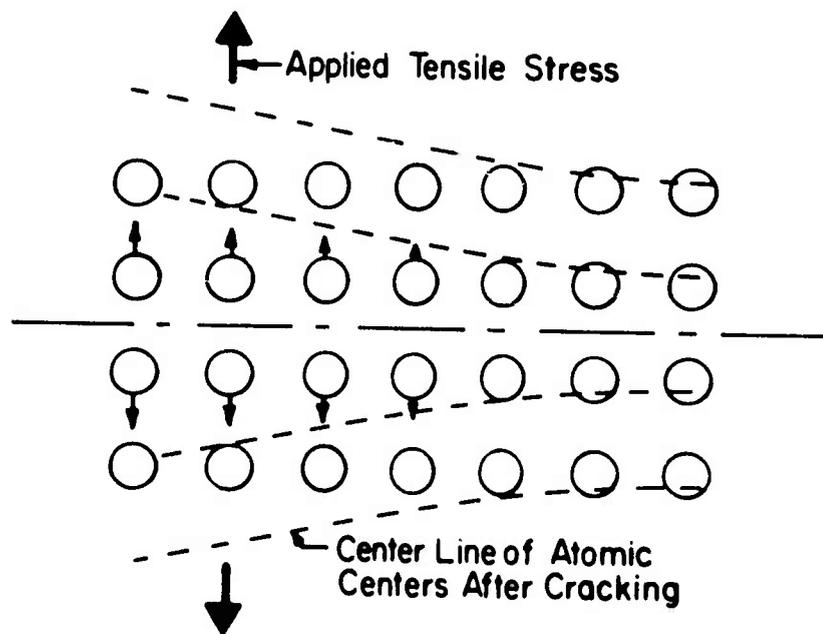
(b) Crack Growth

Figure 2.1: Two fundamental modes of failure of an ideal material.
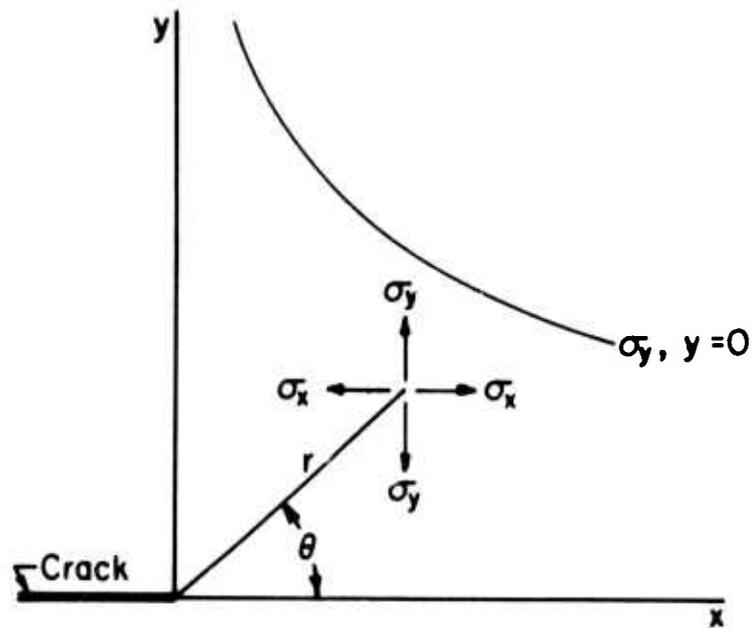
$$\sigma_x = K \frac{\cos\theta/2}{\sqrt{2\pi r}} \left(1 - \sin\frac{\theta}{2} \sin\frac{3\theta}{2}\right)$$

$$\sigma_y = K \frac{\cos\theta/2}{\sqrt{2\pi r}} \left(1 + \sin\frac{\theta}{2} \sin\frac{3\theta}{2}\right)$$

$$\sigma_{xy} = K \frac{\cos\theta/2}{\sqrt{2\pi r}} \sin\frac{\theta}{2} \cos\frac{3\theta}{2}$$

Figure 2.2: Schematic illustration of the elastic stress distribution near the tip of a crack, K is the stress intensity factor.

Figure 2.3: Typical crack growth experiment.

Soft System

Stiff System

Energy Change $= \dfrac{F}{2}\left\{F\left[\dfrac{1}{M}+\delta\left\{\dfrac{1}{M}\right\}\right]-\dfrac{F}{M}\right\}$

$\dfrac{F^2}{2}\delta\left\{\dfrac{1}{M}\right\}$

Energy Change $=$

$\dfrac{F}{2M}\left\{F-\dfrac{F}{M}\left[\dfrac{1}{\dfrac{1}{M}+\delta\left[\dfrac{1}{M}\right]}\right]\right\}$

$=\dfrac{F^2}{2M}\left\{1-\dfrac{1}{1+M\delta\left[\dfrac{1}{M}\right]}\right\}$

$=\dfrac{F^2}{2}\delta\left\{\dfrac{1}{M}\right\}$

Compliance Charge, $\delta\left[\dfrac{1}{M}\right]$, Results from a Change in Crack Area, ΔA.

Energy Change per Unit Fracture Area in Both Cases Converges to

$\dfrac{F}{2}\dfrac{d}{dA}\left\{\dfrac{1}{M}\right\}$ as ΔA Approaches Zero.

Figure 2.4: Illustration of applied-force-stiffness in failure criterion.
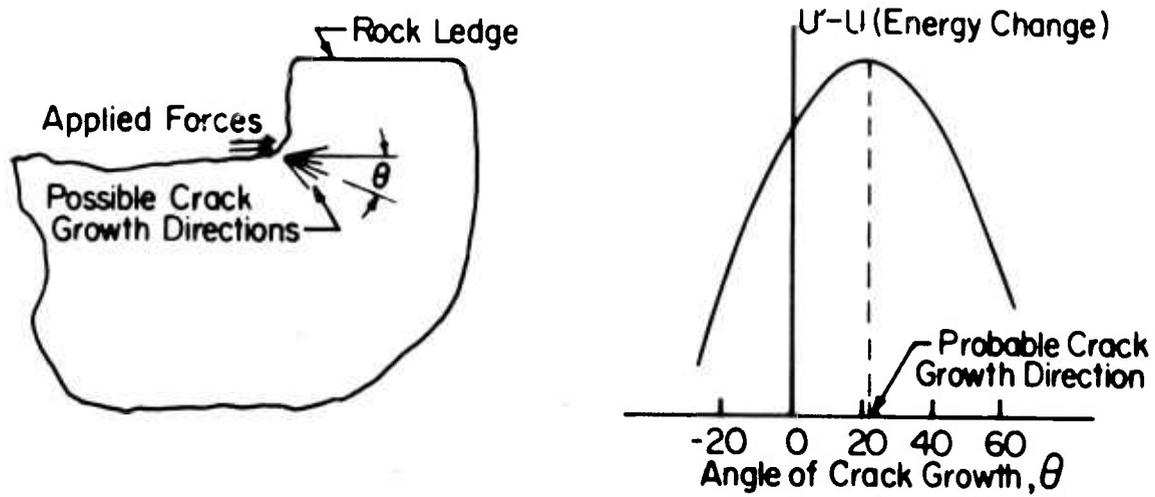
(a)
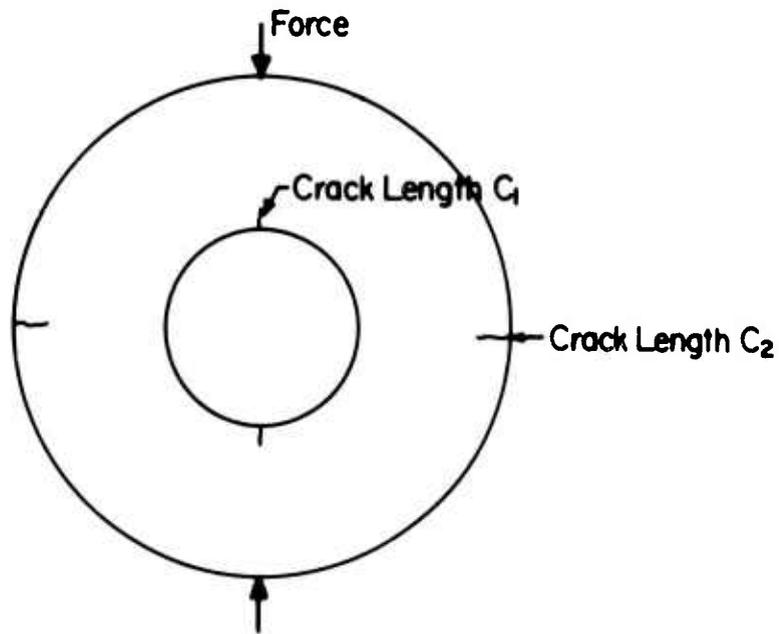
(b)

Figure 2.5:   a) Determinational crack growth direction.
              b) Multiple crack growth in ring test.

Test Name	Test Geometry	Finite Element Representation	Fraction Represented by Mesh	Number of Nodes in F.E. Mesh	Number of Elements in F.E. Mesh	Number of Different Crack Lengths
Beam Test			1/2	178	155	8
Direct Tension Test			1/4	173	150	9
Brazilian Test			1/4	478	450	11
Ring Test			1/4	476	444	13
Hydraulic Tension Test			1/4	331	370	9
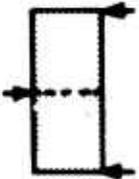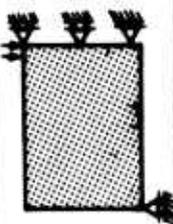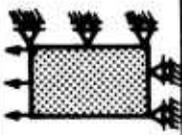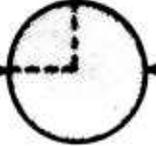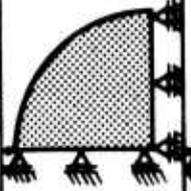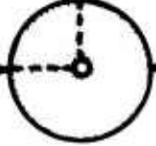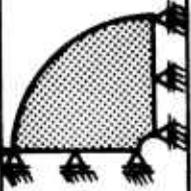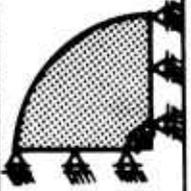
Figure 2.6: Summary of finite element meshes and crack lengths used in crack simulation
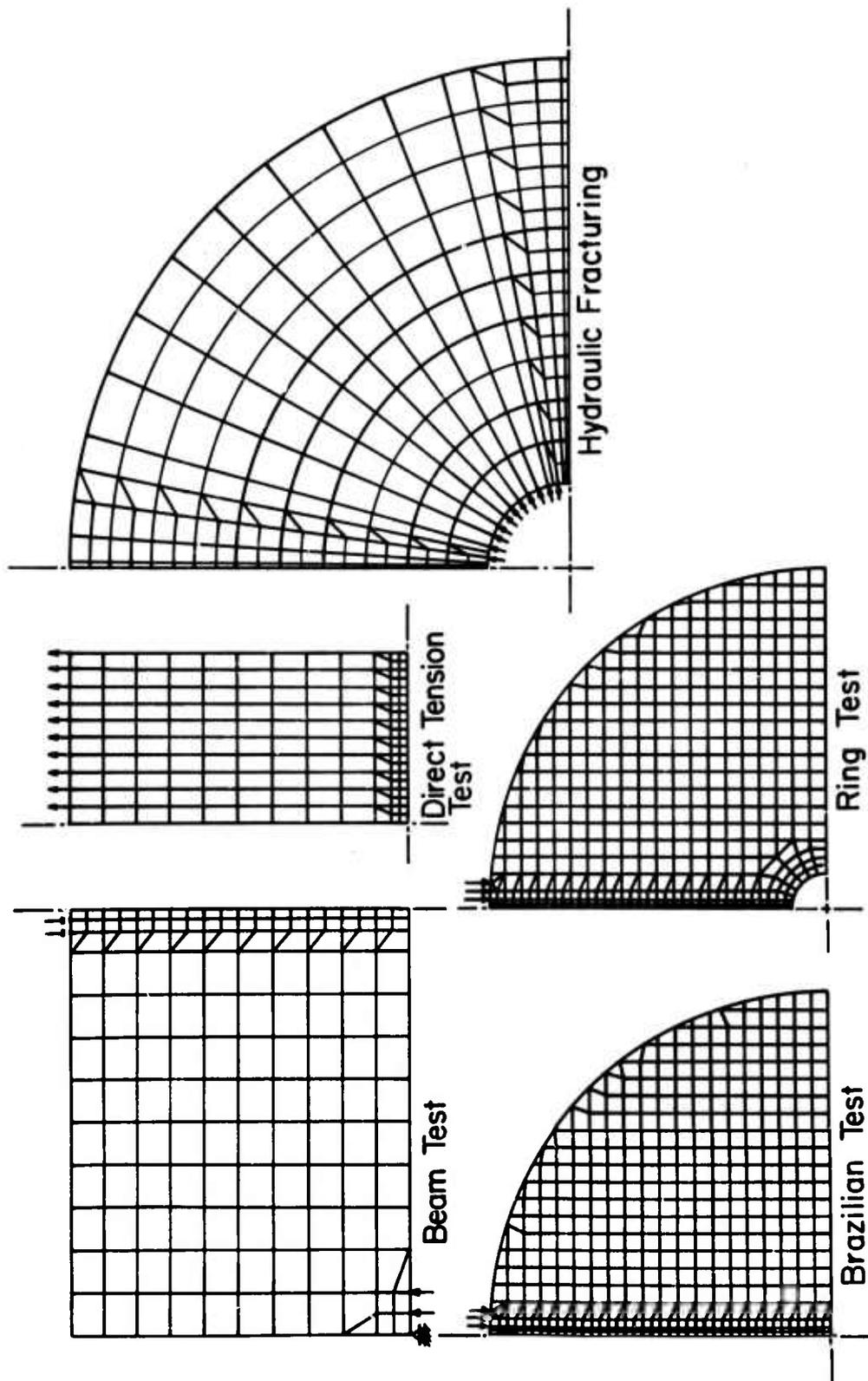
Figure 2.7: Finite element meshes used in crack growth simulation.
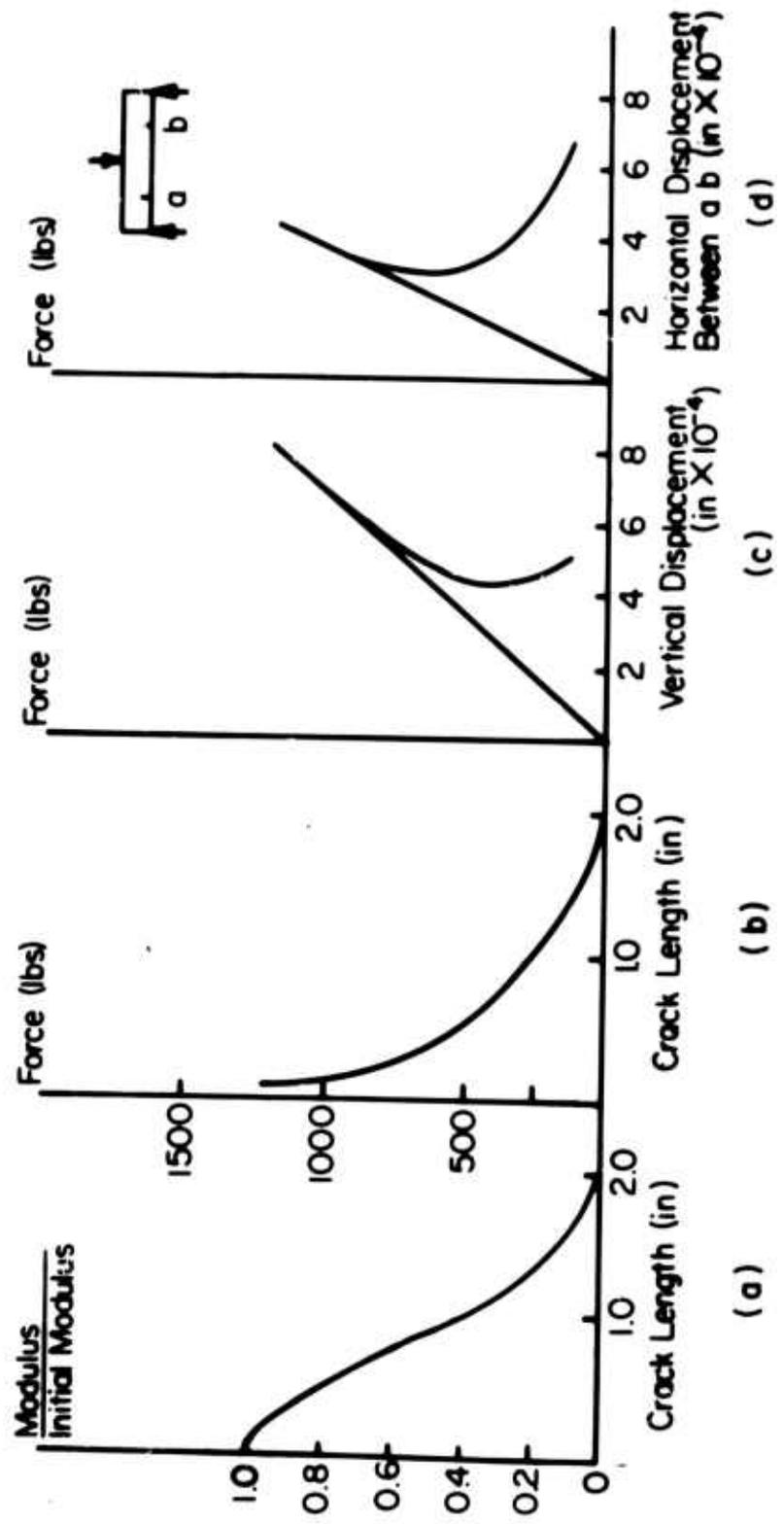
Figure 2.8: Theoretical prediction for the beam test.
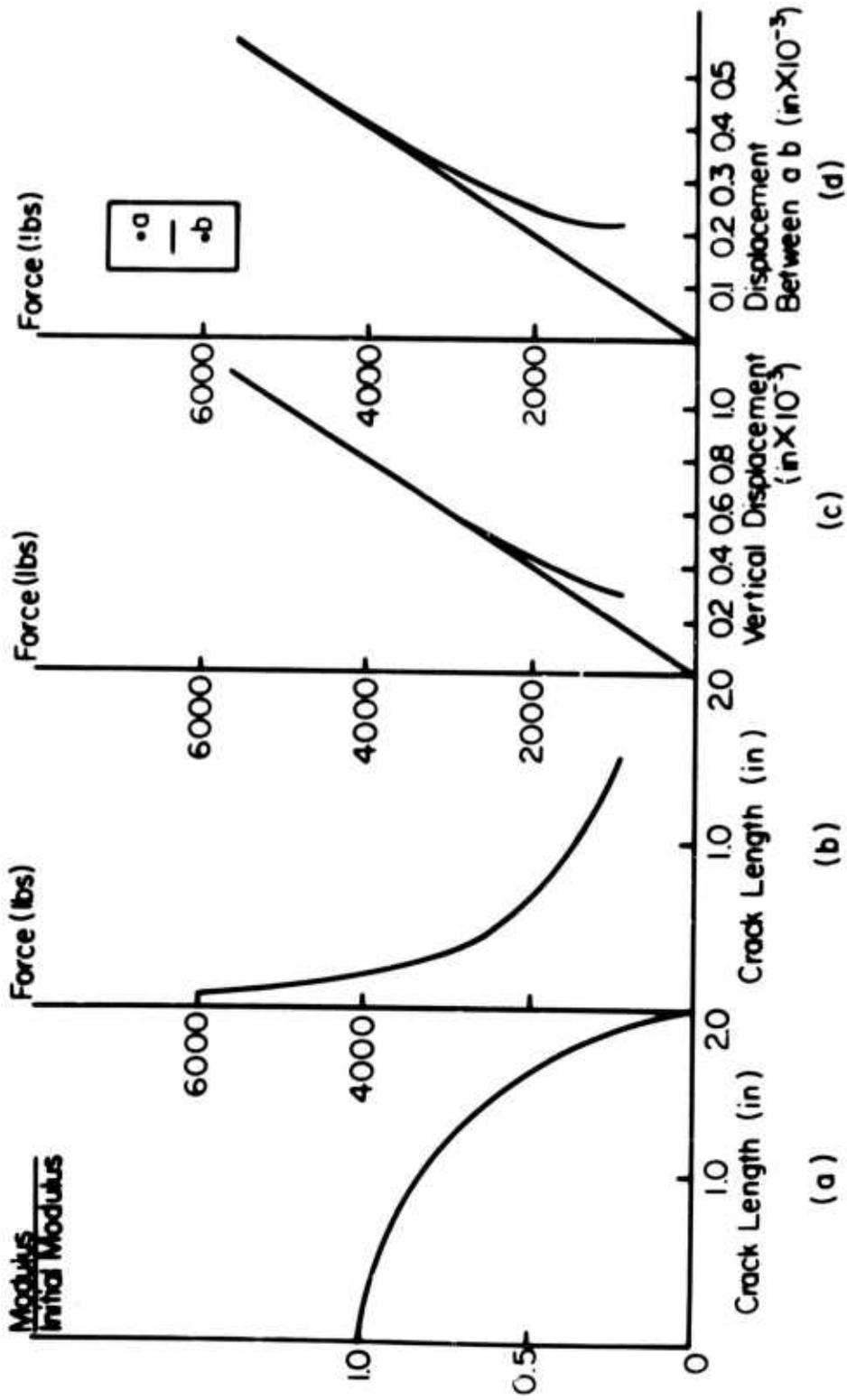
Figure 2.9: Theoretical prediction for the direct tension test.
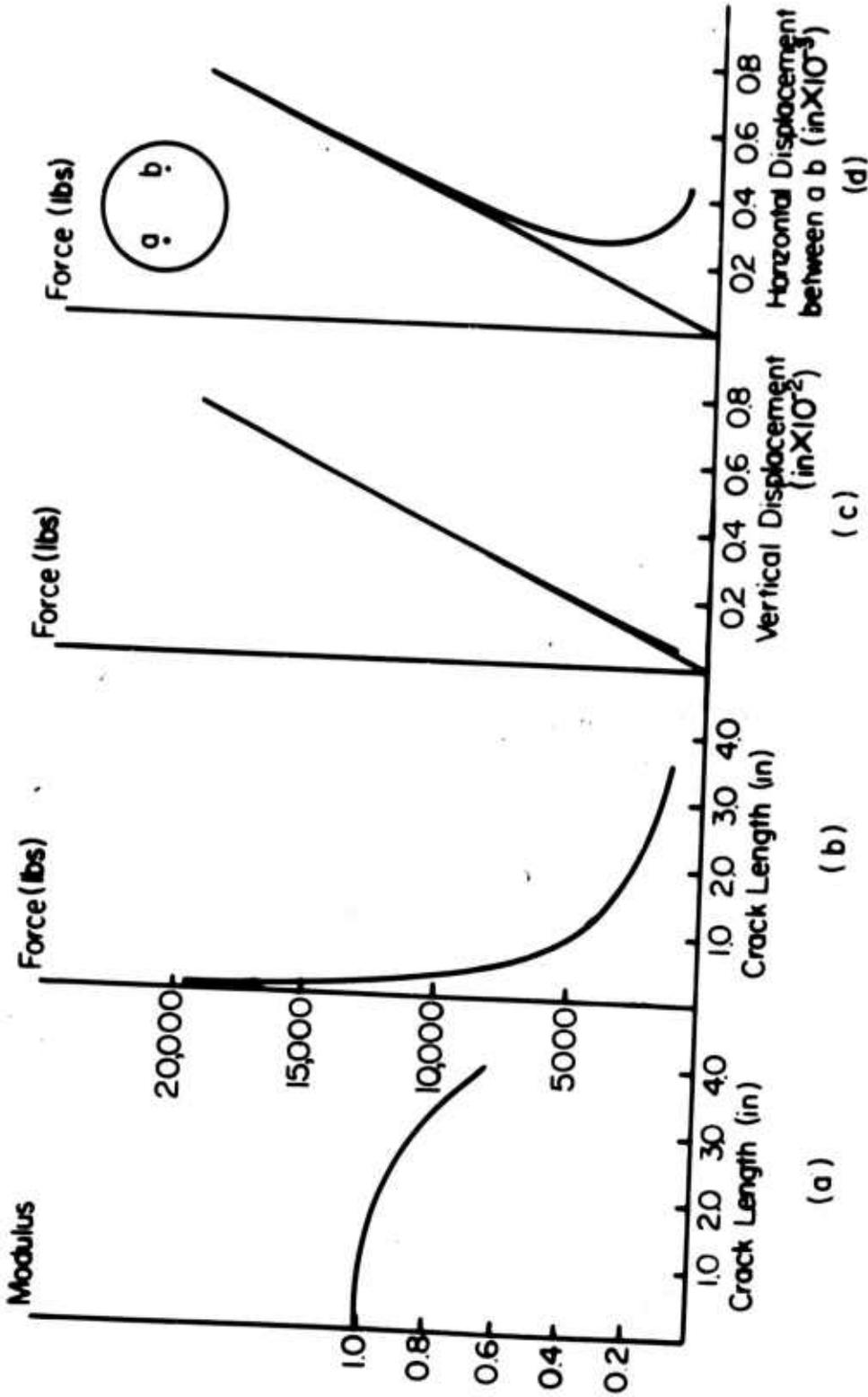
Figure 2.10: Theoretical predictions for brazilian test.
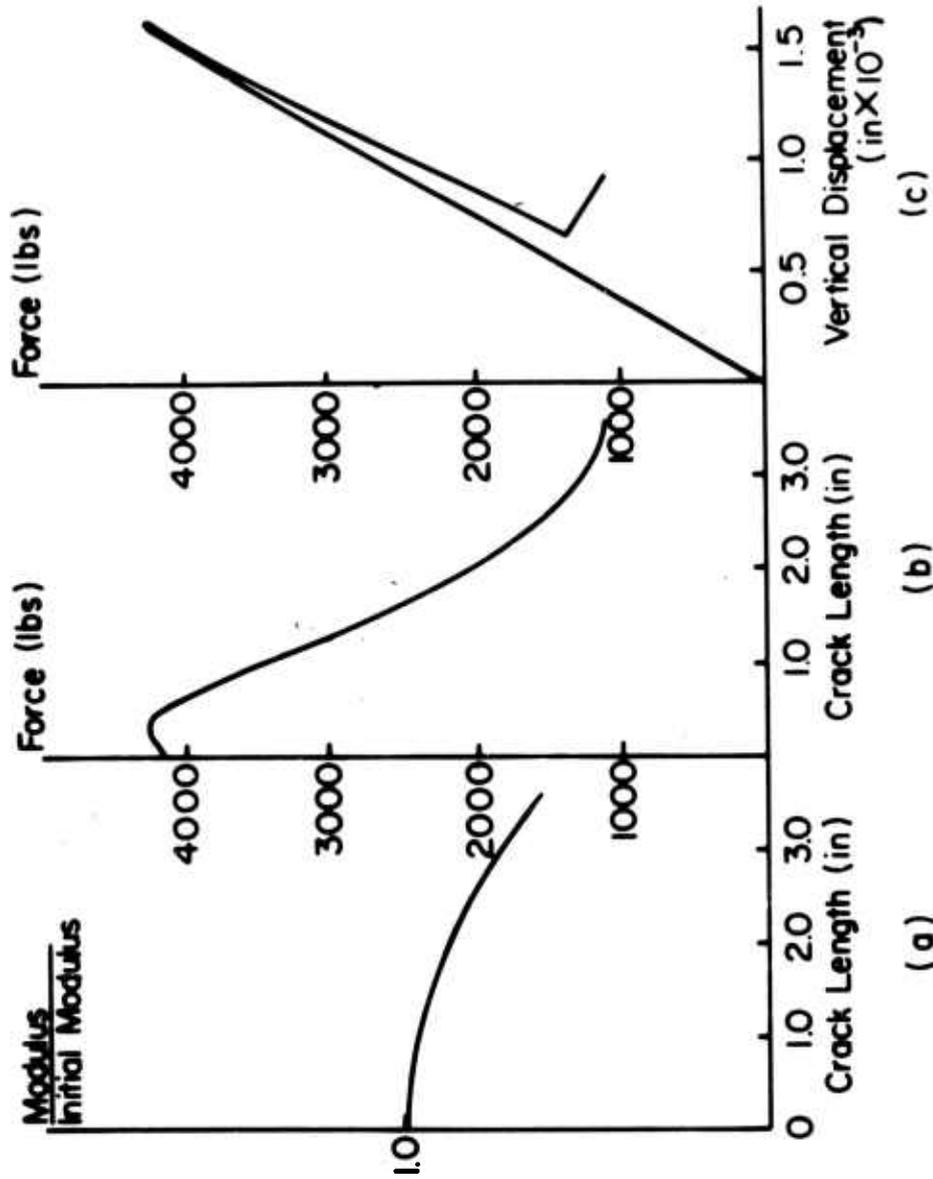
Figure 2.11: Theoretical predictions for the ring test, small hole.
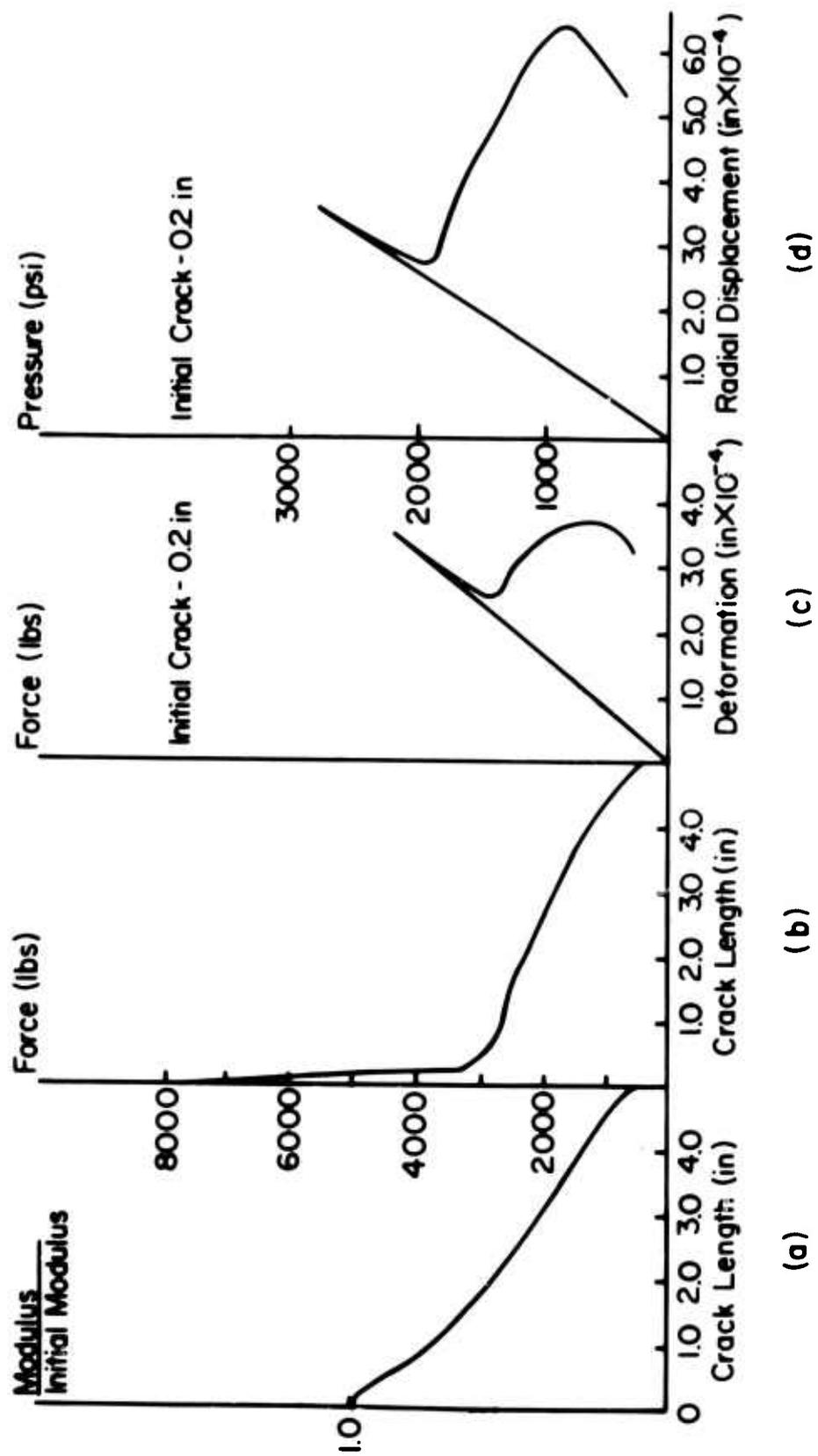
Figure 2.12: Theoretical predictions for the hydraulic fracturing test.
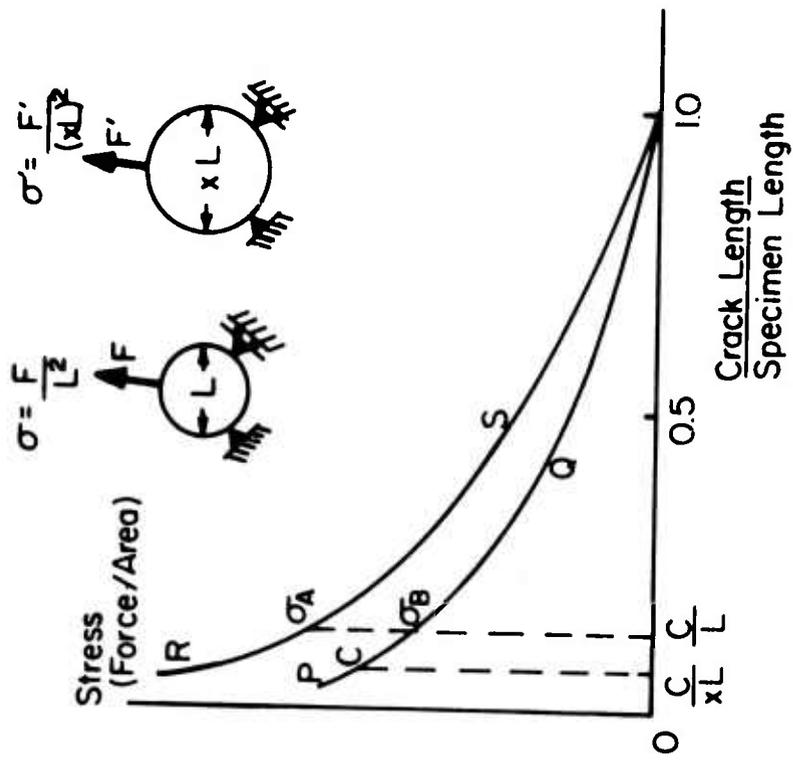
Figure 2.13. The effect of specimen size upon observed stress at failure.
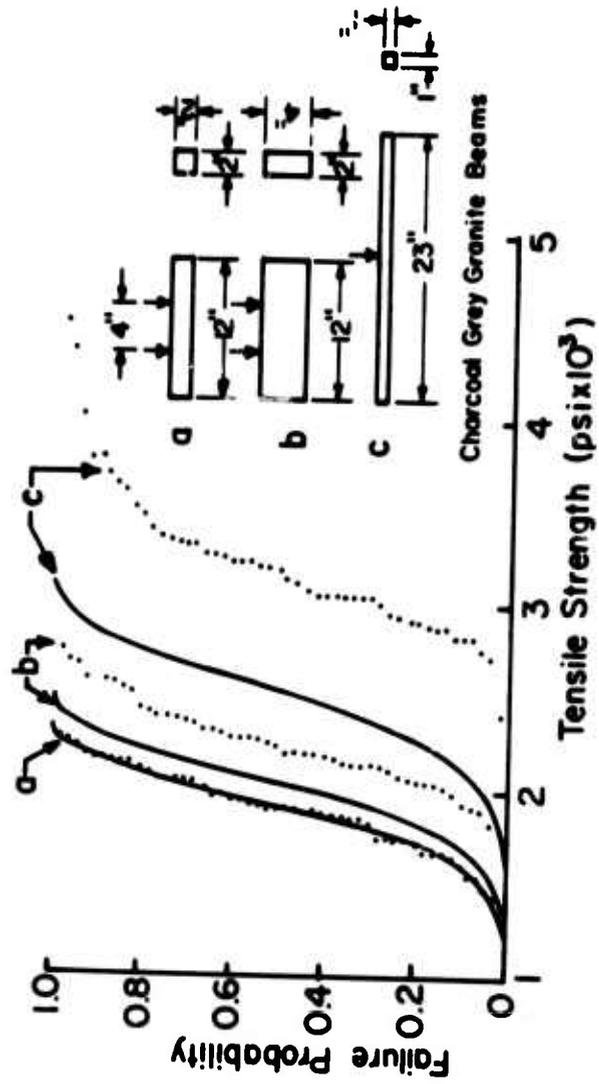
Figure 2.14: Comparison of predicted, using Weibull's theory, and experimental tensile strength distributions for charcoal grey granite, after HUDSON (1971).
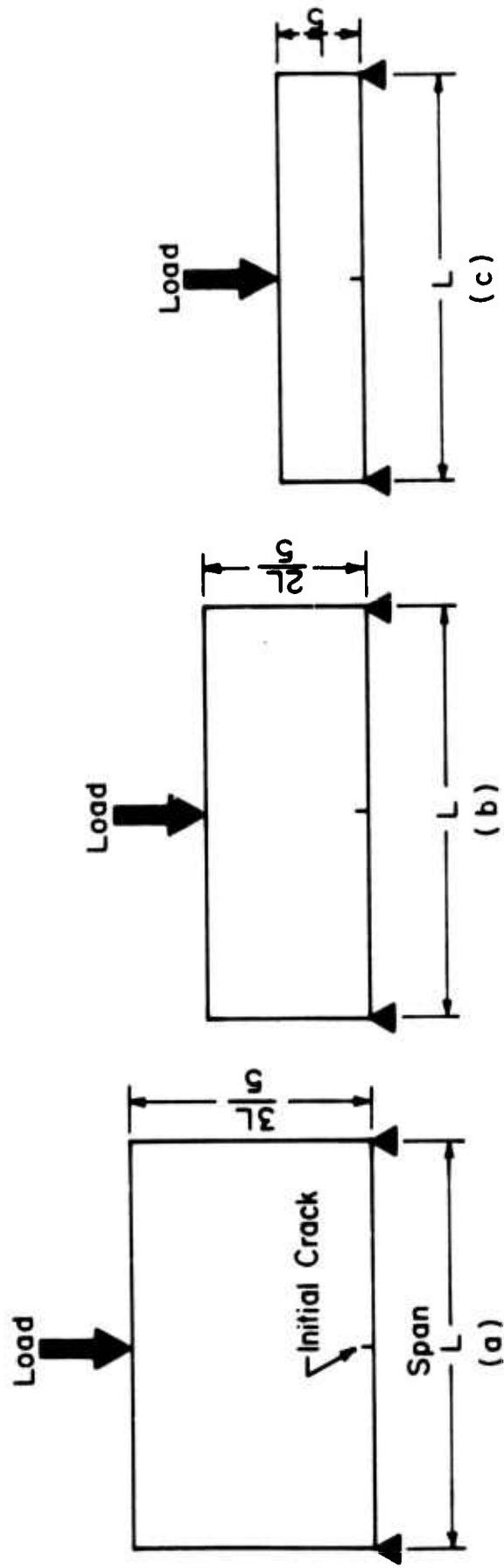
Figure 2.15: Three beams used to check the effect of shape on strength.
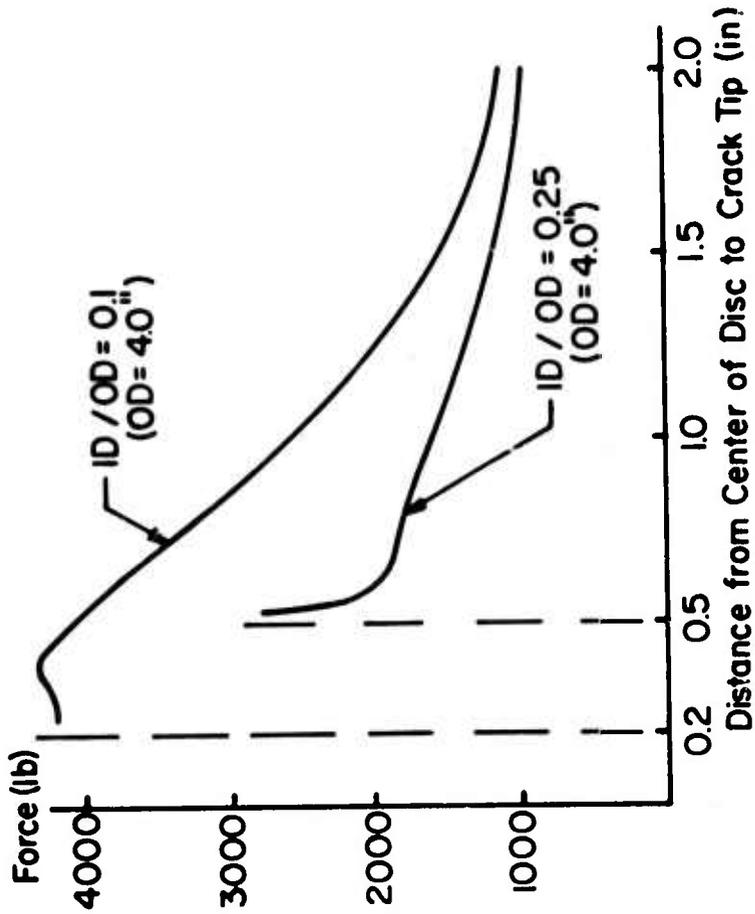
Figure 2.16: Comparison of theoretical predictions for the ring tests with small and large hole.
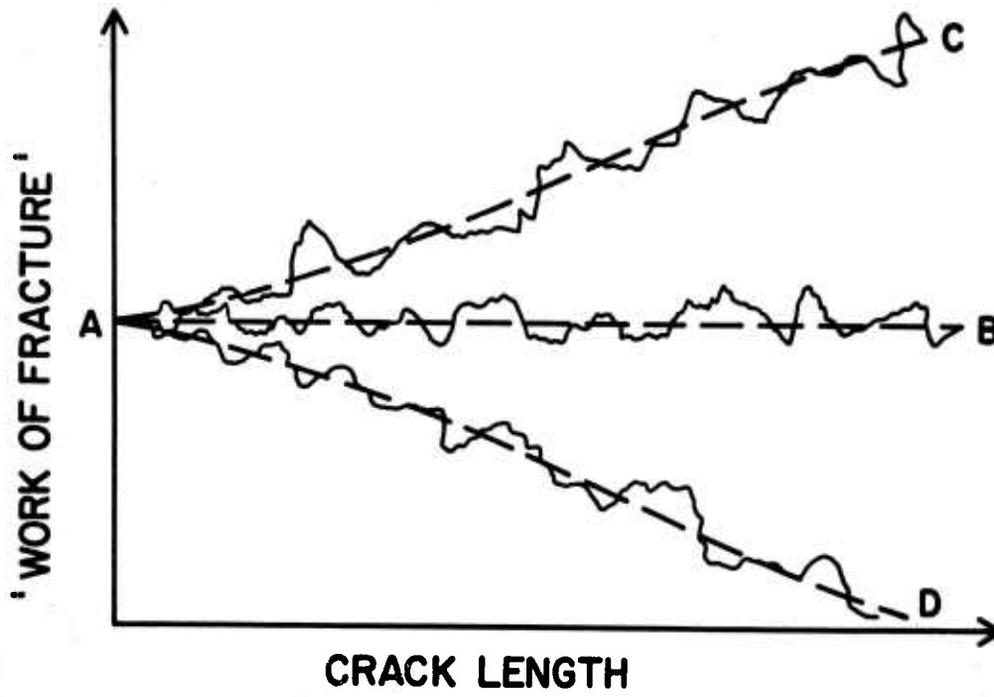
Figure 2.17: Possible variations of work of fracture with crack length.
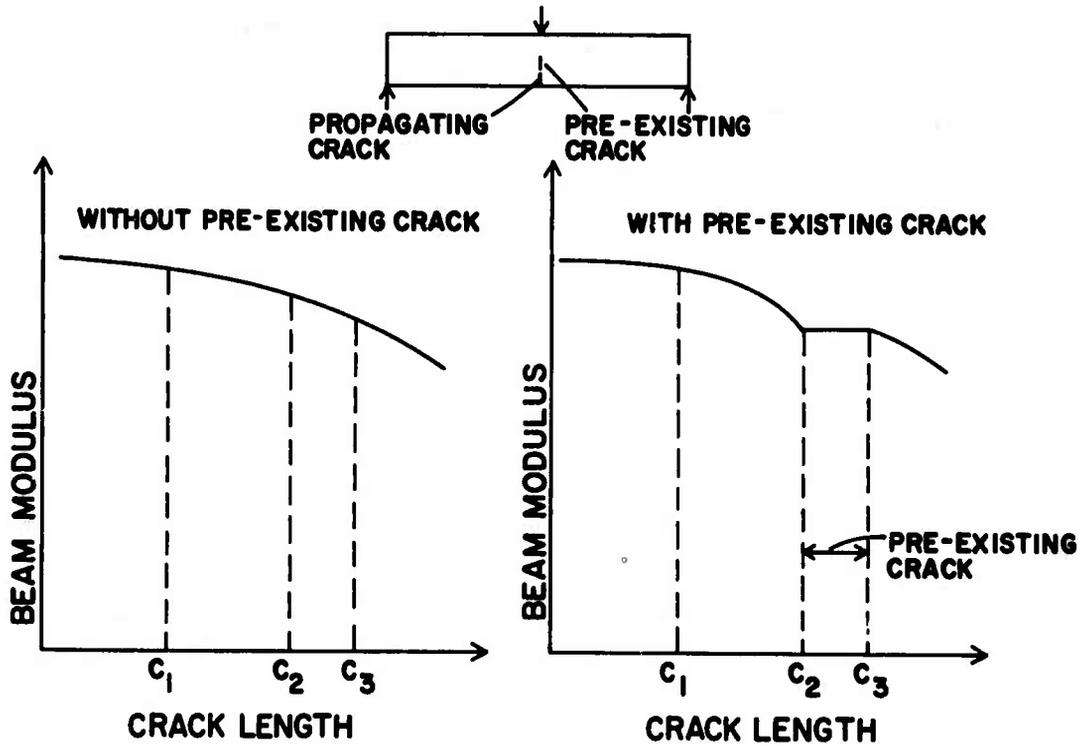
Figure 2.18: Variation in beam modulus for different crack lengths – illustrating the effect of a pre-existing crack.
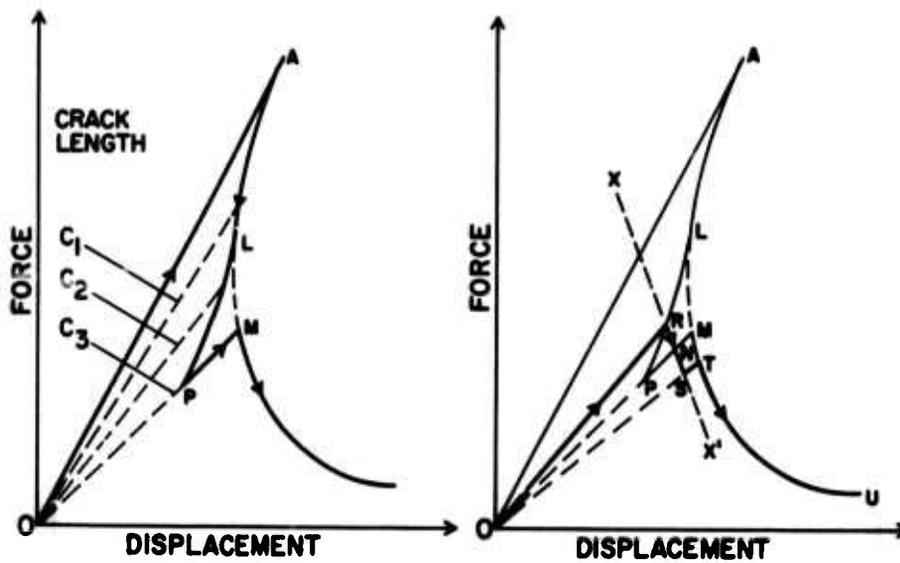
Figure 2.19:   The influence of a pre-existing crack and testing machine stiffness on the complete force-displacement.
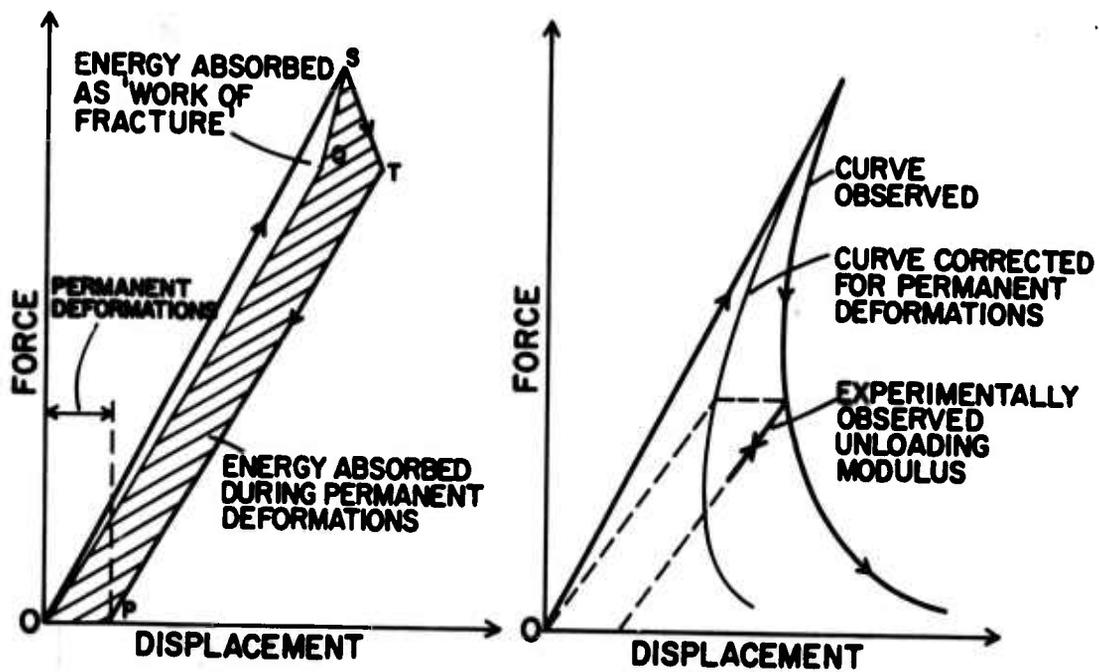
Figure 2.20:   The influence of permanent deformations on the complete force-displacement curve.
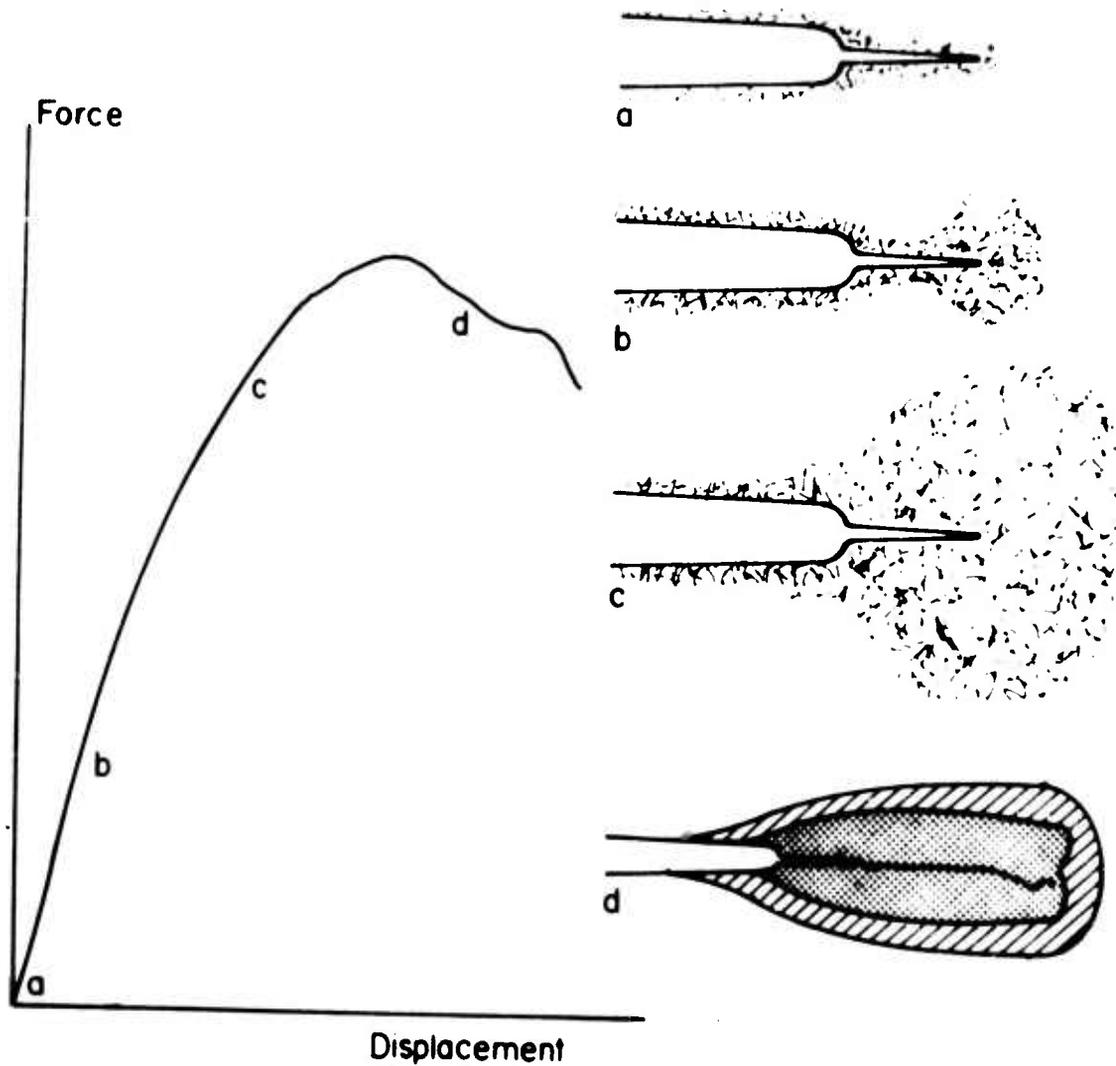
Figure 2.21: A schematic representation of the stages of development of a damage zone around a machined slot in rock. Initially only a few fresh microcracks are present as in (a). On loading the rock first responds elastically corresponding to Region I and only a few microcracks are produced on weakest interfaces, (b). Then in (c) the damage has become intense and spreads rapidly leading to inelastic behavior as in Region II. Finally, the Region III behavior is shown at (d) where the main crack and the damage zone extend together. After HOAGLAND et.al. (1972).
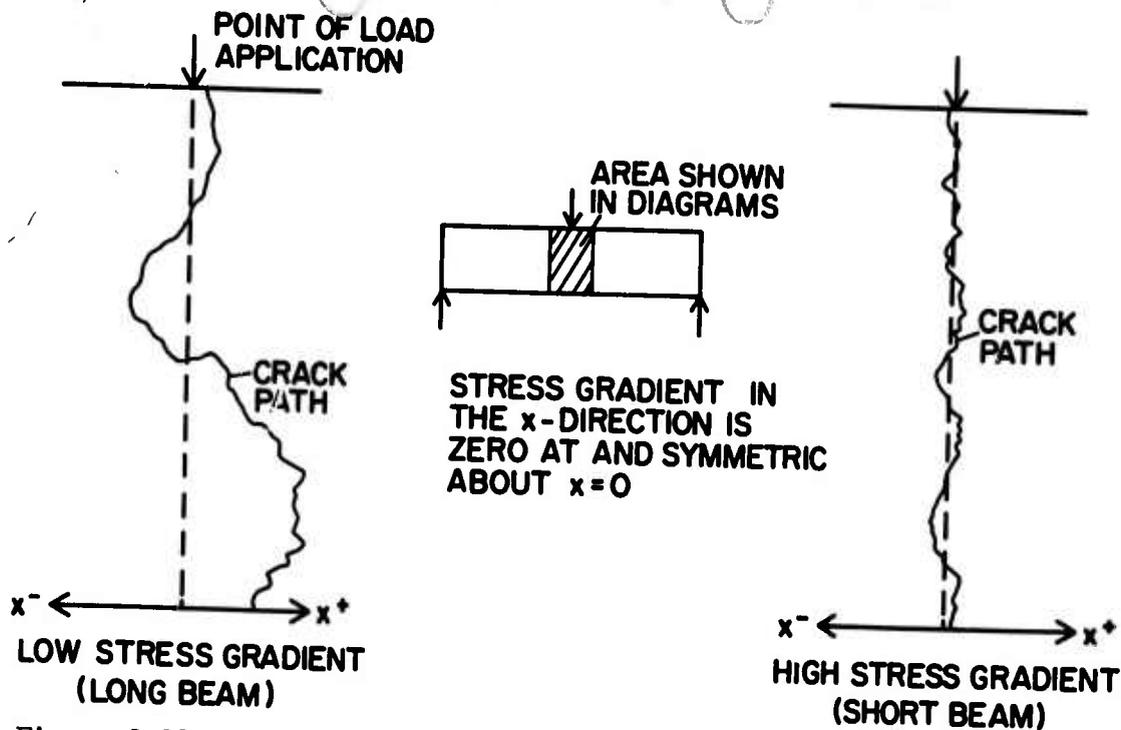
Figure 2.22: Degree of Fracture Path Deviation from a Straight Line is a Function of the Stress Gradient.
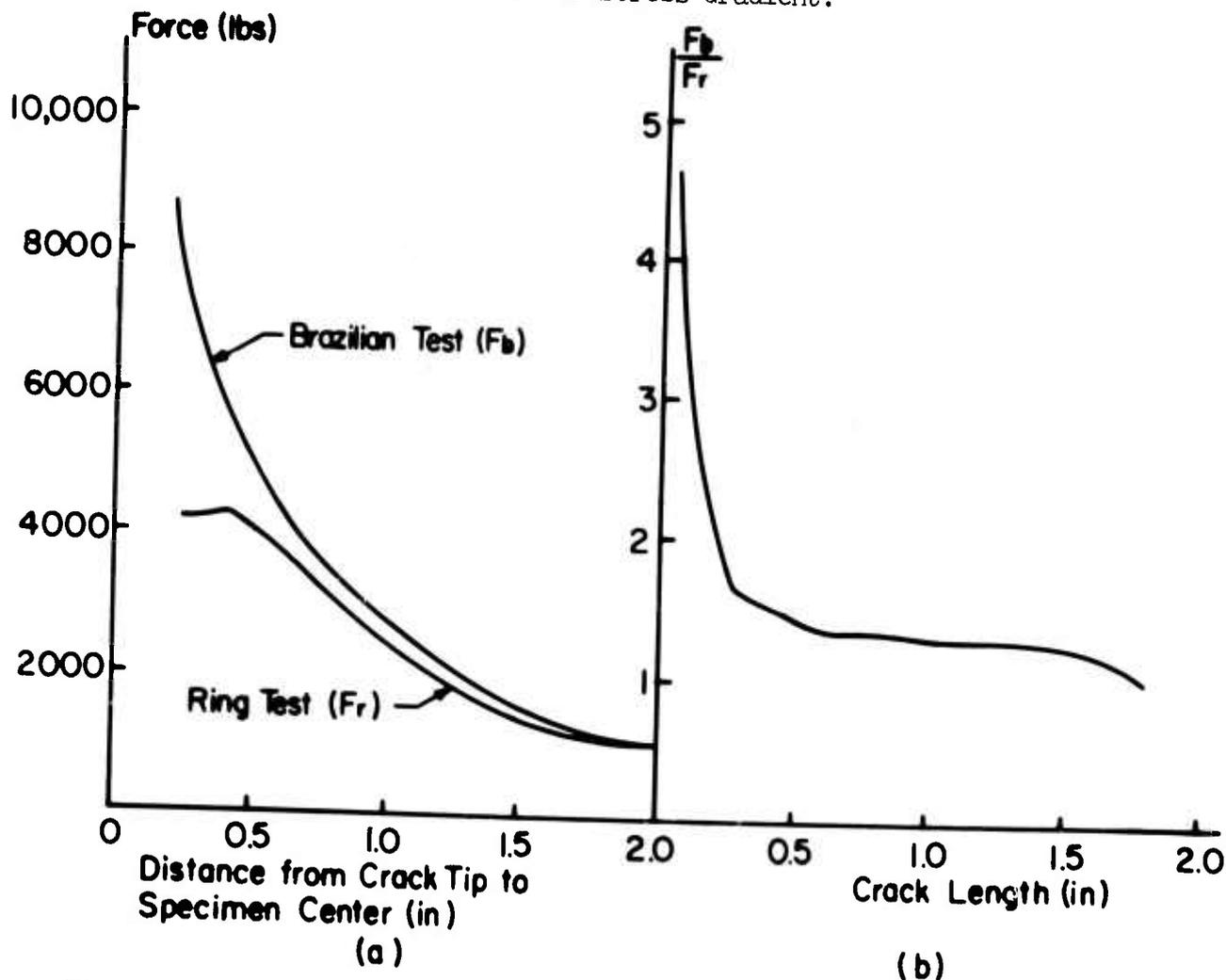
Figure 2.23: Comparison of Brazilian and Ring Tests.
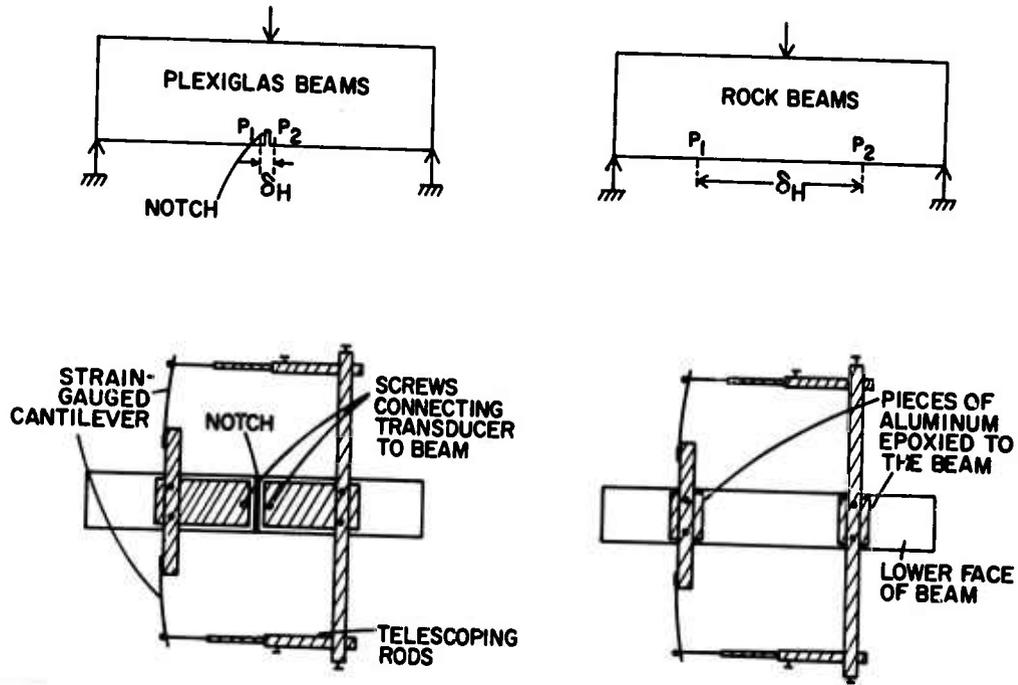
Figure 2.24: Generation of Feedback Signal for Beam Test.
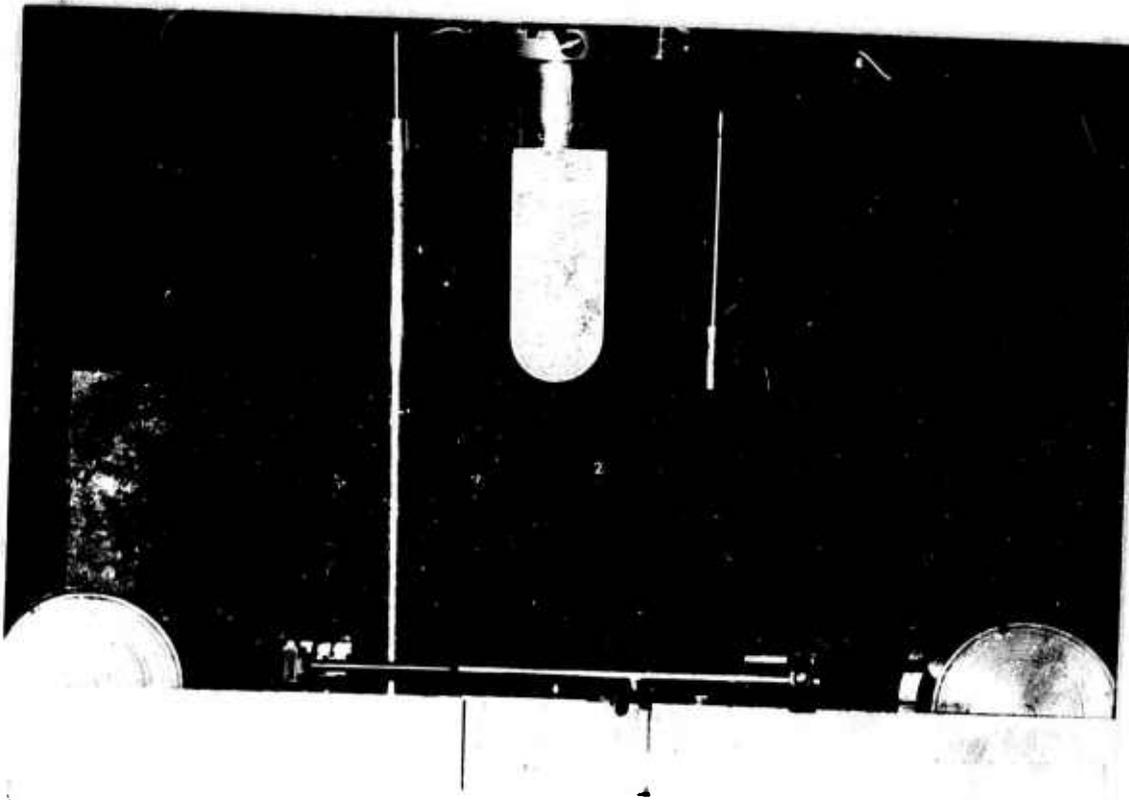
Figure 2.25: The Beam Bending Apparatus.
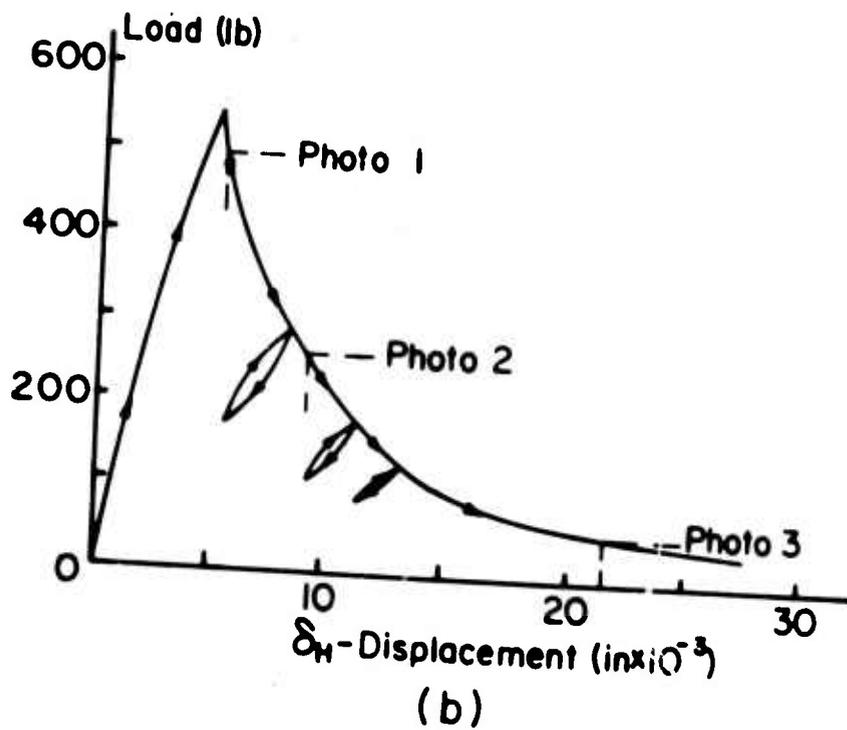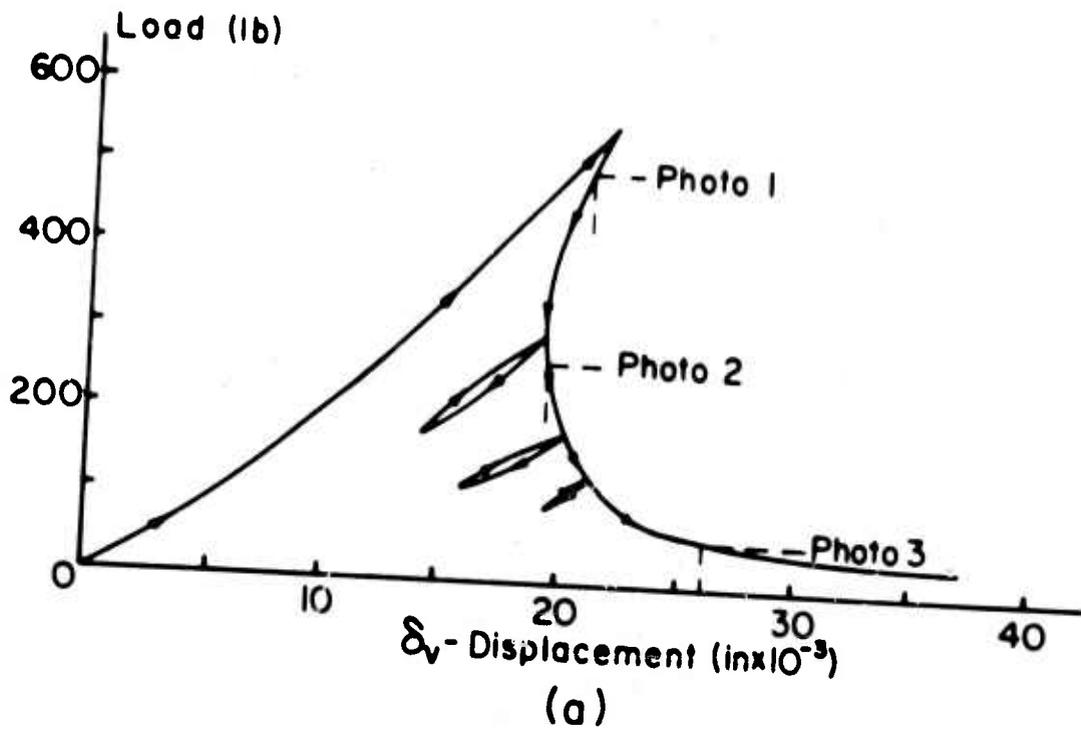
Figure 2.26: Force -'vertical' displacement and force - 'horizontal' displacement curves characterizing controlled plexiglas beam failure.
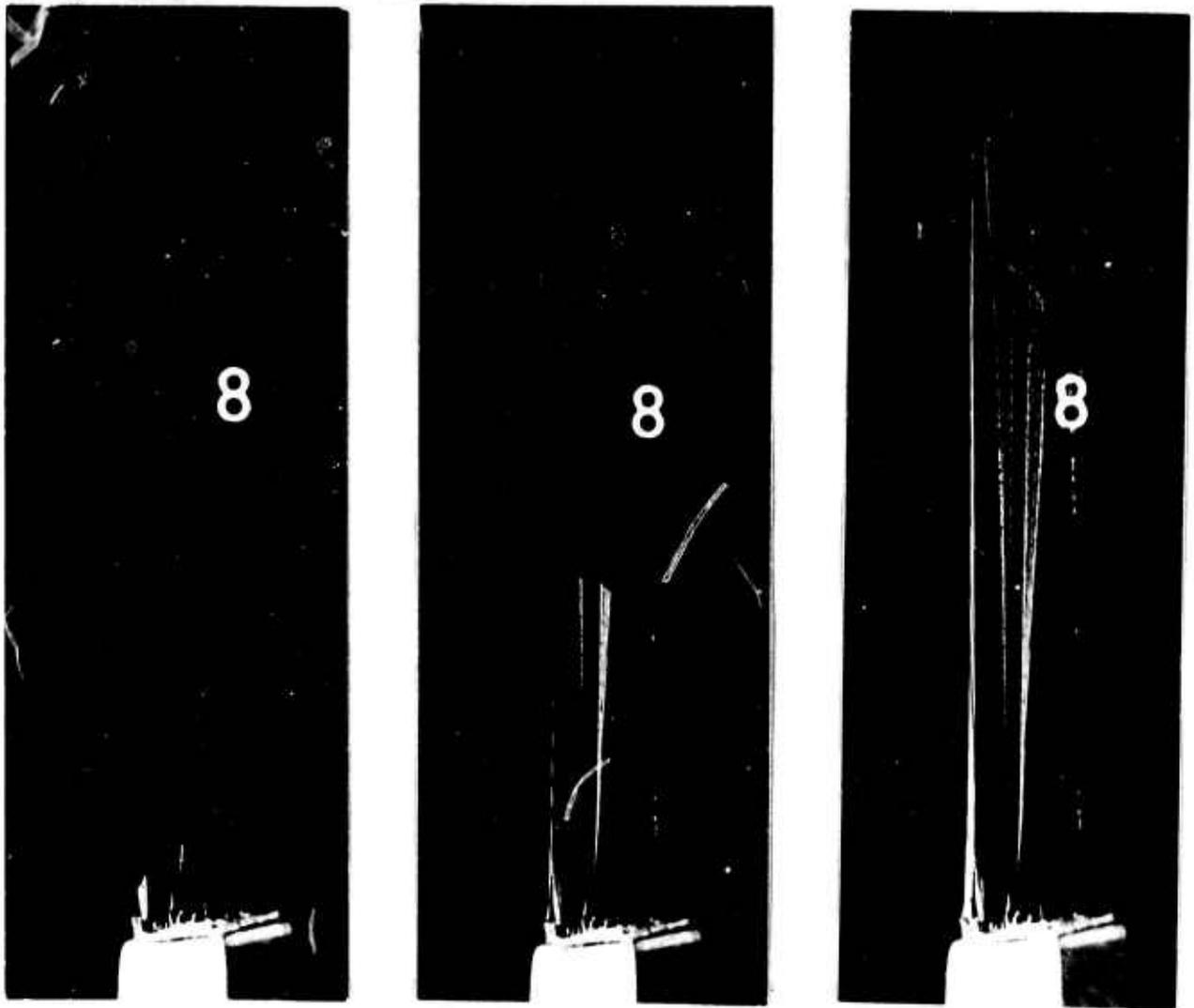
Figure 2.27: Photographs of crack growth in plexiglas.
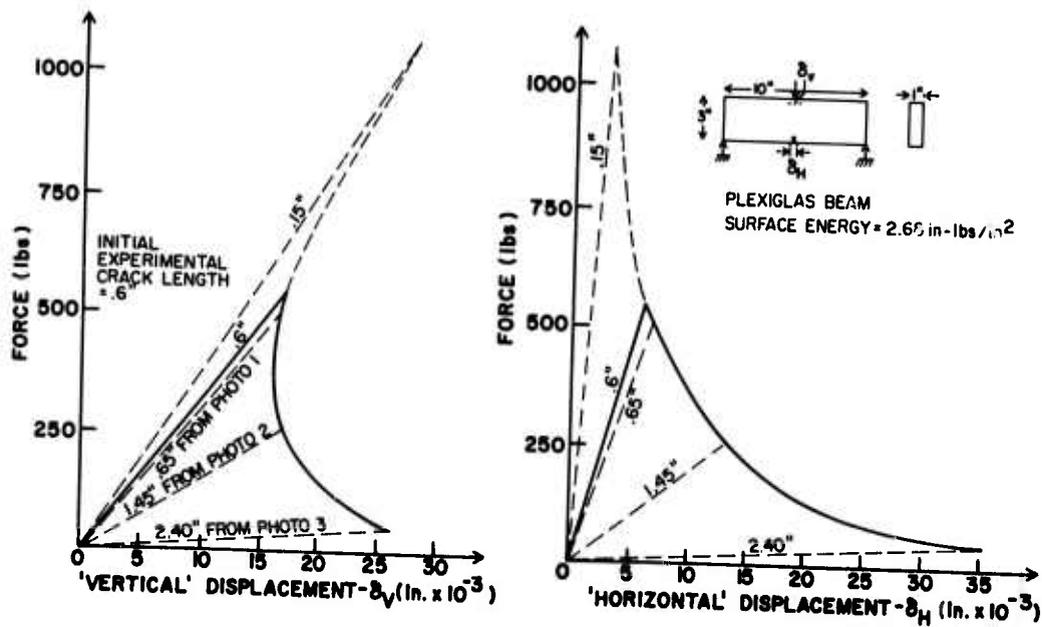
Figure 2.28: Predicted complete force-displacement curves for plexiglas beam failure.
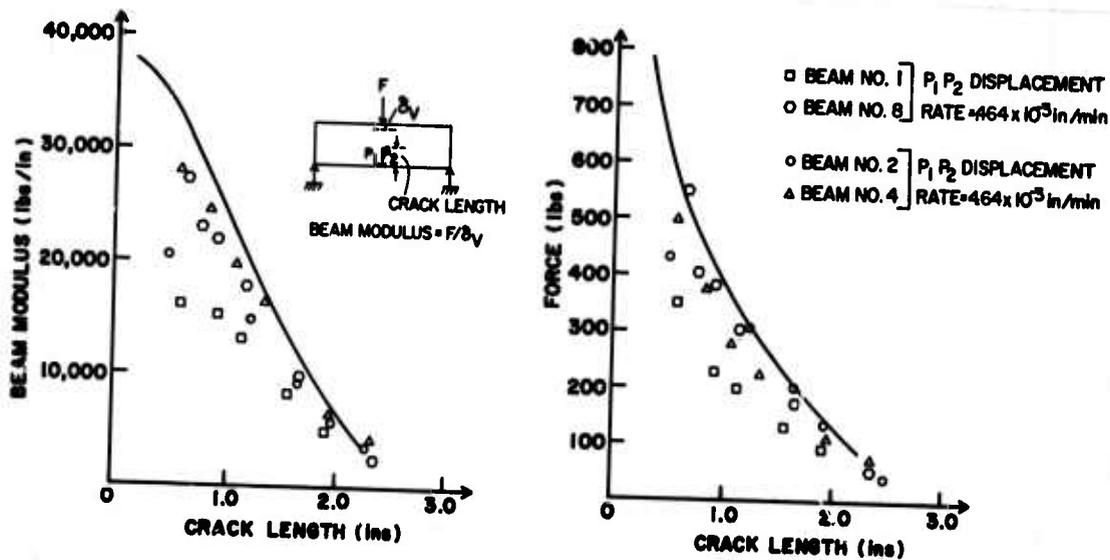
Figure 2.29: Comparison of theoretical and experimental modulus versus crack length and load versus crack length curves.

66
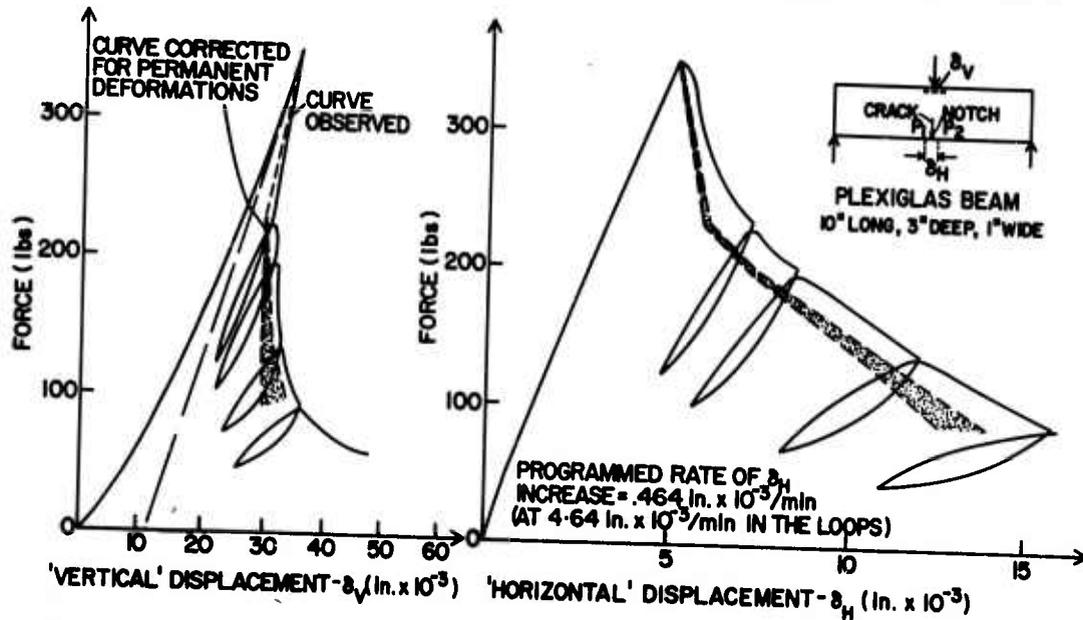
Figure 2.30: Reduction in unloading modulus during crack propagation in a plexiglas beam.
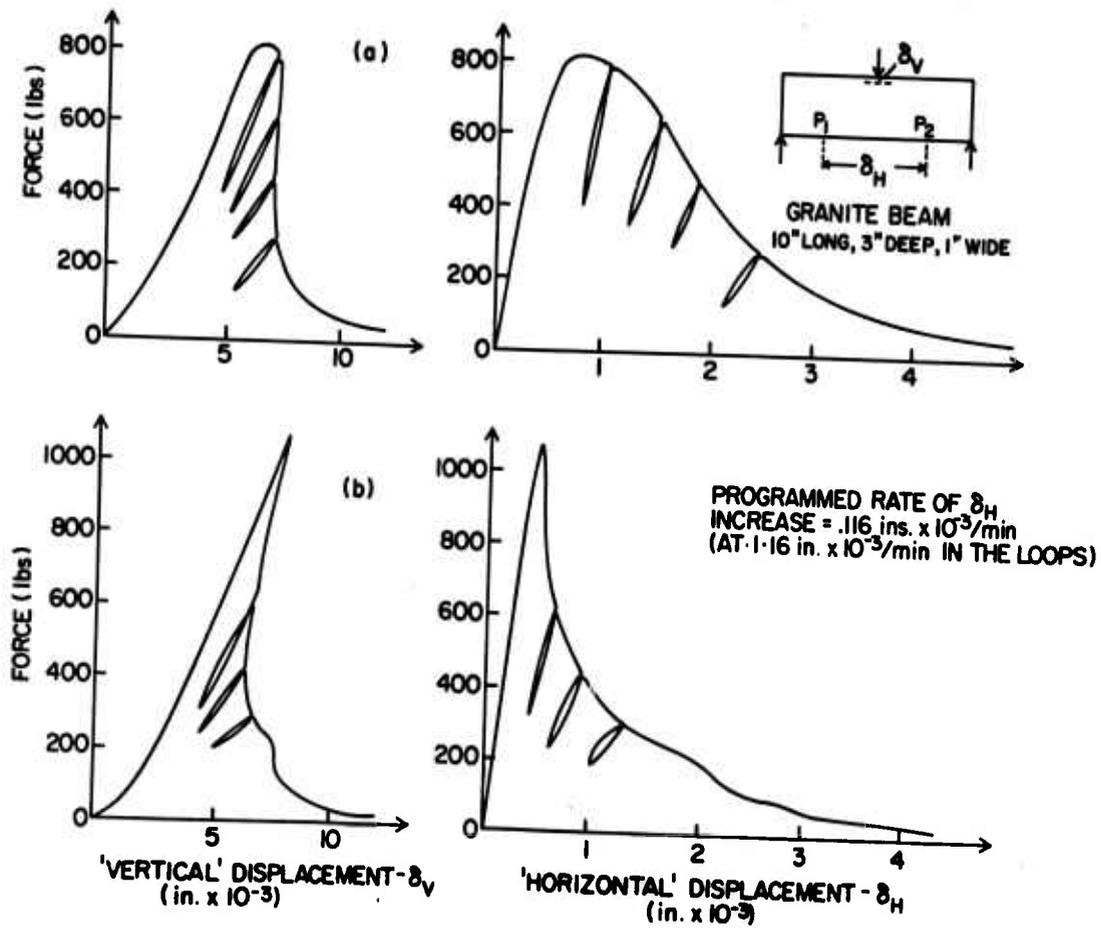
Figure 2.31: Force -'vertical' displacement and force -'horizontal' displacement curves characterizing controlled granite beam failure.
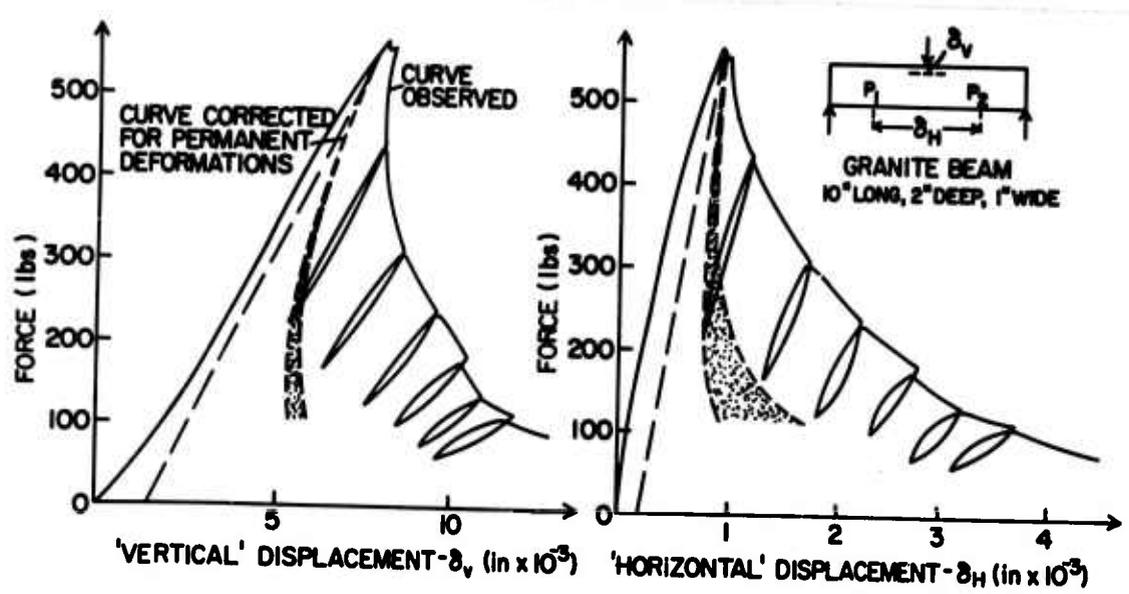
Figure 2.32:   Complete force-displacement curves illustrating the progressive reduction in beam unloading modulus.
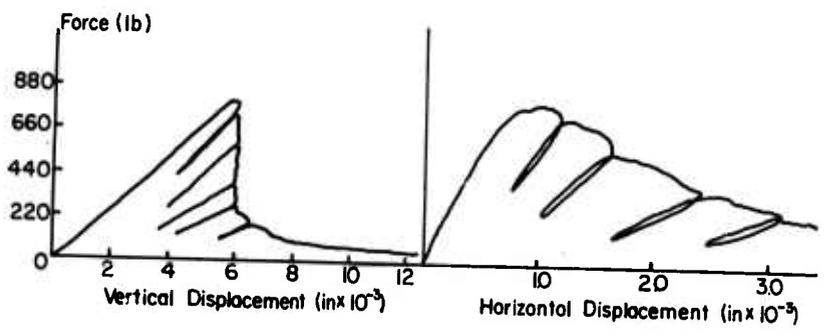
Figure 2.33:   Experimental Output for Notched Granite Beam. (10" x 3" x 1").

71
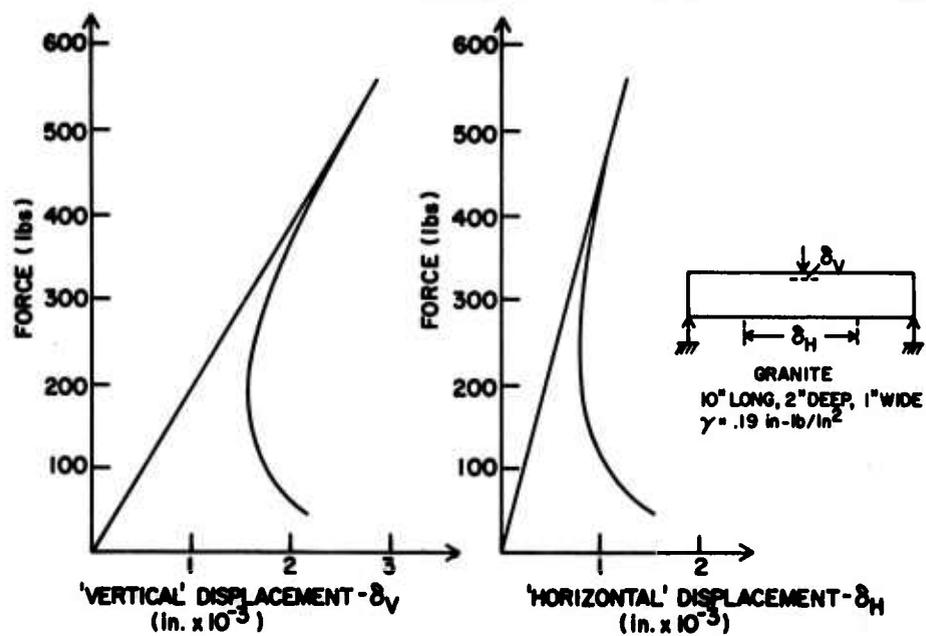
Figure 2.34: Predicted complete force-displacement curves for granite beam failure.
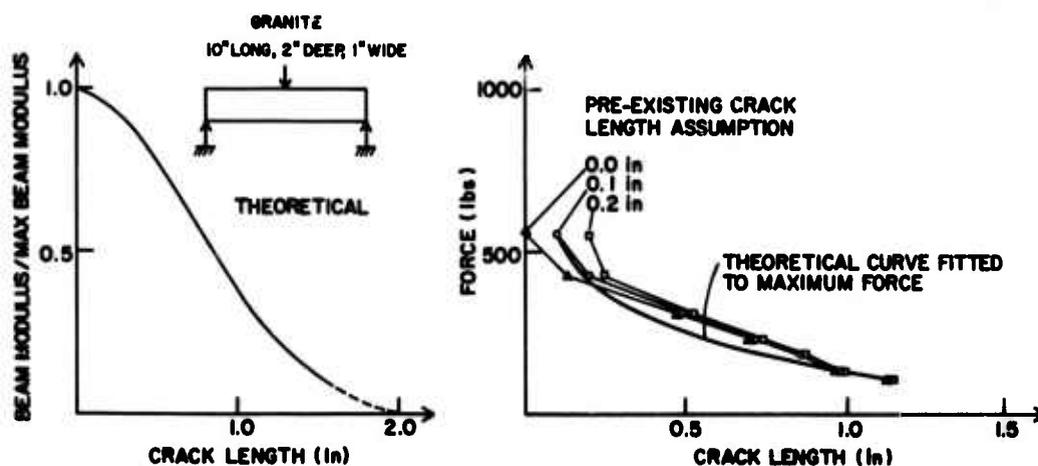
Figure 2.35: Theoretical and experimental relationship between beam modulus and crack length.

Brazilian Test

Wire Strain Gage

Ring Test, Small Hole

Bonded Area
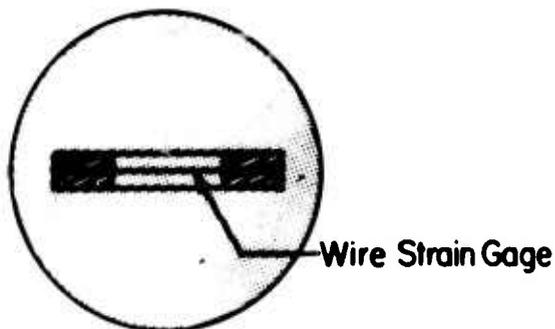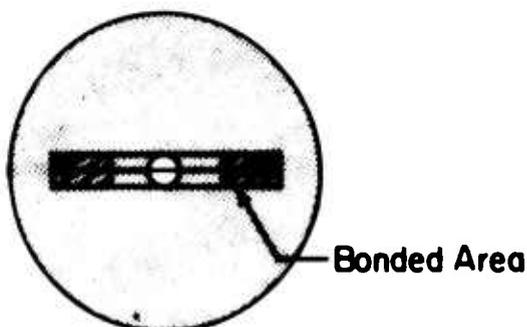
Ring Test, Small Hole

Ring Test, Large Hole

Strain Gage on
Cantilever Beam
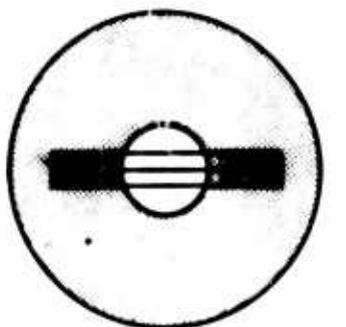
Ring Test, Large Hole

Granite Tests
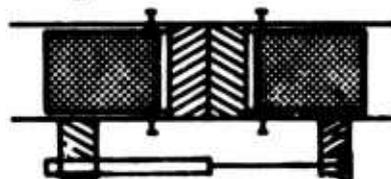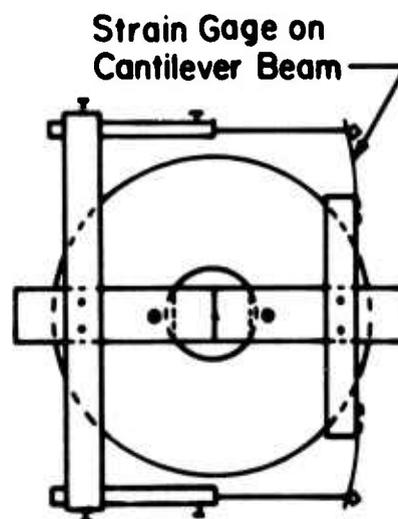
Plexiglas Tests

Figure 2.36: Experimental feedback systems for the brazilian and ring tests.
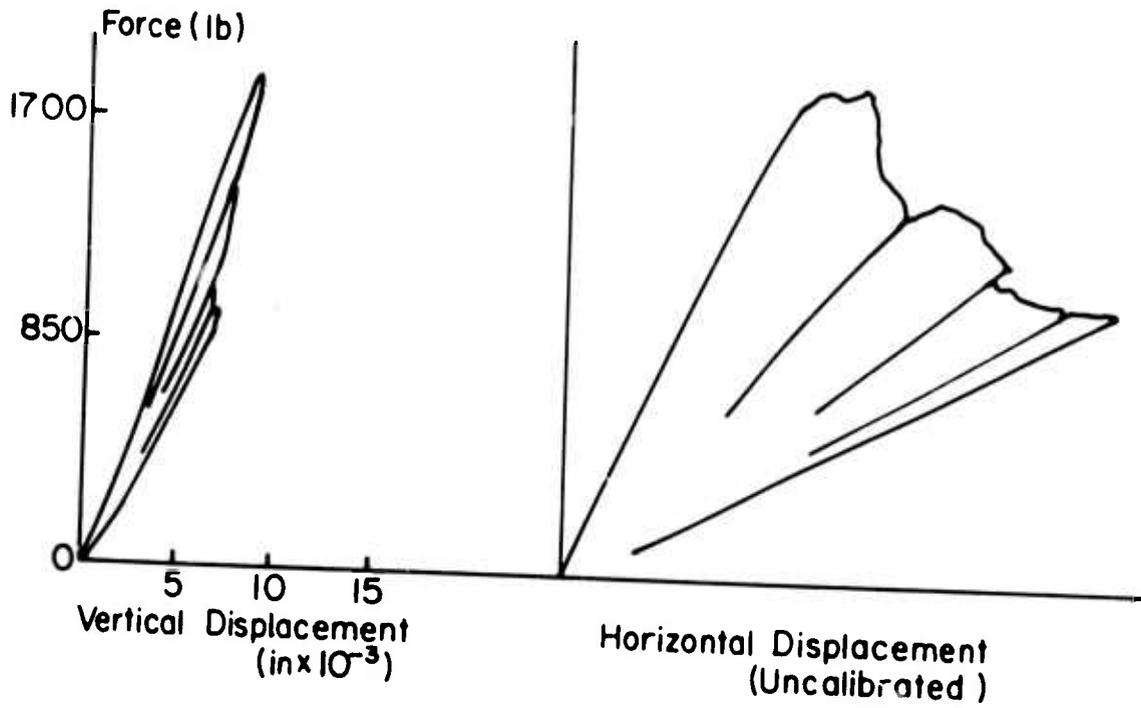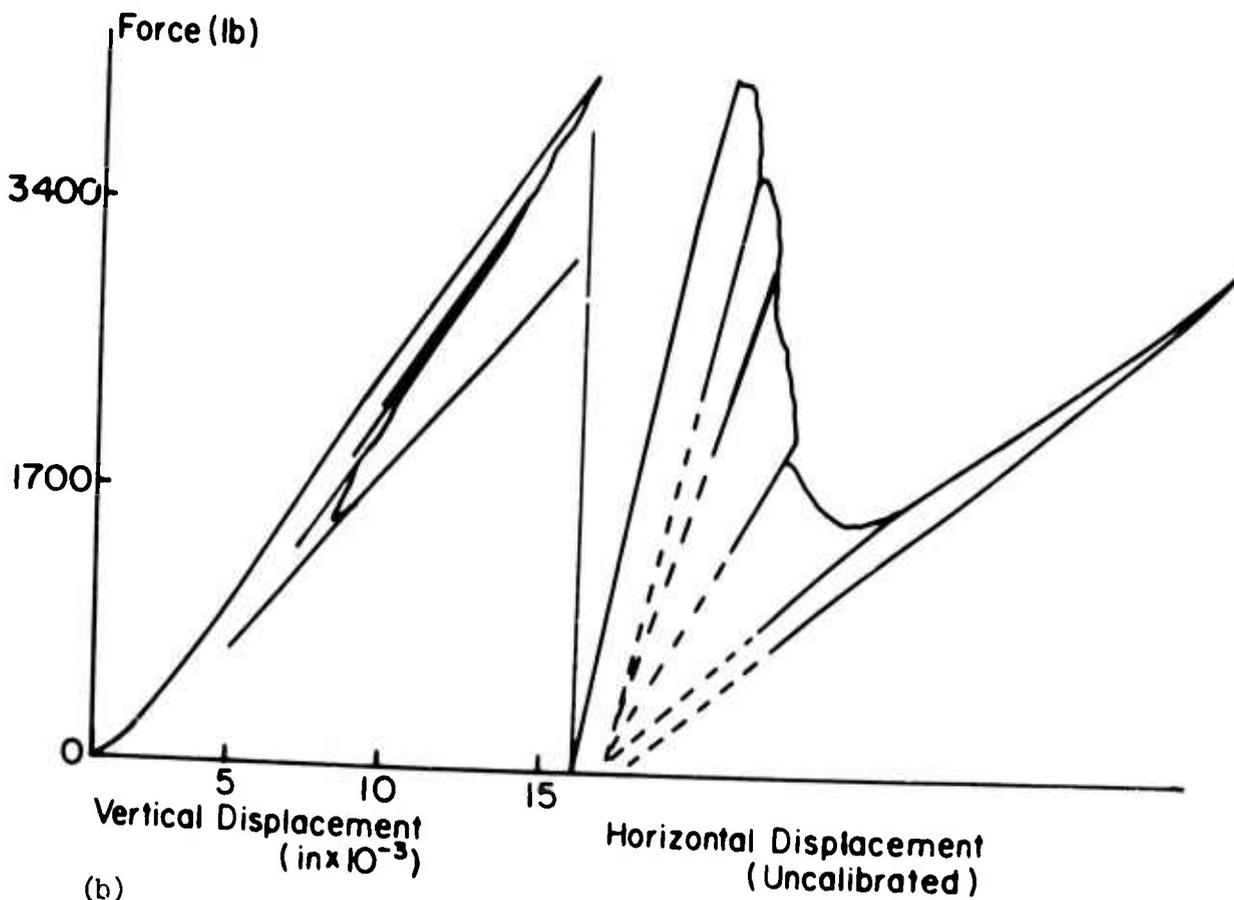
Figure 2.37: Experimental results of the Controlled failure of plexiglas ring tests. (a) Ring with large hole, (b) Ring with small hole.
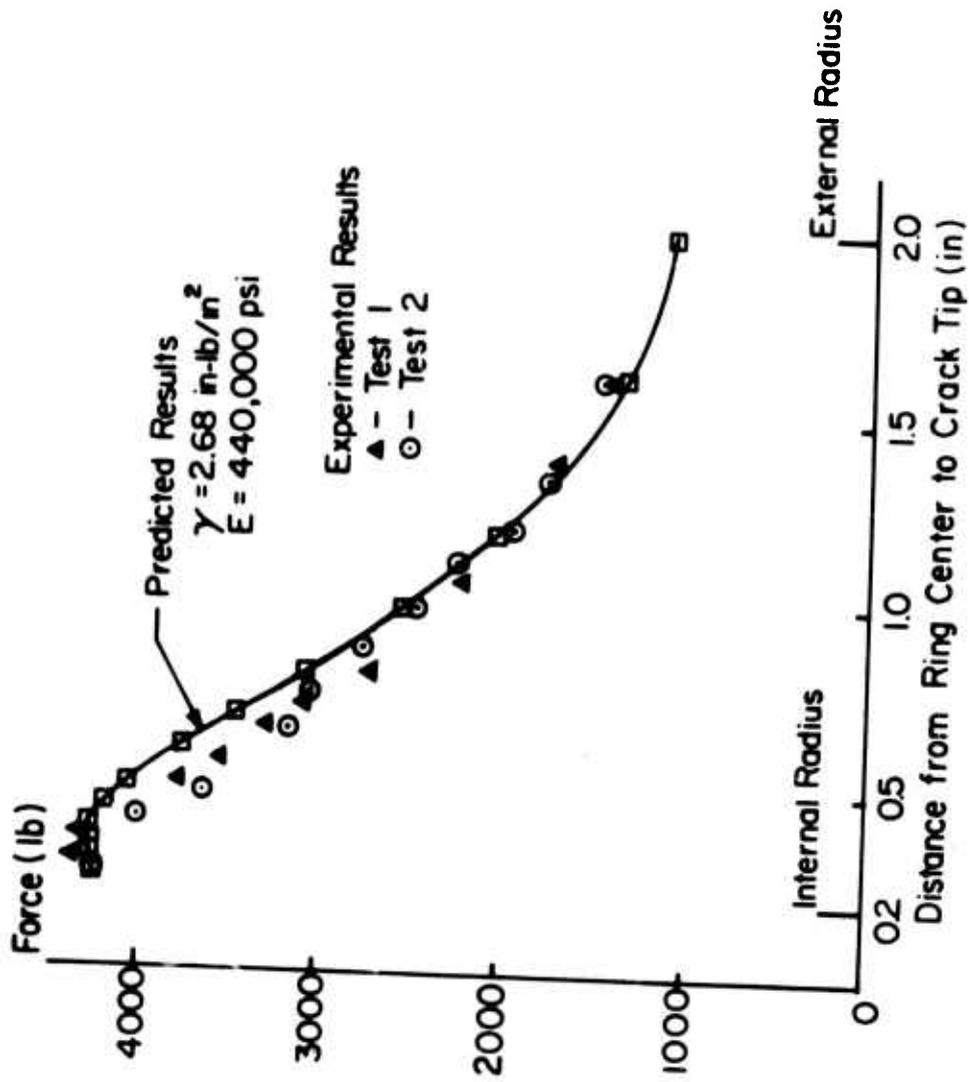
Figure 2.38: Comparison of experimental and predicted results for ring test with small hole (plexiglas).
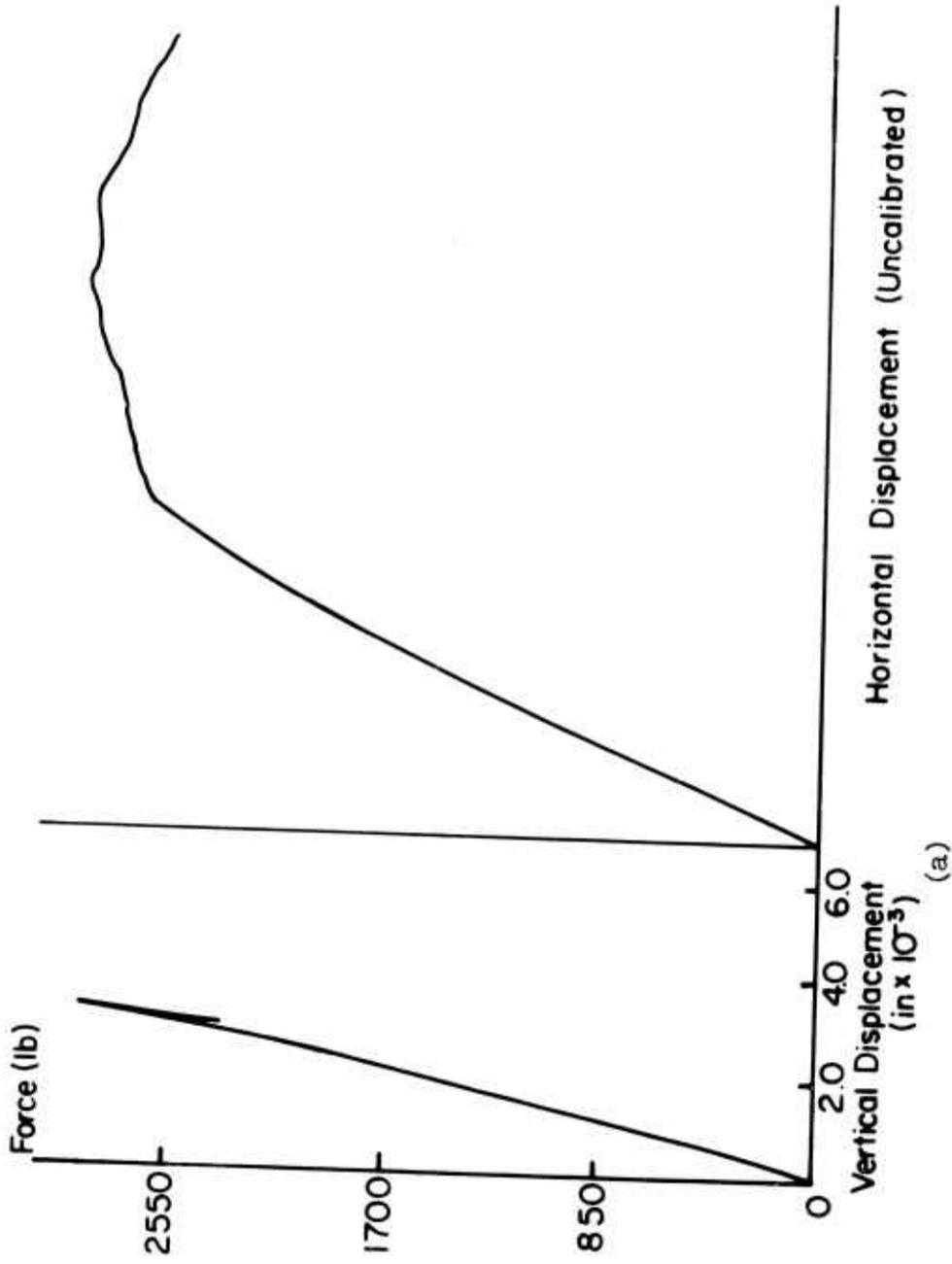
Figure 2.39: Experimental results of controlled failure of charcoal grey granite rings and discs. (a) Ring test large hole.
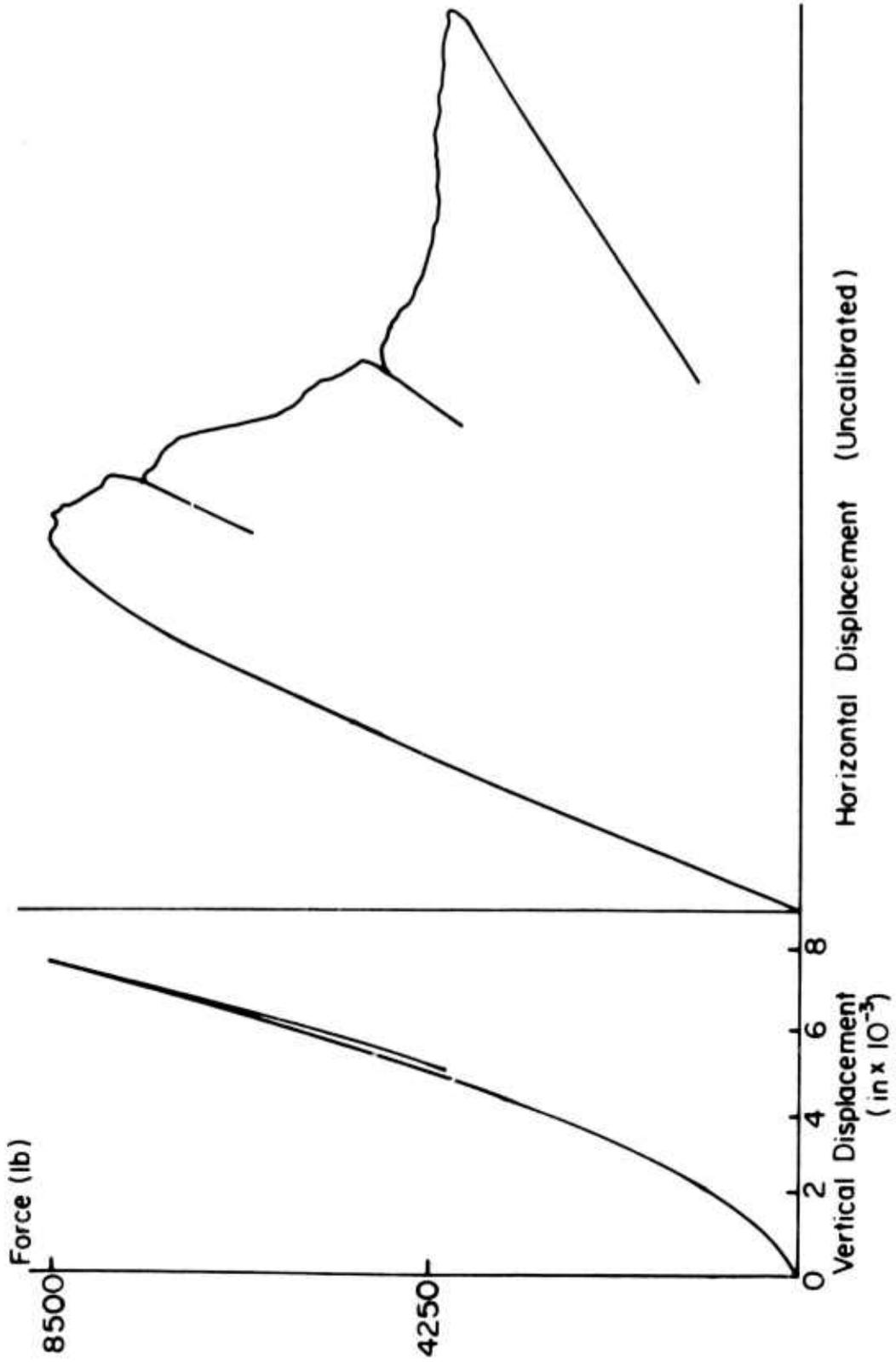
Figure 2.39: Continued: (b) Ring test small hole.
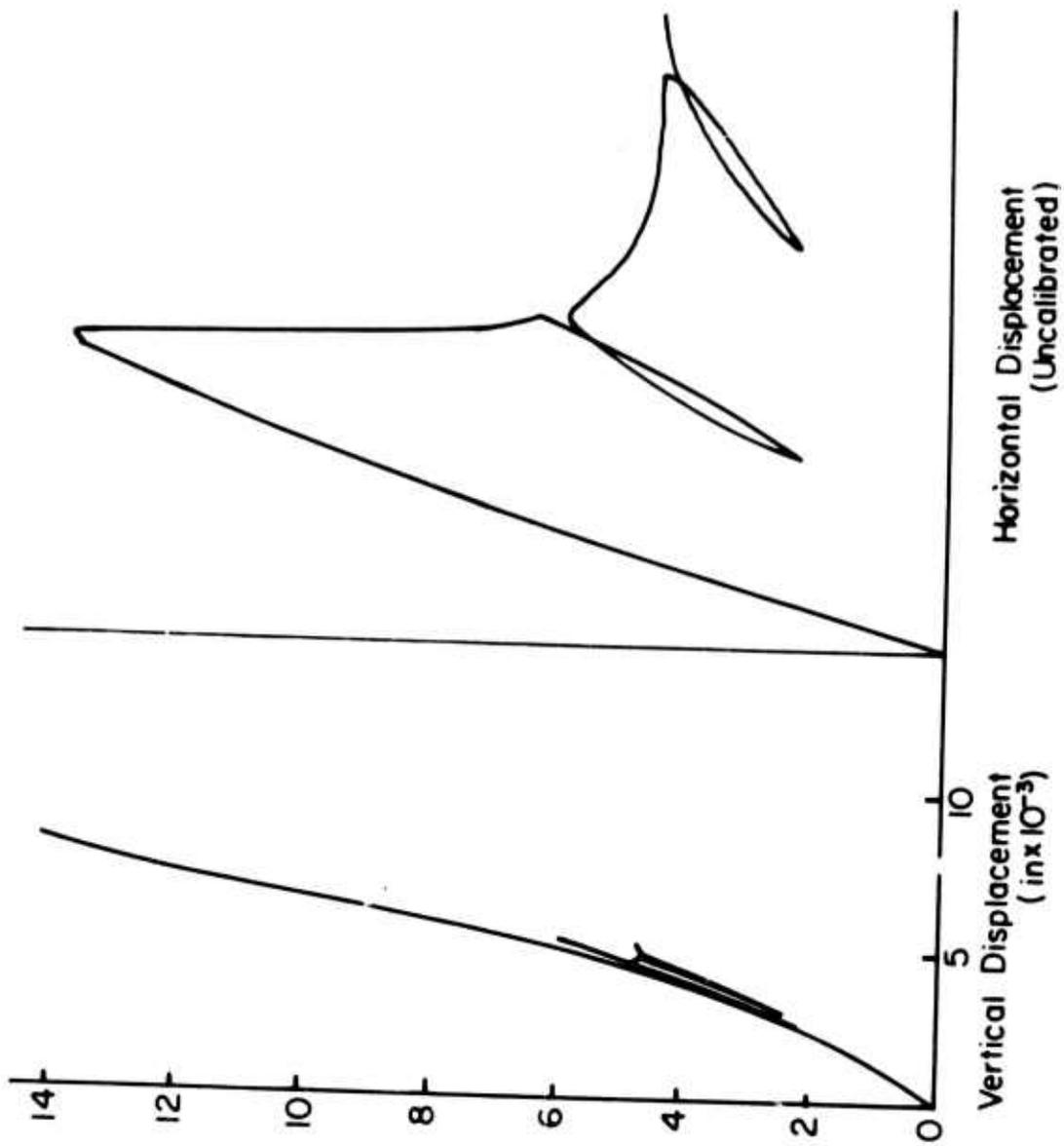
Figure 2.39: Continued: (c) Disc (no hole).
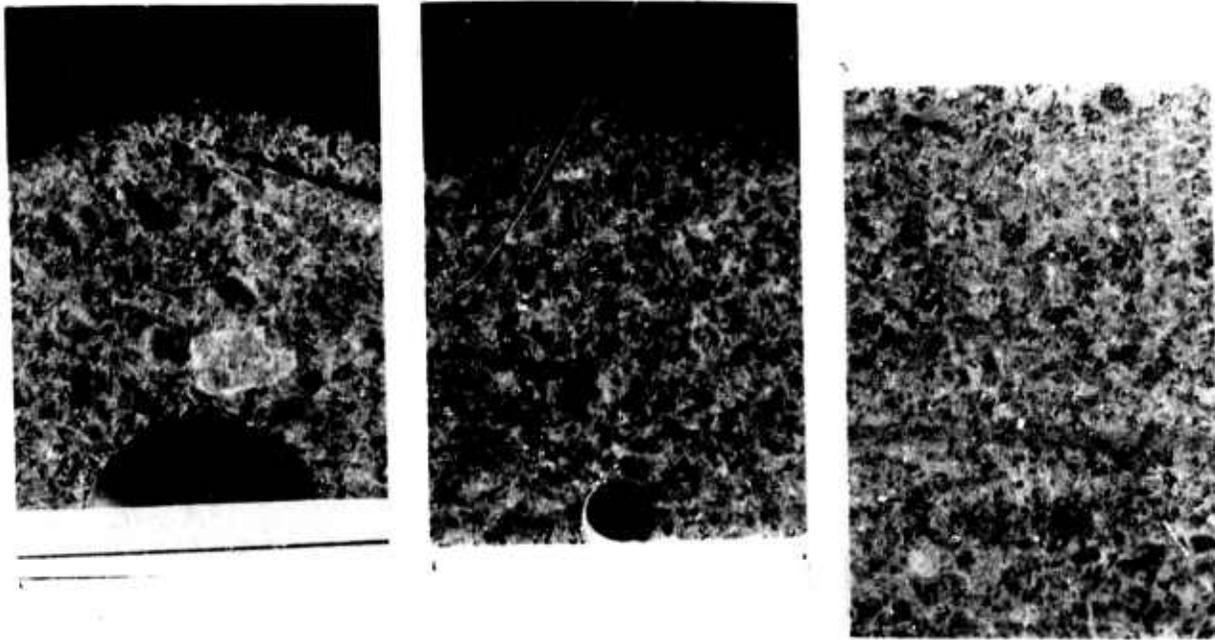
Figure 2.40: Photograph of Cracked Granite Rings.
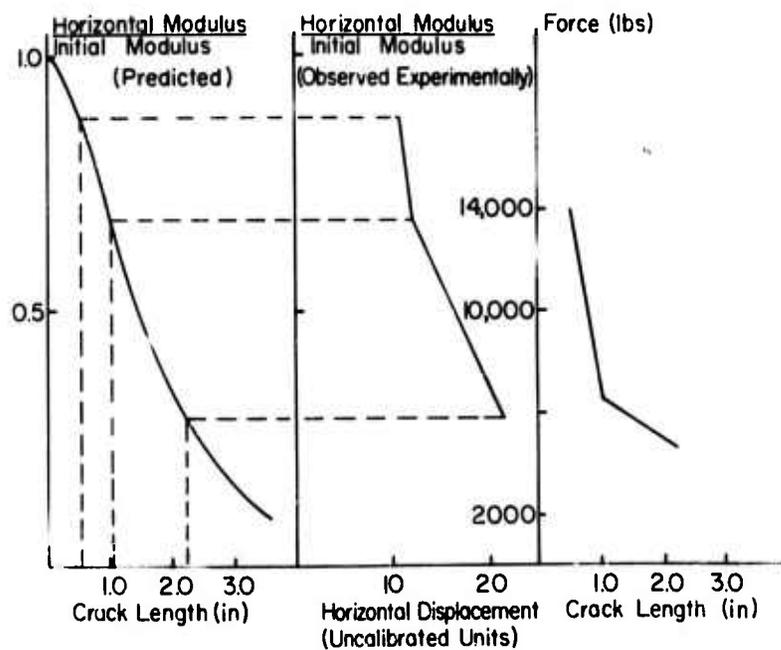
Figure 2.41: Determination of Crack Length in Cracked Granite Disc.

CHAPTER 3

PROGRESSIVE COLLAPSE OF SIMPLE BLOCK-JOINTED SYSTEMS

Introduction

This paper describes the initial phase of an investigation which it was hoped would be developed to include general polyaxial loadings. This work was proposed after an extensive review of the literature pertaining to the failure of block jointed systems, this review is presented in Appendix I.

The present concern is with the simplest possible loading pattern, uni-axial compression. This was chosen as the first step in the program because, despite its' apparent simplicity, and some might argue triviality, it provides the opportunity to develop experimental techniques and study at least one load-ing situation in some detail. As more complicated loadings are applied, it becomes necessary to contain the specimen in a test vessel of some kind so that it is no longer possible to observe the specimen directly as can be done in uniaxial compression. Thus the uniaxial compression test can be used to obtain data on mechanisms of deformation and fracture which may not be obtainable from other types of tests.

Taking the decision that all specimens would be tested in uniaxial compression automatically eliminated certain specimen configurations from the program. Speci-mens containing throughgoing joints for example, will be unstable under self-weight when the inclination of the joint to the horizontal exceeds the angle of friction of the joint (for smooth joints with zero "cohesion"). The case of slip on a continuous joint is further complicated by the need to provide for lateral trans-lation at the specimen ends if the effect of unknown later restraining forces are to be eliminated (Ref. 1, 2). Because of these factors, the case of a system containing sets of continuous inclined joints was not included in this program of uniaxial compression tests.

Without exception, previous model tests have been carried out using conventional or "soft" loading systems. This has been a serious impediment to the complete study of failure mechanisms involving brittle fracture. The question of machine-specimen interaction has been accorded due attention in the recent literature (e.g. Refs. 3, 4, 2) and its' significance need not be repeated here. The experiments reported herein were carried out in a servo-controlled testing system which permitted control and detailed study of the fracture process in a manner not previously possible.

In the past, little attention has been given to the measurement of deformations in general, and volume changes in particular. The limited evidence available, most notably that obtained by Rosenblad(Ref. 5), suggests that in a block-jointed mass, the gradients of principal strain magnitudes and directions are much larger and more unpredictable than those in an intact block of the same material under identical loading. It seems imperative, therefore, that attention should be given to the accurate recording of deformations in any basic investigation.

EXPERIMENTAL METHOD AND RESULTS

Experimental Model Material

The material used was a high strength gypsum plaster specifically chosen because of its very brittle nature. One of the many difficulties encountered in attempting to produce an exact material model of a given rock mass is that the resulting model material is usually very soft (Ref. 6, 7), and so cannot accurately reproduce the brittle post-peak behaviour of the prototype rock (Refs. 1, 2). In the present case, no attempt was made to accurately model any particular rock mass, the investigation being regarded as a very general one with the inherently brittle nature of the material being a prime consideration.

The model material was produced by mixing plaster and water in the ratio of 1:0.35 by weight, stirring in a mechanical mixer for 5 minutes, pouring into specially designed steel moulds, vibrating gently to remove entrapped air bubbles, and following initial setting and stripping of the moulds, curing in an oven at 40°C until constant weight was achieved.

Three types of unit block were produced:

(a) 4-in. x 4-in. x 8-in. (10.3 cm x 10.3 cm x 20.5 cm) rectangular prisms (the unjointed specimens),

(b) 1-in. x 1-in. (2.5 cm x 2.5 cm) square x 4-in (10.3 cm) long blocks,

(c) blocks with a hexagonal cross-sectional area of 1-in^2 (6.5 cm^2) and 4-in. (10.3 cm) long.

These unit blocks were arranged to form four specimen types:

1) Unjointed specimen (solid)
2) Square blocks (SO specimens)
3) Hexagonal Blocks at 60° (H60)
4) Hexagonal Blocks at 30° (H30)

which are illustrated in figure 3-1. All specimens were 4-in. x 4-in. x 8-in. (10.3 cm x 10.3 cm x 20.5 cm) rectangular prisms. The use of these four specimen types permitted the investigation of block-jointed systems with two dimensional extents of jointing of zero, one third and one. Two additional tests were conducted containing transverse holes, these two specimens are shown in Figure 3-1.

Experimental Apparatus

The University of Minnesota's 1 million lbs. (4.45 MN) closed look servo-controlled testing system was used to apply the axial load to the specimens. Axial deformations were monitored by a pair of strain gauged cantilever devices, the output from which was used as the feedback signal. A digital ramp generator was used to program axial strain to increase at a fixed rate.

X-Y plots of axial load against axial deflection were obtained as experimental output. Values of axial deflection so obtained were corrected for the effects of

compression of the various steel components in the loading system, these corrections having been pre-determined in a series of calibration tests.

In some tests, a second set of cantilevers was mounted laterally on the specimen to monitor lateral deformations. While not giving a true measure of the total lateral component of volumetric strain of the specimen, these results were used to give some qualitative indication of the volume changes to be expected in block-jointed systems.

A simple, but apparently effective system was devised for transmitting machine load to the specimen uniformly over its top and bottom surfaces. This system consisted of a 4-in. (10.3 cm) square x 0.25-in. (0.64 cm) thick copper "flat-jack" filled with oil and sealed, a steel platen which constrained the flat-jack laterally and through which the machine load was applied, and 64 ground, one-half inch cubical steel pieces through which the load was transmitted to the specimen must have been closely uniform (this loading system is diagramatically shown in figure 3-2, and an actual photo loading system after a test can be seen in figure 3-4).

During each test, 25-30 photographs were taken at regular intervals in relation to the complete load-deflection curve so that a detailed record of the behaviour of specimens would be available for subsequent analysis.

Progressive Collapse mechanisms

Unjointed Specimens

Ten photographs showing progressive collapse of one of the solid specimens, together with the associated complete load-axial deflection curve are shown in figure 3-3.

The curve is linear up to 80% of the peak load where the first of many local peaks occur. The first visible fracture occurred at the side of the specimen (photograph 2 in figure 4-2) at about 70% of peak load but was not reflected by a change in slope of the load-deflection curve. The next cracks to appear developed just before the peak load was reached (point 3) and, like the first crack, were clearly axial and very much longer than the cracks observed in most rocks tested under similar conditions. The fact that the cracks which developed in this and other specimen types were generally axial, point to similarity between the behaviour of the plaster and that of rock. Recent research into the brittle fracture of rock has shown that at low ambient pressures, fracturing in rock primarily occurs parallel to the direction of the major principal stress, and that the shear fracture commonly assumed to be dominant is, in fact, a secondary feature (Refs. 3, 4, 8, 9).

A notable feature of the load-deflection curve obtained for this and other solid specimens is the sudden drop in load which occurs in the immediate post-peak region. It would appear that this results from the very rapid propagation of a fracture which is not detected and arrested by the servo-control system until the load bearing capability of the specimen has been significantly reduced. It should be noted that in tests previously carried out on similar specimens in a conventional hydraulic testing machine (Refs. 10, 11), explosive fracture of the specimens occured at this point.

The brittleness of the plaster as indicated by the steepness of the load-deflection curve in the immediate post-peak region, probably results from its' fine-grained and relatively homogeneous structure. In this regard, the behaviour of this material in uniaxial compression is similar to that of some fine-grained rocks such as Solenhofen limestone, basalt and fine-grained granites in which fractures has proven difficult to control even with the most advanced techniques (Ref. 3, 4, 9).

With continued deformation beyond the peak load, the load-axial deflection curve shows a series of local peaks, each followed by a sudden drop off in load. Each of these reductions in load results from the rapid propagation of a crack which is not immediately detected by the servo-system operating in axial strain control. Following each of these local load reduction, the load on the specimen is less than that which the specimen can sustain at that point. Consequently, when further energy is supplied to the system via the servo-controlled hydraulic pump, an increase in load occurs. As deformation continues and the mean load on the specimen steadily decreases, the magnitude of the local oscillations in load reduces until a smooth curve finally results. This occurs because, at the lower loads, there is less energy stored in the specimen to drive the propagating cracks which can then be controlled at an earlier stage of their development. Similar behaviour was observed in the SO and H60 models.

Square Blocks (SO)

The load axial deflection curve for one of the SO specimen and the associated photographs illustrating the progressive failure of this specimen are given in figure 3-4.

The first fractures observed in this test appeared in the extreme upper left-hand and lower right-hand blocks at a load slightly less than the peak (see photograph 2). In the region of the peak further axial cracking developed causing a rapid reduction in load to 66% of the peak value. At this point, no major through-going fractures had appeared, fracturing being a comparatively localised phenomenon.

At about this stage, the short shear plane shown in the upper left-hand block in Photograph 5 developed. To accommodate shear deformation along this fracture, the left-hand column of blocks progressively rotated in an anti-clockwise direction causing the left-hand vertical joint to open progressively along its length from bottom to top. With the development of this mechanism, load was transferred from the left-hand to other columns of blocks, ultimately resulting in severe axial cracking and total collapse of the right-hand column.

Obvious differences between the behaviour of this block-jointed specimen and the solid specimen are that individual cracks are shorter in the jointed specimen, being generally confined to within single blocks, and that the presence of jointing permits rotation of blocks or columns of blocks with associated local concentrations and reductions in load not found in the solid specimen.

Hexogonal Blocks at 60° (H60)

Eleven photographs showing progressive break-down of the central section of one of the H60 specimens together with the associated complete load-axial deflection curve are shown in figure 3-5. A latex rubber membrane orginally placed around

the specimen for added stability during setting up was cut at approximately 2-in. from either end of the specimen so that the middle 4-in. could be photographed.

The load-axial deflection curve obtained for this specimen is linear up to 93% of the peak load when the first observable cracks appeared and a small local reduction in load occured. These cracks (photograph 2) were vertical or sub-vertical and did not propagate from block to block across horizontal joints. In some cases the cracks extended to these horizontal joints, while in others they did not reach the boundaries of the block, suggesting that they were initiated somewhere near the center of the block. This observation is supported by the results of a stress analysis of hexagonal blocks carried out using the finite element method. Lateral tensile stresses of up to 17% of the applied pressure are developed at the center of the hexagon. Approximately 56% of the cross-sectional area of the hexagon carries a lateral tensile stress. Towards the loaded faces the stress field becomes entirely compressive, giving some idnication of why fractures initiated near the centers of blocks. Even a cursory examination of the fracture surfaces showed that these and almost all other fractures produced in the investigation were of a tensile rather than shear nature. The fine white powder characteristically produced when shear movements take place between surfaces in this plaster was notably absent in all but the few isolated cases referred to elsewhere.

A second major mechanism observed in these tests was the progressive opening of the inclined joints which developed with increasing axial deflection. This contributed significantly to the development of large lateral deflections and resulted in an increased tendency for the specimen to act as a number of independent columns.

In the post-peak region of the curve (photograph 4) a third mechanism which has some influence on the ultimate behaviour of the specimen appeared. This was shear displacement of one half of a cracked block with respect of the other half. This generally resulted in the displaced portion of the block becoming wedged into a lower inclined joint causing further opening of that joint and eventual rotation of the outer adjacent block.

As the axial deflection was increased and the load-bearing capability of the specimen decreased further, existing cracks widened, new cracks developed and joints continued to open. Associated with this progressive breakdown of the specimen was the development of quite large lateral deflections. At points 3, 6 and 9, for example, the lateral extensions were measured as 2, 6 and 10 times the corresponding axial deflections. Obviously, the number of degrees of freedom associated with behaviour of jointed and unjointed specimens. Any attempt to mathematically analyse the complete behaviour of blocky discontinua must necessarily take this factor into account if it is to be successful (e.g. Ref. 12).

Hexagonal Blocks at 30° (H30)

The behaviour of the H30 specimens as illustrated in Figure 3-6 varies considerably from that of the other specimen types tested. The form of the load-deflection curve differs from that recorded in other tests, and the peak load-bearing capability is quite low.

The first visible cracks appeared in 3 blocks at approximately 20% of the peak load, while at the peak, cracks had developed in approximately two-thirds of the blocks included in the photographs. These cracks differ from those developed in other specimen types in that they were generally curved and ran from one inclined face of a hexagon to another, rather than being straight and vertical or sub-vertical. These differences in crack development must arise from differences in the distribution of stresses within the unit blocks. It is apparent that in the H30 case, the axial compressive load msut result in the application of shear as well as normal stresses to the inclined surfaces of the hexagonal blocks. Thus the internal distribution of stresses could be expected to be quite different from that in the blocks in the H60 type specimens were a normal load applied to two opposite faces of the hexagon is the fundamental loading case.

The second essential feature of the deformational behaviour of this specimen was the progressive opening up of vertical joints from the very beginning of load-ing. Obviously, this can only result from slip on the inclined joints or, in some cases, rotation of isolated blocks. The slip on inclined joints and associated opening up of vertical ones resulted in the formation of stepped "shear" planes having a mean orientation of 60° to the base of the specimen. Despite the obvious significance of this slip mechanism, the lateral deflections measured were not as great as those in the H60 specimens. At the maximum axial deflection reached in the test represented in figure 3-6, the lateral expansion was three times the axial contraction. In the H60 specimen, the lateral expansion was twenty times the axial contraction at the same vlaue of axial deflection.

Block Jointed Models Containing Transverse Holes.

Figure 3-7 shows the observed load axial displacement for the hexagonal blocks containing a transverse hole, and the associated photographs illustrating the failure development.

Later expansion seemed to develop as load was applied, with some splitting of the block adjacent to the hole occurring before the peak load carrying capacity was reached. Subsequently, splitting occurs in the opposite block and slippage along the inclined surfaces of the blocks results in considerable dilation. Even-tually, two well formed cores of essentially undestorted wedges move into the opening illustrating the confirming or restrictive nature of the end condition to large lateral deformations.

Comparative Peak Strengths:

It is obvious from the experimental evidence presented that the peak load reached in the deformational history of a specimen is not associated with the devel-opment of any particular fracture of slip phenomenon, i.e. fracture or slip does not occur at that point alone. Thus the peak load would appear to be of little consequence from a mechanistic viewpoint other than for the fact that it marks the point at which the slope of the characteristic to be followed by the machine changes from positive to negative. Nevertheless, the peak strength is significant engineer-ing parameter and should be studied in its own right. The peak laods sustained by specimens tested in this program are listed in Table 3.1.

It should be noted that the dramatic reduction in strengths of the jointed specimens below that of the unjointed specimens has been obtained using specimen

types in which slip along a critically oriented and continuous joint plane was not the mechanism of "failure" involved. Rather, it was obtained using specimens in which fracture of the model material was the prinicpal mechanism operating. The observed differences in load-bearing capability almost certainly arise from differences in the stress distributions produced in specimens with different joint patterns. This sounds the significant practical warning that the influence of jointing on the strength of rock masses should not be disregarded even when limit equilibrium methods of analysis (Refs. 13, 2) indicate that one of the joints are critically oriented for slip.

TABLE 3.1

Specimen Type	Peak Loads, lbf. (kN)	Mean Peak load, lbf. (kN0	Equivalent average axial stress, lbf/in^2 (MNm^{-2})
SOLID	79,000 (352) 78,000 (347) 76,400 (340)	77,800(346)	4,860 (33.5)
SO	42,100 (187) 58,800 (262) 44,600 (198)	48,500(216)	3,030 (20.9)
H60	21,000 (93) 25,800 (115) 29,300 (130)	25,400 (113)	1,590 (11.0)
H30	5,500 (24.5) 4,960 (22.0) 6,020 (26.8) 6,090 (27.1)	5,640(25.1)	350 (2.4)

CONCLUSIONS

The collapse of simple block-jointed systems prepared from a brittle material and tested in uniaxial compression is a progressive phenomenon involving several possible mechanisms including

a) Fracture of individual blocks, generally in extension,
b) rotation of individual blocks,
c) collapse of columns of blocks by rotation or buckling,
d) slip on joint planes,
e) shear deformation of individual blocks, generally along fracture surfaces.

The relative importance of these mechanism varies with the orientation and continuity of joint sets and with the shape of unit blocks. The fact that fractures generally develop parallel to the direction of the major principal stress is of considerable significance and must be accounted for in any acceptable theory of failure.

The peak load bearing capability of specimen varies with the joint pattern and shpae of unit blocks. Even when fracture of blocks is the dominant break-down mechanism, strengths of jointed specimens can be considerably lower than those of unjointed specimens. This feature of the behaviour of jointed media is seen to be the result of the vastly different distribution of stresses which can exist in blocks of different shapes and orientations. Shears and moments which do not exist in unjionted specimens can be easily set up in jointed media. Any initial lack-of-fit, an inherent feature of natural rock masses, will add to the inhomogeniety of the distribution of stresses with blocks.

Deformability of jointed media is largely a function of the degree to which slip can occur on joint planes. Vertical joints, although not directly involved in slip mechanisms, can open and so add to lateral deformations. The very large lateral deformations estimated from the results of uniaxial compression tests carried out in this program are probably of little practical significance since in most engineering situations the applied loading will be biaxial or polyaxial so that some degree of constraint will be offered. Future work will involve investigation of these situations.

Theoretical or predictive approaches to the problems under consideration must take into account all aspects of the discontinuous nature of jointed media if they are to produce realistic results. In particular, the fact that some blocks are free to both rotate and translate must be recognized. These mechanisms not only influence displacements but can also give rise to major redistributions of stresses within blocks.

REFERENCES

1. ROSENGREN, K.J., - Rock Mechanics of the Black Star Open Cut, Mount Isa. Thesis (Ph.D.) Australian National University, 1968.
2. JAEGER, J.C., - Friction of Rocks, and Stability of Rock Slopes. Geotechnique, Vol. 21, No. 2, June 1971, pp97-134.
3. WAWERSIK, W.R. and C. FAIRHURST, - A Study of Brittle Rock Fracture in Laboratory Compression Experiments. Int. Journal Rock Mechanics and Min. Sciences, Vol. 7, No. 5, September, 1970, pp561-575.
4. BROWN, E.T., - Brittle Fracture of Rock at Low Confining Pressures. Proc. First Aust. - N.S. Conf. Geomech., Melbourne, 1971, Vol. 1, pp31-36.
5. ROSENBLAD, J.L., - Failure Modes of Models of Jointed Rock Masses. Proc. Second Congress Int. Soc. Rock Mechanics, Belgrade, 1970, Vol. 2, Paper 3-11.
6. BARTON, N.R., - A Model Study of the Behaviour of Steep Excavated Rock Slopes. Thesis (Ph.D.) University of London, 1971.
7. STIMSON, B., - Modelling Materials for Engineering Rock Mechanics and Min. Sciences, Vol. 7, No. 1, January 1970, pp77-121.
8. RUMMEL, R., and C. FAIRHURST, - Determination of the Post-Failure Behaviour of Brittle Rock Using a Servo-Controlled Testing Machine Rock Mechanics, Vol. 2, No. 4, December 1970, pp 189-204.
9. HUDSON, J.A., BROWN, E.T. and C. FAIRHURST, - A Method of Optimizing the Control of Rock Failure in Servo-Controlled Laboratory Tests. Rock Mechanics, Vol. 3, No. 4, December 1971, pp217-224.
10. BROWN, E.T. and TROLLOPE, D.H., - Strength of a Model of Jointed Rock. Proc. A.S.C.E., Jour. Soil Mechanics and Foundation Div., Vol. 96, No. SM2, March 1970, pp685-704.

11. JOHN, K.W., - Engineering Methods to Determine Strength and Deformability of Regularly Jointed Rock. In Rock Mechanics - Theory and Practice, Proc. Eleventh Symp. Rock Mechanics, New York, A.I.M.E., 1970, pp69-80.

Figure 3.1: Specimen types tested under uniaxial loading.
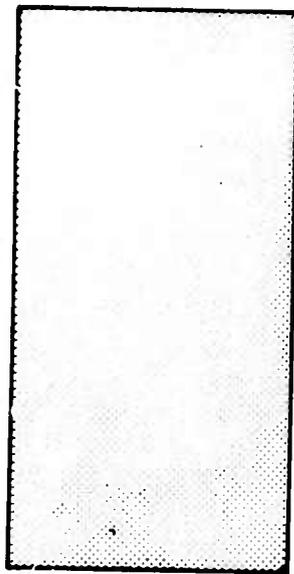
Solid
(a)
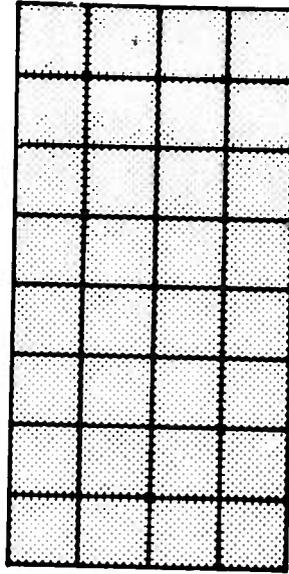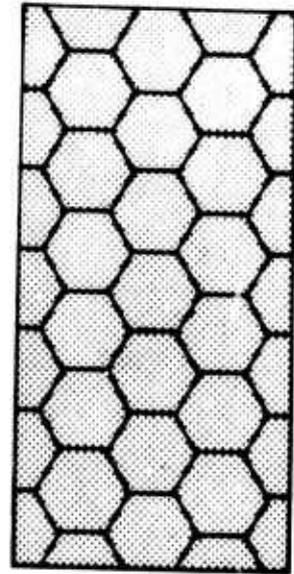
Square
(b)

Hexagonal (60°)
(c)
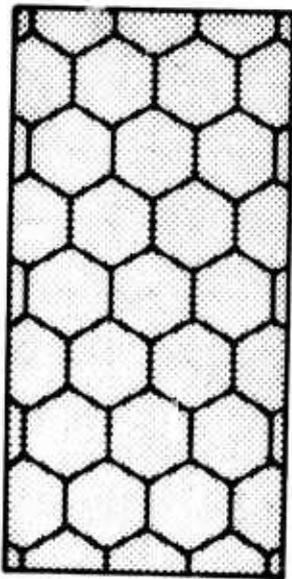
Hexagonal (30°)
(d)
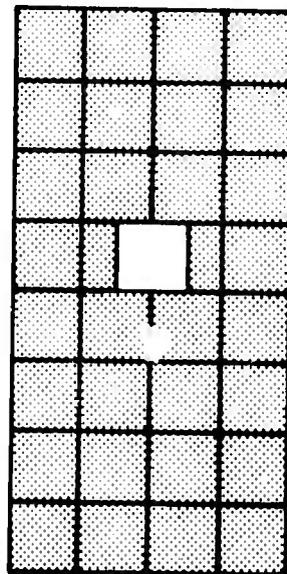
Square with Hole
(e)
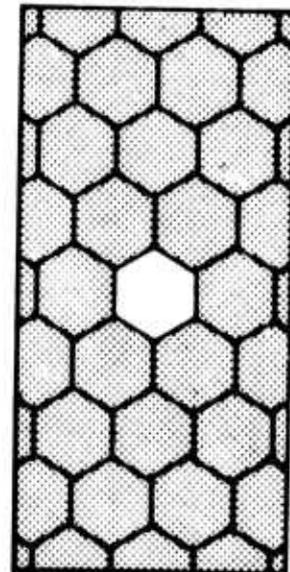
Hexgonal with Hole
(f)
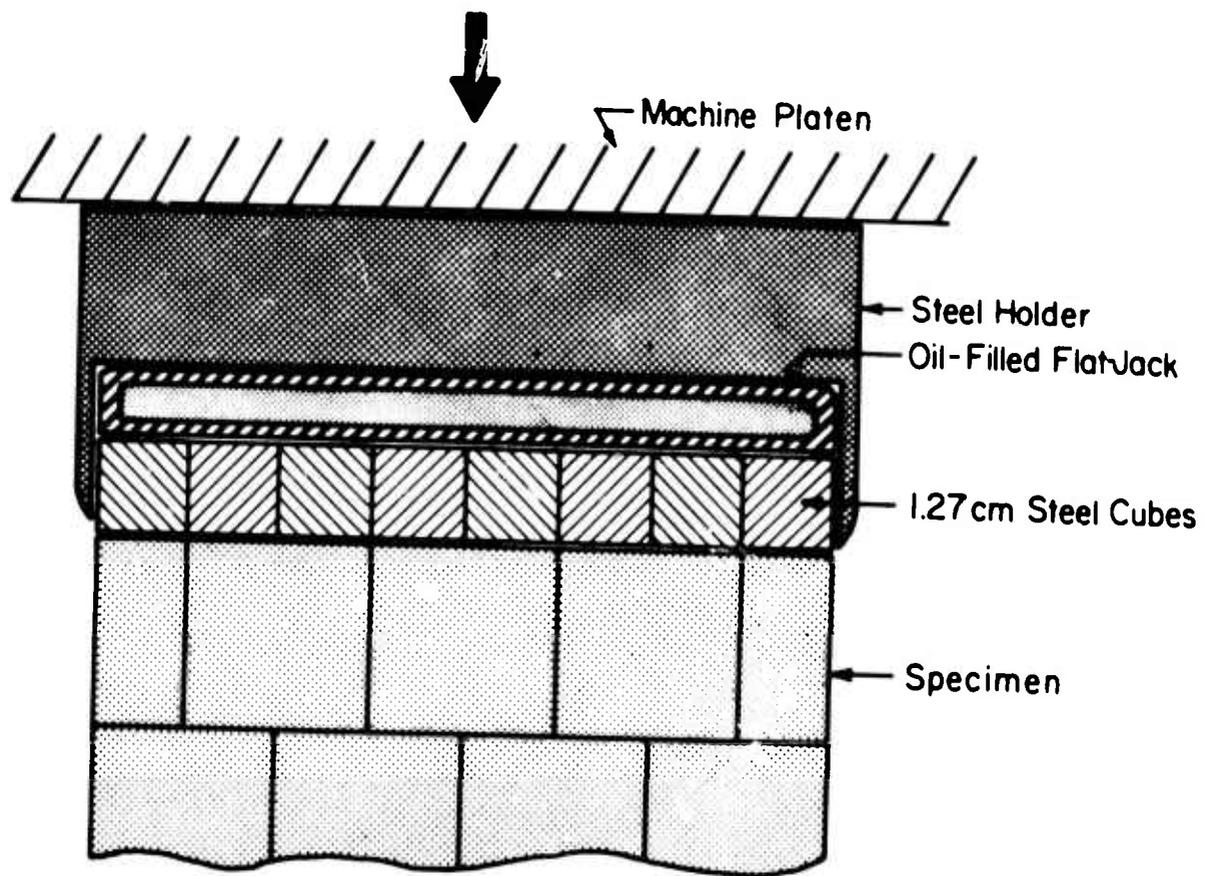
Figure 3.2: Loading system to ensure the application of a uniform load.
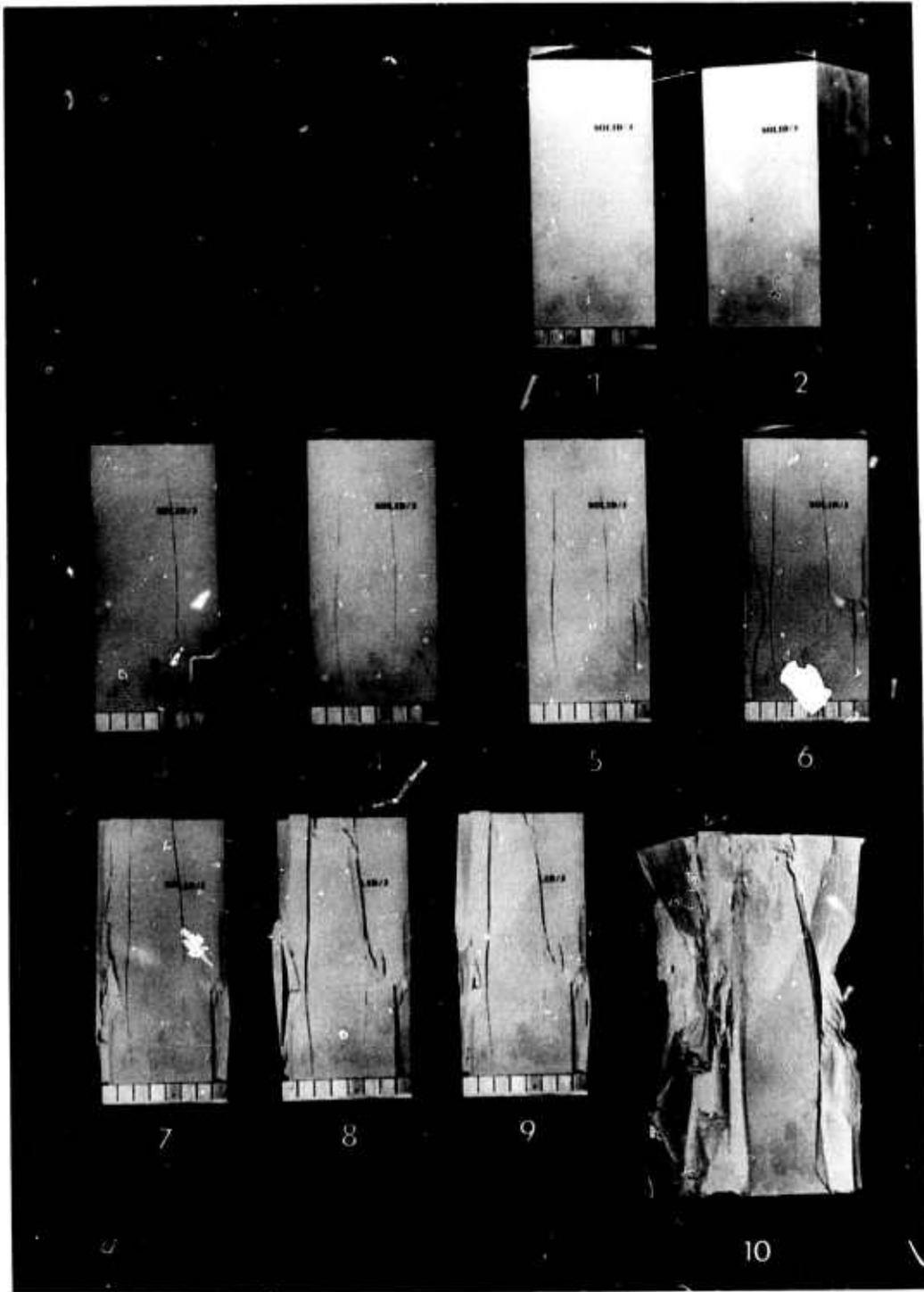
Figure 3.3: Experimental output for solid block.
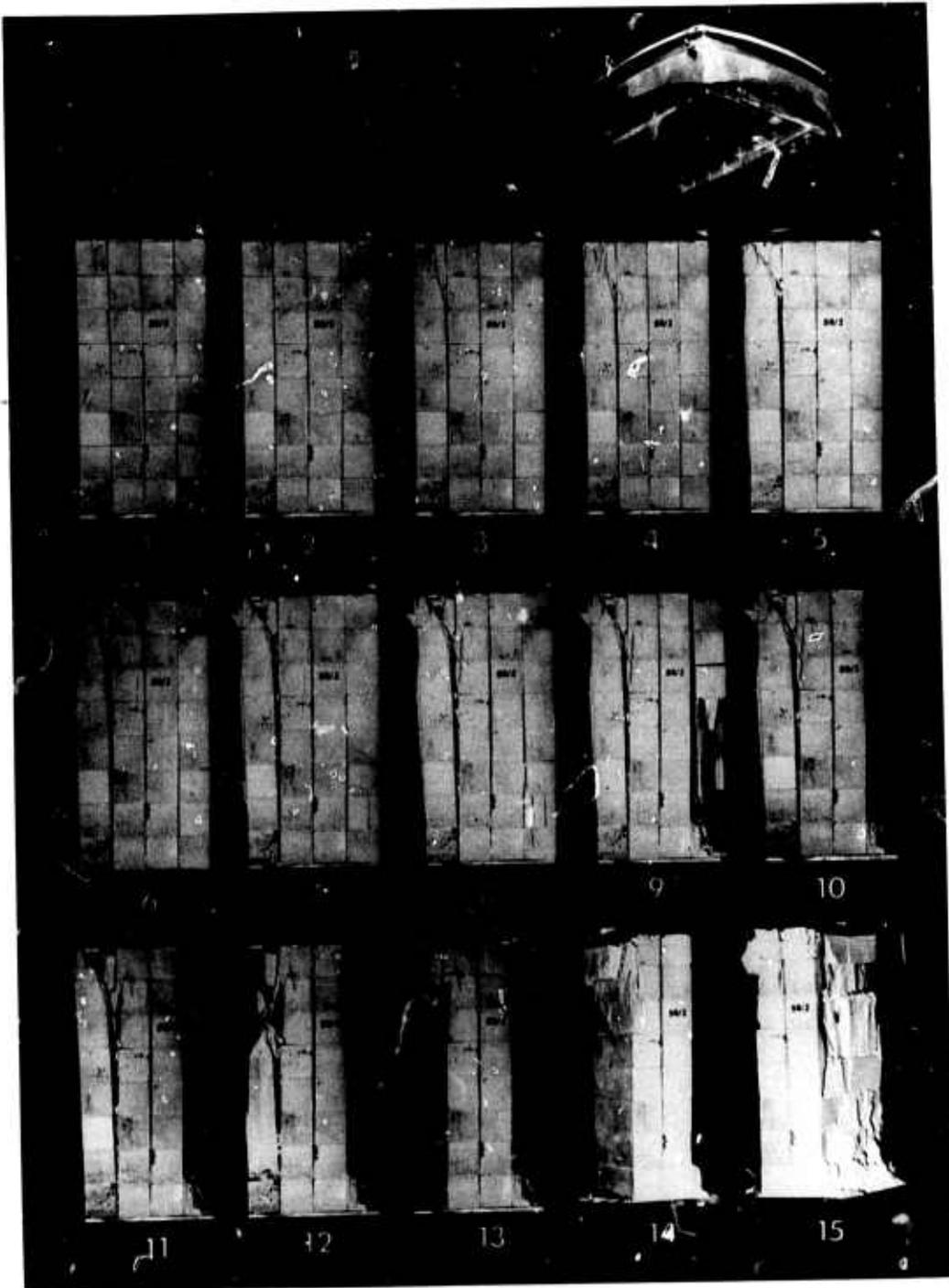
Figure 3.4: Experimental output for square blocks.
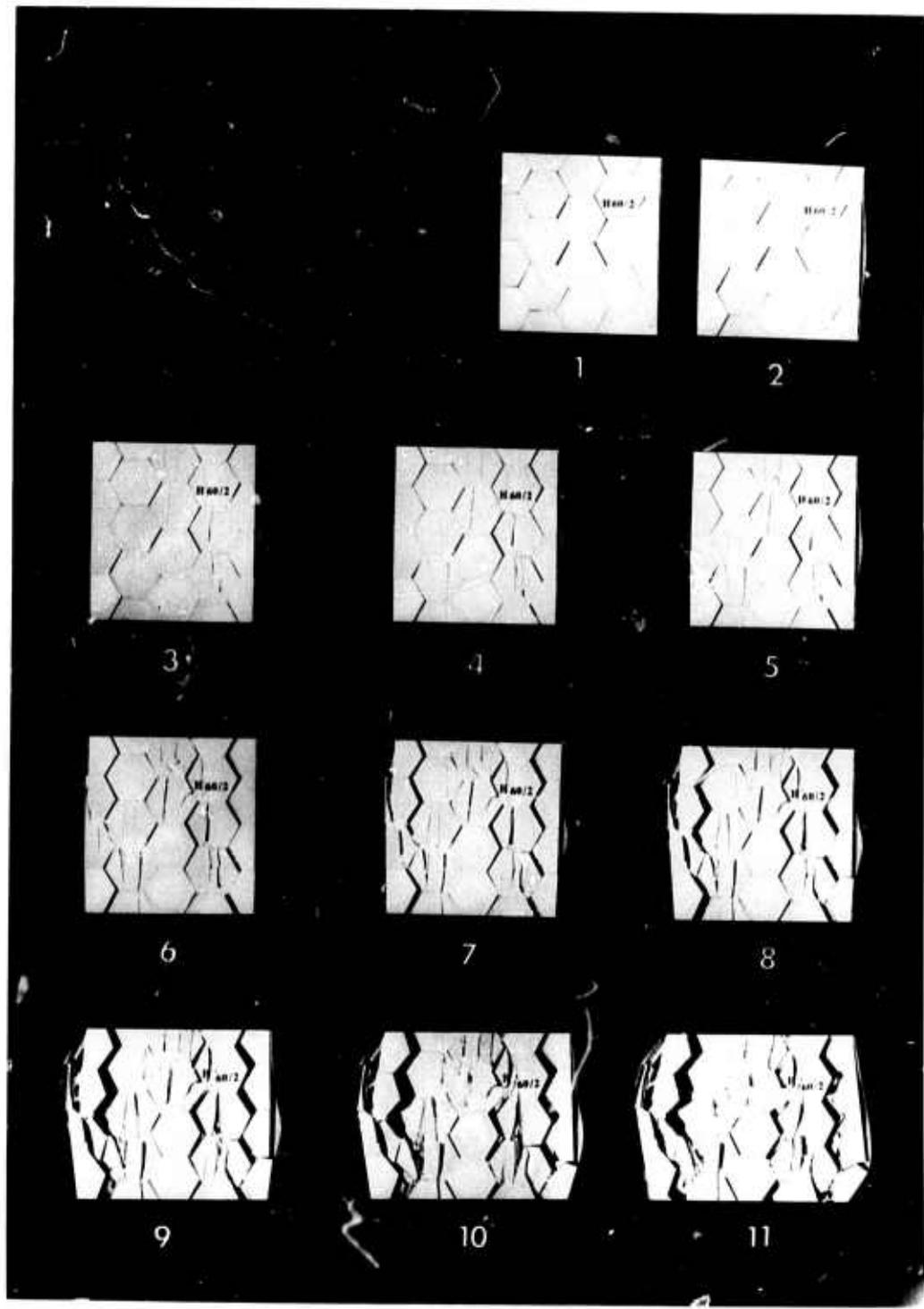
Figure 3.5: Experimental output for hexagonal blocks inclined at 60°.
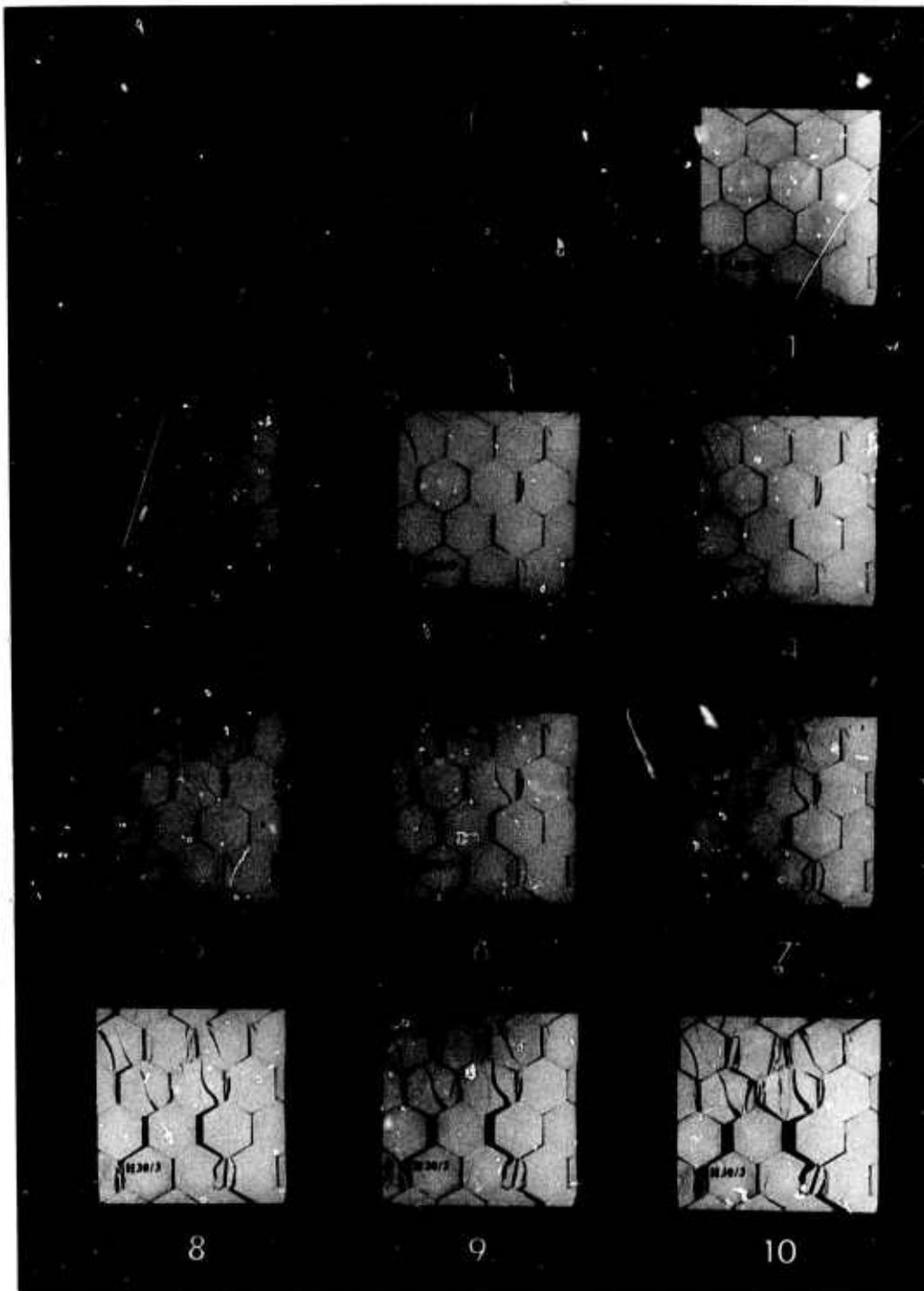
Figure 3.6: Experimental output for hexagonal blocks inclined at 30°
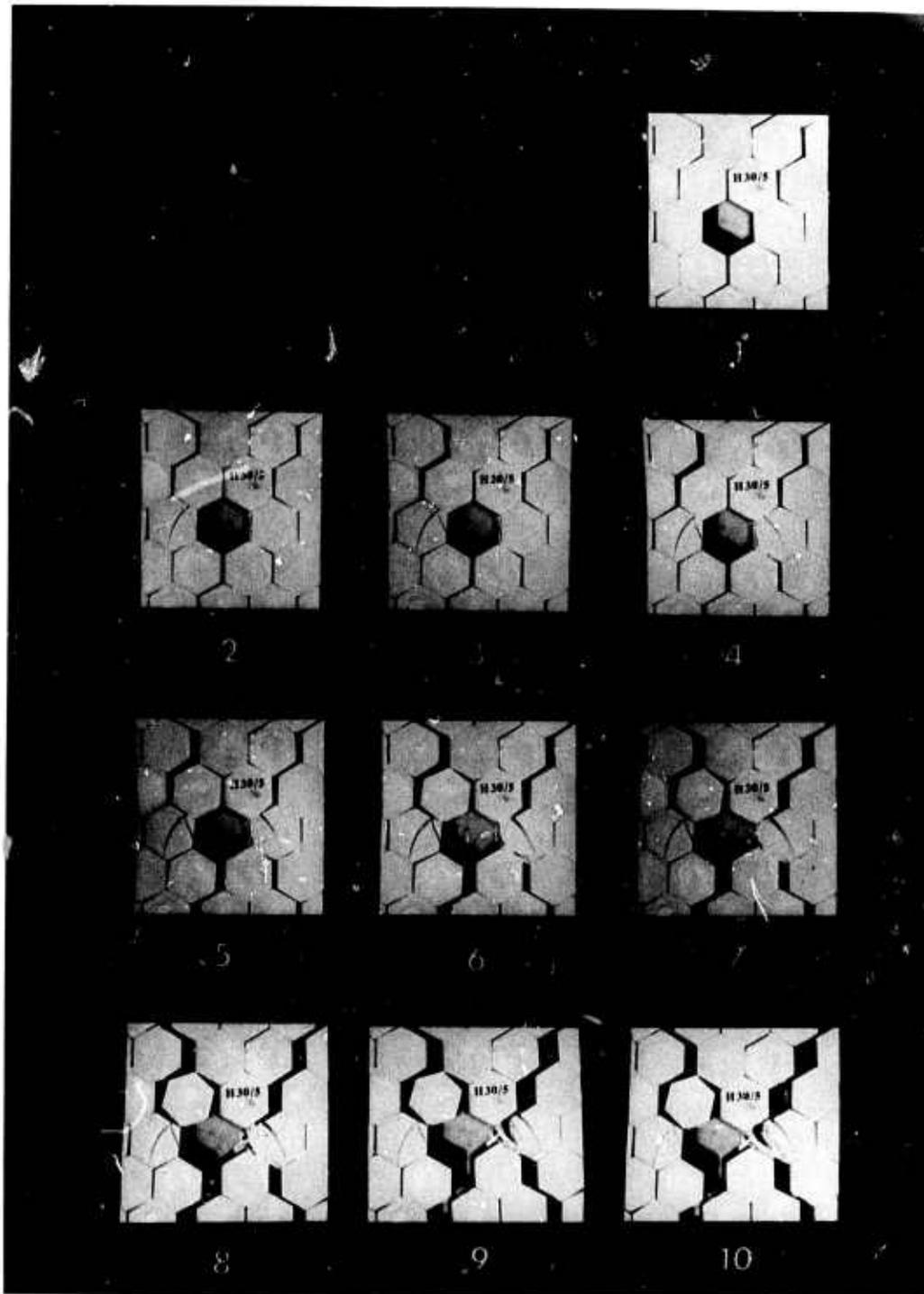
Figure 3.7: Experimental output for hexagonal blocks with a hole.

CHAPTER 4

VOLUMETRIC STRAINS IN TRIAXIAL COMPRESSION TESTS ON BLOCK JOINTED MODELS

Introduction

Previous phases of this investigation have been concerned with the behaviour of block-jointed systems under uniaxial stress. Although these studies have proven useful in identifying possible collapse mechanisms in jointed media and pointing to major differences in the mechanical behaviour of jointed and unjointed rock, they are of limited practical value because the loading pattern used in one rarely met in practice.

As an initial stage in the investigation of the behaviour of jointed rock masses under general polyaxial stress, a series of "triaxial" compression tests in which the intermediate and minor principal stresses are equal, were carried out on idealized block-jointed models. Recent studies of the behaviour of intact rock in triaxial compression have shown that volumetric strain measurements provide a sensitive indicator of the initiation and subsequent growth of cracks in rock[1-3]. In carrying out such studies, Crouch[2] developed a reliable and accurate method for measuring volumetric strains. It seemed that there was much to be gained by applying this method to block-jointed models in which volumetric strains must assume considerable significance because of the previously demonstrated tendency of block rotation, joint slip and opening of joints under load.

EXPERIMENTAL PROGRAM

Tests were carried out on idealized models of jointed rock prepared from gypsum plaster using techniques described elsewhere. All specimens were rectangular prisms approximately 8 in. (20.3 cm) high by 4 in. (10.2cm) square. Four specimen types were tested.

   a)   SOLID specimens cast as one block to simulate unjointed rock.

   b)   SO specimens prepared from 4 in. (10.2 cm) long by 1 in. (2.54 cm) square blocks such that they contained two sets of mutually perpendicular joint planes oriented parallel to the boundaries of the specimens.

   c)   H60 specimens prepared from hexagonal blocks such that they contained three sets of intermittent joints oriented at angles of 60°, 60° and 0° to the base of the specimen.

   d)   H30 specimens prepared from hexagonal blocks such that they contained three sets of intermittent joints oriented at angles of 30°, 30° and 90° to the base of the specimen.

These specimen types are illustrated in Figure 4-1.

Triaxial compression tests were carried out on each of these specimen types at confining pressures of 50 lb/in^2 (345 kNm^{-2}) and 250 lb/in^2 (1724 kNm^{-2}). These low confining pressures were used because the brittle - ductile transition pressure

of the plaster used as a model material is quite low, and it was considered important that brittle rather than ductile behaviour should be investigated. Furthermore, confining pressures are low in many engineering situations of practical interest (e.g. around some underground openings and in slopes).

EXPERIMENTAL TECHNIQUE

Tests were carried out in the closed-loop electro-hydraulic testing system described previously. Specimens were enclosed in a specially constructed triaxial test vessel. Axial loads were applied to the specimens via a 3.0 in. (7.62 cm) dia. high tensile strength steel ram and the loading heads described elsewhere. Latex rubber membranes sealed to the loading heads with O-rings were used to isolate the specimens from the oil under pressure in the test vessel. Axial loads applied to the specimens were monitored by a load cell placed between the ram and the upper platen of the testing machine. Total axial deformation of the specimen and the loading system, used as the feedback signal through which experiments were controlled, was measured by two LVDT's connected in series. In all tests, continuous plots of differential axial load against total axial deformation were obtained on an X-Y recorder.

The method used for measuring the volume changes occurring in the specimen under test depends on the fact that the volume of a fluid-filled pressure vessel must be adjusted to compensate for lateral expansion of the specimen if the fluid is to be kept at constant pressure. If, as in Crouch's tests, the ram is of the same diameter as the specimen the amount by which the volume must be adjusted provides a direct measure of the lateral component of volumetric strain. If, as in the present case, the cross-sectional area of ram and specimen differ an axial strain dependent correction must be applied to the measured volume change to obtain the volume change in the specimen.

The pressure in the test vessel was controlled by a pressure intensifier with a threaded (20 threads/in.) plunger 0.50 in. (1.27 cm) in diameter. During tests the confining pressure as indicated on a pressure gage could be kept constant to within about 0.5 lb/in^2 by manual displacement of the pressure intensifier plunger. This displacement was transferred to a 40 turn potentiometer by a friction drive. The output of the potentiometer and the differential axial load were plotted continuously on a strip chart recorder throughout each test.

The tests were carried out by first applying a small axial load of sufficient magnitude to prevent the ram being forced upwards as the cell pressure was being applied. When the cell pressure had reached the test valve, all recorders were zeroed. Thus the axial forces recorded were the differential rather than total axial forces, and the volumetric strains recorded did not include the component of volumetric strain resulting from the application of the confining pressure. Once this initial equilibrium position had been established, the machine was switched to strain control and the specimen was loaded in the usual way.

Careful calibration tests were carried out using an 8 in. (20.3 cm) by 4 in. (10.2 cm) square block of aluminium as the test specimen. From the results of these runs, the corrections that must be applied to the measured total axial deformations and volumetric strains in order to determine specimen behaviour were computed.

RESULTS AND DISCUSSION

Load Bearing Capability

Mean values of peak load-bearing capability found in the present tests and in a previous series of uniaxial compression tests are shown in Table 4-1. These results confirm a previous finding that in the low confining pressure range, the strengths of the jointed models, particularly those with inclined joints (the H60 and H30 models), are more highly confining pressure-dependent than is the strength of the unjointed material. It is important to note that the difference in the strengths of the H30 and H60 models, so apparent in the unconfined case, is of a minor nature at $\sigma_3 = 250$ lb/in^2. The fact that the mean values of peak load-bearing capability given in Table 1 are derived from the results of only two, three of four tests in each case makes it difficult to draw other than the most general conclusions from them.

Specimen Type	Mean Peak Differential Load (lb.)		
	$\sigma_3 = 0$	$\sigma_3 = 50$ lb/in^2	$\sigma_3 = 250$ lb/in^2
SOLID	77,800	82,200	89,700
SO	48,500	61,600	84,000
H60	25,400	37,100	56,500
H30	5,600	24,700	59,600

TABLE 4.1

Load-Deformation Curves

Sample differential axial load (F_a) - axial deformation (Δ) curves are shown in Figures 4.1 to 4.8. The curves presented have, of necessity, been replotted from the test records, and in this process have been smoothed out considerably so that minor local jumps in the curves, typical of the model material during fracture, are not shown.

It is noteworthy that the shapes of the post-peak portions of these curves are markedly affected by changes in confining pressure. This is particularly notice-able in the case of the SOLID and SO specimens, both of which have very steep post-peak courves in unconfined compression. Even at the low confining pressures used in the present tests, the slopes of the post-peak portions of the curves have been reduced considerably. A similar phenomenon has been well documented for rock, al-though the confining pressures required to produce changes of the type recorded for most rocks are many times those used in these tests on plaster models.

Volumetric Strains

Figures 4.1 to 4.8 also show plots of ΔV, the total volumetric strain occurring in the specimen during application of the differential axial load against axial deformation. These curves provide dramatic illustration of the major differences that exist between the behaviour of jointed and unjointed materials.

Figures 4.1 and 4.2 show that for the SOLID (unjointed) specimens, the volume initially decreases, reaching a minimum value prior to or in the region of the peak of the $F_a - \Delta$ curve. The reversal in the sense of the volumetric strain occurring at this point is interpreted as being due to the onset and subsequent development of cracking within the specimen. With increasing axial deformation past the peak, lateral expansion of the specimen occurs at an increasing rate, and the nett change in specimen volume soon becomes positive or dilatational. Such behaviour is fairly typical of rock tested at low confining pressures[1,2], although in most rocks, the onset of cracking and associated dilation of the specimen occurs at a lower percentage of the peak load than in the case of plaster. In this regard, the behaviour of the plaster is more like that of dense, fine-grained rocks such as basalt and Solenhofen limestone. The behaviour of the SOLID specimens is also similar to that previously observed for rock[2] in that the amounts of volumetric and lateral expansion occurring decrease with increasing confining pressure.

As shown in Figures 4.3 and 4.4, the volume change behaviour of the SO specimens (containing sets of vertical and horizontal continuous joints) is not markedly different from that of the SOLID specimens. Here again, an initial decrease in specimen volume is followed by dilation which decreases in magnitude with increasing confining pressure. The fact that the SOLID and SO specimens exhibit similar behaviour in triaxial compression is hardly surprising. In fact, if the fit of the constituent blocks is the SO configuration were perfect, the behaviour of the two specimen types could be expected to be identical.

The $\Delta V - \Delta$ curves for both SOLID and SO specimens are initially non-linear and become more closely linear at large values of Δ in the post-peak range. Although plots of the lateral component of volumetric strain against axial deformation have not been prepared, it is obvious that these curves would be non-linear in the initial stages of the test when the $F_a - \Delta$ curves are sensibly linear. Crouch[2] has previously obtained a similar result for a number of different rock types.

The volume change characteristics of the two specimen types prepared from hexagonal blocks are quite different from that described for the SOLID and SO specimens. Excepting for the H60 specimens tested at a confining pressure of 250 lb/in² in which small initial contractions occur (figure 4.6), all H60 and H30 specimens dilate from the commencement of loading (figures 4.5, 4.7, 4.8). Generally, the rate of volume increase with axial deformation is initially small, but accelerates presumably with the onset of cracking, and becomes linear in the range of post-peak deformation. Ultimate linearity of the $\Delta V - \Delta$ curves also occurs for the SOLID and SO specimens and would appear to be associated with slip on a major shear plane formed during post-peak deformation. When the H60 and H30 specimens were removed from the cell it was found that they did, in fact, contain major shear planes or shear zones in addition to the wide-spread local axial cracking described elsewhere for the unconfined case.

The fact that dilation occurs at an earlier stage of the test and attains a greater magnitude in the H60 and H30 specimens than in the other types considered is directly attributable to the mobility of blocks in the H60 and H30 cases. Detailed studies of the failure of these specimen types in uniaxial compression have shown that in addition to fracture of the parent material, H60 and H30 specimens may deform by block rotation and slip on joint planes with consequent openings of

gaps throughout the specimen. Although these modes of deformation may be inhibited to some extent by the application of low confining pressures, it is unlikely that their influence will be completely suppressed in tests such as those under consideration here.

Although the response of the volumetric strain when specimens are unloaded was not specifically investigated, the limited evidence produced would suggest that when jointed specimens are unloaded in the post-peak region, volumetric strains are largely irrecoverable.

CONCLUSIONS

Crouch's method for measuring volumetric strains in triaxial compression tests on rock has been successfully applied to models of jointed rock. The tests carried out show that the volumetric strain behaviour of jointed specimens can be vastly different from that of comparable unjointed specimens. This provides additional support for the now well documented phenomenon that in certain circumstances the mechanical behaviour of jointed rock masses may bear no relationship to that of the parent rock material.

A wide range of possible volumetric strain responses have been shown to exist. Some specimen types may initially contract and subsequently expand as does intact rock, while for other jointing patterns, specimens may dilate from the commencement of loading. In all cases, the amount of expansion decreases with increasing confining pressure, and the lateral component of volumetric strain may vary non-linearly with axial deformation even when the axial force - axial deformation curves are linear. Non-linear and irregular behaviour is likely to be more marked in jointed than in unjointed rock.

REFERENCES

1. BRACE, W. r., PAULDING, B. W. and SCHOLTZ, C., Dilatancy in the fracture of crystalline rocks. J. Geophys. Res., 71, 3939-3953 (1966).

2. CROUCH, S. L., Experimental determination of volumetric strains in failed rock. Int. J. Rock Mech. Min. Sci., 7, 589-603 (1970).

3. CROUCH, S. L., The post-failure behaviour of norite in triaxial compression. Engng. Geol., 6, 19-30 (1972).

4. BROWN, E. T., Strength of models of rock with intermittent joints. J. Soil Mech. Foundns. Div., Am. Soc. Civ. Engrs., 96, (SM6), 1935-1949 (1970)
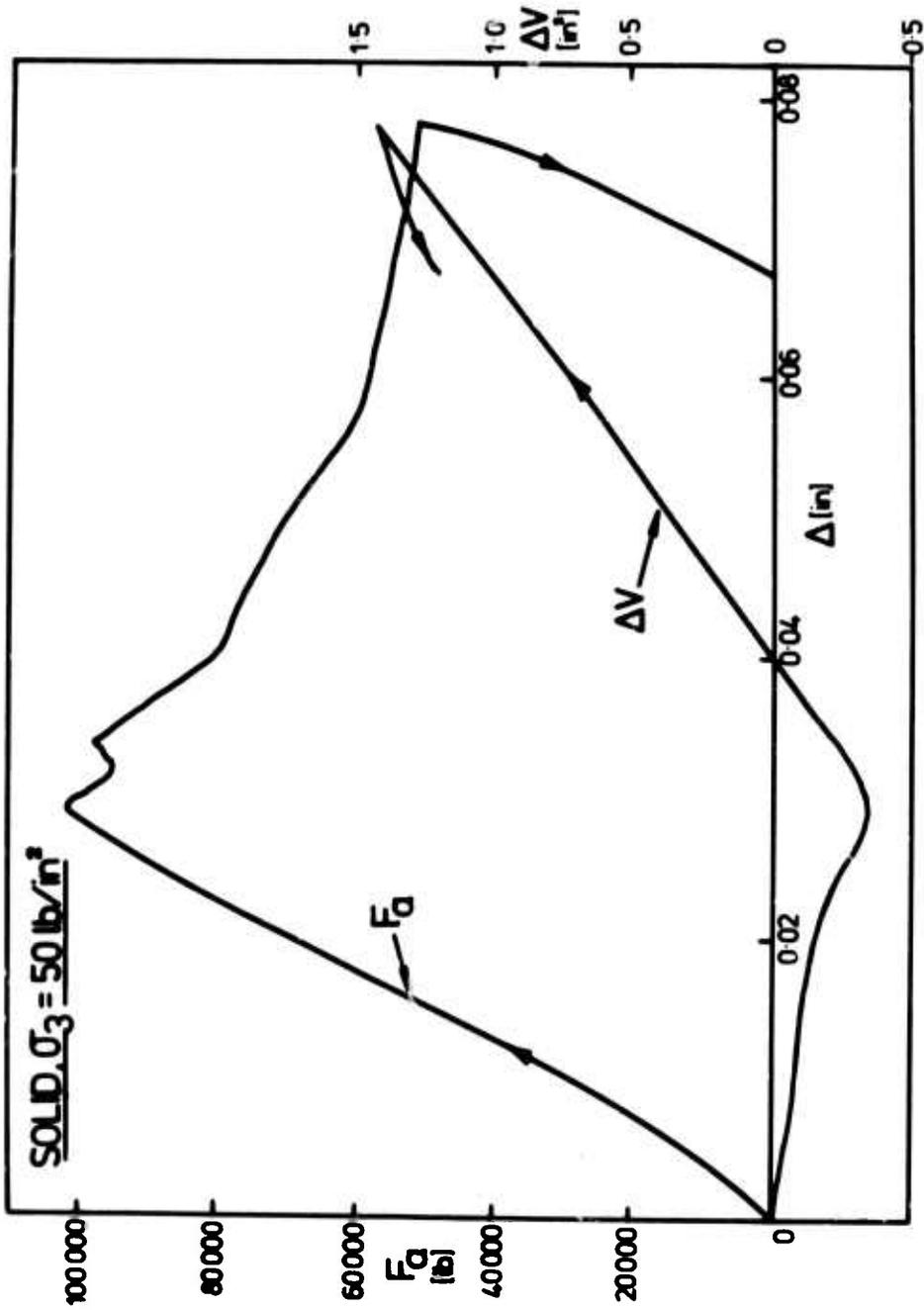
Figure 4.1: Experimental results of triaxial tests on solid block showing vertical force, F_a, and volume change, ΔV, as a function of vertical displacement, Δ.
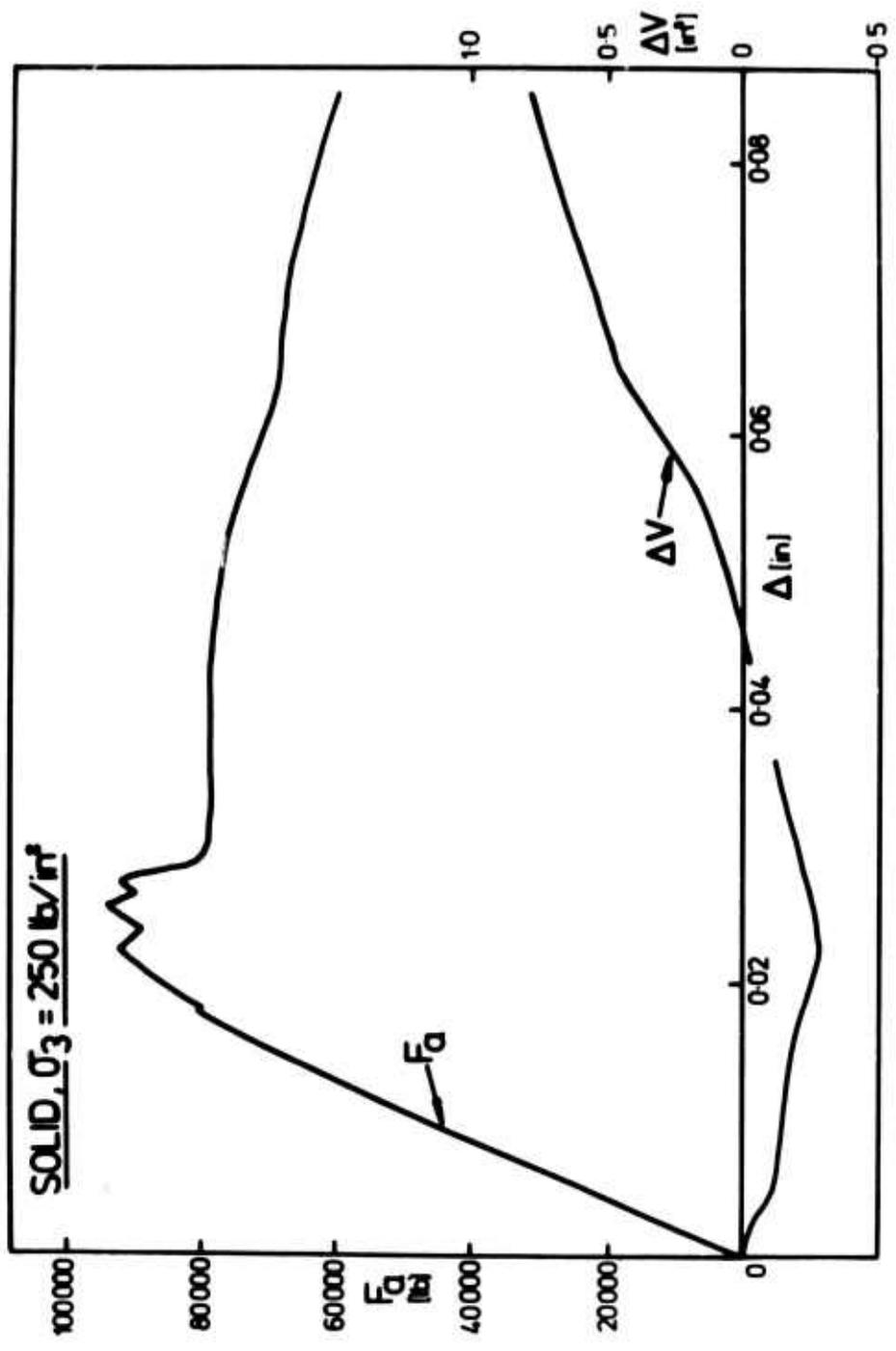
Figure 4.2: Experimental results of triaxial tests on solid block showing vertical force, F_a, and volume change, ΔV, as a function of vertical displacement, Δ.
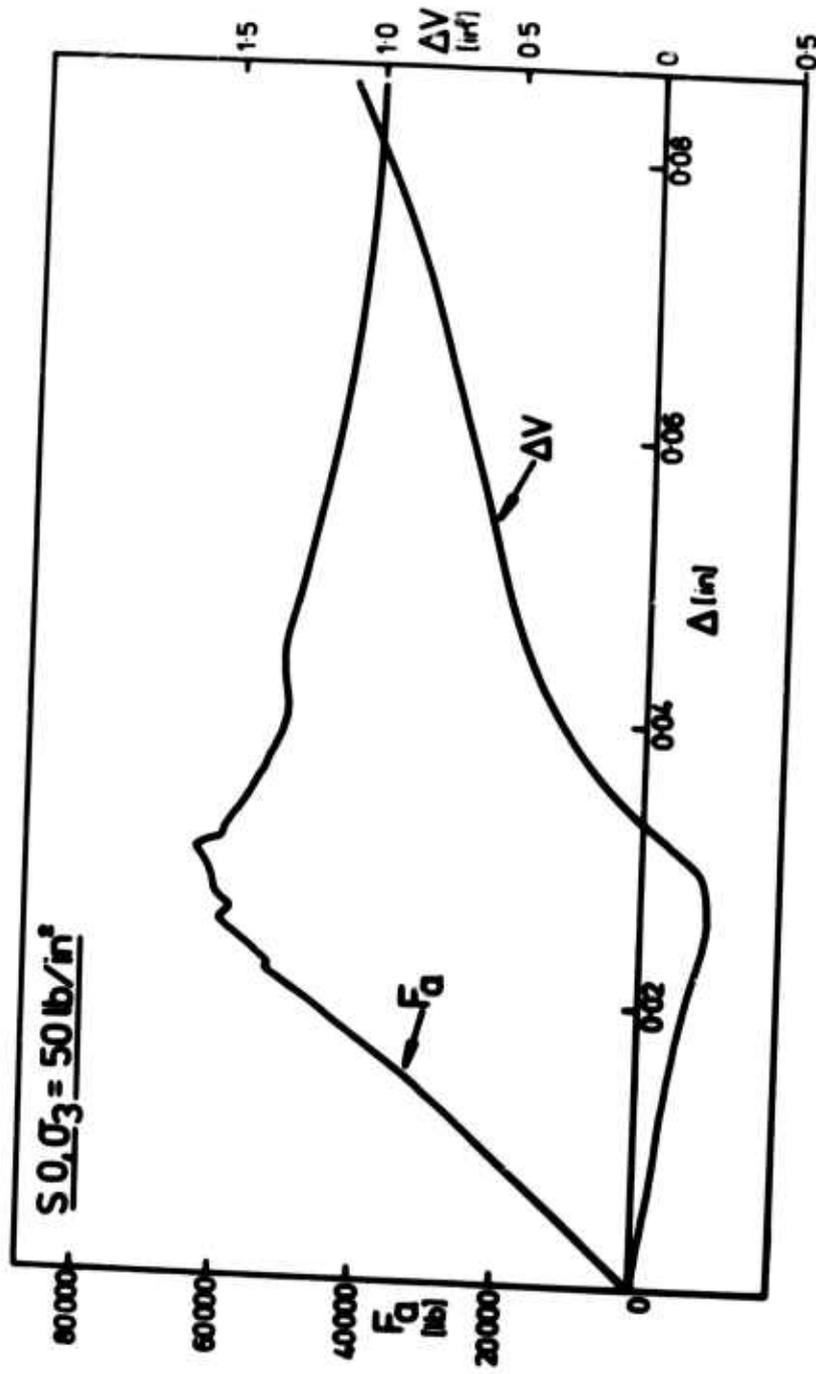
Figure 4.3: Experimental results of triaxial tests on square blocks showing vertical force, F_a, and volume change, ΔV, as a function of vertical displacement, Δ.
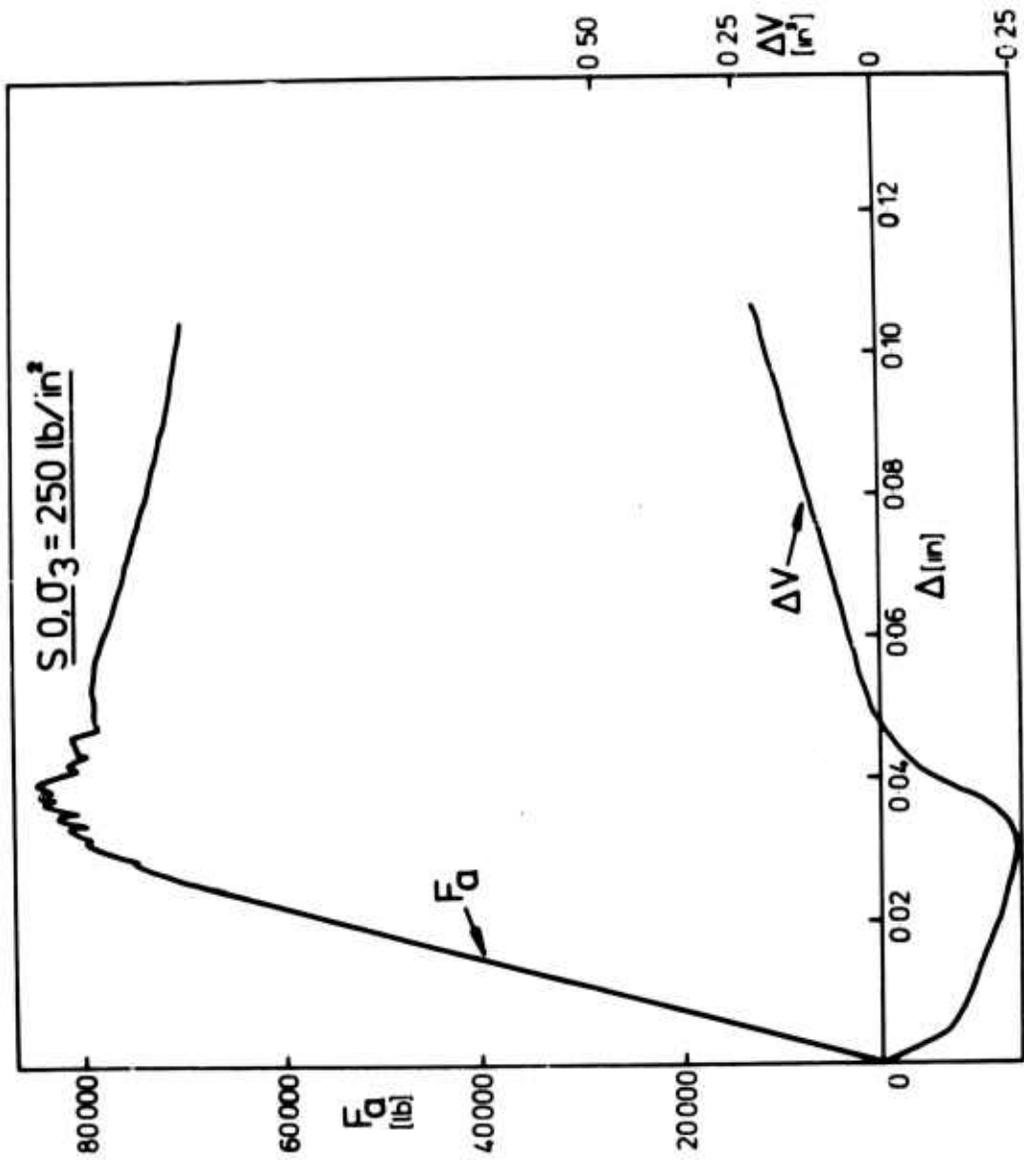
Figure 4.4: Experimental results of triaxial tests on square blocks showing vertical force F_a, and volume change, ΔV, as a function of vertical displacement, Δ.
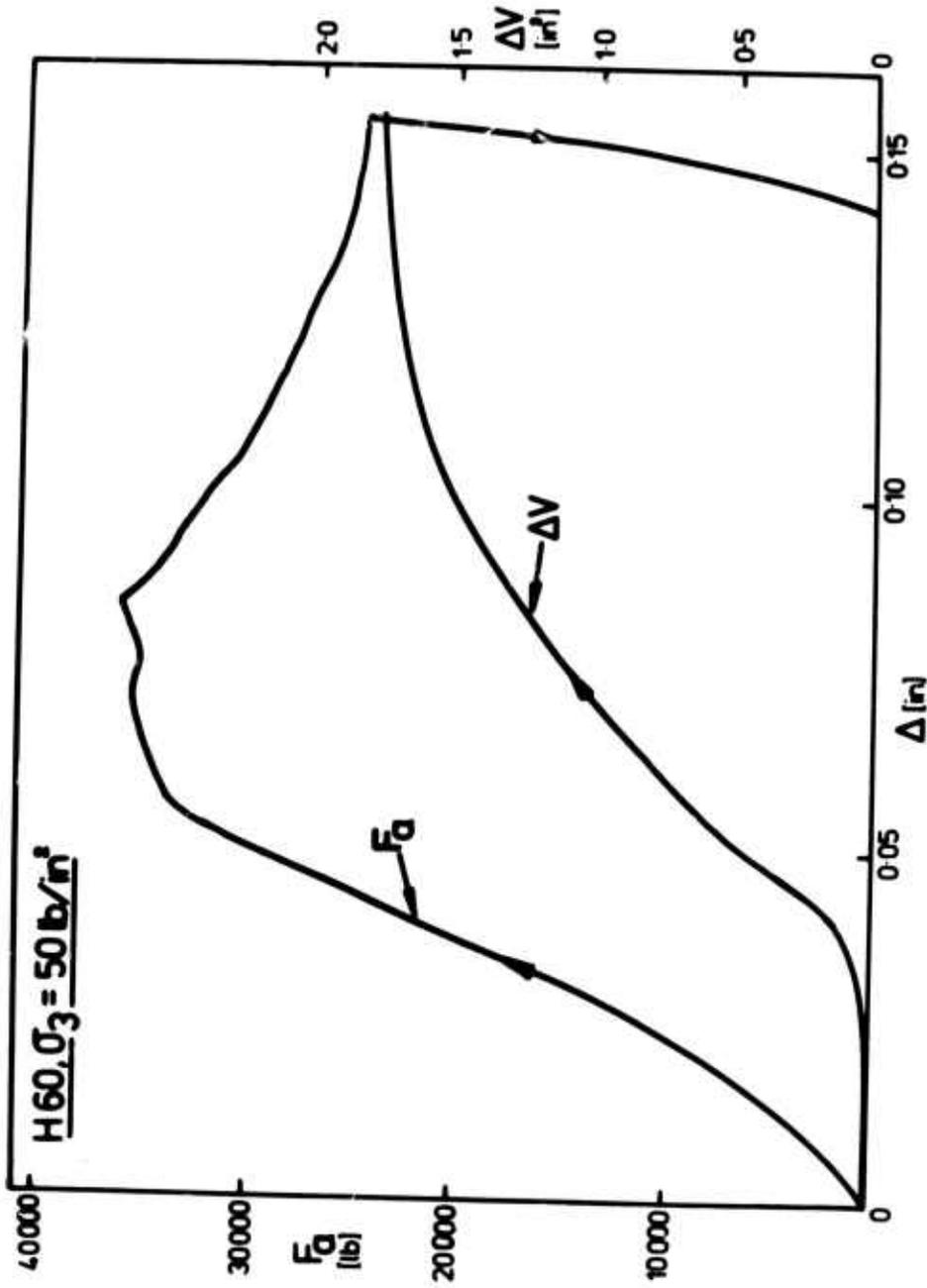
Figure 4.5: Experimental resutls of triaxial tests on hexagonal blocks at 60° showing vertical force, F_a, and volume change, ΔV, as a function of vertical displacement, Δ.
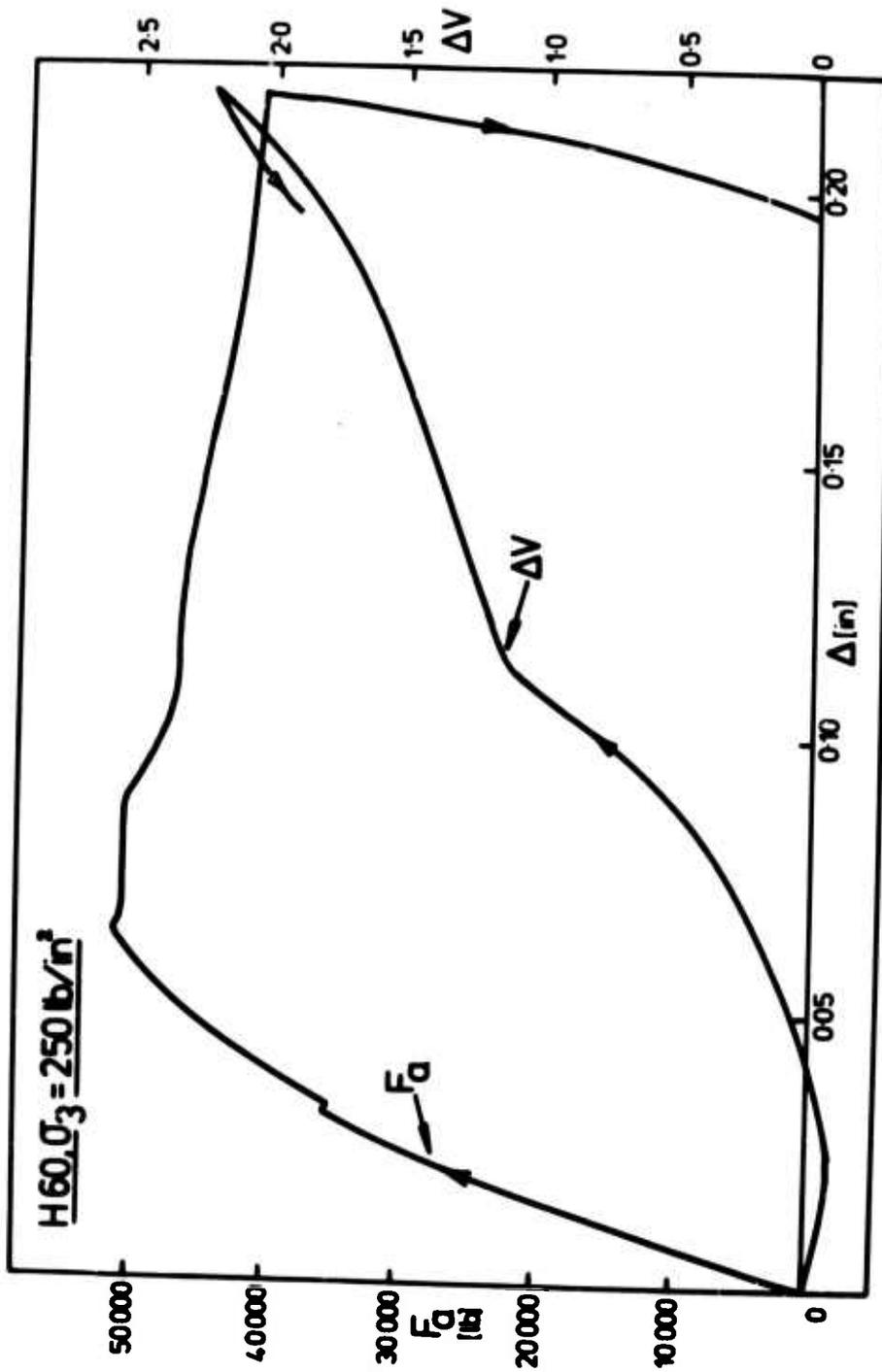
Figure 4.6: Experimental results of triaxial tests on hexagonal blocks at 30° showing vertical force F_a, and volume change, ΔV, as a function of vertical displacement, Δ.
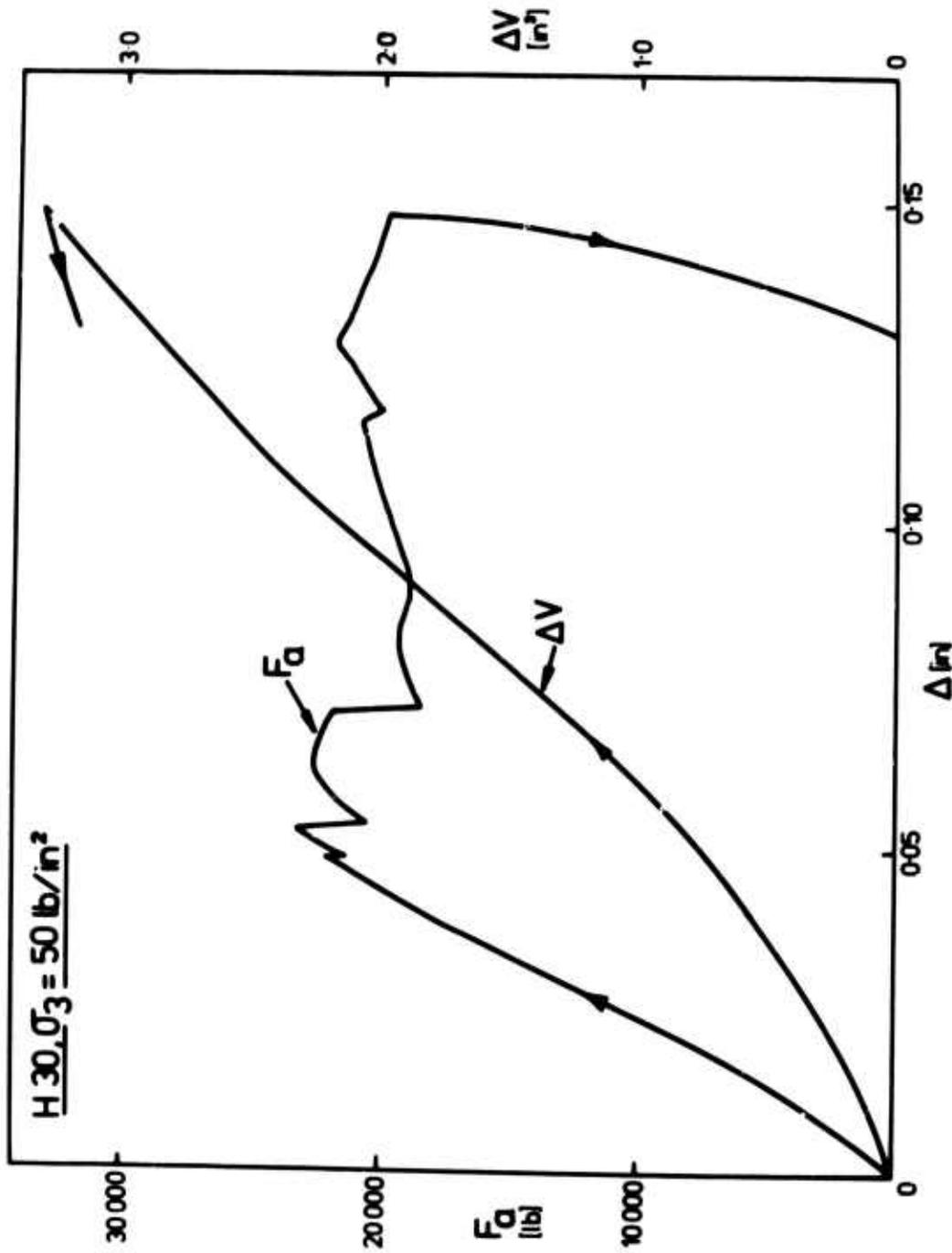
Figure 4.7: Experimental results of triaxial tests on hexagonal blocks at 30° showing vertical force, F_a, and volume change, ΔV, as a function of vertical displacement, Δ.
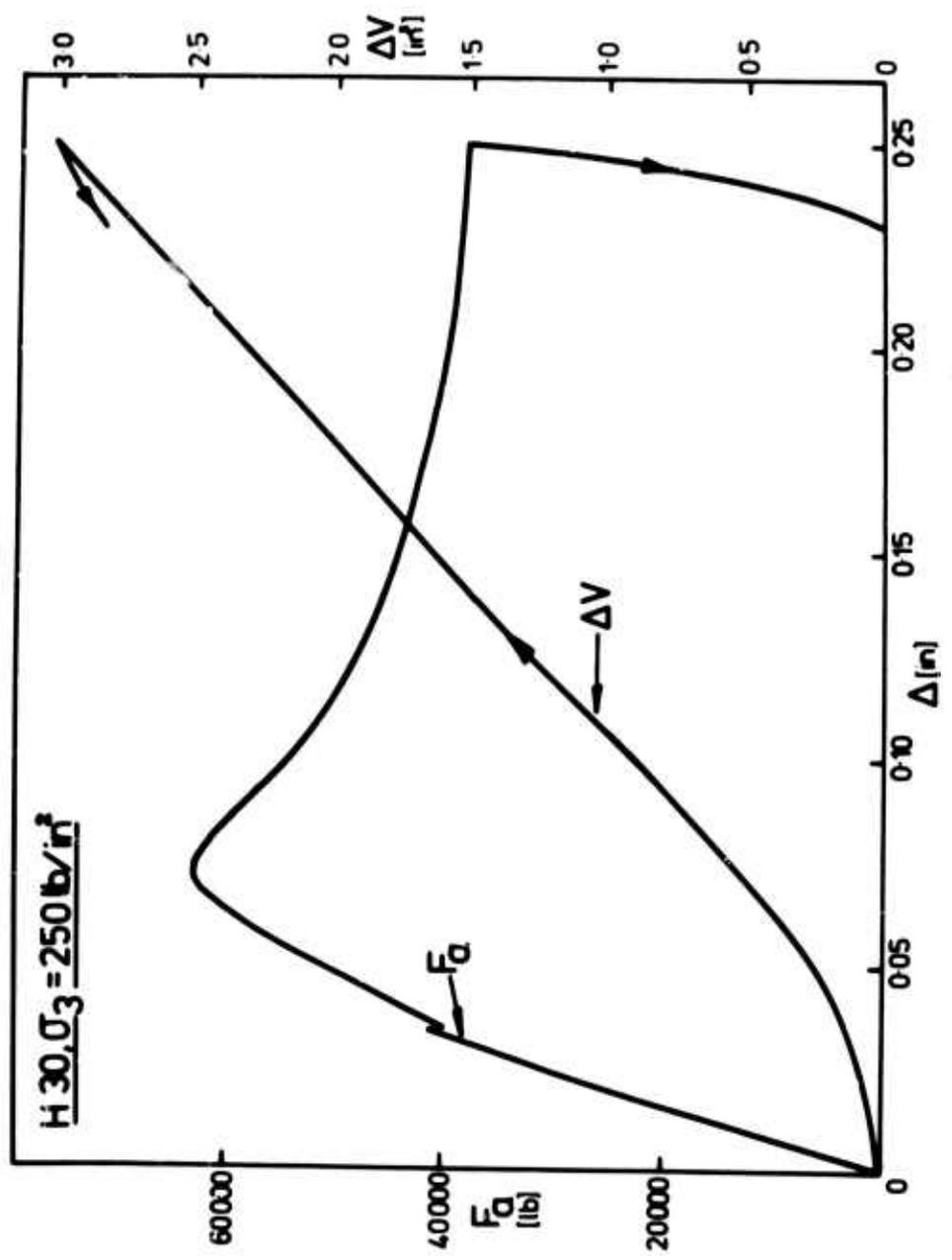
Figure 4.8: Experimental results of triaxial tests on hexagonal blocks at 30° showing vertical force, F_a, and volume change, ΔV, as a function of vertical displacement, Δ.

Chapter 5

THEORETICAL STUDY OF DEFORMABILITY OF JOINTED ROCK MASSES

INTRODUCTION

The theoretical work briefly reviewed in this chapter was completed in the first stage of this contr. (U.S. Bureau of Mines Research Contract No. H0101610) and funds were made available in the current contract to collate this work in the form of three publications. These publications have been prepared and have been submitted for publication, with copies forwarded to the Project monitor. These papers are:

i) "Continuum Characterization of Rock Masses - Part I The Constitutive Equations" by B. Singh.

ii) "Continuum Characterization of Rock Masses - Part II Significance of Low Shear Modulus" by B. Singh.

iii) "Reliability of Dilatometer Tests in the Determination of the Modulus of Deformation of a Jointed Rock Mass" by B. Singh.

The first two papers have been submitted for publication to the International Journal of Rock Mechanics and Mining Science, while the third has been submitted to ASTM Symposium on Field Testing and Instrumentation of Rock, September 1973.

These three papers are summarized below with details in the published papers.

CONTINUUM CHARACTERIZATION OF JOINTED ROCK MASSES Part I, The Constitutive Equations.

HILL (5) has proved that the average strain energy density in any region of an elastic and inhomogeneous material can be calculated from the average values of the stresses and strains within that region. This concept has been used to derive the general constitutive equations of a rock mass containing an orthogonal set of discontinuous joints intersecting an anisotropic rock material. The constants required for the continuum characterization of the jointed mass are the "joint stress concentration factors" B_{N1} and B_{T1} (see Fig. 5.1). These are defined as the ratio of stresses along the joint to the overall stresses in the rock. Exact expressions for the stress concentration factors have been obtained for the case of a rigid rock (i.e. the intact material between the joints) containing staggered compliant joints as follows:

108

$$B_{T1} = (1 + \frac{K_{N2}S}{K_{T1}S_2} (1 - \frac{S_1}{S_2}))^{-1} \qquad (1)$$

$$B_{N1} = (1 + \frac{K_{T2}S}{K_{N1}S_2} (1 - \frac{S_1}{S_2}))^{-1} \qquad (2)$$

and a correction is proposed for the case where the rock is (elastically) deformable. These results suggest that interlocking between blocks of rock may become significant even for a slight offset along the joints, such as may occur during shear deformation of a rock mass containing an initially continuous orthogonal joint set.

Stress concentration factors computed independently from the results of a finite element program for a jointed mass compare excellently with the above mentioned theoretical results.

It is further shown that tensile stresses are developed inside a rock with staggered joints, and may be as high as twice the overall shear stresses or the overall compressive stresses.

It is concluded that a rock mass is rendered anisotropic by any joint set having a preferred orientation. Expressions from which the elastic moduli of the equivalent continuum of anisotropic rock mass may be obtained.

Table 1

Elastic Moduli of the Anisotropic Continuum Model of a Jointed Rock Mass (Fig. 5.1)

Moduli of rock mass / Joint sets	$E_1 = RF_1 E_r$ / $\frac{1}{RF_1}$	$E_2 = RF_2 E_r$ / $\frac{1}{RF_2}$	$\nu_1 =$ ϵ_2/ϵ_1 due to only σ_1	$\nu_2 =$ ϵ_1/ϵ_2 due to only σ_2	$\frac{1}{G_{12}}$
Single joint set normal to axis 2	1	$1 + \dfrac{E_r}{S_2 K_{N2}}$	ν_r	$\nu_r \cdot RF_2$	$\dfrac{1}{G_r} + \dfrac{1}{S_2 K_{T2}}$
Orthogonal joint sets normal to axes 1 and 2	$1 + \dfrac{E_r}{S_1 K_{N1}}$	$1 + \dfrac{E_r}{S_2 K_{N2}}$	$\nu_r \cdot RF_1$	$\nu_r \cdot RF_2$	$\dfrac{1}{G_r} + \dfrac{1}{S_1 K_{T1}} + \dfrac{1}{S_2 K_{T2}}$
Orthogonal joint sets with staggered cross joints normal to axis 1 (obtain B_{N1} and B_{T1} from equations 1 & 2)	$1 + \dfrac{B_{N1} E_r}{S_1 K_{N1}}$	$1 + \dfrac{E_r}{S_2 K_{N2}}$	$\nu_r \cdot RF_1$	$\nu_r \cdot RF_2$	$\dfrac{1}{G_r} + \dfrac{B_{T1}}{S_1 K_{T1}} + \dfrac{1}{S_2 K_{T2}}$

Note: Elastic moduli are defined by following constitutive equations:

$$\epsilon_1 = (\sigma_1/RF_1 - \sigma_2 \nu_r - \sigma_3 \nu_r)/E_r$$

$$\epsilon_2 = (-\sigma_1 \nu_r + \sigma_2/RF_2 - \sigma_3 \nu_r)/E_r$$

$$\epsilon_3 = (-\sigma_1 \nu_r - \sigma_2 \nu_r + \sigma_3)/E_r$$

$$= \tau_{12}/G_{12}$$

where suffix:

r = denotes properties of intact rock material,

1,2 = denotes axes of anisotropy which are orthogonal to joint sets 1 and 2

3 = denotes third axis orthogonal to axes 1 and 2.

Part II.   The Significance of Low Shear Stiffness

Finite element analysis is used to compare the displacement fields given by an anistropic continuum model of a jointed rock mass with that obtained from the discrete joint model. These computations reveal excellent agreement between the finite element predictions of the join'. model and the continuum model, except in the region of steep stress gradients near the loaded area. In the special case where the mass consists of a single joint set of very low shear stiffness, this model breaks down due to excessive bending of rock layers.

The anisotropic continuum model predicts a stress distribution that is significantly different from Flamant's solution for a strip load on a semi-infinite rock mass and is in good agreement with experimental observations of GAZIEV and ERLIKHMAN (4). Stresses are transmitted to a considerably greater depth along joints and to some extent across joints . (see fig. 5.2). This tendency is more pronounced in a medium of very low shear modulus, which corresponds to a joint set of low shear stiffness.

Three case histories have been analysed to evaluate the elastic behavior of rock masses. MAURY (6) observes in his photo-elastic model of layered rock mass that the stresses are transmitted to a considerable depth in a narrow zone below the strip load. WARD et al (7) reported that displacements diminish rapidly away from the edge of the loaded area in a large scale plate load test on weathered chalk. BERRY (8) reported that the subsidence above a coal mine area is quite localized. These observations could not be explained by conventional theory of isotropic elastic material. The observed behavior of rock mass can be simulated successfully by a medium of low shear modulus. In this paper attention has been focused on the adverse effects of low shear modulus on the stability of rock masses.

RELIABILITY OF DILATOMETER TESTS IN THE DETERMINATION OF THE MODULUS OF DEFORMATION OF A JOINTED ROCK MASS.

The available results from radial jacking and dilatometer tests are inadequate for the proper assessment and comparison of the reliability of these test procedures. In order to arrive at a rational evaluation of such tests, a computer program was devised to simulate a jointed rock mass, and sets of test data were then developed by performing (i.e. mathematically simulating) a series of dilatometer tests at various locations within the rock mass.

The mean displacement of the dilatometer was computed for random spacing, orientation and stiffness of the joints, and random location of the dilatometer. These results were then analyzed to determine the minimum number of tests required, in terms of the average joint frequency and the modulus reduction factor (MRF), in order that the error in predicting the mass modulus would be less than 30% with a confidence interval of 95% (see fig. 5.3).

It was concluded that the optimum orientation of the dilatometer with respect to a joint set is in the range of 10° to 20° in order to assess most accurately the influence of the joints. Further, the statistical distribution of individual elastic moduli, as determined from repeated tests, is highly skewed and bimodal.

The harmonic mean of these test measurements provides a better measure of the mass modulus than does the arithmetic mean.

A finite element study was made of the problem of a strip load acting on the surface of a rock mass containing inclined joints. The position of the strip load on the surface was varied in order to examine the effect on the indicated mass modulus, as conventionally computed from the average settlement vertically below the load. It was observed that the mean value obtained from several (simulated) tests was independent of the width of the strip load.

REFERENCES

1. SINGH, B., Continuum characterization of jointed rock masses Part I - The constitutive equations, to be published in Int. J. Rock Mech. and Min. Sci., vol. 10 (1973).

2. SINGH, B., Continuum characterization of jointed rock masses Part II - The significance of low shear modulus, to be published in Int. J. Rock Mech. and Min. Sci., vol. 10 (1973).

3. SINGH, B., Reliability of dilatometer tests in the determination of the modulus of deformation of jointed rock mass. Submitted to ASTM Symp. on Field Testing and Instrumentation of Rock, Sept. (1973).

4. GAZIEV, E.G. and ERLIKHMAN, S.A., Stresses and strains in anisotropic rock foundations (Model Studies). Rock Fracture Symp., Int. Soc. Rock Mechanics, Nancy II-1 (1971).

5. HILL, R., Elastic properties of reinforced solids: some theoretical principles, J. Mech. Phys. Solids, vol. 11, 357-372 (1963).

6. MAURY, V., Distribution of stress in discontinuous layered systems, Water Power, May-June (1970).

7. WARD, W.H., J.B. BURLAND, and R.W. GALLOIS, Geotechnical assessment of a site at Mundford Norfolk for a large proton accelerator, Geotechnique, vol. 18, 399-431 (1968).

8. BERRY, D.S., A theoretical elastic model of the complete region affected by mining a thin seam, 6th Symp. on Rock Mechanics, University of Missouri, Rolla, 310-329 (1969).
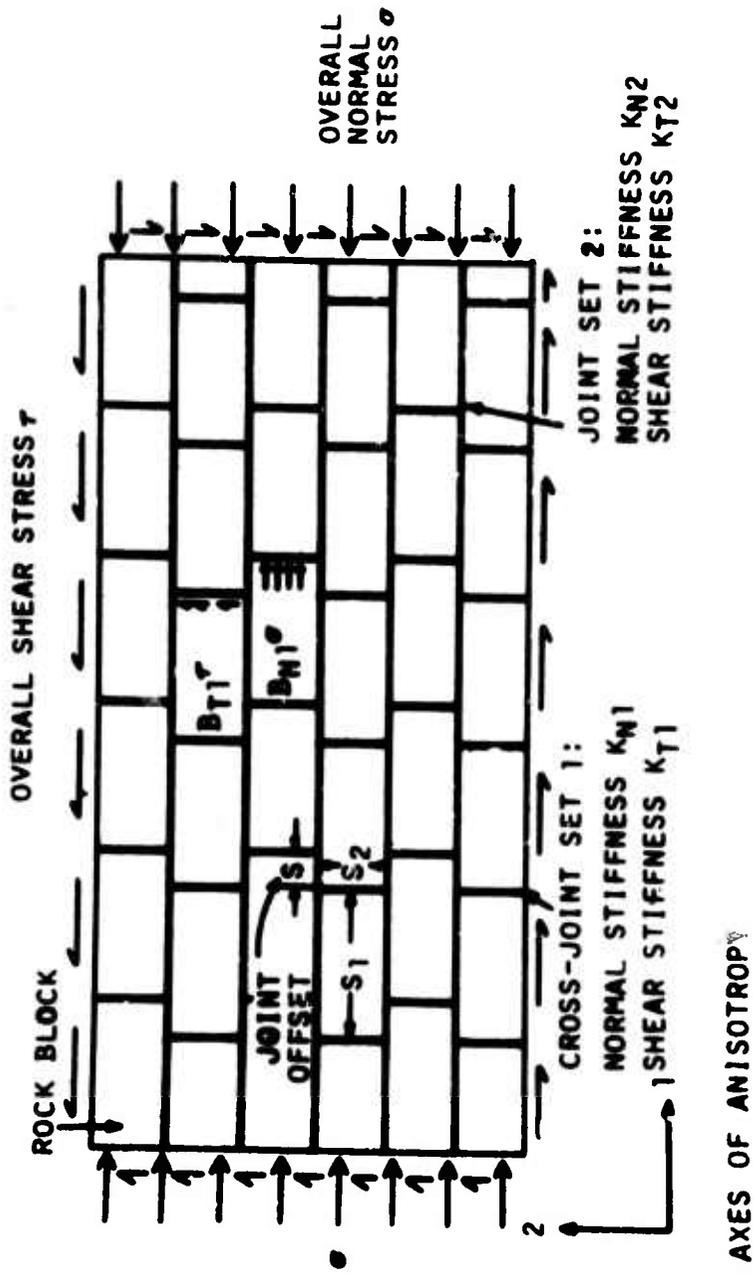
Figure 5.1: Rock mass containing staggered joints.
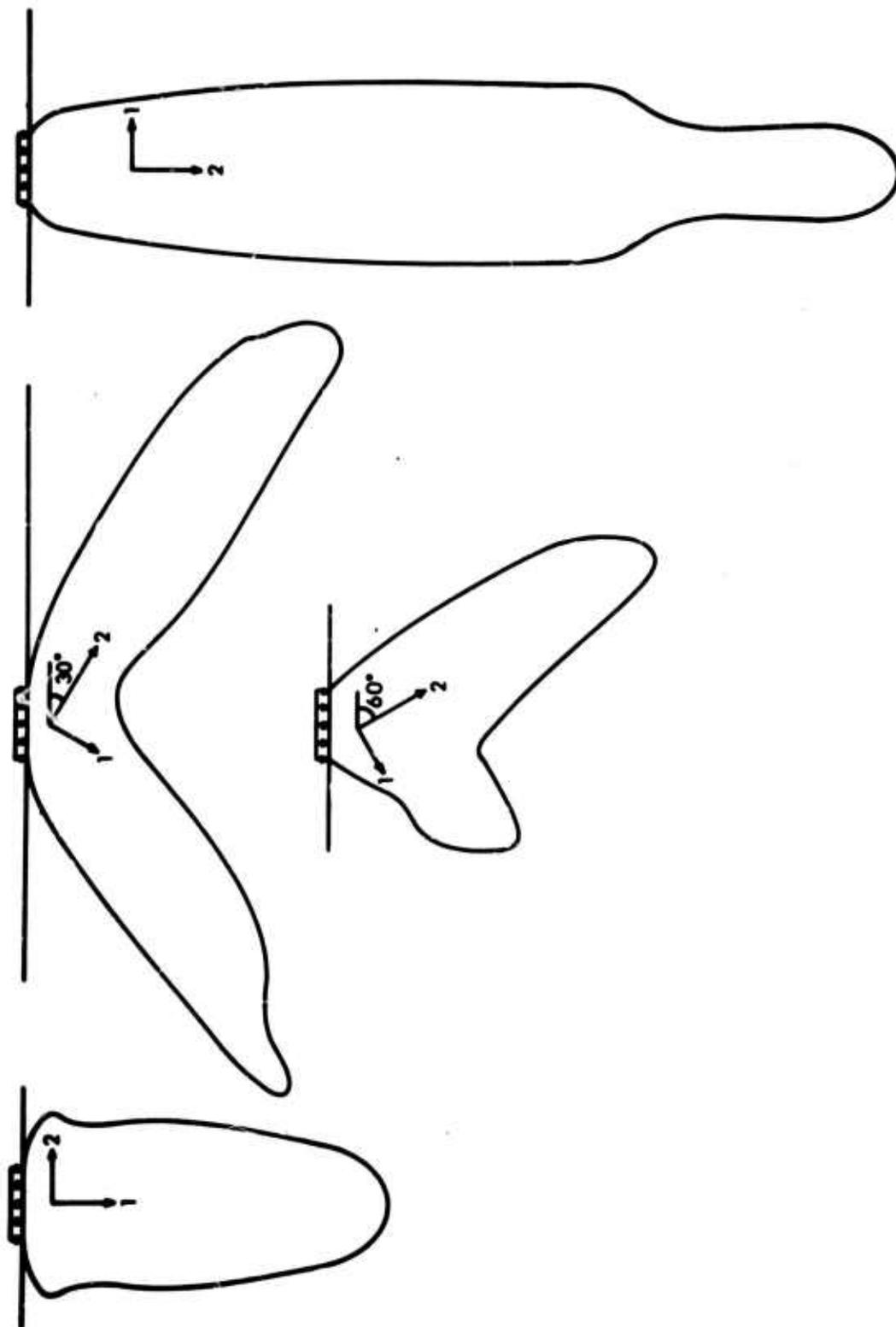
Figure 5.2: Pressure bulb for the strip load on a rock mass containing one set of joints of low shear stiffness ($K_T = K_n/10$). Joints are perpendicular to the axis 1.
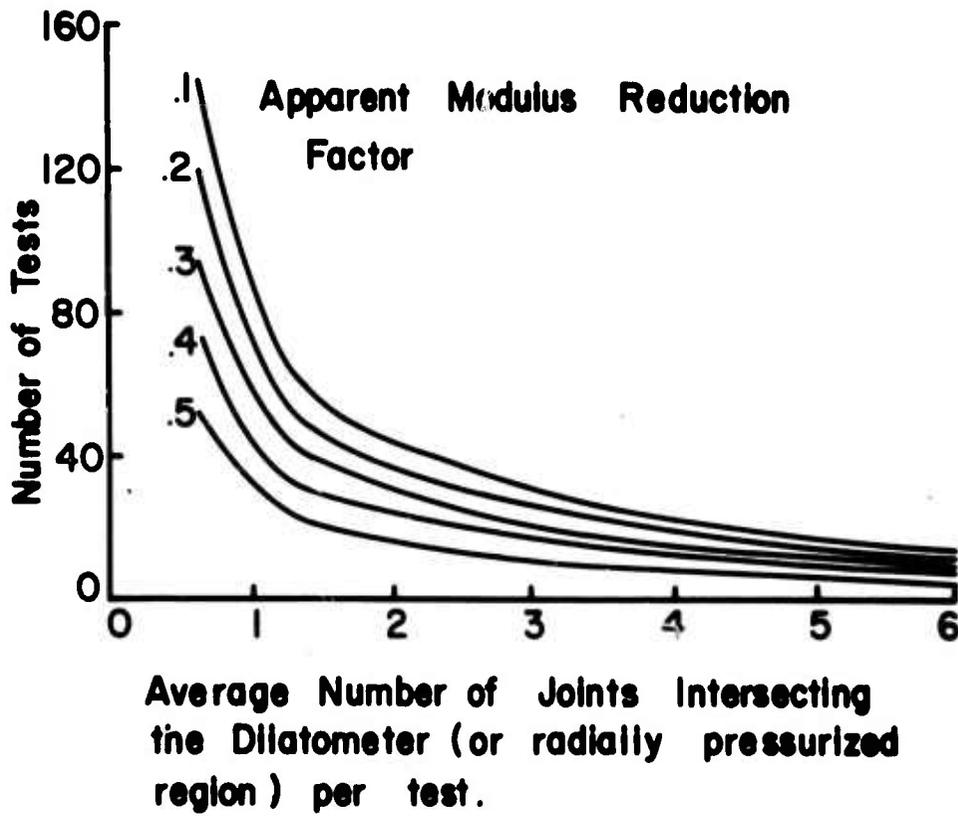
Figure 5.3: Number of dilatometer tests required to estimate modulus
reduction factor of a jointed rock mass within plus or minus
30% error.

CHAPTER 6

CLOSURES

The research presented in this report logically falls into three categories: the intrinsic properties of rock, the mechanical properties of block jointed models and the continuum characterization of rock masses. Each of these sections represents a major contribution to the problem of understanding the mechanical properties of rock masses.

The conclusion of the study of block jointed models suggest that the progressive failure of rock masses cannot be predicated from an individual understanding of the intact rock of the rock joints alone. The interaction of these two components of the system has been shown to produce fracture within the intact rock at average stress levels much below that to cause fracture in the solid specimens. These fractures contribute an increase in the degrees of freedom within the jointed system such that block rotations and joint slippage can more readily occur. The complete force displacement response, and hence the stress strain characterization of such a system cannot be predicted by any simple theory such as the single plane of weakness theory on the two dimensional intent of jointing concept, however the experimental results offer a useful comparison for the developing numerical models such as finite elements and finite difference techniques outlined in appendix II section 2.3a . One of the mechanisms involved in the collapse process of the clock jointed models, vertical splitting or cleavage, has been studied in detail in the section on intrinsic properties of rock, but much more work is necessary on the numerical methods of predicting block interactions before the sophistication of the fracture analysis can be incorporated into the description of the collapsed block jointed models.

The observations of the behavior of jointed block models under confinement confirm the belief that these types of systems are initially more highly pressure dependent than is the strength of the unjointed material. The shape of the post peak curves are markedly affected by even a small change in confining pressure. The models very quickly become more 'stable' as confinement is increased. Volumetric changes due to fracture of models has shown a considerable variation. Some models initially contracted due to essentially elastic deformations, but others dilated with the application of the load. All block jointed models dilated more than the unjointed model with the amount of expansion decreasing with increasing confinement pressure.

The continuum characterization of jointed material presents material which should be of direct practical value. The anisotropic elastic constants for the rock mass are presented in terms of the intact rock and the joint characteristics. Numerical comparisons of the anisotropic continuum model and the finite element model with joint elements indicate that the continuum characterization gives excellent results for the rock mass, but differences become apparent between the

two models in areas of high stress gradient. The significance of low shear stiffness on the anisotropic continuum model is described and discussed with reference to several published papers dealing with jointed rock masses. The reliability of dilatometer tests in relation to spacing and location of joints is discussed. It is concluded that the optimum orientation of the dilatometer with respect to a joint set is in the range of 10° to 20° in order to assess most accurately the influence of the joints.

The studies of the intrinsic properties of rock have produced two material properties, 'the work of fracture' and the 'effective rock length'. With these two properties and the correct energy analysis of cracked structures the apparent variations of the tensile strength, based on a stress criterion, are explained. Experimental results support these claims. Integration of tensile splitting to explain the total compressive failure of rock is not at this stage practical but the approach outlined in this study is considered applicable to one of the individual mechanisms of failure in compression. This splitting mechanism has also been shown to be extremely important to the development of the peak strength of the block jointed models, as splitting of blocks appears to initiate failure. These studies of intrinsic properties of rock have produced information that can be applied to practical problems involving both large scale volumes of rock and small scale volumes of rock. The analytical (numerical) procedures described can be used on the large scale to determine quasi-static fracture paths due to either gas pressures in blasting or hydraulic pressures in hydraulic fracturings or, on the small scale, it can be used to determine fracture paths due to cutting or drilling of rock.

The mechanical properties of rock masses is not easily defined. The work presented here represents a valuable contribution to the understanding of rock mass behavior, but additional work is needed to integrate the various approaches of this and other studies to develop useful methods of rock mass characterization particularily as failure progresses.

APPENDICES

117

CONTENTS OF APPENDICES

CONTENTS OF APPENDICES (Cont.)

SHEAR STRENGTH OF ROCK JOINTS

1 INTRODUCTION

The resistance to slip developed in a rock joint (or its shear strength) is one of the prime determinants of the strength and deformation properties of a rock mass containing that joint. In the present context, the term "joint" is used to describe any plane of weakness in the rock mass, including those features which may be more accurately described as bedding planes, cleavage planes, veins, shear zones, etc.

Present knowledge of the frictional properties of rock surfaces and the strength of naturally occurring rock joints is extremely limited. Moreover, there is no generally accepted method for determining these properties. As a consequence of this, oversimplified concepts of rock joint behavior are used in engineering practice where some attempt must be made to provide workable solutions.

The present appendix discusses the laws of friction which have been applied to rock, previous experimental investigations, methods of determining joint strength, and the influence of surface texture or joint strength. The material presented draws heavily on extensive analyses of the problem made by Rosengren [1,2] and Jaeger [57].

2 LAWS OF FRICTION APPLIED TO ROCK

2.1 Amontons Law

The classical laws of friction, namely that frictional resistance is proportional to normal force and independent of nominal contact area, were first proposed by Leonardo da Vinci and subsequently rediscovered by Amontons some 200 years later [3]. Amontons' first law can be written as

$$F = \mu N \qquad \qquad \dots(1)$$

where F is the frictional resistance, N the normal force, and μ the coefficient of friction. Dividing each side of Eqn. 1 by A, the nominal contact area, gives

$$\tau = \mu \, \sigma_n \qquad \qquad \dots(2)$$

where σ_n and τ are the normal and shear stresses respectively.

Amontons' laws are explained by the Bowden-Tabor adhesion theory of friction [3,4] in which it is postulated that contact between two surfaces occurs only at the tips of asperities so that the true area of contact is much less than the nominal area, A. Due to the high normal stresses, the material at the tips of the asperities deforms plastically and "welding" occurs. The frictional resistance arises from the force necessary to shear these contact given by

$$F = S.A_c \qquad \qquad \dots(3)$$

where S is the shear strength of the material and A_c is the true area of contact.

If the deformation of the asperities is perfectly plastic,

$$A_c = \frac{N}{Y} \qquad \qquad \ldots(4)$$

where Y is the yield stress of the material.

Substitution for A_c from 4 and 3 gives

$$F = \frac{S}{Y} \cdot N \qquad \qquad \ldots(5)$$

or $\quad F = \mu \cdot N \qquad \qquad \ldots(1)$

where $\mu = \frac{S}{Y}$ is a constant for the material.

This theory was developed primarily for metals and most of the experimental verification of it has been for this class of materials [3,4]. Although the asperity concept appears to be fundamental to any theory of friction, the theory outlined above is not always applicable to rocks. Perhaps the most significant of the many reasons for this is that the very brittle minerals making up many rocks will not always behave plastically (see Sections 2.2 and 2.3 below).

Carlisle [5] argued that the Bowden-Tabor theory cannot be expected to apply to rocks for several other reasons:

(a) It neglects the frictional resistance due to ploughing of a hard body sliding on a soft one, a mechanism which has been discussed by Jaeger and Cook [6].

(b) It neglects the effects of the inherent granularity, porosity and anisotrophy of rocks and their constituent minerals, these effects including dilatancy, pore pressure development, the reorientation of minerals and the creation of new minerals along the sliding surfaces.

(c) Since the strengths of materials are known to be sensitive to temperature, confining pressure and strain rate, the classic law cannot be expected to hold through the whole range of environmental conditions encountered in nature.

To these various difficulties must be added the fact that the classic theory does not allow for the effects of interlocking of irregularities occurring on the rock surfaces. The component of strength arising from this source is often allowed for by the inclusion of a constant strength term, τ_0 , in the shear strength law which then becomes

$$\tau = \tau_0 + \mu \, \sigma_n \qquad \qquad \ldots(6)$$

or $\quad \tau = \tau_0 + \sigma_n \tan \phi \qquad \qquad \ldots(6a)$

It is in this form that the shear strength of rock surfaces is usually expressed.

2.2 Power Laws.

A number of investigators have found that Eqns. 2 and 6 do not fit the frictional behavior or rocks at all well. Very commonly it is found that μ, as defined by τ, decreases with increasing normal stress [7-10]. Such results may be fitted by a power law

$$\tau = K \sigma_n^c \qquad \ldots(7)$$

or

$$\tau = \tau_0 + K \sigma_n^c \qquad \ldots(8)$$

where K and c are constants.

Some theoretical justification for such a law can be put forward on the grounds that deformation at some asperities may be elastic rather than plastic. In his classic work, Hertz demonstrated that for elastic deformation of spherical asperities in contact, $A_c \propto N^{2/3}$ [11], while Archard [12, 13] has shown that as the complexity of asperity geometry increases, the index approaches unity. Jaeger and Cook [6] nave further pointed out that it is reasonable to expect that deformation of some asperities will be elastic while that of others will be plastic.

On this basis then there is some justification for suggesting that in the general case,

$$\tau = \tau_0 + K \sigma_n^c \qquad \ldots(8)$$

where $2/3 \le c \le 1$.

A disadvantage of this law is that the coefficient K is not a dimensionless quantity. This difficulty can be overcome by rewriting Eqn. 8 in dimensionless form [14] as

$$\frac{\tau - \tau_0}{\sigma_c} = K' \left(\frac{\sigma_n}{\sigma_c}\right)^c \qquad \ldots(9)$$

where σ_c is a material property, taken by Hoek [15] to be the uniaxial compressive strength of the rock.

2.3 A Theory of Friction for Brittle Rock.

Byerlee [16] has postulated that in many rocks the asperities will fail in a brittle manner rather than by plastic shear. He assumed that asperities are wedge-shaped and that the forces exerted by one asperity on another can be represented by normal and tangential stress acting at the apex of the wedge. Using the theory of elasticity to calculate stresses, and assuming that all values of α, the half-angle of the wedge, between 0 and $\frac{\pi}{2}$ are equally likely and that, on the average, the load will be shared equally by all angles of asperities, Byerlee was able to show that the coefficient of friction may be calculated as

$$\mu_o = \frac{1 + \frac{T}{C}}{\frac{\pi}{2}} \int_o^{\frac{\pi}{2}} \cot \alpha \left[\frac{\alpha - \frac{1}{2} \sin 2\alpha}{\alpha + \frac{1}{2} \sin 2\alpha} \right] \qquad \qquad \ldots (10)$$

where T and C are the uniaxial tensile and compressive strengths of the material. Taking $\frac{T}{C} = 0.1$ as a typical value for rock, numerical integration gives $\mu_o = 0.15$ which is lower than the values commonly measured for rock surfaces.

Byerlee suggested that for rough surfaces asperities may interlock so that the forces will be applied at the sides rather than the tips of asperities, in which case his theory will not apply. In direct shear experiments, Byerlee found that the measured coefficient of friction increased markedly with surface roughness. The coefficient of friction of Westerley granite increased from 0.2 to 0.6 as the CLA (centre line average) roughness increased from 20 to 300 micro-inches (Fig. 1) while the coefficient of a freshly fractured surface of the same rock was between 0.8 and 1.3. Further experiments involving the sliding of quartz, microcline, hornblende and calcite on sapphire showed a similar dependence of friction on surface roughness.

3 METHODS OF MEASUREMENT AND THEIR RESULTS.

3.1 Direct Shear Tests on Minerals.

The classical method of measuring friction [3] shown in Fig. 2a consists of a flat surface, A, which slides under a spring loaded button, B, of the same, or another, material under a given normal load, N. The frictional force, F, is measured by the deflection of the spring, S. The samples are usually small, and the normal load, N, does not exceed a few tens of pounds. However, a wide range of variables including temperature, speed of sliding and surface contamination can be investigated. The data obtained by Bowden and Tabor [3,4] for minerals such as rock salt, diamond, mica and graphite are of little significance in the present context.

The most comprehensive study of the friction of minerals was made by Horn and Deere (17) with a similar apparatus. They showed that massive structured minerals such as quartz, microcline and calcite have low coefficients of friction of the order of 0.1 when oven dried and much higher values (0.4 to 0.8) when saturated with water. On the other hand, layer-lattice minerals such as muscovite, phlogopite, biotite, chlorite, serpentine, steatite and talc showed the reverse behaviour, the coefficient being of the order of 0.5 when dry and 0.25 when wet. These results were obtained for "very smooth" surfaces at low normal loads of up to 10 lbs. Further observations were that quartz, when saturated, showed pronounced "stick-slip" behaviour and that increased surface roughness increased the coefficient of friction, but reduced the anti-lubricating effect of water on quartz.

Other studies of the frictional behaviour of minerals, notably quartz, have arisen in soil mechanics from attempts to correlate the properties of individual grains with those of an aggregate. Terzaghi [18], Tschebotarioff and Welsh [19], and Penman [20] have all found higher values of the coefficient of friction for saturated quartz than for oven dry quartz. Penman measured the friction between two fragments of quartz in a shear box (Fig. 2b) and obtained values of $\mu = 0.65$ for the saturated condition and $\mu = 0.19$ for the oven-dry condition for normal stresses up to 126 psi. For "much higher" normal stresses, μ decreased to 0.35 when saturated.

3.2 Direct Shear Tests on Rocks.

A first approach to the measurement of the frictional properties of rocks in direct shear has been to use the simple soil mechanics shear box. The normal load, N, is usually not greater than a few hundred pounds and is applied by a dead weight hanger which is free to translate with the top part of the box. Maximum normal stresses of the order of 200 psi can be applied to a 2 in. square sample in this way. This is generally too low for rock mechanics work. A second major disadvantage of the simple soil mechanics shear box is that the specimen size is too small (usually up to 6 cm. square) for practical purposes.

Disadvantages of shear box tests generally are that overturning moments are almost invariably introduced, and that the boundary conditions represented by the lateral confinement offered by the sides of the box are extremely variable. Overturning moments are set up when the shear load and its reaction are applied through the sides of the top and bottom halves of the shear box (Fig. 2b) rather than in the plane of the joint being tested, and when one half of the box rides up on a high point on a rough surface in the other half. Rotation in the horizontal plane is also possible in the latter case.

Ripley and Lee [21] used a soil mechanics shear box to study the behaviour of both ground and naturally rough surfaces of sandstone, siltstone and shale. The ground surfaces gave coefficients of friction in the range 0.47 to 0.60. The rough surfaces gave residual coefficients which were somewhat higher, but when corrections were made for the effect of riding over surface irregularities, the results could be correlated with those for the ground surfaces. This was perhaps the first attempt to quantify the effect of surface roughness on joint behaviour. This aspect of the subject is discussed in detail in Section 5 below.

In rock mechanics work, the use of normal stresses of up to a few thousand p.s.i. is desirable. This requires the design and construction of special high capacity direct shear machines in which the normal load is applied by a hydraulic jack. Since one half of the shear box must translate across the face of the jack, some method such as roller bearings or teflon slides must be used to minimize friction in the apparatus, and even then a correction must be applied to the indicated shear force.

A number of these shear machines have been built in recent years. Krsmanovic and Langof [22] used a machine with a normal load capacity of 60 tons and a maximum sample size of 16 in. square in tests on bedding planes and joints in limestone. Residual coefficients of friction varied from 0.2 for clay-filled joints to over 1.0 for very rough stratification planes. The latter showed a peak strength of up to twice the residual strength which was attained after some 1-1/2 in. of sliding. Tests on intact samples of sandsone, limestone, and conglomerate [23], gave residual coefficients of friction of approximately 0.7.

A machine with normal and shear load capacities of 100 tons and maximum specimen size of 15 in. x 12 in. is in operation at Imperial College, London [24,25]. The shear surface can be displaced over a distance of 6 in. at rates of between 0.1 in./min. and 2 in./month. Friction in the apparatus is minimized by a teflon bearing surface. The machine has a very high stiffness in relation to the stiffness of the rock joint which means that most of the deformation in the system takes place in the rock and not in the machine, and that the rate of failure of the discontinuity can be carefully controlled. The results of tests on large samples of natural joints in porphyry obtained using this machine are shown in Fig. 3. In this case both peak and residual strengths are represented by linear laws with $c = 100$ kg/m^2 and $\phi = 37$ 1/2° (peak) and $c = 0$ and $\phi = 30°$ (residual).

A very high capacity direct shear machine has been built at the James Cook University of North Queensland, Townsville [26]. This machine, which can accept of up to 12 in. square specimens can operate at normal pressures of up to 4,000 p.s.i. applied via flat jacks, and uses a 1.2×10^6 lbf. compression machine to provide the shearing force. As with most of the other modern machines, dilation normal to the direction of sliding is measured during each test.

Rengers [27] has carried out direct shear tests at the University of Karlsruhe, using a sophisticated medicine in which the shear plane has an area of 600 cm^2. Normal and shear forces of 50 Mp can be applied, and a relative movement of 200 mm. is possible. The normal force is applied via air pressure in rubber bellows which obviates the need to apply a correction for friction such as that required in the case of the James Cook machine. Other large direct shear machines have been used by Bernaix [28,29] and by Guiseppe [30] who used the Jugoslavian design [22,23]. Goodman [31] has recently given a useful summary description of a number of these machines.

The direct shear method is, of course, the method used in most in-situ tests for determining rock strength. Examples of the techniques used and results obtained are given by Serafim and Lopes [32], Krsmanovic and Popovic [33], and Wallace and Olsen [34] among many others. Generally surfaces tested are of the order of size as those which can be accommodated in the larger laboratory machines, although in some cases very large surfaces have been tested.

3.3 Double Shear Tests.

In the double shear test (Fig. 2c), a flat block (C) is sandwiched between two other blocks (A and B), supported on packers (P), and the normal load (N) is supplied by jacks reacting against a loading frame. This system eliminates the difficulty of part of the machine translating across the face of the jack as in the case of direct shear, but suffers from the disadvantage that only the average frictional resistance on each of two faces can be measured. It is therefore preferable that the faces be identical, and for this reason, the method is virtually limited to artificially ground rock surfaces.

Maurer [8,35] used this method for testing the frictional behaviour of surfaces of various rocks after fracture in the same apparatus. The samples were only 0.5 in. x 1.0 in. in section. His results were expressed in terms of a power law (Eqn. 1.7) with the constant K varying between 3.7 and 60.0 (in lb.-in. units) and the exponent c between 0.46 and 0.80.

Hoskins, Jaeger and Rosengren [36] used the double shear apparatus in a study of the behaviour of 12 in. square artificially ground surfaces of several rocks. They found that the sliding behaviour for any rock is profoundly influenced by the degree of surface finish. "Rough" surfaces showed steady sliding (Fig. 4) whereas "smooth" surfaces exhibited stick-slip oscillations (Fig. 5). The critical roughness separating the two types of behaviour was found to be approximately 100 microinches. Obviously, these "rough" surfaces are still very smooth and flat compared with almost any natural joint surface.

For all the surfaces tested, a linear shear strength law was applicable for normal stresses up to 1000 p.s.i., the coefficient of friction varying from 0.51 to 0.75 for "rough" surfaces and from 0.18 to 0.63 for "smooth" surfaces. The cohesion intercept was less than 200 p.s.i. in both cases. This difference in friction between "rough" and "smooth" surfaces of the same rock varied with rock type. All surfaces showed significant variations in friction with displacement, the rate of increase depending on the type and roughness of the surface. Some surfaces, such as sandstone, reached a steady value after less than 0.1 in. of sliding, while others, such as trachyte, showed a rising characteristic even after 0.5 in. of sliding.

Rosengren [1] extended this work using 3 in. square blocks and higher normal loads, confirming the general patterns of behaviour observed in the earlier study.

3.4 Triaxial Compression Tests.

The technique of sliding on a pre-determined plane of weakness in the triaxial test appears to have been first used by the U.S.B.R. [37] for testing the bond strength between concrete and rock. It was adapted for measurement of sliding friction between the surfaces of a joint by Jaeger [38] and has since been used extensively for this purpose. In this method, a length of core containing a natural or artificial joint is jacketed in rubber tubing and tested under confining pressure in a conventional triaxial

apparatus (Fig. 2d). Provided the joint is favourably oriented, failure will occur by sliding along the joint rather than in the solid rock. Peak and residual frictional properties may be deduced from load–deformation curves obtained at various confing pressures.

This method is attractive for the following reasons:

(a) The apparatus is simple and usually readily available in rock mechanics laboratories.

(b) Minimal specimen preparation is required since ordinary diamond drill core can be used.

(c) High normal stresses on the joint plane can be applied more readily than in other types of test.

(d) Pore pressures can be more readily introduced and measured than in other type of test.

(e) The specimen is not subject to mechanical constraint and sliding can occur along the direction of least resistance.

On the other hand, there are some uncertainties which require clarification:

(a) The normal stress on the joint plane is not constant during a test but varies with the shear stress.

(b) The area of contact between the faces continually changes as sliding proceeds.

(c) Unknown lateral stresses may be set up at the ends of the cylinder during a test.

These factors make the test difficult to interpret, and the system is generally regarded as not being a good one when large displacements on the shear plane are required. Rosengren [1] has analysed this test in detail, clarifying a number of the questions raised above and providing methods of calculating corrections for these various factors. This important contribution of knowledge is discussed in Section 4 below. The remainder of the present section is devoted to a brief catalog of results obtained using the triaxial method.

Jaeger [38] used 2 in. diameter cores and confining pressures in the range 3,000 to 15,000 p.s.i. For plaster-filled joints the τ-σ failure line was slightly curved and μ varied from 0.4 to 0.78. For sawn and ground bare surfaces, stick-slip oscillations occurred and μ varied from 0.53 to 0.61. For natural fracture surfaces of porphyry, marble, sandstone and gneiss, μ varied from 0.52 to 0.86. Wet surfaces of sandstone and gneiss gave slightly lower values of μ. The intercept τ_0 was not measured accurately but in all cases was less than 3,000 p.s.i. Similar tests using lower confining pressures on natural joints in quartz monzonite carried out by Lane and Heck [39] yielded τ_0 = 200 psi and μ = 0.62. Handin and Stearns [40] used 0.75 in. diameter cores and confining pressures up to 30,000 psi to obtain μ = 0.4 for ground surfaces of dolomite.

Murrell [7] measured the frictional properties of fracture surfaces of sandstone in the course of a more comprehensive study on the strength of rocks. He fitted his results to the power law (Eqn. 7) with constants K = 2.10 and c = 0.89. His results for σ<20,000 p.s.i. can also be fitted to the linear law (Eqn. 6) with τ_0=500 psi and μ=0.70. Raleigh and Paterson [41] measured the residual friction on faults in serpentinite and found that μ (= τ/σ) reduced from 0.73 to 0.40 as the confining pressure increased from 11,000 to 75,000 psi.

A very comprehensive series of tests using the triaxial apparatus has been reported by Brace and Byerlee in recent years. The object of this work was to investigate the significance of friction, particularly of stick-slip, as an earthquake mechanism [42]. Consequently the tests were carried out mainly at high confining pressures, up to 10 kb (150,000 psi), and the specimens were small, 0.5 and 0.6 inch in diameter.

The early work [42] used Westerley Granite. For both ground and fracture surfaces the linear relation (Eqn. 6) was found to hold with τ_0 = 7,500 psi and μ = 0.6 in the range of normal stresses 2 to 10 kb. For ground surfaces with additional pore water pressure, μ remained at 0.6 but c was reduced to 1,500 psi; this way attributed to reduction in strength of the asperities by water. Later work on other rocks [44] led to the adoption of a curved friction relation, particularly at lower normal stresses.

3.5 Rotating Friction Tests.

In these methods, one surface rotates against a stationary slider (Fig. 2e), or two discs rotate in opposite directions about their common axis (Fig. 2f). The frictional resistance can be calculated by measuring the torque, T, required to rotate the cylinder under a given normal load, N. The advantage of these methods is that they are capable of producing infinite displacements without change in geometry and are thus well suited for studying variations in frictional behaviour with displacement, a subject of great practical significance.

The first of these methods was used by Rae [45] for a sandstone wheel and sandstone and limestone sliders tested at very low normal loads. For the sandstone slider, μ = 0.7 and was independent of sliding speed. For the limestone slider, μ reduced from 0.75 to 0.2 as the speed increased from 0 to 15 ft./sec. A similar technique in which one piece of drill core is rotated while in contact with a stationary second piece at right angles to the first is being developed at Imperial College, London [46] with a view to its adoption as a simple field test for the friction of fairly smooth rock surfaces.

A device using the second method has been successfully used at the Chamber of Mines of South Africa [47], and a similar device is also under development at Imperial College. Details of the results obtained have not yet been published.

4 ANALYSIS OF FRICTION MEASUREMENT IN THE TRIAXIAL TEST

4.1 Elementary Theory.

Consider a cylinder containing a planar joint inclined at angle α to its axis (Fig. 6) and subject to principal stresses σ_1 and σ_3. The normal and shear stresses on the joint plane are given by

$$\sigma = \sigma_1 \sin^2\alpha + \sigma_3 \cos^2\alpha \qquad \ldots 11$$
$$= \sigma_3 + (\sigma_1 - \sigma_3) \sin^2\alpha$$

$$\text{and } \tau = (\sigma_1 - \sigma_3) \sin\alpha \cos\alpha \qquad \ldots 12$$

Eqns. 11 and 12 can be combined to give

$$\sigma_1 = \sigma_3 + \tau \tan\alpha \qquad \ldots 13$$

The conditions under which sliding on the joint plane can occur were first given mathematically by Jaeger [37] and are considered in detail in Appendix II. The problem can be conveniently represented on a Mohr diagram (Fig. 7).

It is assumed that the shear strength of the joint is given by the simple linear relationship

$$S = c + \sigma \tan\phi \qquad \ldots 14$$

which is the line DE in Fig. 7. Under hydrostatic pressure σ_3 before the differential stress $(\sigma_1 - \sigma_3)$ is applied, the shear stress on the plane is zero and the normal stress equal to σ_3, point A in Fig. 7. As the differential stress increases, both normal and shear stresses on the plane increase, following the path AC inclined at angle α to the τ axis, which is given in Eqn. 13. Distances such as AL along this stress path are equal to $(\sigma_1 - \sigma_3) \sin\alpha$ and these are also the chords of the Mohr circles originating at A. Eventually the stress path will reach the failure line DE and sliding will commence under the normal and shear stresses corresponding to point C.

This representation shows how the differential stress required to initiate sliding increases with confining pressure and also with α. AH is the stress path for a direct shear test with $\alpha = 0$ and σ constant. As α increases towards ϕ, the intersection point C becomes poorly defined and instability may occur leading to very large changes in differential stress for small change in α. An example will be given later. Clearly, if $\alpha = 90° - \phi$ the stress path will never intersect the failure line and sliding on the joint is impossible. In this case, the differential stress will increase until the Mohr circle based on A reaches the failure envelope for the intact rock. Fracture will then occur in the rock, ignoring the joint. Depending on the strength of the rock this situation can occur for values of α somewhat less than the cirtical value. Fracture will also theoretically occur for small values of α since the Mohr circle will reach the failure envelope before the chord AL reaches the joint failure line DE. However, in practice the lower limit of α is determined by the geometry of the system and for a 2:1 cylinder is of the order of 27°.

If the joint is sufficiently interlocked, or a weakness plane or vein is being tested, stresses correspoinding to point C will be insufficient to initiate sliding.

The stress will then follow the path AB to point K, at which stage shear failure of the filling or shearing of the asperities will occur and the stresses will return along AB to point C which now defines the residual strength of the joint. The peak strength defined by point K lies on the line defining the failure criterion of the filling or of the asperities, which may be assumed to have the linear form

$$S_o = c_o = \sigma \tan \phi_o \qquad \ldots 15$$

where $\tan \phi_o$ is a coefficient of internal friction. The situation is undoubtedly more complex than this (see Section 5) but additional refinements seem unjustified for purposes of the present analysis.

4.2 Change in Contact Area with Sliding

An expression for the instantaneous contact area has previously been presented by Chandler [48]. However, for the following theory additional information is required and a fuller analysis follows.

If the relative displacement along the joint is s, the ends of the cylinder come together by a, and the axis of the cylinder is displaced by b (Fig. 8a). These quantities are related by:

$$a = s \cos \alpha \qquad \ldots 16$$
$$b = s \sin \alpha \qquad \ldots 17$$

The elliptical faces of the joint are displaced by distance s and the true area of contact is A_1, Fig. 8b. On each face of the joint an area A_2 is no longer in contact. Corresponding areas on a horizontal projection are A_1' and A_2' (Fig. 8c). These areas are given by

$$A_1' = \frac{D^2 (2\theta - \sin 2\theta)}{4} \qquad \ldots 18$$

$$A_2' = \frac{D^2 (\pi - 2\theta + \sin 2\theta)}{4} \qquad \ldots 19$$

where D is the diameter of the cylinder and θ is as shown in Fig. 8c and given by

$$\cos \theta = \frac{a \tan \alpha}{D} \qquad \ldots 20$$

The areas on the joint faces are then given by

$$A_1 = \frac{D^2 (2\theta - \sin 2\theta)}{4 \sin \alpha} \qquad \ldots 21$$

and

$$A_2 = \frac{D^2 (\pi - 2\theta + \sin 2\theta)}{4 \sin \alpha} \qquad \ldots 22$$

A convenient approximation when s is small can be calculated by reference to Fig. 8d. The area A_2 is given approximately by

$$A_2 = D.s \qquad \ldots 23$$

and

$$A_1 = \frac{\pi D^2}{\sin \alpha} - D.s \qquad \ldots 24$$

There is, therefore, an approximately linear relation between true area of contact and small displacements on the shear plane.

4.3 Sliding with Large Displacements.

The above analysis strictly applies only to the initiation of sliding with frictionless end conditions for the cylinder. As sliding proceeds, the situation is complicated by change in geometry of the system. If rigid platens are used in the triaxial cell, the ends of the sample must translate (Fig. 6b) and work must be done by the differential stress to overcome frictional resistance at the platens. Most previous investigators have used one spherical seat in the system. However, as noted by Jaeger [37] the situation becomes that of Fig. 6c. as sliding proceeds and it is impossible to maintain uniform normal stress across the joint. The sample then usually fails by secondary splitting. The only other way to maintain uniform contact between the joint faces is to use a spherical seat at each end of the specimen (Fig. 6d).

Both the system of Fig. 6b and 6d have been used in experiments described by Rosengren [1] and the theory for each is set out below. In the analysis it is convenient to work in terms of resultant forces. Stresses can be calculated at any time if the appropriate areas are known. During each stage of a test the confining pressure, σ_3, is held at a constant known value and the axial force, R_1, required to maintain sliding is measured by a testing machine. The "differential stress" obtained is not generally a principal stress because of frictional shear stresses at the ends of the specimen. However, the notation $(\sigma_1 - \sigma_3)$ has been retained in order to make the results comparable with those from elementary theory.

As a preliminary, consider a solid in the shape of two displaced half cylinders of diameter D and cross sectional area A, immersed in a fluid pressure, σ_3. The resultant forces in the plane of the paper are shown in Fig. 9a and are given by

$$P_1 = \sigma_3 \, A \qquad \qquad \ldots 25$$

$$P_2 = \sigma_3 \, \frac{A}{\tan \alpha} \qquad \qquad \ldots 26$$

$$P_3 = \sigma_3 \, A_2 \qquad \qquad \ldots 27$$

where A_2 is given by Eqn. 22. Other forces act on the curved surfaces of the cylinder, but since they are equal, opposite and collinear they may be omitted from further discussion. Since the solid is under hydrostatic pressure, the forces P_1, P_2 and P_3 must be in complete equilibrium and it is possible to calculate the point of action of force P_3, if required, without knowing the centroid of the area A_2. Therefore, any additional non-hydrostatic forces applied to the body must themselves be in complete equilibrium.

4.4 Sliding with Lateral Translation.

This is the situation shown in Fig. 3.6b. In addition to the forces generated by the confining pressure and shown in Fig. 3.9a, there is the differential force R_1, which is measured by the testing machine, and a lateral force R_2 due to frictional restraint at the platens (Fig 9.b). The point of action of R_1 is indeterminate but since the non-hydrostatic forces must be in complete equilibrium and resultant forces at each end of the cylinder must be collinear and therefore the line of action of the resultant makes an angle, $\psi = \tan^{-1} \left(\dfrac{R_2}{R_1} \right)$, with the axis of the cylinder.

In fact, the point of action of R_1 is not relevant in the statics of the problem and for the symmetrical case, (Fig. 9b) it will be assumed that the resultant passes through the centroid of the contact area A_1.

With regard to the relation between R_1 and R_2^1 during sliding there are two possible experimental arrangements: -

(i) The sliding platens may be enclosed with the specimen inside the rubber jacket. In this case, the confining pressure contributes to the normal stress between the platens and

$$R_2 = k (R_1 + \beta P_1) \qquad \qquad ...29$$

where K is a coefficient of friction between the sliding platens, and assumed constant. The coefficient β is introduced since the area of contact between the platens decreases as sliding proceeds, and

$$\beta = \frac{A_3'}{A} \qquad \qquad ...30$$

where A_1' is the contact area given by Eqn. 18 and A is the cross-sectional area of the cylinder.

(ii) The sliding platens may be exposed to the confining fluid. In this case:

$$R_2 = k R \qquad \qquad ...31$$

and it is, mathematically, a special case of Eqn. 29 with $\beta = 0$.

The low half of the specimen (Fig. 9c) is an equilibrium under the action of forces P_1, P_2, P_3 from the confining pressure; forces R_1 and R_2 as discussed above; the normal and shear forces, N and F respectively, from upper half of the specimen on the shear plane. Resolving these forces and using Eqn. 29, we have:

$$N = R_1 (\sin\alpha + \cos\alpha) + P_1 (\sin\alpha + \beta k \cos\alpha) + P_2 \cos\alpha - P_3 \qquad ...32$$

$$F = R_1 (\cos\alpha - k \sin\alpha) + P_1 (\cos\alpha - \beta k \sin\alpha) - P_2 \sin\alpha \qquad ...33$$

The normal stress σ and shear stress τ can be obtained by dividing the resultant forces by the contact area A_1 (Eqn. 21). One case of interest is that at the initiation of sliding when $A_1 = \frac{A}{\sin\alpha}$, $\beta = 1$ and $P_3 = 0$. Eqns. 32 and 33 yield

$$\sigma = \sigma_1 \sin\alpha (\sin\alpha + k \cos\alpha) + \cos^2\alpha \qquad \qquad ...34$$

$$\tau = \sigma_1 \sin\alpha(\cos\alpha - k \sin\alpha) - \sigma_3 \sin\alpha \cos\alpha \qquad \qquad ...35$$

valid for $\alpha > 0$. When the ends of the cylinder are frictionless, k = 0, and these equations reduce to Eqns. 11 and 12.

Since a differential force – displacement curve is the output from a test it is also instructive to investigate the variation of differential stress with displacement for a rock with a constant value of the coefficient of friction (equivalent to tan ϕ in Eqn. 14). Although most rock surfaces show a cohesion intercept

when the results are reduced in terms of μ = constant [35], for purposes of illustration the equations are simplified, but of the same form, by ignoring the cohesion term. Therefore, putting F = N Eqns. 32 and 34 give

$$R_1 = \frac{P_1 \ (\mu+k\beta) \ \sin\alpha-(1-\mu k\beta) \ \cos\alpha) + P_2(\mu\cos\alpha+ \ \sin\alpha) - \mu P_3}{(1-\mu k)\cos\alpha- \ (\mu+k)\sin\alpha} \qquad \ldots 36$$

or dividing by the appropriate areas,

$$\sigma_1-\sigma_3 = \sigma_3 \ \left\{ \frac{\frac{\mu}{\sin\alpha} + \beta k \ \sin\alpha + \beta\mu k \ \cos\alpha - \frac{A_2}{A}}{(1-\mu k) \ \cos\alpha - (\mu+k) \ \sin\alpha} \right\} \qquad \ldots 37$$

The corresponding relation for the case when the platens are exposed to the confining fluid is

$$\sigma_1-\sigma_3 = \sigma_3 \ \left\{ \frac{\frac{\mu}{\sin\alpha} - \mu\frac{A_2}{A}}{(1-\mu k) \ \cos\alpha - (\mu+k) \ \sin\alpha} \right\} \qquad \ldots 38$$

To illustrate the effect of platen friction on the interpretation of this test, values of the ratio $(\sigma_1-\sigma_3)/\sigma_3$ at the initiation of sliding are shown in Table 1, for the case $\alpha = 40°$ and various values of μ and k.

TABLE 1

Values of $(\sigma_1-\sigma_3)/\sigma_3$ At Initiation of Sliding

K	0.3	0.4	0.5	0.6	0.7	0.8
0	0.82	1.22	1.75	2.45	3.45	4.94
0.001	0.82	1.23	1.76	2.46	3.46	4.97
0.005	0.83	1.24	1.78	2.50	3.53	5.09
0.01	0.84	1.27	1.81	2.56	3.62	5.25
0.05	0.96	1.45	2.11	3.04	4.46	6.92
0.01	1.14	1.73	2.57	3.86	6.09	10.90
0.2	1.61	2.55	4.11	7.22	16.50	*
0.3	2.34	4.05	7.93	25.50	*	*
0.4	3.64	7.75	34.60	*	*	*
0.5	6.60	32.00	*	*	*	*

*Indicates sliding on joint not possible.

It is evident that unless these frictional effects are eliminated, or at least precisely known so that corrections can be made, very significant errors may be introduced by assuming that there are no end effects on the specimen.

Typical differential stress-displacement curves predicted by Eqn. 37 for the case $\alpha = 40°$ and several values of k and μ are shown in Fig. 10. These show an almost linear decrease in differential stress with displacement.

4.5 Sliding with Rotation

This is the case shown in Fig. 6d with a spherical seat at each end of the specimen. The geometric constraints of this system are: -

(i) Each half of the specimen must rotate about the center of its respective spherical seat.

(ii) The centres of the spherical seats must move along the axis of the apparatus. This only applies if the outer parts of the spherical seats are fixed relative to the apparatus. If the spherical seats are free to translate laterally it is possible to have the more complicated situation of combined rotation and lateral translation. However, only the case of pure rotation will be considered here.

With regard to the geometry of the spherical seats there are three basic cases.

Case A: The center of each spherical seat may lie within its respective half of the specimen (Fig. 11a).

Case B: The spherical seats may be reversed so that the centers lie outside of, but on the same side of the shear plane as, the respective halves of the specimen (Fig. 11b).

Case C: The centers of each spherical seat may lie on the opposite side of the shear plane to its respective half of the specimen (Fig. 11c).

There is no restriction on the radii of the spherical seats and the two seats need not have the same radius. Any combination of the three cases above is possible but not necessarily practical. The only inadmissable situation is that where the centers of the two seats coincide, in which case the system is unstable since the specimen can rotate as a rigid body. Clearly, if the centers are close together the system is quasi-stable since large rotations will be required to accommodate small displacements on the slip plane.

In cases A and B, the shear plane rotates away from the axis of the apparatus and the centers of the spherical seats approach each other as shearing proceeds. In case C, the shear plane rotates towards the axis and the centers move apart. The case of pure translation discussed previously is a special case of case C, with seats of infinite radius.

The full mathematical treatment will not be given here but the equation corresponding to Eqn. 38 is.

$$\sigma_1 - \sigma_3 = \sigma_3 \left\{ \frac{k'\sin(\alpha+\delta) + k'\cos(\alpha+\delta) + \dfrac{\mu}{\sin\alpha} - \mu\dfrac{A_2}{A}}{(1-\mu k')\cos(\alpha+\delta) - (\mu+k')\sin(\alpha+\delta)} \right\} \quad \ldots 39$$

where k' is the equivalent coefficient of friction in the spherical seat and δ is the instantaneous angle of rotation of each half of the specimen about its spherical seat.

Theoretical differential stress-displacement curves are shown in Fig. 12. It is clear that even for rock surfaces with a constant coefficient of friction the interpretation of this test is by no means straightforward.

4.6 Apparatus.

Due to its inherently simpler nature the lateral translation method has been adopted although some tests using two spherical seats have also been performed (1). To minimize frictional restraint two hardened and polished steel disc lubricated with Molybond GA50 are placed at each end of the specimen. Molybond GA50 has an unusually low coefficient of friction of 0.005 under high normal loads.

The results of a large number of tests carried out by Rosengren (1) both with and without pore pressure, on rough (500 microinch) surfaces of Narrandera quartite are shown in Fig. 13. This rock surface closely obeys the linear relation with $\mu = 0.70$ and clear obeys the effective stress law. Comparative tests using this rock and

(i) lubricated discs
(ii) unlubricated ends and one spherical seat

indicated that the conventional method (ii) can lead to very large overestimates of frictional properties.

One further point is that interaction between the ends of the specimen and the platens may contribute to some of the effects observed during sliding. Some exploratory experiments with composite specimens in the direct shear apparatus (1), indicate that the stick-slip oscillations commonly occur in the sliding of quartzite of steel. It is therefore possible for stick-slip to occur at unlubricated platens in a triaxial test. This effect may have contributed to the stick-slip oscillations recorded for very rough surfaces of granite by Brace and Byerlee (42).

4.7 Frictional Properties of Natural Joints.

Most previous work on rock friction has been done with surfaces prepared by cutting and grinding to a known roughness. These surfaces may not be representative of natural joints since the roughness, and surface coatings, are often vastly different. Lane and Heck (39) gave a few results for natural joints in granitic rocks but there is little other information available other than that recently obtained in large direct shear machines (22-29).

The procedures outlined in the previous section were developed by Rosengren (1) primarily for testing natural joints in diamond drill core in connection with a slope stability investion at Mount Isa Mines, Australia. The core was NMLC size, 2.045 in. nominal diameter, obtained by careful drilling with a split inner

tube, triple tube core barrell so that most of the joints were well preserved. The rock types involved were shale, siltstones and slates, and a variety of different joints in terms of orientation, roughness and surface coating were available. Most of the joints discussed here were remarkably planar in the dimensions of the drill core. On appearance they could be divided into two broad classes:

(i) Shear fractures or faults. These tend to be slickensided or polished and have mainly chlorite or sometimes graphite coatings.

(ii) Extension fractures. These tend to be more interlocked on a fine scale and their coatings are usually limonite, pyrite, quartz, dolomite or occasionally they may be clean.

From the outset, it became apparent that different joints showed vastly different behaviour during the initial stages of sliding. They could be divided into four groups with some intermediate behaviour. The types of initial load – displacement curve obtained are shown in Fig. 14 and tabulated in Table 2.

TABLE 2 (after Rosengren [1,2])

LOAD-DISPLACEMENT CURVE CHARACTERISTICS FOR NATURAL JOINTS.

Type of Behaviour	Characteristic Joints
A. No slip until peak load then gradual drop off to residual value. Fig. 14a.	Joints with large interlocking asperities; bedding planes with cross ripples; faults with cross slickensides or grooves.
B. Well defined initial slip which continues at constant load. Fig. 14b.	Joints with hard, fairly smooth surfaces; also Narrandera quartzite.
C. Well defined initial slip which continues with rising load. Fig. 14c.	Relatively rough, chlorite or graphite coated surfaces; very smooth hard surfaces.
D. Continuous curvature of load displacement curve. Fig. 14d.	Faults with smooth or polished chloritic surfaces.

Goodman (31) has similarly identified four types of shear stress-displacement relationship for naturally occurring planes of weakness. The recognition of these types of load-deformation curve is of great practical significance since they provide guidelines to the type of joint characteristic which should

be incorporated in analyses. The significance of such curves in respect of finite element analyses incorporating joint-elements is discussed in Section 2.3, of Appendix II of this report.

Significant findings of Rosengren's testing program carried out using the modified triaxial technique were:

(i)   Despite the wide variation in types of surface tested, the coefficients of friction nearly all fell in the narrow range 0.5 to 0.7. The principal exceptions were the graphite coated faults which, as would be expected, give lower values of the range 0.2 to 0.3.

(ii)   Those joints which were tested with pore pressure appeared to obey the effective stress law. There was no significant difference in frictional behaviour of wet and dry surfaces. One test indicated that the coefficient of friction for polished chlorite coated surfaces may be lowered by the presence of water (c/f. Horn and Deere (17)).

(iii)   All joints tested showed a small residual cohesion of up to 200 p.s.i.

Rosengren (1,2) recognized that the major deficiency of this work is that the size of the joints tested is extremely small compared with the size of joints influencing an engineering structure in rock. The longer wavelength undulations found in natural joint planes (see Section 5 below) are not taken into account, and so it appears likely that the friction parameters measured would be minimum values, at least in terms of peak resistance. Rosengren's techniques have been adapted to 6 in. diameter specimens by Jaeger (49) and by the author at the James Cook University of North Queensland, Australia. Results obtained for graphite coated joints in the rocks tested by Rosengren have given similar friction parameters to those obtained using 2 in. diameter specimens. Obviously much more work is required before an answer to the question of the influence of size on joint strengths can be answered.

5   INFLUENCE OF THE SURFACE TEXTURE OF JOINTS.

5,1   The General Problem.

The variations in surface texture occurring from joint to joint or over a given joint surface cause difficulties in the determination of the strength of rock joints not met in measuring the frictional properties of most other engineering materials. Until very recently, most work on the frictional properties of rock surfaces or natural surfaces which have been qualitatively described as "rough" or "smooth". The area most needful of further research is undoubtedly the quantification of the relationship between surface texture and joint strength.

The problem of the influence of size on joint strength referred to in Section 4.7 above is intimately linked with that of surface texture. Deere et al (50) have provided a useful illustration of how laboratory tests and in in-situ tests may measure the influence of surface features different from those governing prototype behaviour (Fig. 15).

5.2   Elementary Theory.

For the ideal case shown in Fig. 16a, the limiting conditions of equilibrium are given by the relation

$$H = V \tan \phi_\mu$$

or

$$\tan \phi_\mu = \frac{H}{V} \qquad \qquad ...(40)$$

where V is the vertical or normal force, H is the horizontal or shear force, and $\tan \phi_\mu$ is the true coefficient of friction between the two surfaces.

If the joint is inclined at an angle i to the shear direction as in Fig. 18b, the resultant force on the joint plane is inclined at $(\phi_\mu + i)$ to horizontal in the limiting equilibrium condition. In this case,

$$H = V \tan (\phi_\mu + i)$$

or

$$\tan (\phi_\mu + i) = \frac{H}{V} \qquad \qquad ...(41)$$

and the apparent coefficient of friction given by $\frac{H}{V}$ is greater than the true value. Eqn. 41 also holds for negative values of i (Fig. 16c) if the correct algebraic value of i is used.

The true coefficient of friction for the surfaces may be obtained by expanding the term $\tan (\phi_\mu + i)$ to get

$$\tan \phi_\mu = \frac{\frac{H}{V} - \tan i}{1 + \frac{H}{V} \tan i} \qquad \qquad ...(42)$$

Bray, (12,13) has shown how the apparent friction angle can change with displacement as slip proceeds. For the idealized surface profile shown in Fig. 17a, an initial apparent friction angle of $\phi + \lambda_1$ will be recorded for slip on the A planes. With continued movement in the same direction, the position shown in Fig. 17b will eventually be reached, with slip proceeding down the B surfaces. The apparent angle of friction

is now $\phi_0 - \lambda_2$. As movement continues, the apparent friction angle alternates between these two limiting values as shown in Fig. 17c.

Withers (51) investigated the validity of this elementary theory using flat and sinusoidal surfaces of mild steel, copper and plexiglass. For the sinusoidal surface shown in Fig. 18, he found that the resistance to the first relative movement is the peak resistance and is given by

$$H = V \tan (\phi_\mu + i) \qquad \qquad ...(41)$$

After the initial movement, the angle $\phi_\mu + i$ decreases for sinusoidal surfaces, and the resistance to sliding is lowered. If $(\phi_\mu + i) > \frac{\pi}{2}$, initial movement can take place only by shearing through the intact material.

Where the normal load increases linearly with deformation, the sliding resistance also increases with deformation and is given by

$$H = (V_1 + kZ) \tan (\phi_\mu + i) \qquad \qquad ...(43)$$

where V_1 is the normal load when movement on the joint surfaces is initiated, k is the slope of the load-deformation curve for the material, and Z is the vertical component of movement on the sliding surface.

Patton (52,53) has also examined the validity of Eqn. 41 using plaster of paris with sand or kaolin filler as a model material in tests on samples in which the sliding surfaces were either smooth and flat or contained moulded rectangular or saw teeth as illustrated in Fig. 19. A linear relation between N and S was found for the flat surfaces with ϕ_μ in the range $27\frac{1}{2}°$ to $31°$. In the models with saw teeth, two types of behaviour were observed. Under low normal loads, the upper half of the specimen rode up over the teeth on the lower half, the S/N relation being a straight line through the origin with a slope of $(\phi_\mu + i)$. Under higher normal loads, the teeth were sheared off and the failure relation was another straight line of slope $\phi_r = \phi_\mu$, and an intercept on the S axis corresponding to the load required to shear through the teeth. This intercept increased with the number of teeth in a specimen (Fig. 20). Patton therefore suggested that for real rock surfaces a single linear failure relation may be unrealistic in view of the possibility of multiple nodes of behaviour.

5.3   Measurement and Description of Surface Texture.

American Standard ASA B 46.1-1962 (54) defines surface texture as the repetitive or random deviations from the normal surface which form the pattern of the surface. Surface texture has four components:

(i)   Roughness consisting of the fine scale irregularities, or asperities, in the surface which contribute to the surface "finish".

(ii)   Waviness consisting of the larger scale, long wavelength, undulations in the surface.

(iii)   Lay, which is the direction of the predominant surface pattern.

(iv)   Flaws which are irregularities which occur at one place or at relatively infrequent or widely varying intervals in a surface.

Instruments for the measurement of surface finish are widely used in metal cutting. These consist of a fine radius diamond stylus which follows the asperities as it is moved across the surface. The surface profile is continuously recorded on a chart and/or electrically averaged and displayed on a meter as the arithmetic average root mean square deviation from the mean surface. Examples are the Talysurf used by Byerlee (43) and the Brush Surfindicator used by Hoskins, Jaeger and Rosengren (36). The maximum range of such instruments is usually 1000 microinch deviation and so they are only useful for measuring "smooth" surfaces produced in the laboratory.

The standard roughness width-cutoff of these instruments is usually 0.030 in. and waviness of wavelength greater than this value is therefore not included in the surface measurement. Horino, Hoskins, and Ellickson (54) have developed an instrument consisting of an LVDT probe with a maximum range from 200 to 40,000 microinch. The probe is mounted relative to the traversing table of a milling machine and so can measure both roughness and waviness.

Waviness can be measured with a coarse measuring instrument such as dial gauge moving on a fixed baseline relative to the rock surface. This is a time consuming operation and an LVDT feeding an X-Y recorder is a more sophisticated method.

The roughness and waviness of a ground rock surface will depend on the method of grinding, the type of grinding medium and the mineralogy of the rock. As an example, grinding with 600 grit carborundum powder will give a roughness of 30 to 100 microinch for most rock types. Much smoother surfaces can be obtained using alumina powder or diamond paste. The lay of the surface will be determined by the grinding method. For example, an oscillating diamond wheel will produce a linear lay whereas grinding by hand on a glass plate will produce a circular type lay.

It is only very recently that any quantitative information on the surface texture of natural joints has been produced. All four texture components are important with waviness and lay probably the most significant. A number of techniques for collecting data on surface texture have been recently developed so that this aspect of the problem does not present any great difficulty at the present time. The greater difficulty lies in the presentation and use of this data. Should an attempt be made to relate "mean" surface roughness to joint strength as is done in the case of "smooth" surfaces described above, or should only the major surface features be considered? These questions as yet remain unanswered.

Rengers (27) has developed a unique form of presentation of surface data which could lead to a solution of this problem. Different measuring techniques are used for specimens in different size ranges. For surfaces on the scale of hand specimens, a stereodepth measurement microscope is used with both horizontal and vertical displacements being recorded with arbitrary enlargement on an X-Y recorder. For profiles of a size between 20 cm. and 2 m, a specially developed "profilograph" (55) is used. The profilograph traverses the rock surface in a series of straight lines and records surface roughness with 1:1 correspondence by mechanical means. Terrestrial photogrammetry is used for recording profiles of larger in-situ surfaces.

Rengers' method of describing surfaces using data so obtained is illustrated in Fig. 21. A reference plan is chosen parallel to the largest observable extension of the joint plane. The intersection of this plane with the plane of a given profile is the line indicated by "ref" in Fig. 21a. On the recorded profiles, measuring points are set out with a mutual separation measured parallel to ref of L = 1 mm which in fact represents real steps of 0.1mm, 1 mm and 2 cm on stereomicroscope, profilograph and photogrammetric profiles respectively. From every such point on the profile, connection lines are drawn to other points at pre-determined stepsizes, nL, away. The connection lines make positive and negative angles α with the reference line. Fig. 21b shows a plot of tan α against real stepsize for the profiles shown in Fig. 21a.

Using this form of presentation of profile data, some very important aspects of the relative moment of two surfaces can be easily demonstrated. For example, the roughness pattern can obviously be different for positive and negative angles of α indicating that the two different senses of relative movement along a profile will show different frictional properties. This distinction cannot be made using other methods of presentation such as departure from a mean surface. Further, a relationship between dilatation and relative movement can be plotted from this data, assuming that all asperities will be overridden rather than sheared through.

Mathews (56) used a method for measuring surface profiles of laboratory specimens in which dial gauge readings were taken on a grid pattern over the surface. For specimens of approximately 9 in. long x 6 in. wide dial gauge readings were taken at 0.125 in. intervals along lines spaced 0.5 in. apart and parallel to the long direction of the specimen. A plane of best fit was determined for each surface using a multiple linear regression analysis, and a contoured plot of heights above and below this plane produced on a computer. Mathews' approach has been modified at the James Cook University of North Queensland where profiles are continuously recorded by the outputs of longitudinally and vertically mounted LVDT's produced when the specimen mounted in a milling machine is moved forward (c/f. Horino, Hoskins and Ellickson (54)).

From these surface profile measurements and measurements of shear and normal displacements occurring during direct shear tests, Mathews was able to show how the two surfaces moved relative to each other during a test, and locate local zones of shearing. As an example, consider the results of a

test carried out on a 6 in. x 6.6 in. sample of a carbon coated bedding plane joint in a shale. The mean and maximum departures from the plane of best fit were measured as 0.032 in. and 0.089 in. respectively. Two runs were carried out at a normal load of 19,750 lb. Shear force-displacement and dilatation-shear displacement curves for these two runs are shown in Fig. 22. The relative positions of the two sections at one edge of the specimen after 1 in. of sliding are shown in Fig. 23.

In a series of tests on such specimens taken from the same bedding plane joint, Mathews obtained peak angles of friction varying between 15° and 44°, the result obtained for a given specimen apparently depending on surface roughness. It is interesting to note, however, that Mathews was unable to correlate this variation with either the mean or maximum roughness values calculated by his method of presenting surface texture data. As a consequence of these results, Mathews suggested that limiting angles of friction determined from relatively smooth natural joints should be used in design, on the grounds that an assessment of the influence of abnormal roughness will be extremely difficult.

REFERENCES

1. ROSENGREN, K.J. - Rock mechanics of the Black Star open cut, Mount Isa. Ph.D. thesis, Australian National University, Canberra, June, 1968.
2. ROSENGREN, K.J. - Frictional properties of rock surfaces. Vacation School in Rock Mechanics, Univ. College of Townsville, May, 1969.
3. BOWDEN, F.P. and TABOR, D. - The friction and lubrication of solids, Vol. 1. Oxford, Clarendon Press, 1950, 337 pp.
4. BOWDEN, F.P. and TABOR, D. - The friction and lubrication of solids, Vol. 2. Oxford, Clarendon Press, 1964, 337 pp.
5. CARLISLE, D. - Sliding friction and overthrust faulting. J. Geol., Vol. 73, Mar., 1965, pp. 271-290.
6. JAEGER, J.C. and COOK, N.G.W. - Fundamentals of Rock Mechanics. London, Methuen, 1969, 513 pp.
7. MURRELL, S.A.F. - The effect of triaxial stress systems on the strength of rocks at atmospheric temperatures. Geophys. J.R. astr. Soc., Vol. 10, No. 3. Dec., 1965, pp. 231-281.
8. MAURER, W.C. - Shear failure of rock under axial and hydrostatic pressure. Proc. 1st Congr., Int. Soc. Rock Mech., Lisbon, 1966, Vol. 1, pp. 337-341.
9. HOBBS, D.W. - The strength and stress-strain characteristics of coal in triaxial compression. J. Geol., Vol. 72, No. 2, March, pp. 214-231.
10. HOBBS, D.W. - A study of the behaviour of broken rock under triaxial compression and its application to mine roadways. Int. J. Rock Mech. Min. Sci., Vol. 4, No. 1, March, 1966, pp. 11-43.
11. TIMOSHENKO, S. and GOODIER, J.N. - Theory of elasticity, 2nd ed. New York, McGraw-Hill, 1951, pp. 506.
12. ARCHARD, J.F. - Elastic deformation and the contact of surfaces. Nature, Vol. 172, 1953, pp. 918-919.
13. ARCHARD, J.F. - Elastic deformation and the laws of friction. Proc. Roy. Soc., Series A, Vol. 243, pp. 190-205.
14. BROWN, E.T. and TROLLOPE, D.H. - Strength of a model of jointed rock. J. Soil Mech. Found. Div., ASCE, Vol. 96, No. SM2, Mar., 1970, pp. 685-704.
15. HOEK, E. - The brittle fracture of rock. In Rock mechanics in engineering practice, K.G. Stagg and O.C. Zienkiewicz (eds.), London, John Wiley, 1968, pp. 99-102.
16. BYERLEE, J.D. - Theory of friction based on brittle fracture. J. Appl. Phys., Vol. 38, No. 7, June 1967, pp. 2928-2934.
17. HORN, H.M. and DEERE, D.U. - Frictional characteristics of minerals. Geotechnique, Vol. 12, No. 4, Dec., 1962, pp. 319-335.
18. TERZAGHI, K. - Erdbaumechanik auf Boden-physikalischer Grundlage. Vienna, Deuticke, 1925, pp. 399.
19. TSCHEBOTARIOFF, G.P. and WELCH, J.D. - Lateral pressures and friction between soil minerals. Proc. 2nd Int. Conf. Soil Mech. Found. Eng., Rotterdam, 1948, Vol. 7, pp. 135-138.
20. PENMAN, A.D.M. - Shear characteristics of a saturated silt measured in triaxial compression. Geotechnique, Vol. 3, No.8, 1953, pp. 312-328.

21. RIPLEY, C.F. and LEE, K.L. - Sliding friction tests on sedimentary rock specimens. Trans. 7th Int. Congr. Large Dams, Rome, 1961, Vol. 4, pp. 657 - 671.

22. DRSMANOVIC, D. and LANGOF, Z. - Large scale laboratory tests on the shear strength of rocky material. Felsmechanik und Ingenieurgeologie, Suppl. 2, 1964, pp. 20-30.

23. KRSMANOVIC, D. - Initial and residual shear strength of hard rocks. Geotechnique, Vol. 17, No. 2, June, 1967, pp. 145-160.

24. HOEK, E. and Pentz, D.L. - The stability of open pit mines. Rock Mech. Res. Rep., No. 5, Imperial College, London, 1968.

25. HOEK, E. - Estimating the stability of excavated slopes in opencast mines. Trans. Inst. Min. Met., Section A, Vol. 79, 1970, pp. A109-A132.

26. BURMAN, B.C. - Some aspects of the mechanics of slopes and discontinuous media. Ph.D. thesis, James Cook Univ. of North Queensland, Townsville, 1971.

27. RENGERS, N. - Influence of surface roughness on the friction properties of rock planes. Proc. 2nd Congr., Int. Soc. Rock Mech., Belgrade, 1970, Vol. 1, Paper 1-31.

28. BERNAIX, J. - La mesure de la resistance des roches. Proc. Geotech. Conf., Oslo, 1967, Vol. 1, pp. 245-257.

29. BERNAIX, J. - New laboratory methods of studying the mechanical properties of rocks. Int. J. Rock Mech. Min. Sci., Vol. 6, No. 1, Ja., 1969, pp. 43-90.

30. GUISEPPE, B. - The shear strength of some rocks by laboratory tests. Proc. 2nd Congr., Int. Soc. Rock Mech., Belgrade, 1970, Vol. 2, Paper 8-24.

31. BOODMAN, R.E. - The deformability of joints. In Determination of the in-situ modulus of deformation of rock. ASTM STP 477, 1970, pp. 174-196.

32. SERAFIM, J.L. and LOPES, J.B. - In-situ shear tests and triaxial tests on foundation rocks of concrete dams. Proc. 5th Int. Conf. Soil Mech. Found. Eng., Paris, 1961, Vol. 1, pp. 533-540.

33. KRSMANOVIC, D. and POPOVIC, M. - Large scale tests of the shear strength of limestone. Proc. 1st Congr., Int. Soc. Rock Mech., Lisbon, 1966, Vol. 1, pp. 773-779.

34. WALLACE, G.B. and OLSEN, O.J. - Foundation testing techniques for arch dams and underground power-plants. In Testing Techniques for Rock Mechanics, ASTM STP 402, 1966, pp. 272-289.

35. MAURER, W.C. - Shear failure of rock under compression. J. Soc. Petrol. Engrs., Vol. 5, 1965, pp. 167-176.

36. HOSKINS, E.R., JAEGER, J.C. and ROSENGREN, K.J. - A medium-scale direct friction experiment. Int. J. Rock Mech. Min. Sci., Vol. 5, No. 2, Mar., 1968, pp. 143-154.

37. U.S. Bureau of Reclamation - Bond strength between concrete and rock from Monticello dam site, Solano project, California. Concrete Lab. Rept., No. C-761, 1954.

38. JAEGER, J.C. - The frictional properties of joints in rock. Geogis. pura e appl., Vol. 43, 1959, pp. 148-158.

39. LANE, K.S. and HECK, W.J. - Triaxial testing for rock joints. Proc. 6th Symp. Rock Mech., Rolla, 1964, pp. 98-108.

40. HANDIN, J. and STEARNS, D.W. - Sliding friction of rocks. Trans. Am. Geophys. Union, Vol. 45, 1964, p. 103.

41. RALEIGH, C.B. and PATERSON, M.S. - Experimental deformation of serpentine and its tectonic implications. J. Geophys. Res., Vol. 70, No. 16, 1965, pp. 3965-3985.

42. BRACE, W.F. and BYERLEE, J.D. - Stick-slip as a mechanism for earthquakes. Science, Vol. 153, No. 3739, 1966, pp. 990-992.

43. BYERLEE, J.D. - Frictional characteristics of granite under high confining pressure. J. Geophys. Res., Vol. 72, No. 14, 1967, pp. 3639-3648.

44. BYERLEE, J.D. - Brittle-ductile transition in rocks. J. Geophys. Res., Vol. 73, No. 14, 1968, pp. 4741-4750.

45. RAE, D. - The measurement of the coefficient of friction of some rocks during continuous rubbing. J. Sci. Instrum., Vol. 40, 1963, pp. 438-440.

46. HOEK, E. - Private communication, 1971.

47. COOK, N.G.W. - Private communication, 1971.

48. CHANDLER, R.J. - The strength of stiff silty clay. Proc. Geotechnical Conf., Oslow 1967, Vol. 1, p. 103.

49. JAEGER, J.C. - The behaviour of closely jointed rock. In Rock Mechanics - Theory and Practice (Proc. 11th Symp. Rock Mech.), W.H. Somerton (ed.), New York, AIME, 1970, pp. 58-68.

50. DEERE, D.U., HENDRON, A.J., PATTON, F.D. and CORDING, E.J. - Design of surface and near-surface construction in rock. In Failure and Breakage in Rock (Proc. 8th Symp. Rock Mech.), C. Fairhurst (ed.), New York, AIME, 1967, pp. 237-302.

51. WITHERS, J.H. - Sliding resistance along discontinuities in rock masses. Ph.D. Dissertation, Univ. of Illinois, 1964.

52. PATTON, F.D. - Multiple modes of shear failure in rock and related materials. Ph.D. dissertation, Univ. of Illinois, 1966.

53. PATTON, F.D. - Multiple modes of shear failure in rock. Proc. 1st Congr., Int. Soc. Rock Mech., Lisbon, 1966, Vol. 1, pp. 509-513.

54. HORINO, F.G., HOSKINS, J.R. and ELLICKSON, M.L. - A method of measuring surface texture of rock. U.S. Bureau Mines R.I. 7095.

55. FECKER, E. - Geologische Kartierung des Gebietes nordwestlich von Neustadt/Weinstrasse sowie Bau und Anwendung eines Profilographen. Diplom Thesis, Univ. of Karlsruhe, W. Germany, 1970.

56. MATHEWS, K.E. - Excavation design in hard and fractured rock at the Mount Isa Mine, Australia, M.E. thesis, Univ. of Queensland, Australia, July, 1970.

57. JAEGER, J.D. - Friction of rocks and stability of rock slopes. Geotechnique, Vol. 13, No. 2, June 1971, pp. 97-134.

58. LADANYI, B. and ARCHAMBAULT, G. - Simulation of shear behavior of a jointed rock mass. In Rock Mechanics - Theory and Practice (Proc. 11th Symp. Rock Mech., W.H. Somerton (ed.), New York, AIME, 1970, pp. 105-125.
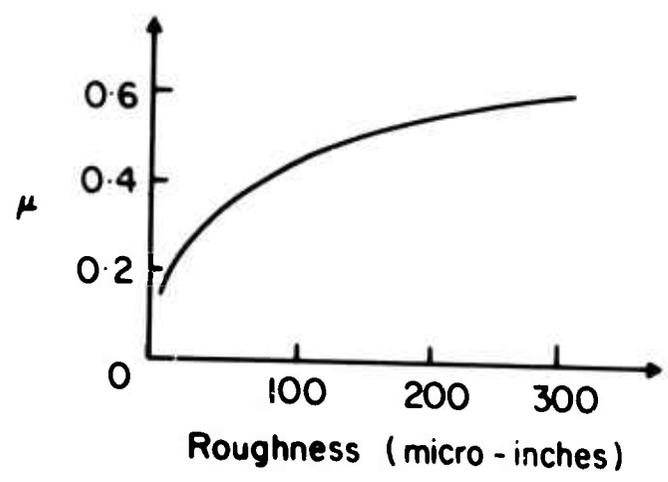
Fig. 1: Variation of the Coefficient of Friction (μ) with Roughness.
(After Byerlee [16]).
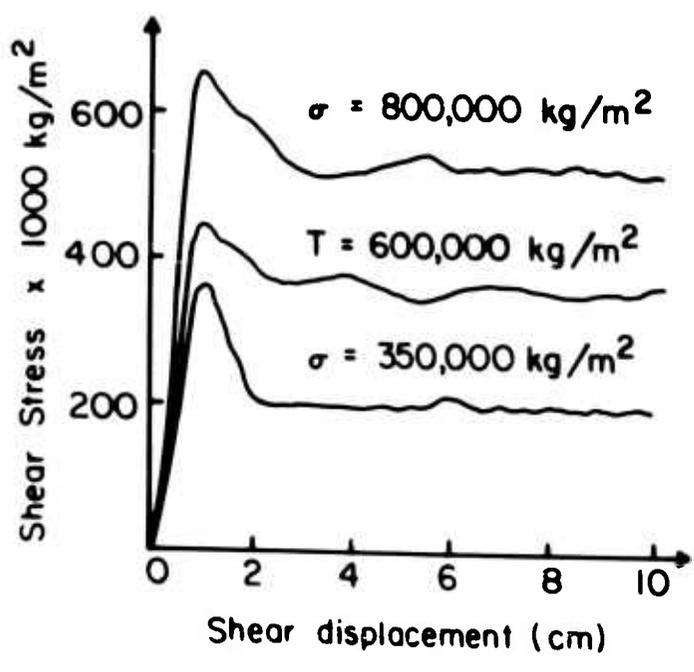
(a)
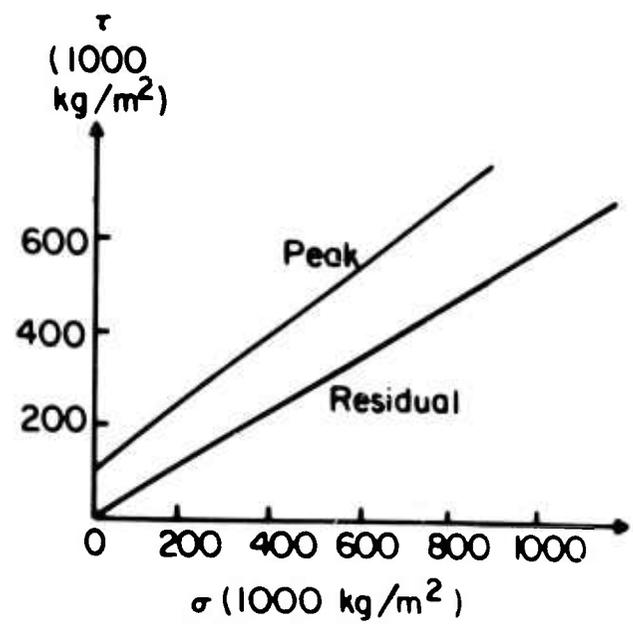
(b)

Fig. 3: Results of Direct Shear Tests on Joints in Porphyry.
(After Hoek [25]).

146
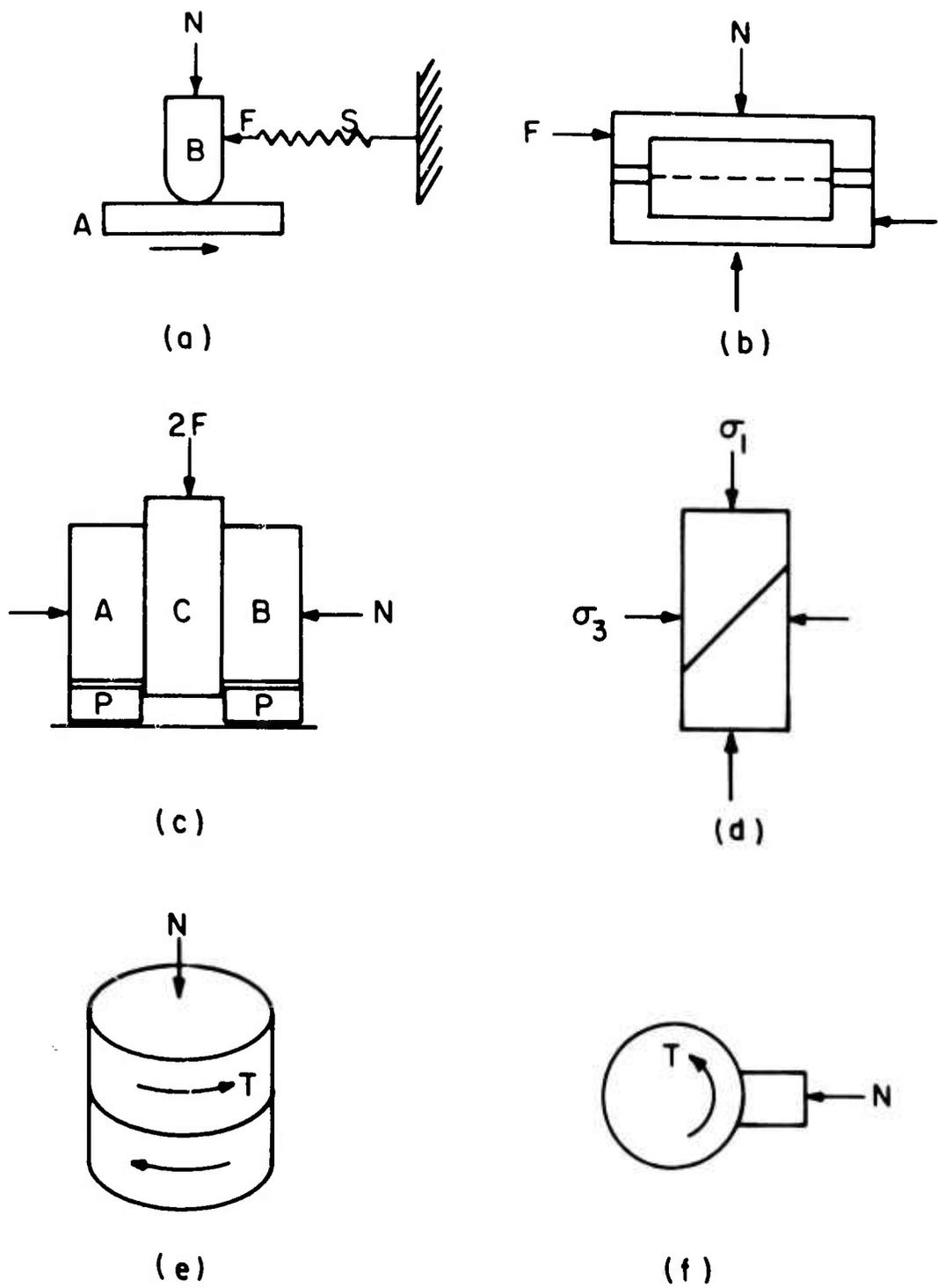
Fig. 2: Methods of Measuring Friction for Rock. (After Rosengen [1]).
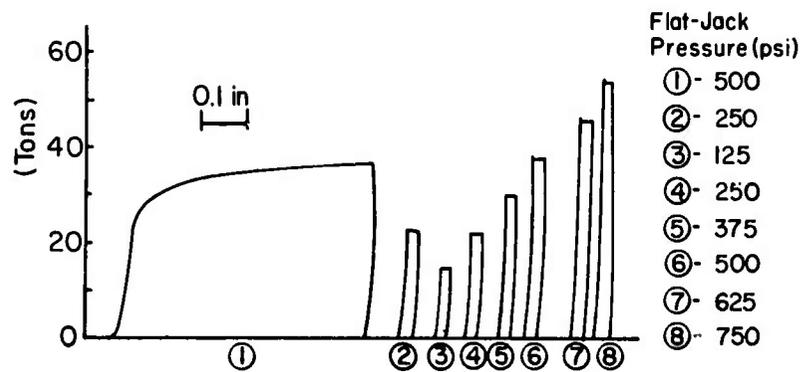
Fig. 4: Load Displacement Curves for Rough Trachyte.
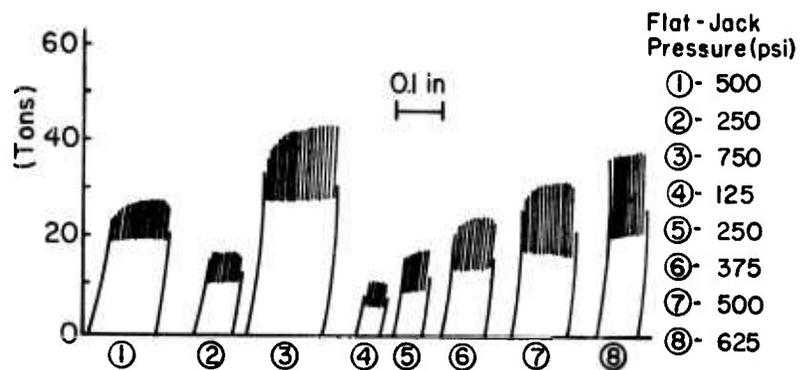
Fig. 5: Load Displacement Curves for Smooth Red Granite with Surface Roughness 35 ± 5 μ in.
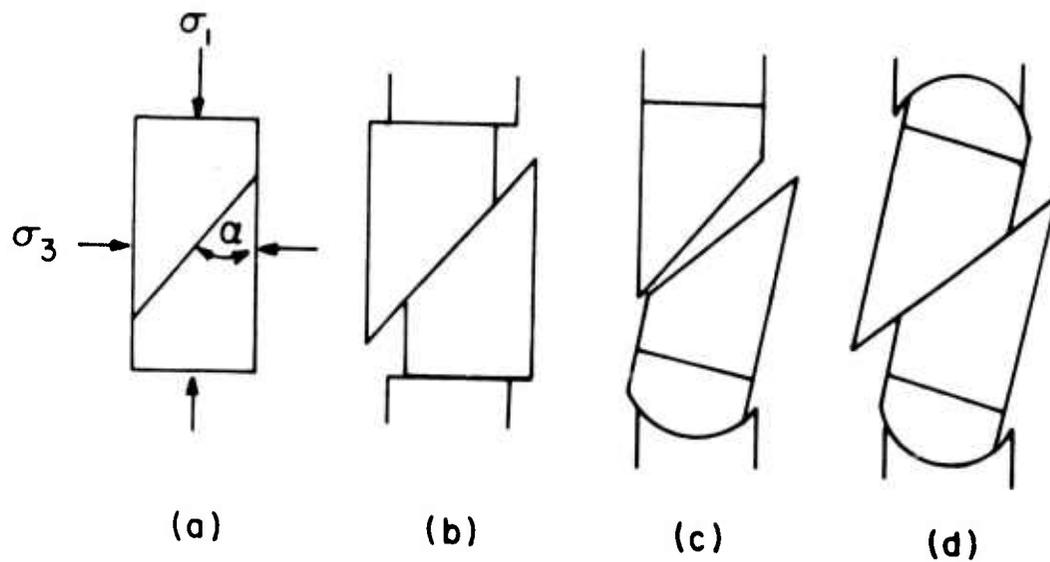
Fig. 6: Motion of Faulted Rock Specimen in Triaxial Test.
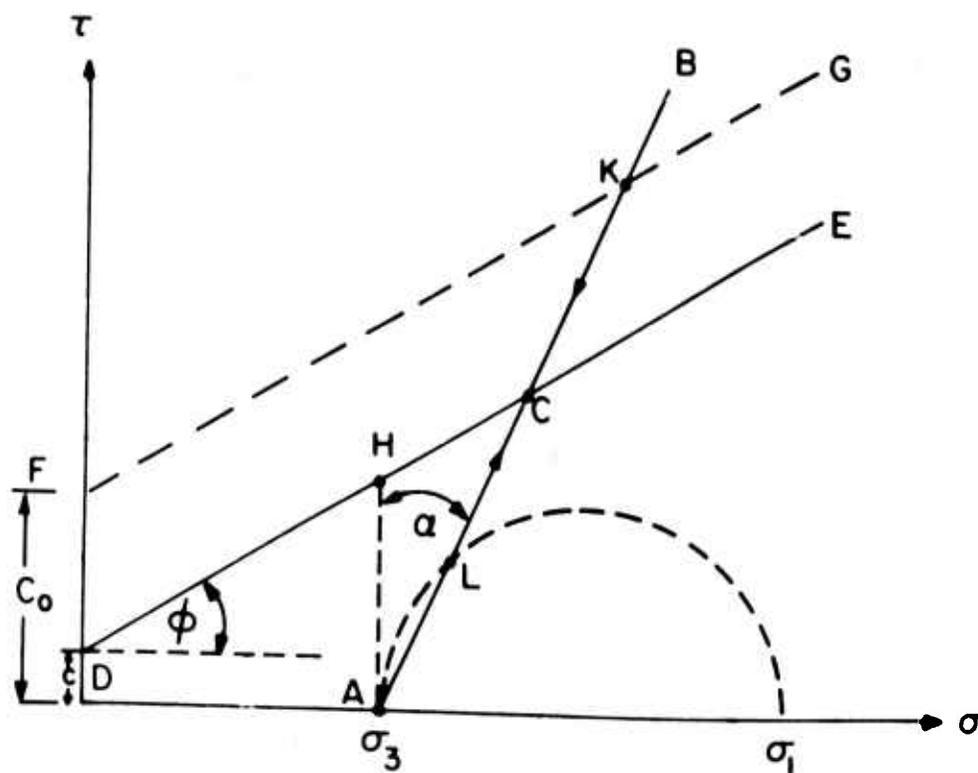
Fig. 7: Mohr Diagram of Triaxial Test.
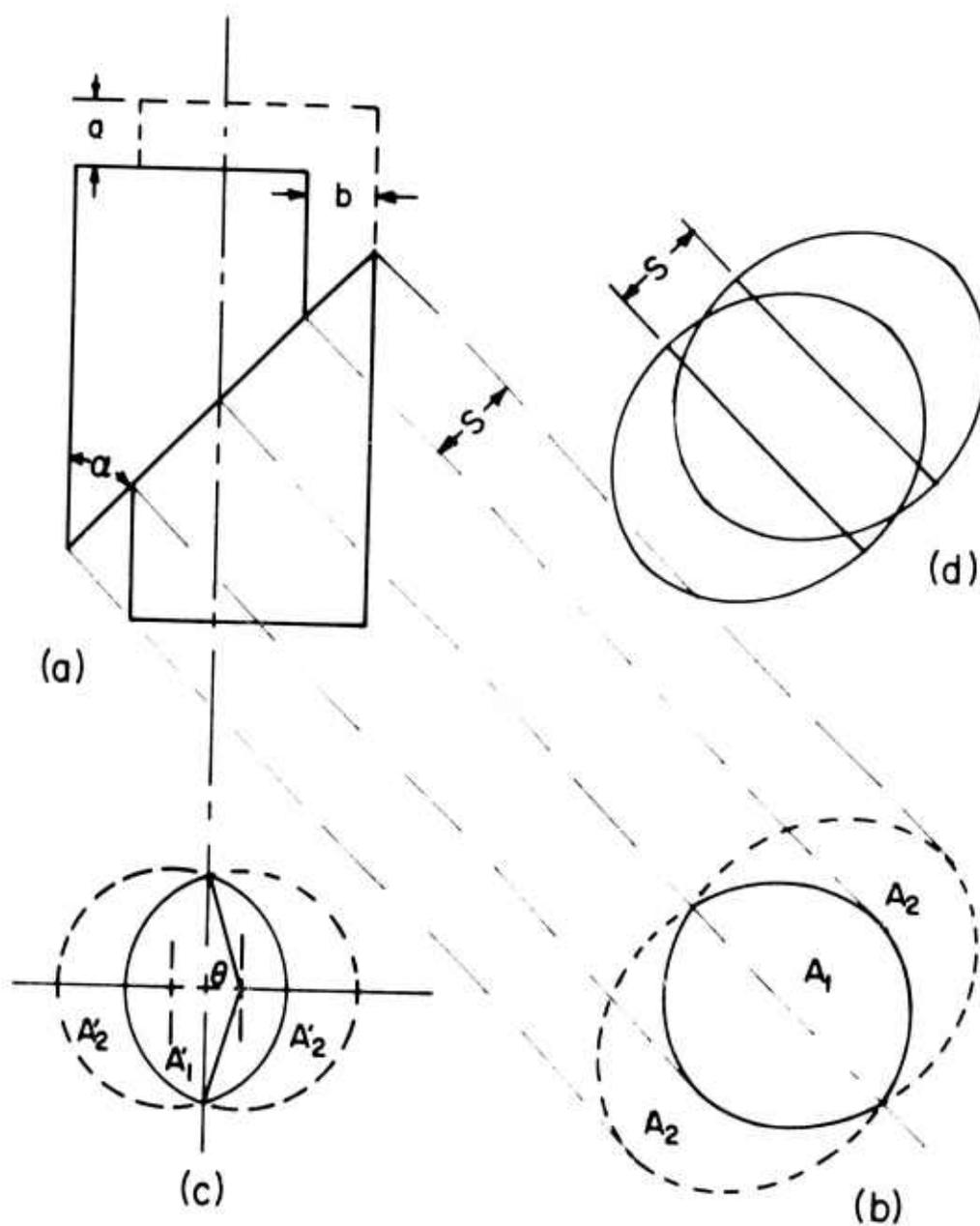
Fig. 8: Changes in Contact Area with Sliding.
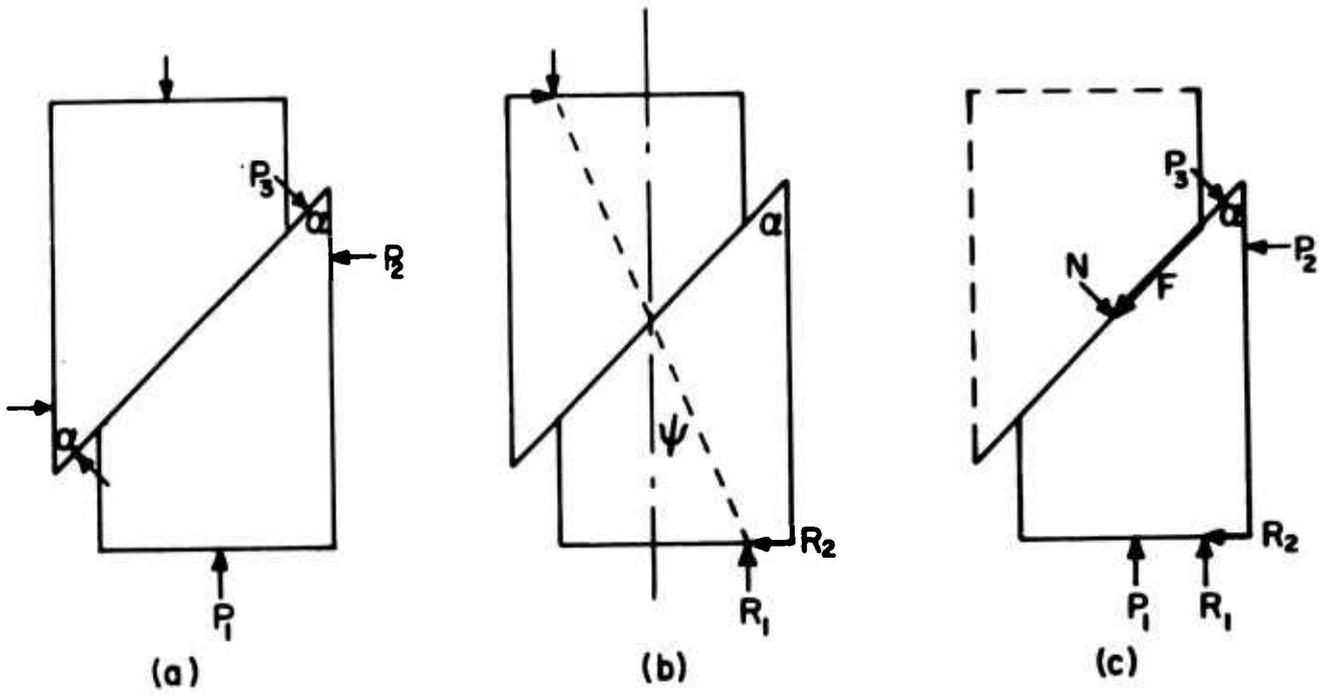
Fig. 9: Forces Involved in Triaxial Test with Sliding.
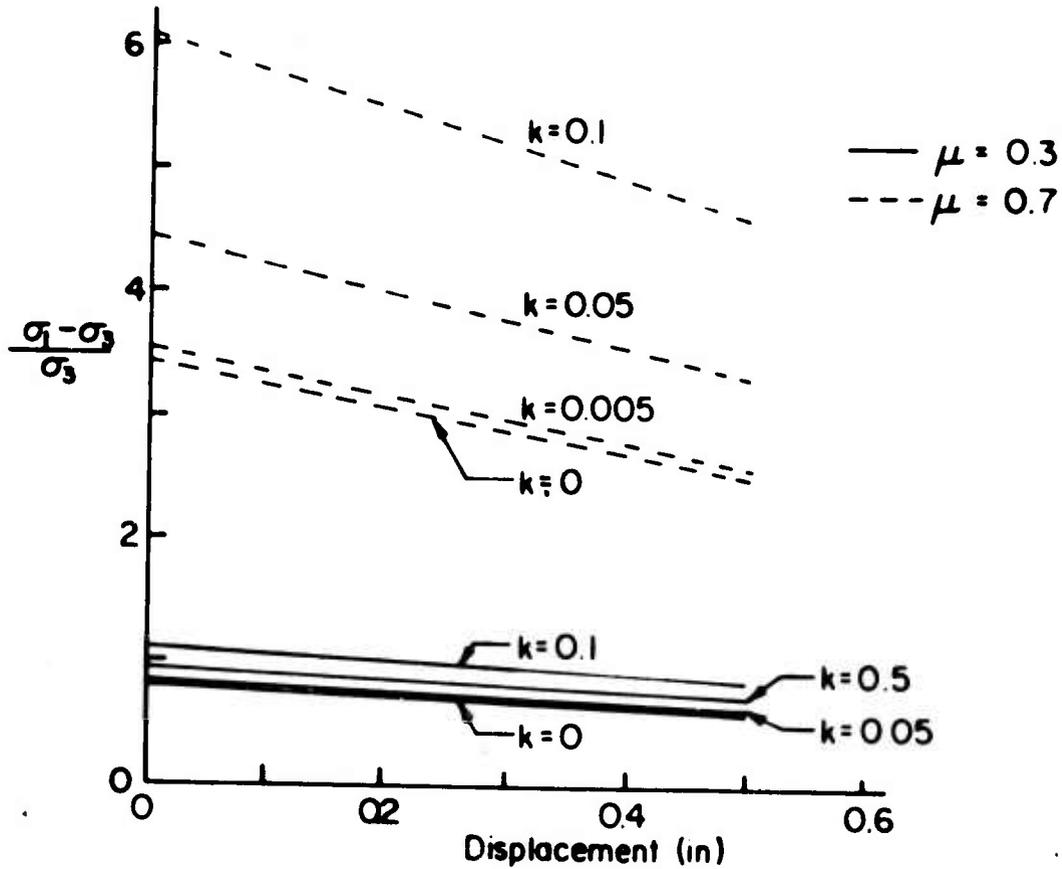
Fig. 10: Differential Stress-Displacement Curve for Triaxial Test with
Sliding.
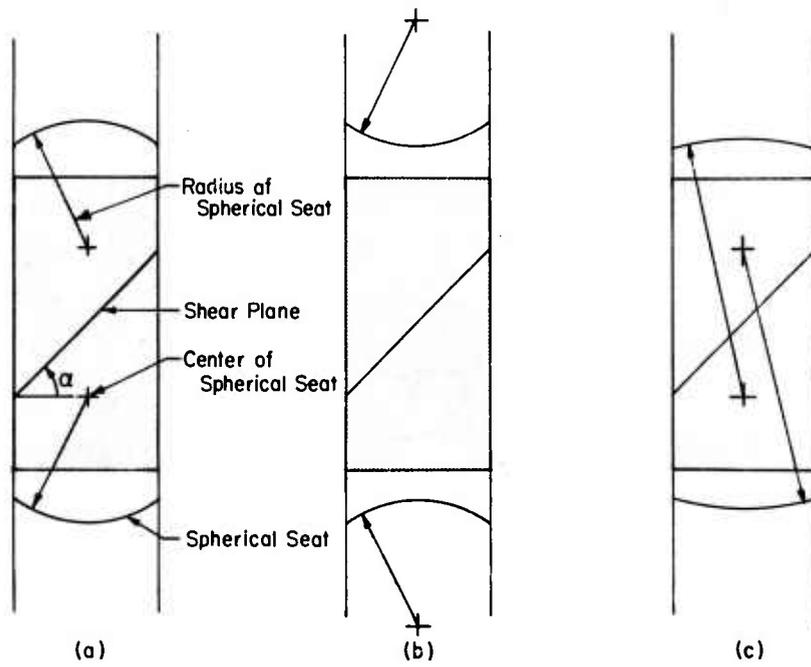
Fig. 11: Possible Geometries of the Spherical Seat in Compressive Testing.
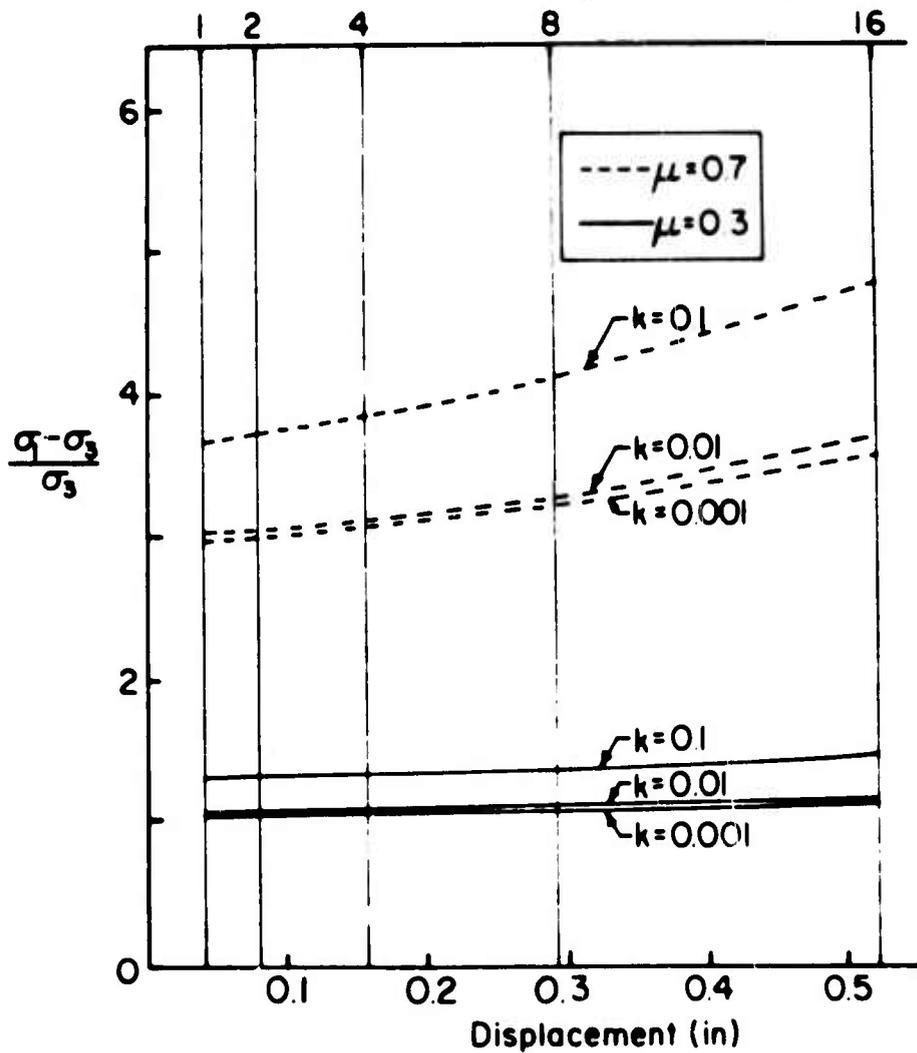
Fig. 12: Differential Stress-Displacement Curve for Triaxial Test with Rotation.
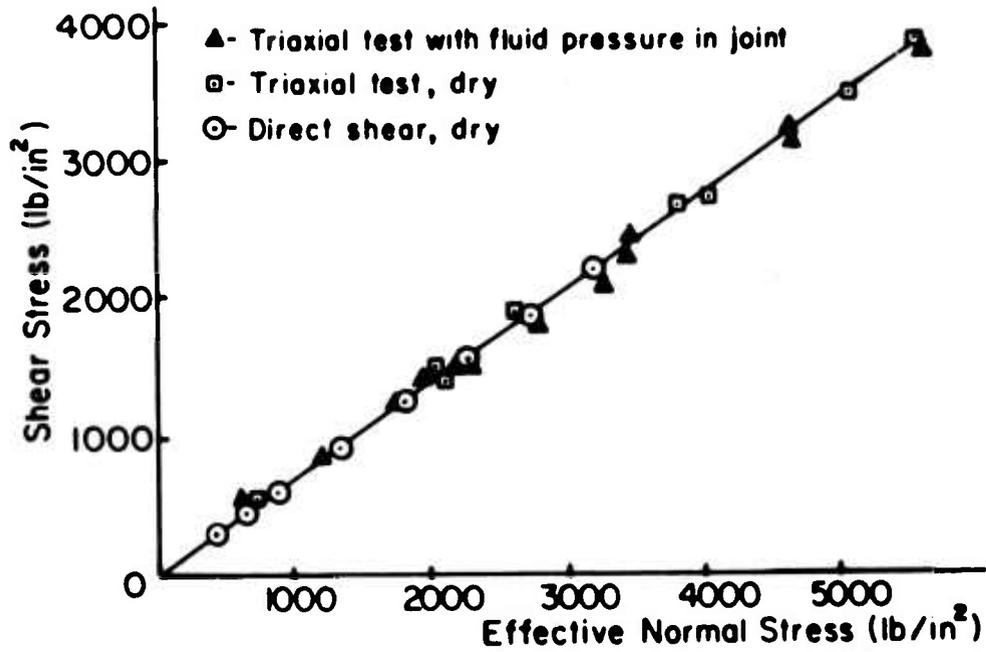
Figure 13: Sliding of Narrandera Quartzite under Various Conditions. (After Rosengren [1]).
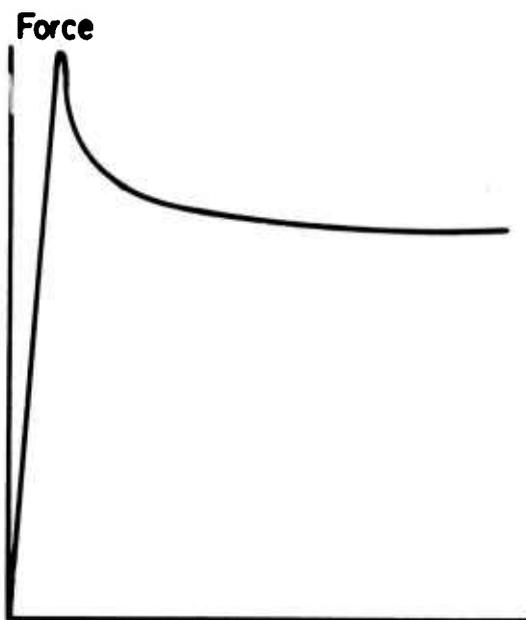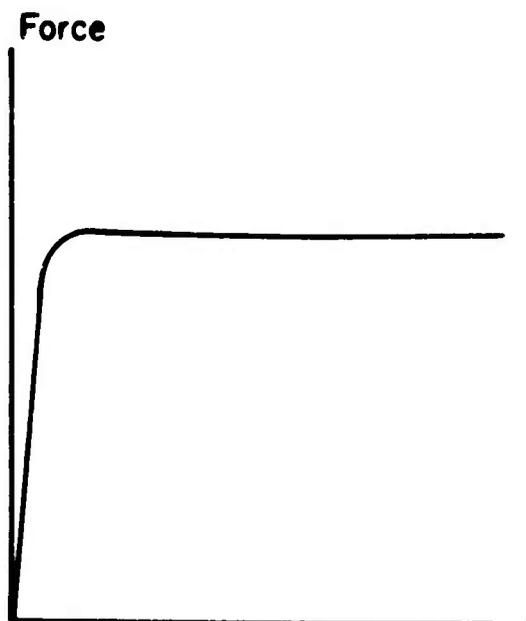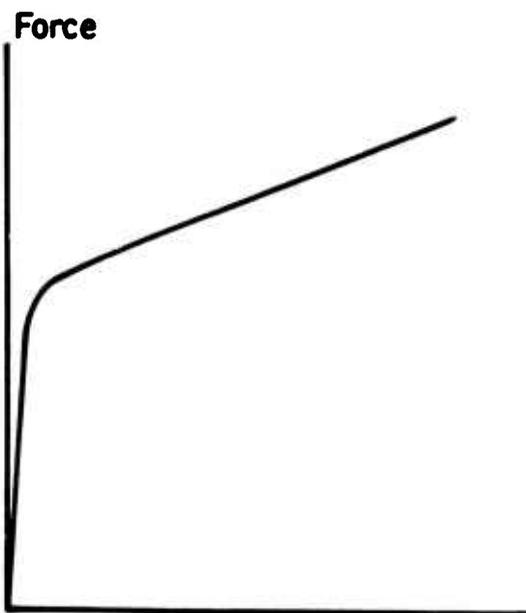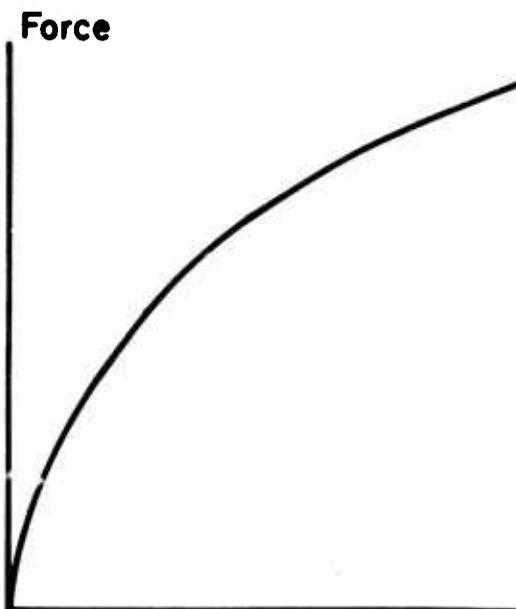
Figure 14: Load Displacement Curves for Natural Joints in Triaxial Experiments.
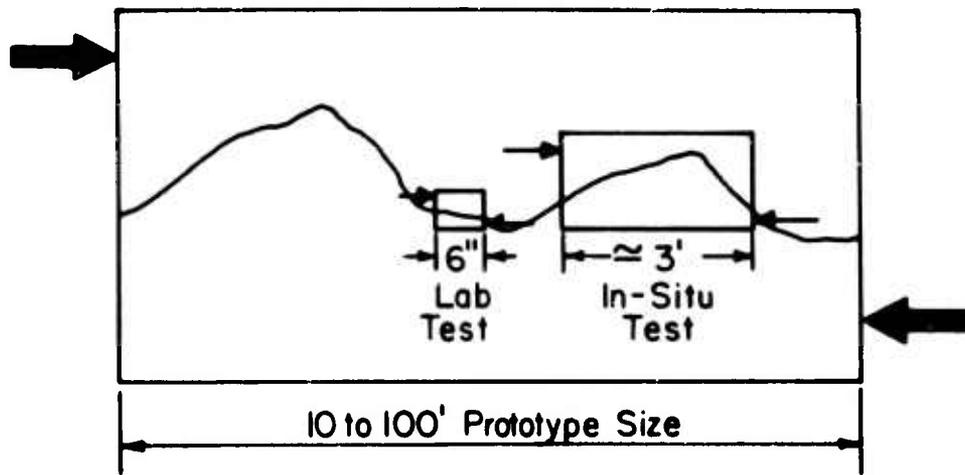
Figure 15:   Size of Laboratory Test Related to Size of Prototype.

(a)   (b)   (c)
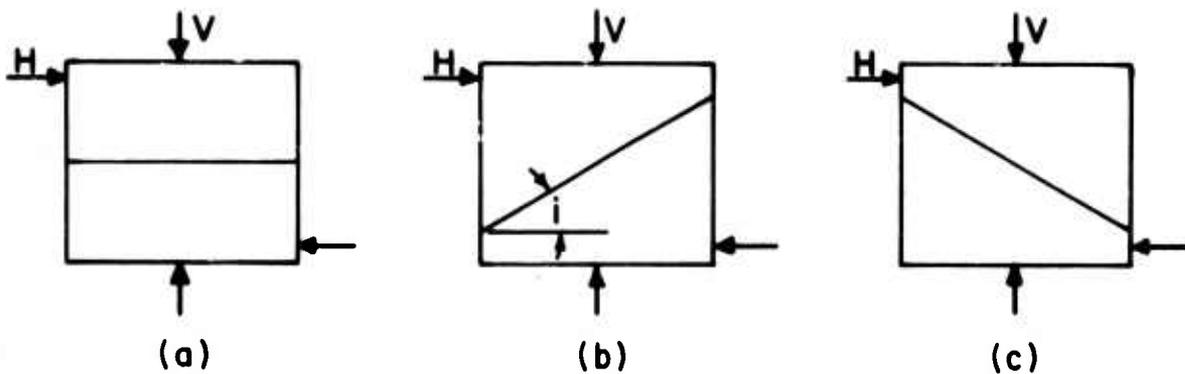
Figure 16:   Effect of Joint Inclination on Apparent Angle of Friction.
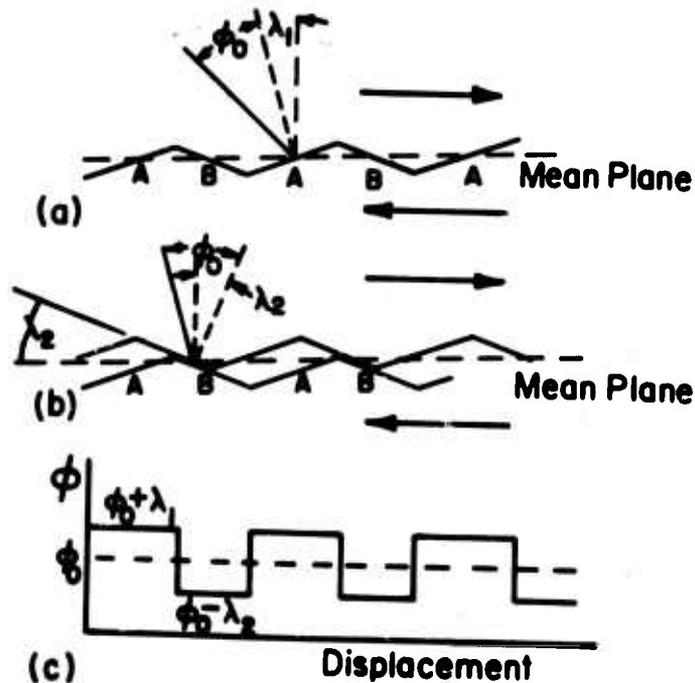
Figure 17:   Effect of Displacement upon Apparent Angle of Friction.
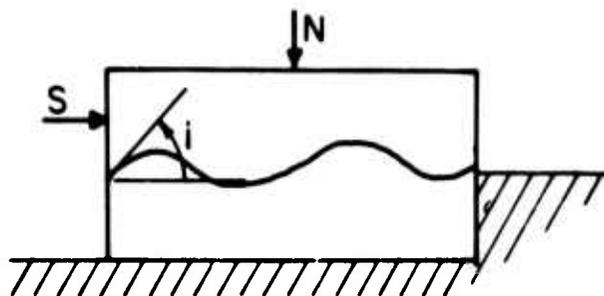
Figure 18: Sinusoidal Frictional Surface.
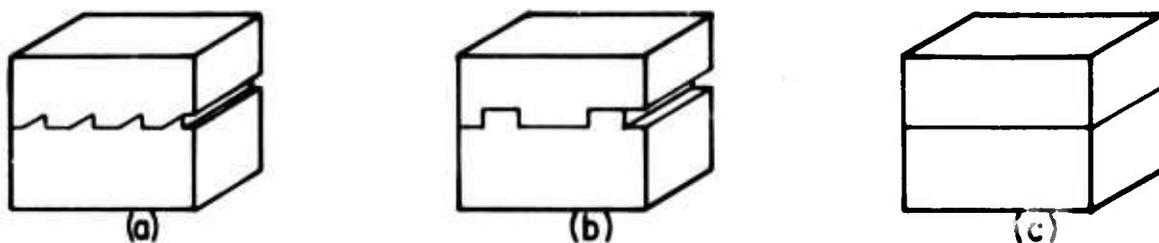
Figure 19: Friction Surfaces Investigated by Patton [52].
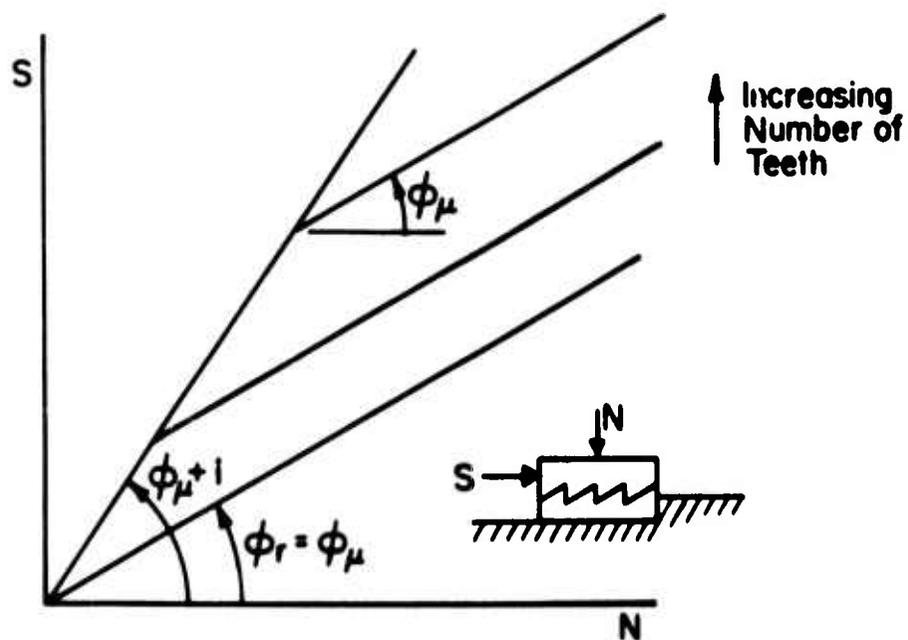
Figure 20: Experimental Results from Shearing a Sawtooth Model of
a Friction Surface. (After Patton [52]).
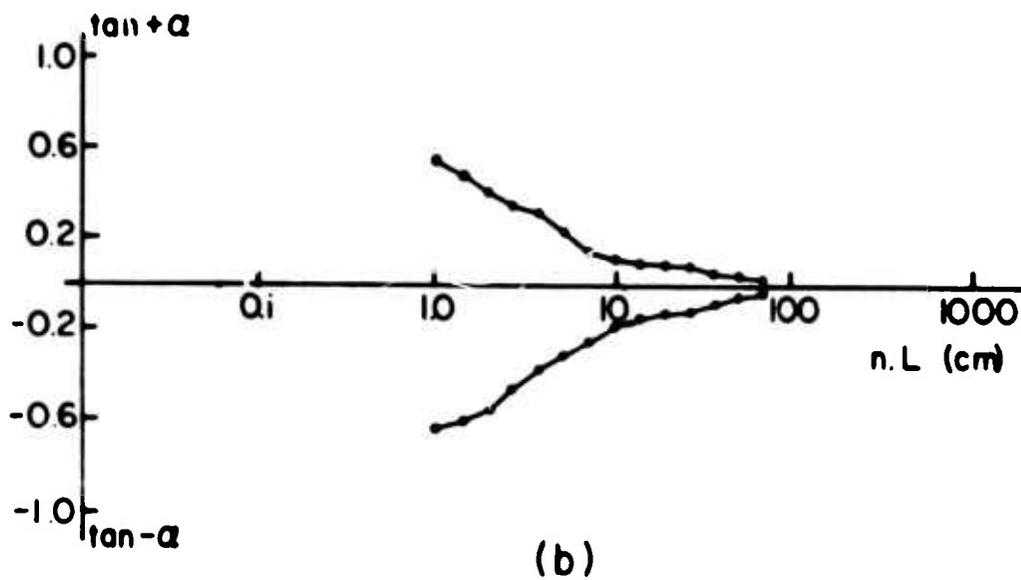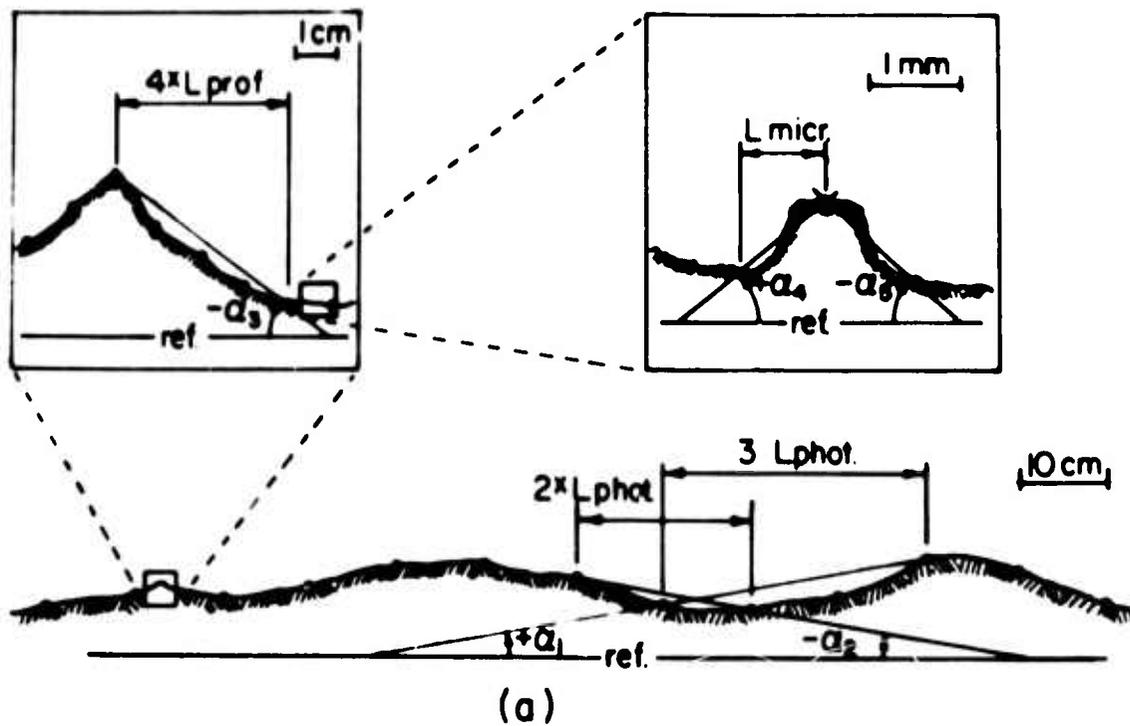
Figure 21: Rengers Method of Surface Description [27].
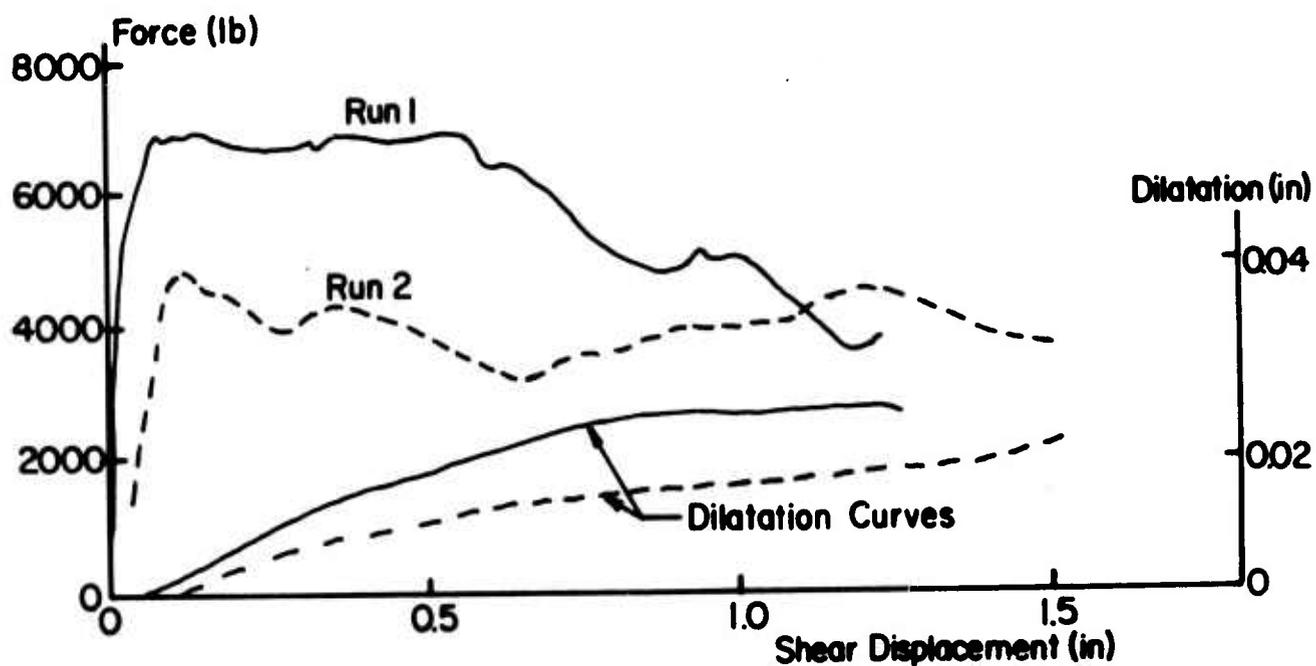
Figure 22: Experimental Results from Shearing a Carbon Coated Bedding Plane of Shale.(After Mathews [56]).
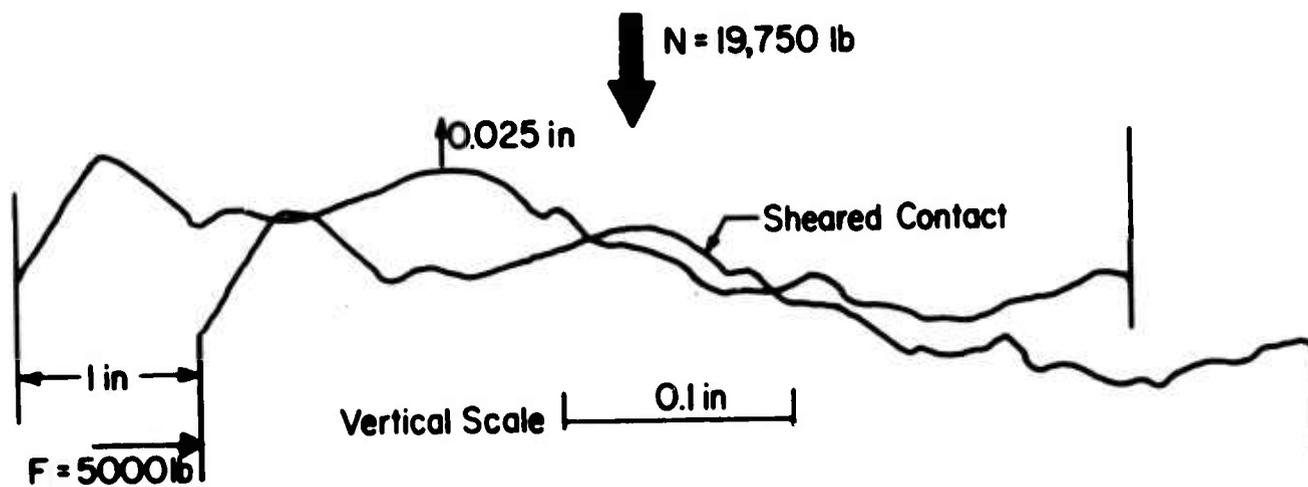
Figure 23: Relative Position at One Edge of Specimen of Experiment Shown in Figure 22.

THE COLLAPSE OF BLOCK-JOINTED SYSTEMS - PREVIOUS WORK

1 SCOPE.

In the present chapter previous investigations into the failure and strength of block-jointed rock masses will be reviewed. Generally, the problem to be considered is one in which the unit block size is an order of magnitude smaller than the rock mass being loaded and involved in collapse. Thus, we will not consider the simple case of slip of a single large block from a slope, a case which has been analysed extensively by rigid body mechanics (1-5), but rather, will consider situations in which a number of unit blocks are involved in the deformation and collapse of the rock mass. Both experimental and analytical approaches to the problem will be discussed.

2 ANALYTICAL METHODS.

2.1 Limiting Conditions for Slip on a Single Joint.

A logical and frequently used starting point for discussions of the strength of jointed systems is Jaeger's analysis of the conditions required for sliding on a single plane of weakness (6,7). Consider the two-dimensional situation shown in Fig. 1 in which a joint or other plane of weakness, AB, is inclined at an angle β to the direction of the minor principal stress, σ_3. The normal and shear stresses on the plane of weakness are given by

$$\sigma_n = 1/2 \ (\sigma_1 + \sigma_3) + 1/2 \ (\sigma_1 - \sigma_3) \ \cos 2\beta \tag{1a}$$

and

$$\tau = (\sigma_1 - \sigma_3) \ \sin 2\beta \tag{1b}$$

Assuming that the linear shear strength law

$$s = c_j + \sigma_n \tan \phi_j \tag{2}$$

holds for the plane of weakness, the conditions for slip on AB are given by

$$\tfrac{1}{2} \ (\sigma_1 - \sigma_3) \sin 2\beta \geq c_j + (\tfrac{1}{2} \ (\sigma_1 + \sigma_3) + \tfrac{1}{2} \ (\sigma_1 - \sigma_3) \ (\cos 2\beta) \tan \phi_j$$

or

$$\sigma_1(\sin(2\beta-\phi_j) - \sin\phi_j) - \sigma_3(\sin(2\beta-\phi_j) + \sin\phi_j) \geq 2 \ c_j \ \cos \phi_j \tag{3}$$

For those combinations of σ_1, σ_3, β, ϕ_j and c_j for which the left hand side of Eqn. 3 is less than $2\,c_j\,\cos\phi_j$, failure can only take place through the rock material, and presumably will be unaffected by the presence of the discontinuity, AB. Jaeger has also described these conditions for failure in terms of a Mohr's circle construction. If in Fig. 1 the point D representing the state of stress on a given plane lies in the arcs AQ or RC, slip cannot occur, but for D in the arc QR, slip on the joint will take place. If σ_1 is increased until the Mohr's circle becomes tangent to the failure envelope for the rock material, failure through the rock material can occur when slip on the joint plane is inhibited.

The conditions for slip given by Eqn. 3 may be expressed in several alternative forms. By introducing the principal stress ratio $k = \dfrac{\sigma_3}{\sigma_1}$, Eqn. 3 can be re-written to give an expression for the value of the major principal stress required to produce slip.

i.e.
$$\sigma_1 \geqslant \frac{2c_j\,\cot\phi_j}{\sin(2\beta - \phi_j)\,\operatorname{cosec}\phi_j\,(1 - k) - (1 + k)} \qquad \ldots(4)$$

In many cases it is more useful to be able to express these conditions in terms of the principal stress difference $(\sigma_1 - \sigma_3)$ required to produce slip at constant σ_3.

i.e.
$$\sigma_1 - \sigma_3 \geqslant \frac{2(c_j + \sigma_3\,\tan\phi_j)}{(1 - \tan\phi_j\,\cot\beta)\,\sin 2\beta} \qquad \ldots(5)$$

It is instructive to plot the variation in the value of $(\sigma_1 - \sigma_3)$ required to produce slip against the angle β. Note from Eqn. 5 that

$$\sigma_1 - \sigma_3 \to \infty \text{ as } \sin 2\beta \to 0$$

i.e. as $\beta \to 0$ or $\dfrac{\pi}{2}$,

and that $\sigma_1 - \sigma_3 \to \infty$ as $(1 - \tan\phi_j \cdot \cot\beta) \to 0$

i.e. as $\beta \to \phi_j$

To find the angle at which the principal stress difference at slip $(\sigma_1 - \sigma_3)$ takes a minimum value put the derivative $\dfrac{d\,(\sigma_1 - \sigma_3)}{d\beta}$ equal to zero. It is found that the minimum occurs when

$$\tan 2\beta = -\frac{1}{\tan\phi_j} = -\frac{1}{\mu}$$

and that this minimum value is

$$(\sigma_1 - \sigma_3)\,\text{min.} = 2(c_j + \mu \cdot \sigma_3)\,((1 + \mu^2)^{\frac{1}{2}} + \mu) \qquad \ldots(6)$$

As noted previously, fracture of the rock material must occur if σ_1 is increased beyond some critical value in those cases in which the joint orientation is unfavorable for slip. Assume for the purposes of the present discussion that fracture of the rock will take place according to the Mohr-Coulomb criterion

$$s = c_0 + \sigma_n \tan \phi_0 \qquad \qquad \ldots (7)$$

It can be shown that in this case,

$$(\sigma_1 - \sigma_3)_f = \frac{2(c_0 \cos \phi_0 + \sigma_3 \sin \phi_0)}{1 - \sin \phi_0}$$

or alternatively,

$$(\sigma_1 - \sigma_3)_f = 2 (c_0 + \mu_0 \cdot \sigma_3) ((1 + \mu_0^2)^{\frac{1}{2}} + \mu_0) \qquad \ldots (8)$$

where $\mu_0 = \tan \phi_0$.

The information given by Eqns. 5, 6, and 8 is best represented graphically using one of three forms of presentation. Fig. 2a shows a Cartesian plot of $(\sigma_1 - \sigma_3)_f$ against the angle β. This form of presentation was used by Jaeger in his original work and has been used by Nelson and Hirschfeld (8) to present the results of a comprehensive analysis of the conditions for failure of a set of jointed plaster models. Fig. 2b shows the same information in polar co-ordinates, a form of presentation favored by the Austrian School of rock mechanics (9-11). Fig. 2c shows a plot of the principal stress ratio at failure, k, against β. This form of presentation has been used by Bray (12, 13) and may be thought of as some kind of reciprocal of the curve shown in Fig. 2b. The polar representation shown in Figs. 2b and 2c has an advantage over the Cartesian system in that for practical problems it provides a slightly more convenient way of representing the full range of β from 0 to 180°, although the Cartesian method has been used for this purpose (e.g. Lombardi (14)). A plot of limiting stress against the angle β is sometimes referred to as the <u>failure characteristic</u> of the system.

2.2 Application to Block-jointed Systems.

An obvious approach to the problem of determining the stability of block-jointed rock masses is to apply the single plane of weakness theory in several parts. Bray (12, 13) considered the situation shown in Fig. 3a in which the shear strength of each of the two sets of orthogonal joints is given by

$$s = \sigma_n \tan \phi \qquad \qquad \ldots (9)$$

and it was assumed that fracture of the blocks themselves would not occur. For this case, the limiting conditions for slip on either set of joint planes is as shown in Fig. 3b. From this analysis of this simple problem Bray was able to point to a feature of considerable practical consequence. If a certain amount of slip takes place on the horizontal set of joint planes shown in Fig. 3a, the position shown in Fig. 4a will be reached. The vertical joints will now be staggered and, as shown in Appendix I, will have a different apparent friction angle from that of the original planar surface. The failure characteristic will now be that shown by the broken line in Fig. 4c. If slip on the vertical joints now occurs, the new configuration will be that shown in Fig. 4b in which both sets of joints are staggered. The failure characteristic for this system is that given by the full line in Fig. 4c. Lobe A on this diagram represents the conditions for slip on the A planes when movement occurs in the direction indicated by the arrows in Fig. 4b. In this case the apparent angle of friction is reduced to $\phi = 30^\circ - 9^\circ = 21^\circ$ and the overall volume tends to decrease. Lobe A_2 corresponds to slip in the opposite direction, the apparent friction angle being increased to $\phi = 30^\circ + 9^\circ = 39^\circ$, and the volume increased. Similar results are obtained for slip on the B planes.

Bray extended the analysis to cases in which more than two sets of joints traverse the mass. He defined an index of anisotropy

$$r = \frac{k_{max.} - k_{min.}}{k_{max.}} \times 100\% \qquad \qquad ...(10)$$

where $k_{max.}$ and $k_{min.}$ are maximum and minimum values of the principal stress ratio $k = \frac{\sigma_3}{\sigma_1}$ at slip. For an isotropic material, $k_{max} = k_{min}$ and $r = 0$. When $k_{min} = 0$, $r - 100\%$ and if k_{min} is negative (indicating failure under tensile stresses), $r > 100\%$. A plot of the index of anisotrophy, r, against N, the number of sets of equi-anqularly spaced planes in the system (Fig. 5) illustrates how dramatically anisotropy decreases with increasing numbers of differently oriented planes. Calculations also show that the degree of anisotropy in strength behaviour decreases with increased joint friction.

In considering how practical problems may be treated it is as well to remember that not all joints existing in natural rock masses are continuous. A set of joints may be said to be continuous if it is possible to construct sections through the rock mass that nowhere cut across intact rock. A useful concept in the treatment of intermittent jointing is the two-dimensional extent of jointing, defined by John (10) as the <u>ratio of the areal extent of the set of joints along a section plane parallel to the areal extent of the entire section</u>. For the situation shown in Fig. 6 where a plane of area A passes through three joints having areas A_1, A_2 and A_3, the two-dimensional extent of the set of joints is given as

$$\chi = \frac{A_1 + A_2 + A_3}{A} \qquad \qquad ...(11)$$

If a joint is continuous, $\chi = 1$, and if no jointing exists, $\chi = 0$.

It should be noted here that the determination of the value of χ for any given joint set is one of the more difficult aspects of any field joint survey. In theory, it is necessary to trace a particular joint across at least two surfaces approximately at right angles, but this is often not possible and averaging must be resorted to. The two dimensional extent can be approximated by assuming rectangular shapes for the joints and measuring the linear continuities of two intersections with exposed surfaces at right angles.

The concept of the two-dimensional extent of jointing has been combined with the single plane of weakness theory to provide an approach to the estimation of the strength of a rock mass containing intermittent jointing. This approach assumes that for a jointed rock mass such as that illustrated in Fig. 7a, failure may take place by shear of the rock material, by slip on a continuous joint plane, by combined slip on an intermittent joint plane and shear through the rock material, or by tension failure of the rock material should one of the principal stresses be tensile. (It will be shown later that modes of failure other than these should be allowed for at low ambient pressures.) Assuming that Mohr-Coulomb criteria apply for both joints and rock material, the three following shear strengths could be assigned to our hypothetical rock mass:

(i) $\qquad S = c_o + \sigma_n \tan \phi_o$ $\qquad\qquad\qquad$ ...(12)

This describes the shear strength of the rock material and is presumed to apply for failures on all planes other than those given by $0 = 60^\circ$ and $0 = 105^\circ$ in Fig. 7a. It is an implicit assumption of the method that failure conditions in this case will be unaffected by the presence of the joints.

(ii) $\qquad S = c_j + \sigma_n \tan \phi_j$ $\qquad\qquad\qquad$ ...(13)

This describes the shear strength of the joint planes inclined at $0 = 60^\circ$ to the reference direction.

(iii) $\qquad S = (\chi c_j + (1 - \chi) c_o) + \sigma_n (\chi \tan \phi_j + (1 - \chi) \tan \phi_o)$ $\qquad$ ...(14)

This gives the shear strength of the rock mass in the direction of the intermittent joint planes ($0 = 105^\circ$) and represents a simple averaging of joint and rock strengths. Whether this approach can be related to the mechanics of failure is extremely doubtful since it is unlikely that peak joint friction and peak rock strength could be mobilized simultaneously. Lajtai [15] has introduced a mobilization factor, C, which may take any value between 0 and 1, and indicates the degree to which the strength of a joint plane may be mobilized in shear. Thus, Eqn. 14 may be modified to

$$S = (C\chi c_j + (1 - \chi) c_o) + \sigma_n (C\chi \tan \phi_j + (1 - \chi) \tan \phi_o)$$
$$\text{...(14a)}$$

163

For certain values of β, the angle made by joint set A with the σ_3 direction, slip on either set of joint planes cannot occur, and failure of the system must be by fracture of the rock material according to Eqn. 12. Over certain other ranges of β, failure of the system will be governed by Eqns. 13 or 14a. The form of the resultant variation in principal stress difference at failure with the angle β is shown in Fig. 7b.

In applying this approach to determine the stability of a rock mass in a given situation it is also necessary to determine the distribution of shear stresses with β. By comparing the shear stresses and the available shear strength for various orientations it is possible to prepare a polar diagram of "factor of safety" or "resistance quotient" against β(10). This procedure generally requires the assumption that a joint will be encountered at the point being considered (the "ubiquitous" joint concept introduced by Goodman (16)).

The preceding analysis assumes that shear failure will occur. If tensile stresses exist an analogous procedure may be applied. John (10) has presented detailed examples for both cases. Obviously, these calculations can be most conveniently carried out on a computer.

2.3 Limitations of this Approach.

The methods outlined in Appendix I, Sections 2.1 and above section 2.2 provide a useful engineering approach to the problem of calculating the strength of rock masses, and currently find widespread use in practice. However, it should be recognized that they considerably over-simplify the problem and suffer from a number of serious limitations.

(a) Stress distributions.

The methods described above implicitly assume that the stress distribution within the mass is a uniform one and is not influenced by the presence of joints. This assumption can be accepted as being valid for those cases in which the two surfaces forming a joint are perfectly matched and in which no slip has occurred (17). As soon as slip on any joint occurs, the stresses redistribute and can depart quite markedly from the uniform. Photo-elastic investigations by Chappell (18) for example, show this to be the case in the simple situation in which the central block in a group of three slips on the joint planes formed with the other two, as well as in more complex situations such as in the roof of an underground opening excavated in blocky rock.

More realistic stress distributions than those calculated from the simple equations for the transformation of plane stress, may be calculated using finite element methods incorporating joint elements (16, 19-26). In this approach, the rock blocks are assigned the usual elastic properties and divided into finite elements while the joints are treated as elements of finite length and small thickness with certain normal and shear stiffnesses and shear stress shear strain characteristics.

Initially, the stress-strain characteristics assumed were highly idealized e.g. elastic - perfectly plastic (16). More recently, however, methods using more realistic non-linear joint characteristics have been developed (22-24). These newer methods permit the modeling of curved and variable thickness joints using curved isoparametric elements. Present methods assume that the shape of the joint shear stress-shear strain curve is independent of normal stress. Thus, a unique dimensionless plot based on residual shear stress (τ_r) and an elastically related value of shear strain (γ_{er}) as shown in Fig. 8 is assumed for each joint type. While this approach represents a considerable advance over former methods, it will not always provide accurate solutions because of the assumption of the uniqueness of the shear stress-shear strain relationship.

Finite-element methods have been applied to the problems of the stability of underground openings in jointed rock subject to static (16, 23,) and dynamic (16) load, the stability of rock slopes (19, 25, 26) and the three-dimensional stability of arch dams (24). Their value is that they permit the evaluation of reasonably realistic stress distributions for complex situations for which solutions could not otherwise be obtained. Nevertheless, they depend on assumptions regarding failure mechanisms which are usually little different from those used in the simple approaches outlined in Sections 2.1 and 2.2 above, and can still only take account of simplified material behaviour and properties. However, they do possess the great capacity to yield solutions for deformations which may not be reasonably calculated by any other method. There is little doubt that in the future these methods will provide an increasingly powerful analytical tool, particularly when alternative collapse mechanisms such as block rotation and translation are incorporated into programs (26).

(b) Slip and Fracture Criteria

The methods of analysis referred to previously all assume linear Mohr-Coulomb failure criteria for the rock material and similar laws for slip on rock joints, although in one case known to the author a parabolic friction law was used (27). It was shown in Appendix 1 that this approach is both over-simplified and mis-leading. Methods which use such concepts of material behaviour may provide useful approximate solutions to some engineering problems, but can never hope to lead to a complete understanding and solution of the general problem. Obviously, improved concepts of the stress-strain behaviour of rock material and rock joints are fundamental to an improved understanding of the complete load-deformation and volume change response of jointed rock masses.

(c) Collapse Mechanisms

Three mechanisms were assumed to be possible:
(i)   Slip on joints
(ii)   Shear failure of the rock material
(iii)   Composite shear failure, partly through
        rock and partly along a joint.

Experimental studies of models of jointed rock have shown that mechanisms other than these are likely to be involved (28, 29). (These studies will be discussed fully in succeeding sections). Obviously, methods of analysis which do not admit a full range of collapse mechanisms are inadequate. A related point is that failure of jointed rock mass is likely to be progressive (30), a factor which is very difficult to allow for in simple analytical methods.

(d) Inter-action of Joints

So far it has been implicify assumed that the strength of a jointed rock mass is unaffected by the number of joints of a given set traversing a particular zone of rock (i.e. by the joint spacing). It seems reasonable to assume that in a real rock mass, the local re-distribution of stress associate with slip will be joint-spacing dependent (i.e. that joints will "inter-act"). Indeed, simple model studies have suggested that strength decreases with joint spacing (31, 32). This factor could only be taken account of by a very tedious and complicated "exact" computer solution for the stress distribution in any given case, or by assuming a "macro" failure criteria for the mass as a whole in which the strength parameters varied with joint spacing. The latter would appear to provide the most useful approach for immediate engineering purposes.

3   EXPERIMENTAL INVESTIGATIONS

3.1   General

A vast majority of the experimental investigations of the failure of jointed media have been carried out in the laboratory using idealized models prepared from substituterock-like materials, such as gypsum plaster or plaster-sand mixtures of one kind or another. In some cases attempts have been made to satisfy the laws of similitude and model a particular rock mass and a particular problem (33, 34), but in many other cases this has not been done for reasons of experimental expediency.

The various investigations that have been carried out to date will be classified and discussed according to the nature of the applied loading. Uniaxial, biaxial and triaxial compressions, direct shear, and special problem categories will be considered.

3.2   Uniaxial Compression

Here, only those investigations in which uniaxial compression was the major loading system used will be considered. Those cases in which uniaxial tests were carried out as part of biaxial or triaxial compression investigations will be discussed in the appropriate section below.

Hayashi (35, 36) carried out a series of uniaxial compression tests on approximately 3" x 3" x 6" plaster prisms containing the systems of pre-formed continuous and intermittent jointing shown in Figs. 9 and 10.

For samples of the type shown in Fig. 9a, the application of a Coulombic failure criterion for slip along the joint plane gives the value of the uniaxial load at failure as

$$P = \frac{c_j A_o}{\cos i (\sin i - \cos i \tan \phi_j)} \qquad \ldots(15)$$

where c_j and $\tan \phi_j$ are the cohesion and co-efficient of friction for the joint surfaces, and A_o is the cross-sectional area of the prism. Hayashi's experimental results showed considerable scatter, but for $i = 30^o$, 45° and 60° were in reasonable agreement with Eqn. 15. For $i = 15^o$, the measured strength was much lower than that predicted by the simple Coulombic theory, because in this case failure was by "tensile cracking" rather than by sliding on the joint plane.

In the samples illustrated in Figs. 9b and 9c, a constant two dimensional extent of jointing of X = 0.5 was used, the total joint area being made up of 1, 2, 3 or 4 individual joints. If the strength of the sample material is given by

$$\tau = c_o + \sigma_n \tan \phi_o \qquad \ldots(16)$$

then the uniaxial load required for shear failure in the plane containing the joint is

$$P = \frac{(c_j + c_o) A_o}{\cos i (2 \sin i - \cos i (\tan \phi_j + \tan \phi_o))} \qquad \ldots(17)$$

As shown in Fig. 10, Hayashi's unconfined compression tests gave results that differ markedly from those predicted by Eqn. 17. This lack of agreement is readily explained by the fact that the mode of failure observed in the tests did not correspond with that assumed in the derivation of Eqn. 17 which will hold only if failure takes place by shear along the plane AB in Fig. 11. In fact, failure occurred by the formation of cracks such as CE and EF under the influence of stress concentration set up at the tips of the prepared discontinuities. Similar behaviour is unconfined compression was observed by Brace and Bombalakis (37) who used the photo-elastic method to study the influence of cracks such as CE in Fig. 11 on the stress distributions in brittle materials.

For samples of the type shown in Fig. 9c, failure loads decreased as the number of joints in a given plane increased, no doubt as a result of the increased effect of stress concentrations at the tips of the joints. The results of triaxial tests on similar samples would have been of great interest since in this case it may have been possible to inhibit the development of tensile failures.

In unconfined compression and direct shear tests on samples containing joints in more than one plane, Hayashi measured a decrease in strength as the number of parallel rows of joints (n) increased. This was accounted for in terms of the statistical theory of the distribution of extreme values developed by Epstein (38). The relationship between n and the load required to induce failure in unconfined compression is found to be

$$P_{n,m} = P_{1,m} \quad (1 - v \sqrt{2} \log n + v\{\frac{\log (\log n) + \log 4}{2\sqrt{2} \quad \log n}\})$$

...(18)

where $P_{1,m}$ is the failure load for the case of m joints in one plane, and v is the co-efficient of variation of values of $P_{1,m}$. Using suitable values of v, Hayshi found that this theory gave an excellent representation of the effects described (see Fig. 12).

Latjai (39) carried out uniaxial compression tests on a number of sample types including one in which the inclined discontinuities were formed by interlocking rectangular "teeth". Depending on the tooth geometry, failure was by shear along a plane partly through joints and partly through plaster itself, by vertical tensile fractures starting from the sharp corners in the discontinuities, or by combined shear and tensile modes. As with Hayashi's tests, the problem of applying the single plane of weakness theory to these results is obvious.

Goldstein et al (31) carried out uniaxial compression tests on cubic samples made up of 2 cm. cubes of plaster of Paris and sand mixed in various proportions to give a range of cube strengths. They found that the strength of the mass (σ_m) and the strength of the unit blocks (σ_b) were related an expression of the form

$$\frac{\sigma_m}{\sigma_b} = a + b \quad (\frac{\ell}{L}) \beta$$

...(19)

where β = a constant considerably less than 1,
$\quad$ b = 1 - a

and $\quad \frac{\ell}{L}$ = ratio of the side length of the unit blocks to that of the sample.

As the ratio $\frac{\ell}{L}$ decreases (i.e. as the blocks become smaller in relation to the mass) the strength of the mass decreases towards the value of σ_b. This suggests that the frequency of jointing is a significant factor in determining rock mass strength. A similar result was obtained by Einstein et al[32].

Sirieys (40, 41) considered the question of the uniaxial compressive behaviour of prismatic samples containing parallel sets of discontinuities in which the two dimensional extent of jointing varied. Sirieys postulated that for the X = 1 case, failure could be by sliding along the joint plane or by vertical splitting with no other possibility being admitted. For x<1, the angle made by the failure plane with the horizontal coincided with that made by the joint plane (α) up to a certain limiting value of α beyond which failure was by combined splitting and sliding along the joint plane giving a stepped failure surface.

Sirieys also considered the behaviour of the "brick-wall" system (Fig. 13) in unconfined compression. He suggested that failure should be in one of three modes depending on the angle α.

(i)   For $0<\alpha<38^{\circ}$ failure is by vertical splitting partly in the joint planes and partly through the sample material.

(ii)   For $38^{\circ}<\alpha<66^{\circ}$ a step-wise failure is predicted with the mean failure "plane" making an angle of 63.4° with the bedding plane.

(iii)   For $66^{\circ}<\alpha<90^{\circ}$ failure is again by splitting.

Panet (41) has also made brief reference to uniaxial compression tests on block-jointed samples in which tensile and composite modes of failure were obtained.

3.3   Biaxial Compression

Significant contributions have been made by biaxial compression tests carried out on plate-like models by Müller and Pacher (43), John (11, 44) Rosenblad (45, 46) and Ergun (17).

Müller and Pacher (43) investigated the influence of a number of parallel, planar intermittent discontinuities on the strength and deformation properties of a 70 cm x 70 cm. Model made up from a cement-like material and loaded in biaxial compression through heavy steel beams and a soft "cushioning" material. In their experimental design they attempted to take account of seven parameters:

(a)   the angle made by the joints with the direction of the major principal stress (α),

(b)   the principal stress ratio (n),

(c)   the degree of separation of the joints (χ),

(d)   the opening of the joints,

(e)   the number of joints in a given direction,

(f)   the strength of the joint material,

and (g)   the strength of the blocks themselves.

Müller and Pacher expressed their test results in terms of the stability quotient (R) or ratio of the strength measured in a given test to that of a solid block tested under identical conditions. Fig. 14 shows the variation in R, and the mode of failure with α for various values of n.

For all tests in which α was less than 60°, the strength of the jointed model was less than that of the solid sample, the strength reductions being greatest for the unconfined case (n = ∞). Several failure modes including brittle fracture of the blocks, sliding on joint planes and composite failures were observed. Deformations were greatest in the unconfined tests but quite probably the high lateral strains measured in the free direction were associated with the development of splitting type failures.

John (11, 44) carried and biaxial compression tests on 800 mm x 400 mm x 120 mm thick block-jointed models prepared from 40 mm square blocks of a soft model material. The loads were applied by hydraulic pressure acting through flexible bags thus ensuring a degree of uniformity in loading not obtained in many other experimental situations. John's unit blocks were reinforced with steel rods in their long direction so that failure of the model by extension in the direction at right angles to the plane of loading was prevented.

A majority of John's tests were carried out with the blocks arranged such that continuous joint planes were produced at various angles to the principal stress directions. In a few cases blocks were staggered so that a two-dimensional extent of jointing of $\chi = \frac{1}{2}$ was produced.

Three modes of failure were observed:

(a)   sliding on joints

(b)   shearing of elements

(c)   shearing of elements affected by joints.

John found that his experimental results were well represented by the analytical procedures presented in Sections 2.1 and 2.2 above except in a "transition zone" in which type (c) failures occurred. In these cases the polar diagram of strength against joint orientation was modified in the manner shown in Fig. 15.

An interesting feature of John's results a specimen with two sets of joint planes each inclined at 45° to the specimen axes. Because of the test configuration, slip on either set of joint planes was inhibited and individual blocks failed by cleavage, apparently under a wedging action. A similar phenomenon has been observed

by Rosenblad (46) and Brown (47, 48). Note also that breakdown of John's model is progressive and apparently time dependent.

Using fine sand and gypsum cement Rosenblad developed a material which closely modeled the properties of a certain schistose gneiss. Pre-cast blocks of this material were used to prepare plane block-jointed models. He developed a special loading system which permitted uniform loads to be maintained along any side of his block-jointed models even though slip on some joint plane may have occurred and the loaded faces were no longer planar. Rosenblad observed four modes of collapse:

(a) Initial - slip along joints

(b) Secondary - vertical tensile fractures (His model was horizontal)

(c) Tertiary horizontal tensile fractures i.e. failures of blocks due to extension in the direction at right angles to the plane in which the loads were applied.

(d) Ultimate - shear failures through intact material.

Type (b) failures were associated with joint orientations of 45° to the principal stress directions as in the case described above for John's tests. Type (c) failures were common and represent a severe limitation in Rosenblad's test system.

Rosenblad measured the percentage of the intact material strength associated with each mode of failure as: Initial 8-17%; Secondary 28-41%; Tertiary 28-41%; Ultimate 45-57%. He obtained the important result that slip along joints in one direction causes an increase in the apparent angle of friction of the joints in the perpendicular direction due to block interaction, a result which was predicted by Bray (12, 13).

Rosenblad also measured relative and absolute deformation of blocks. He found that gradients of principal strain magnitude and direction in a jointed rock mass are much larger and impredictable than those in an intact block of the same material under identical loading conditions.

Ergun (17) was primarily interested in stress distributions in jointed media which he studied using the photo-elastic method. However, as an adjunct to this work he carried out a series of uniaxial and biaxial compression tests on plaster models in which the joint planes were in the principal stress directions. He concluded that in this case the strength of the mass is not affected by the presence of the joints, provided the blocks are flat and square with surfaces parallel to within + 250 microns. A similar result was obtained by Brown (47, 48) for uniaxial and triaxial compression. The goodness of fit of blocks is seen to have a major influence on the behaviour of such block-jointed models.

3.4   Triaxial Compression

Triaxial compression tests on block-jointed media have been carried out less frequently than have uniaxial, biaxial or direct shear tests. The major investigations have been those due to Brown (28, 47-49) and Einstein et al (32, 50). These two investigations have much in common, using similar model materials and some of the same test configurations and producing similar results. However, because the former investigation has been the more extensive of the two it alone will be reported in detail.

Brown carried out an extensive series of triaxial compression tests ($\sigma_2 = \sigma_3$) on block-jointed models made from a high-strength gypsum plaster. All samples were 8" high with a 4" square cross-section and were prepared by assembling pre-cast blocks with one square-inch cross-sectional area. Using cubical, parallelepipedal and hexagonal blocks, samples with a two-dimensional extent of jointing of 1, 1/2 or 1/3 were produced. Examples of each of these three groups of sample types are illustrated in Fig. 16. In all, four sample types were produced using cubic blocks, two using parallelepipedal blocks, and three using hexagonal blocks so that a total of 10 sample configurations were tested when unjointed samples are included. The various block-jointed sample types tested may be described in the following way:

A.   Cubic blocks ($\chi = 1$). The angles i and β shown in Fig. 16a had values of $0°$ and $90°$, $15°$ and $75°$, $30°$ and $60°$, and $45°$ and $45°$ in the four sample types used.

B.   Parallelepidedal blocks ($\chi = \frac{1}{2}$)
  T60 – the $\chi = \frac{1}{2}$ planes were inclined at $60°$ to the base of the sample (Fig. 16b)
  T45 – the $\chi = \frac{1}{2}$ planes were inclined at $45°$ to the base of the sample.

C.   Hexagonal blocks ($\chi = \frac{1}{3}$)
  H60 – the $\chi = \frac{1}{3}$ planes were inclined at angles of $60°$ and $0°$ to the base of the sample (Fig. 16 c)
  H45 – the $\chi = \frac{1}{3}$ joint planes were inclined at angles of $45°$, $15°$ and $75°$ to the base of the sample.
  H30 – the $\chi = \frac{1}{3}$ joint planes were inclined at angles of $30°$ and $90°$ to the base of the sample.

Samples of each type were tested at confining pressures of 0, 200, 500, 1,000 and 2,000 p.s.i. giving a total of 50 tests, many of which were duplicated. Although these pressures may seem low by rock mechanics standards, they were sufficient to enable a wide range of behaviour to be studied since the highest confining pressure used (2000 p.s.i.) is approximately the brittle-ductile transition pressure for the plaster.

In all, eight different failure patterns were observed in these tests. It should be noted, however, that the failure characteristics listed below were observed on removing the samples from the triaxial cell, often following considerable post-peak deformation. Furthermore, since the tests at the lower confining pressures were carried out in a conventional "soft" testing machine, some of the macrofracture characteristics observed could have been influenced by the testing machine stiffness characteristics. For these reasons, the features listed can only be considered as ultimate conditions and may not always be accurate representations of the state of the samples at peak principal stress difference (taken to correspond to "failure"). The eight failure modes observed were:

A. Axial cleavage at low confining pressures.

B. Shear failure of the plaster along a single planar surface inclined at approximately 30° to the sample axis.

C. Collapse at low confining pressures due to block movement involving opening of joints and dilatation of the sample.

D. Slip on continuous pre-formed joint planes.

E. Slip on a planar surface partly along a pre-formed joint plane and partly through intact plaster.

F. Local axial cleavage fractures in the $45^\circ/45^\circ$ case due to wedging action.

G. The formation of complex non-planar shear surfaces partly through plaster and partly along joints.

H. The formation of multiple conjugate shear planes through plaster at high confining pressure (viz. ductile behaviour).

I. The formation of multiple conjugate shear planes partly through plaster and partly along joints.

The envelopes to the Mohr's circle plots of peak stresses were curved and could be described by the equation

$$\tau = \tau_o + Z\sigma_n^{\zeta} \qquad \qquad \ldots(20)$$

The parameter Z has variable dimensions depending on the value of the index ζ, and so it may be preferable to re-express Eqn. 20 in the form

$$\frac{\tau - \tau_o}{\sigma_c} = Z \left(\frac{\sigma_n}{\sigma_c}\right)^{\zeta} \qquad \qquad \dots (21)$$

where σ_c is a material property taken as the unconfined compressive strength of the unjointed material (3000 p.s.i.).

The envelopes passed through the origin of the $\tau - \sigma_n$ axes for all jointed samples so that $\tau_o = 0$. For the unjointed material, $\tau_o = 450$ p.s.i.

The following conclusions regarding rock mass behaviour and the applicability of the method of analysis outlined above may be drawn from the test results:

1. The strengths of jointed samples lie between upper and lower limits set by the strengths of the rock material and smooth joints respectively.

2. Modes of failure other than those commonly recognized in the literature are likely to occur in block-jointed rock masses. Of particular significance in this regard are axial cleavage and block separation modes observed at low confining pressures.

3. For those cases in which planar shear surfaces were formed partly through the plaster and partly through joints, the approach to the calculation of shear strength outlined in Sections 1 and 2.2 was found to be valid. Such failures did <u>not</u> occur at the lower confining pressures.

4. Where shear failure took place through the plaster and not along joints, the strengths of the jointed models were lower than those of the corresponding unjointed samples except at the highest confining pressures.

Some of these conclusions are illustrated by Fig. 17 which shows Mohr envelopes for the unjointed plaster, the strongest (H30) and weakest (T60) of the models with intermittent jointing, and a single joint. In zone 1 the models have lower strengths than those predicted by simple theory which is applicable in zone 2. In zone 3 the material is ductile and the influence of joint patterns on strength is negligible.

In an associated investigation Stanley (51) investigated the behaviour of unjointed samples and the simple $0^\circ/90^\circ$ case under polyaxial stress ($\sigma_1 \neq \sigma_2 \neq \sigma_3$). He obtained modes of failure A and B described above, and found that in the general case, the peak stresses could be related by the equation

$$\tfrac{1}{2}(\sigma_1 - \sigma_3)_f = f(\tfrac{1}{2}(\sigma_1 + \sigma_3 + \alpha.\sigma_2))$$

where the function itself and the value of α are characteristic of both the material of which the mass is composed and the nature of the joint pattern. For the 0°/90° model, α equalled zero i.e. the intermediate principal stress had no effect on the strength of this particular model.

3.5 Direct Shear Tests

Hayashi and Fujiwara (52, 53) and Hayashi (36) have reported on the results of direct shear tests on plaster samples containing a number of parallel planar discontinuities as shown in Fig. 18. The joint planes were said to be cohesionless and to have a co-efficient of friction of approximately 1.0. The most significant of the many conclusions to be drawn from this work is that although the simple theory would suggest that failure should have been through the plaster in all cases except $\theta = 0°$, the shear strength varied with θ, the angle of inclination of the joints to the shearing direction. The mode of failure was not well defined, appearing to be partly due to tensile failures in bending and partly to shear failure of the plaster. In some instances sliding on or opening of the joint planes was noted. Both the mode and direction of failure varied with the angle θ, and it is quite apparent that the linear shear strength theory does not apply. It was also found that the dilatancy of these specimens was highly anisotropic and dependent on the angle θ. More detailed conclusions regarding dilatation in direct shear are difficult to draw from the results presented.

Kawamoto (54) carried out similar direct shear tests on "layered" ($\chi = 1$) and "jointed ($\chi = \frac{1}{2}$) plaster-sand models, the discontinuous joints in the latter case having been prepared by inserting 0.1 mm steel shims. Only when the joint planes were oriented in the direction of the applied shear force did simple shear failures along the discontinuous joint planes occur. In all other cases, failure of the specimen was progressive with combined tensile, shear and slip mechanisms developing. The $\chi = \frac{1}{2}$ specimens were found to be less anisotropic with respect to both strength and deformation than the layered or $\chi = 1$ specimens.

Hayashi (35, 36) extended the scope of his direct shear tests to include samples containing cross-joints within the plaster layers. He concluded that the shear strength is almost independent of the pitch of these cross-joints despite the fact that his results suggest that the strength decreases as the pitch decreases, the effect varying with the orientation of the cross-joints and bedding planes.

Lajtai (15, 55) carried out direct shear tests on plaster and plaster and kavlin blocks containing a single joint, no joints, and intermittent joint with $\chi = \frac{1}{2}$ cast into the specimen, and an intermittent joint with $\chi = \frac{1}{2}$ formed by the interlocking of two sections cast with teeth. He found that by the tensile and shear fractures developed. For the two $\chi = \frac{1}{2}$ cases none of the primary fracture directions co-incided with the enforced shear direction.

The results of these direct shear tests show little more than that quite complex failure mechanisms occur. No doubt many of fracture phenomena observed result from the severe constraints and complex stress patterns imposed by the direct shear test. This severly limits the usefulness of the direct shear test in fundamental studies of the mechanics of jointed media.

3.6 Special Studies

Many model studies have been carried out to investigate the behaviour of jointed rocks as structural foundations (56-60) or the stability of rock slopes (26, 29, 53, 61-64). Although such studies were aimed at solving specific problems and do not attempt to study the overall problem at a fundamental level, they do provide some useful general concepts. As an example, consider the two dimensional model of an arch dam abutment made up of an assembly of square blocks tested by Krsmanovic et al (58, 59). They identified four modes of failure: (1) sliding on joint planes; (2) planes sliding, partly on jointed planes and partly through the blocks; (3) compression failure of the blocks; and (4) composite failures.

The tests on model slopes have been particularly significant in that they have pointed to the importance of block rotation as a significant mode of collapse near the boundaries of jointed rock masses. Such mechanisms, which have also been observed in triaxial compression tests (28, 49), should be given special attention in future investigations.

3.7 Tests on Real Rock Masses

Although the model tests outlined above have contributed to our understanding of the strength of rock masses it is obviously preferable to experiment with real rocks containing natural joint patterns. Because of the enormous difficulties encountered in sampling such materials and in preparing them for testing, very few studies of this type have been carried out.

Rosengren and Jaeger (65) developed an ingenious method of preparing laboratory samples of a randomly jointed rock which enabled them to carry out one of the most significant studies of the problem published to date. They found that if Wombeyan marble is heated to around 500°C the anisotropy of thermal expansion of calcite causes complete grain boundary separation. The resulting material retains its shape and consists of a mass of crystals in contact with a porosity of about 4%. The results of their triaxial compression tests on 2" dia. x 5" long samples show that, as with the model tests described above, the jointed material had low strengths at low confining pressures and strengths approaching those of the unjointed material at higher confining pressures.

Jaeger (66) was able to prepare 6" dia. by 12" long cores of andesite containing "a network of open joints and of veins with a rather weak filling, the spacing of these being so close that a cross-section of the core would usually contain 50 to 100 individual areas separated by planes of weakness". Triaxial compression tests were carried out at confining pressures in the range 0 to 6000 p.s.i. Again it was found that the material had low strength at low confining pressures and that the curved Mohr circle envelope passed close to the origin. The material was so broken up by joints and veins that it was not possible to produce intact cores of the material for purposes of making strength comparisons.

Finally, some mention should be made of in-situ tests on rock masses. Most in-situ strength tests are direct shear tests aimed at determining the shear strength of a certain joint or plane of weakness. Multi-axial compression tests which measure strength properties of a rock mass containing a large number of joints are rarely carried out because of their great expense. In one of the few published reports of such tests, John (10, 67) describes three multiaxial compression tests carried out on 9.3 ft. square by 4.7 ft. wide prismatic samples of jointed and somewhat decomposed granite in the abutments of the Kurobe IV arch dam. He found that the bulk strength of these large samples was about 35% of the core strength, but greater than that of a single joint. Although the available data is extremely limited, the curves published (67) suggest a similar pattern of behaviour to that shown in Fig. 17.

4 COMMENTS AND CONCLUSIONS

This brief review shows that there exists a single analytical method for predicting the strength of jointed media which can provide satisfactory solutions under certain circumstances. However, it is far from being entirely satisfactory because it over-simplifies the calculation of stress distributions within jointed media, does not take account of the full range of collapse mechanisms known to be possible, does not allow for the inter-action of joints, and uses over-simplified concepts of rock material and rock joint behaviour.

Obviously, a great amount of detailed research must be carried out before a satisfactory solution to the difficult problem of determining the load-deformation behaviour and strength of jointed rock masses can be obtained. The primary approach must be an experimental one. This will lead to an understanding of the mechanics of the situation which must then be modeled mathematically in order that useful methods of analysis can be produced.

Previous experiments have been limited in their usefulness as fundamental studies because

(a)   with few exceptions little attention has been given to the problem of ensuring that applied stresses are uniform and remain so after deformation.

(b)   without exception model tests have been carried out in conventional or "soft" testing machines which proves an impediment to the detailed study of progressive failure mechanisms, and

(c)   little attention has been given to the measurement of deformations in general, and volume changes, in particular. The limited evidence available suggests that deformation in jointed media are likely to be quite different from those occurring in the unjointed material. In any event, a knowledge of deformations and volume changes is essential to the complete understanding of the response of any material to load.

The experimental work described in Chapters 3 and 4 were aimed at overcoming some of these deficiencies.

REFERENCES

1. WITTKE, W. - Verfahren zur Berechnung der Standsicherheit belasteter und unbelasteter Feloboschungen (A numerical method of calculating the stability of loaded and unloaded rock slopes). Felsmechanik und Ingeniourgeologie, Suppl. II, 1963, pp. 52-79.

2. GOODMAN, R.E. and TAYLOR, R.L. - Methods of analysis for rock slopes and abutments - A review of recent developments. In Failure and Breakage of Rock (Proc. 8th Symp. Rock Mech.), C. Fairhurst (ed), New York, AIME, 1967, pp. 303-320.

3. JOHN, K.W. - Graphical stability analysis of slopes in jointed rock. J. Soil Mech. Founds. Div., ASCE, Vol. 94, No. SM2, Mar., 1968, pp. 497-526.

4. LONDE, P. - The stability of rock masses. Ann. Inst. Tech. Bat. et Trav. Publ., No. 51, 1968, pp. 1617-1637.

5. LONDE, P., VIGIER, G. and VORMERINGER, R. - Stability of rock slopes - a three-dimensional study, J. Soil Mech. Found. Div., ASCE, Vol. 95, No. SMI, Jan., 1969, pp. 235-262.

6. JAEGER, J.C. - The frictional properties of joints in rock. Geofis. pura et appl., Vol. 43, 1959, pp. 148-158.

7. JAEGER, J.C. - Shear failure in anisotropic rocks. Geol. Mag., Vol. 97, 1960, pp. 65-72.

8. NELSON, R.A. and HIRSCHFELD, R.C. - Modeling a jointed rock mass. M.I.T. Report R68-70 to U.S. Dept. of Transportation, Cambridge, Sept., 1968, pp. 217.

9. MÜLLER, L. - Der Felsbau. Stuttgart, Ferdinand Enke Verlag, 1963, pp. 624.

10. JOHN, K.W. - An approach to rock mechanics. J. Soil Mech. Founds. Div., ASCE, Vol. 88, No. SM4, Aug., 1962, pp. 1-30.

11. JOHN, K.W. - Engineering methods to determine strength and deformability of regularly jointed rock. In Rock Mechanics - Theory and Practice (Proc. 11th Symp. Rock Mech.), New York, AIME, 1970, pp.

12. BRAY, J.W. - Limiting equilibrium of fractured and jointed rock. Proc. 1st Congr., Int. Soc. Rock Mech., Lisbon, 1966, Vol. 1, pp. 531-535.

13. BRAY, J.W. - A study of jointed and fractured rock. Part 1 Fracture patterns and their failure characteristics. Felsmechavik and Ingeniewgeologie. Vol. 5, No. 2-3, 1967, pp. 117-136.

14. LOMBARDI, G. - The influence of rock characteristics on the stability of rock cavities (Part 1). Tunnels and Tunnelling, Vol. 2, No. 1, 1970, pp. 19-22.

15. LAJTAI, E.Z. - Strength of discontinuous rocks in direct shear. Geotechnique, Vol. 19, No. 2, June, 1969, pp. 218-233.

16. GOODMAN, R.E. - Analysis of Strecutres in jointed rock. U.S. Army Engineer District, Omaha, Tech. Report, No. 3, 1967.

17. ERGUN, I. - Stress distribution in jointed media. Proc. 2nd Congr., Int. Soc. Rock Mech., Belgrade, 1970, Vol. 1, Paper 2-31.

18. CHAPPEL, B.A. - Stress distribution in blocky material. Ph.D. thesis, Australian National Univ., Canberra, 1971.

19. DUNCAN, J.M. and GOODMAN, R.E. - Finite element analysis of slopes in jointed rock. Report No. TE-68-1, Univ. of California, Berkeley, 1968.

20. GOODMAN, R.E., TAYLOR, R.L. and BREKKE, T.L. - A model for the mechanics of jointed rock. J. Soil Mech. Found. Div., ASCE, Vol. 94, No. SM3, May, 1968, pp. 637-659.

21. GOODMAN, R.E. - Effect of joints on the strength of tunnels. U.S. Army Engineer District, Omaha, Tech. Report No. 4, 1968.

22. BEST, B.S. - A computer program incorporating non-linear rock joint elements. Report, Univ. of Wales, Swansea, June, 1969.

23. BEST, B.S. - An investigation into the use of finite element methods; for analysing stress distributions in block-jointed masses. Ph.D. thesis, James Cook Univ. of North Queensland, Dec., 1970.

24. ZIENKIEWICZ, O.C., BEST, B.S., DULLAGE, C. and STAGG, K.G. Analysis of non-linear problems in rock mechanics with particular reference to jointed rock systems. Proc. 2nd Congr. Int. Soc. Rock Mech., Belgrade, 1970, Vol. 3, paper 8-14.

25. MALINA, H. - The numerical determination of stresses and deformations in rock, taking into account discontinuities. Rock Mechanics, Vol. 2, p. 1-16, 1970.

26. BURMAN, B.C. - Some aspects of the mechanics of slopes and discontinuous media. Ph.D. thesis, James Cook University of North Queensland, Townsville, 1971.

27. KOBAYASHI, S. - Fracture criteria for anisotropic rocks. Mem. Faculty of Engg., Kyoto Univ., Vol. 32, Part 3, Sept., 1970, pp. 307-333.

28. BROWN, E.T. - Strength of models of rock with intermittent joints. J. Soil Mech. Founds. Div., ASCE, Vol. 96, No. SM6, Dec., 1970, pp. 1935-1949.

29. HOFMANN, H. - Das Verformungsverhalten eines regelmässig geklüftenten Diskontinuums beim Abbau einer steilen Fel böschung (The deformation process of a regularly joined discontinuum during the excavation of a cut). Proc. 2nd Congr., Int. Soc. Rock Mech., Belgrade, 1970, Vol. 3, Paper 7-1.

30. MÜLLER, L. - Der Progressive Bruch in Geklufteten Median (Progressive Failure in jointed media) Proc. 1st Congr., Int. Soc. Rock Mech., Lisbon, 1966, Vol. 1, pp. 679-686.

31. GOLDSTEIN, M. et al - Proc. 1st Congr., Int. Soc. Rock Mech., Lisbon, 1966, Vol. 2, pp. 175-178.

32. EINSTEIN, HH., BRUHN, R.W. and HIRSCHFELD, R.C. - Mechanics of jointed rock - Experimental and theoretical studies. M.I.T. Report R70-62 As U.S. Dept. of Transportation, Cambridge, Aug., 1970, pp. 115.

33. ROSENBLAD, J.L. - Development of a rock-like model material. In Rock Mechanics - Theory and Practice (Proc. 11th Symp. Rock Mech.), New York, AIME, 1970, pp.

34. BARTON, N.R. - A low-strength material for simulation of the mechanical properties of intact rock in rock mechanics models. Proc. 2nd Congr., Int. Soc. Rock Mech., Belgrade, 1970, Vol. 2, Paper 3-15.

35. HAYASHI, M. - Strength characteristics of discontinuous jointy masses - introduction of extreme value stochastics. Tech. Rept. No. 65052, Central Research Institute of Electric Power Industry, Tokyo, 1965, 18 pp.

36. HAYASHI, M. - Strength and dilatancy of brittle jointed mass - the extreme value stochastics and anisotropic failure mechanism. Proc. 1st Congr., Int. Soc. Rock Mech., Lisbon, 1966, Vol. 1, pp. 295-302.

37. BRACE, W.F. and BOMBOLAKIS, E.G. - A note on brittle crack growth in compression. J. Geophys. Res., Vol. 68, 1963, pp. 3709-3713.

38. EPSTEIN, B. - Statistical aspects of fracture problems. J. Appl. Phys., Vol. 19, 1948, pp. 149-157.

39. LAJTAI, E.Z. - The influence of interlocking rock discontinuities on compressive strength (model experiments). Felsmechanik and Ingenieur-geologie, Vol. 5, No. 4, 1967, pp. 217-228.

40. SIRIEYS, P.M. - Phenonomenes de rupture fragile des roches isotropes et anisotropes. In Rheology in Soil Mechanics, Kravtchenko, J. and Sirieys, P.M. (eds). Berlin, Springer - Verlag, 1966, pp. 385-395.

41. SIRIEYS, P.M. - Sur les lois de fragmentation des roches. Proc. 1st Congr., Int. Soc. Rock Mech., Lisbon, 1966, Vol. 2, pp. 81-86.

42. PANET, M. - Etude de la structure d'un massif rocheux. Bull. Liason Labs. Routiers Ponts et Chausses, Paris, No. 28, Nov. - Dec., 1967.

43. MÜLLER, L. and PACHER, F. - Modellversuche gur Klärung der Bruchgefahr geklüfteter Medien (Model tests to investigate the danger of failure of jointed media). Felsmechanik and Ingenieurgeologie, Suppl. 2, 1965, pp. 7-24.

44. JOHN, K.W. - Festigkeit and Verformbarkeit von druckfesten regelmässig gefugten Diskontinuen. Veroffentlichungen des Institutes fui Bodenmechanik and Felsmechanik der Unwersität, No. 37, 1969.

45. ROSENBLAD, J.L. - Development of equipment for testing models of jointed rock masses. In Rock Mechanics - Theory and Practice (Proc. 11th Symp. Rock Mech.), New York, AIME, 1970, pp. 127-146.

46. ROSENBLAD, J.L. - Failure modes of models of jointed rock masses, Proc. 2nd Congr., Int. Soc. Rock Mech., Belgrade, 1970, Vol. 2, Paper 3-11.

47. BROWN, E.T. - The influence of planar discontinuities on the shear strength of a rock-like material. Ph.D. thesis, Univ. of Q'ld., June, 1968.

48. BROWN, E.T. and TROLLOPE, D.H. - Strength of a model of jointed rock. J. Soil Mech. Found. Div., ASCE, Vol. 96, No. SM2, Mar., 1970, pp. 685-704.

49. BROWN, E.T. - Modes of failure in jointed rock masses. Proc. 2nd Congr., Int. Soc. Rock Mech., Belgrade, 1970, Vol. 2, Paper 3-42.

50. EINSTEIN, H.H., NELSON, R.A., BRUHN, R.W. and HIRSCHFELD, R.C. Model studies of jointed rock behaviour. In Rock Mechanics Theory and Practice (Proc. 11th Symp. Rock Mech.), New York, AIME, 1970, pp. 83-103.

51. STANLEY, L.O. - Failure criteria for rock models under controlled traixial stress conditions. M. Eng. Sc. Thesis, Univ. of Q'ld., 1968.

52. HAYASHI, M. and FUJIWARA, Y. - Failure mechanism, anisotropic strength and dilatancy of layer - jointed masses under direct shear. Proc. 3rd Interior Symp. Rock Mech., Jap. Soc. Civ. Engrs., Nov., 1965, pp. 16-22.

53. HAYASHI, M. and FUJIWARA, Y. - A mechanism of anisotropic dilatancy and shear failure of laminately jointed rock masses. Tech. Rept. C67006, Central Research Institute of Electric Power Industry, Tokyo, March, 1968, 17 pp.

54. KAWAMOTO, T. - Mocorscopic shear failure of jointed and layered brittle media. Proc. 2nd Congr. Int. Soc. Rock Mech., Belgrade, 1970, Vol. 2, Paper 3-31.

55. ALJTAI, E.Z. - Shear strength of weakness planes in rock. Int. J. Rock Mech. Min. Sci., Vol. 6, No. 1969, pp. 499-515.

56. FUMAGAILI, E. - Model simulation of rock mechanics problems. In Rock Mechanics in Engineering Practice, K.G. Stagg and O.C. Zienkiewicz (eds.), London, John Wiley, 1969, pp. 353-384.

57. GRISHIN, M.M. et al - The effect of characteristics of geological structure of the rock foundations of dams on their strength and stability. Trans. 9th Congr. Large Dams, Instanbaul, 1967, Vol. 1, pp. 873-889.

58. KRSMANOVIC, D., TUPO, M. and LANGOF, Z. - Some aspects of the rupture of rock masses. Felsmechanik and Ingenieurgeologie, Suppl. 2, 1965, pp. 143-155.

59. KRSMANOVIC, D., TUFO, M. and LANGOF, Z. - Shear strength of rock masses and possibilities of its reproduction in models. Proc. 1st Congr., Int. Soc., Rock Mechan., Lisbon, 1966, Vol. 1, pp. 537-542.

60. TAKANO, M. - Fracture studies on arch-dams foundations by means of models. Geologie and Banwesen, Vol. 26, No. 3, 1961, pp. 99-121.

61. GOLDSTEIN, M. et al - Stability investigations of fissured rock slopes. Proc. 1st Congr., Int. Soc. Rock Mech., Lisbon, 1966, Vol. 2, pp. 175-178.

62. MÜLLER, L. - New considerations on the vaiont slide. Felsmechanik and Ingenieurgeologie, Vol. 6, No. 1-2, 1968, pp. 1-91.

63. MÜLLER, L. and HOFMANN, H. - Selection, compilation and assessment of geological data for the slope problem. Proc. Symp. Theoretical Background to the Planning of Open Pit Mines with Special Reference to Slope Stability, Johannesburg, 1970.

64. RENGERS, N. and MULLER, L. - Kinematische Versuche an geomechanischen Modellen (Kinematic studies on geomechanical models). Rock Mechanics, Suppl. 1, 1970, pp. 20-31.

65. ROSENGREN, K.J. and JAEGER, J.C. - The mechanical properties of an interlocked low-porosity aggregate. Geotechnique, Vol. 18, No. 3, 1968, pp. 317-326.

66. JAEGER, J.C. - The behaviour of closely joined rock. In Rock Mechanics - Theory and Practice (Proc. 11th Symp. Rock Mech.), New York, AIME, 1970.

67. JOHN, K.W. - Die Praxis der Felsgrossversuche (Practical aspects of large-scale rock tests) Geologie and Banwesen, Vol. 27, No. 1, 1961, pp. 9-19.
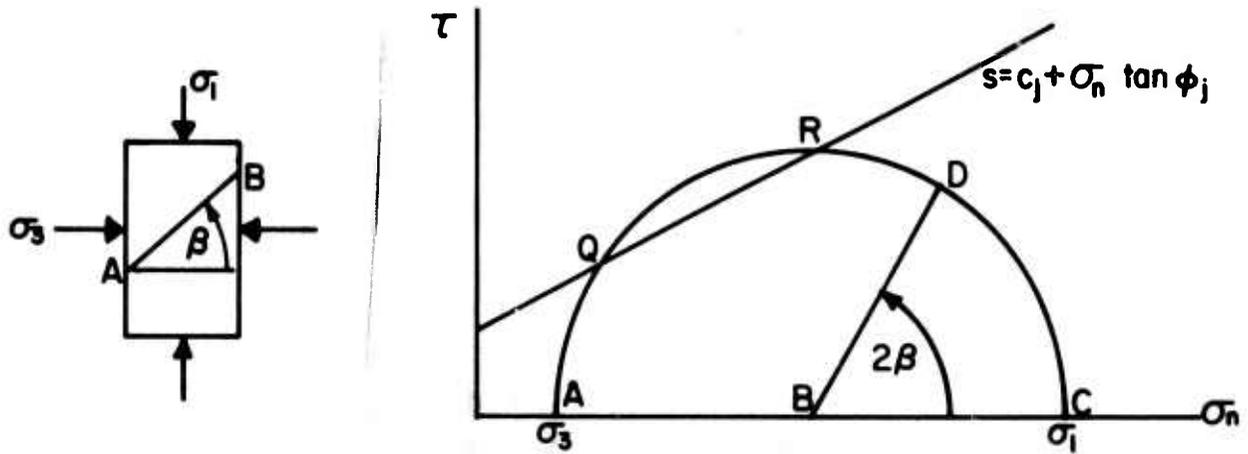
Figure 1: Mohrs Diagram for Specimen with Single Plane of Weakness.

(a)

(b)

(c)
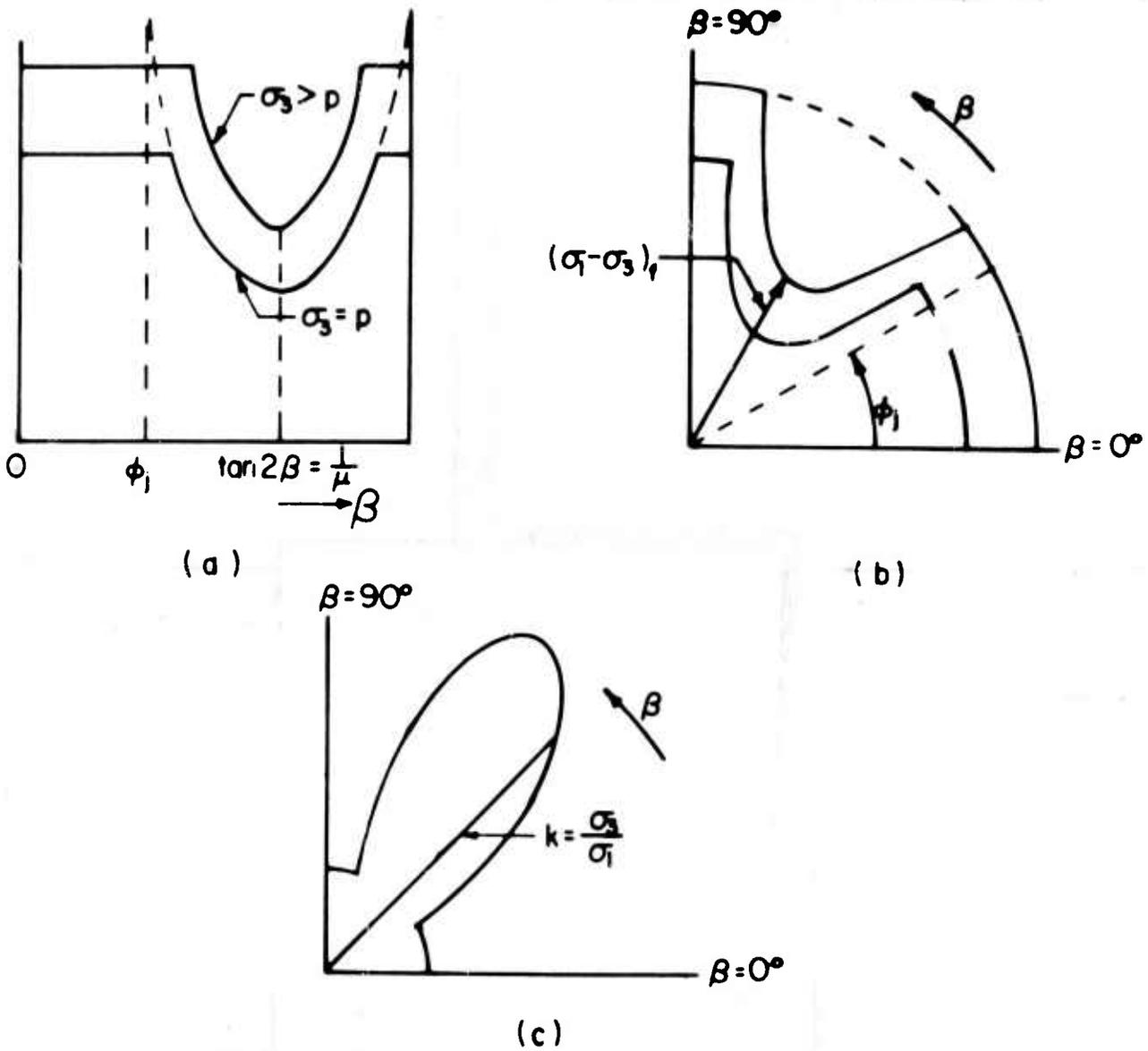
Figure 2: Graphical Representation of Strength of Specimen with a Single Plane of Weakness.

(a)

(b)

$\phi = 30°$
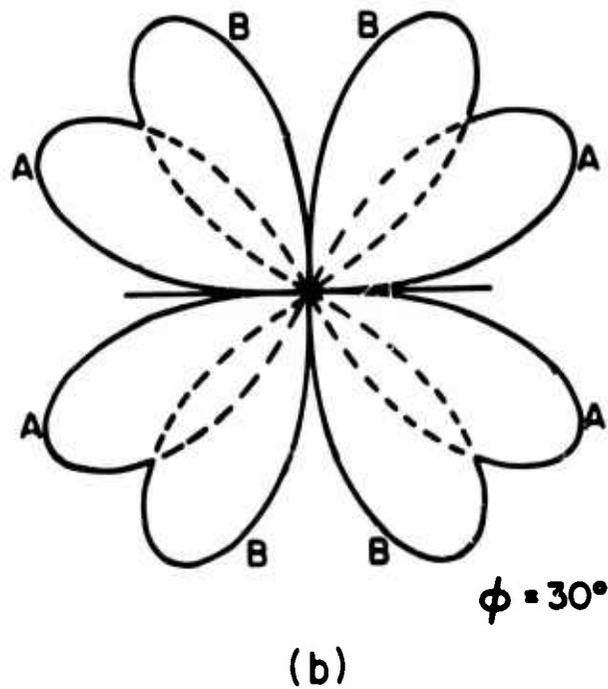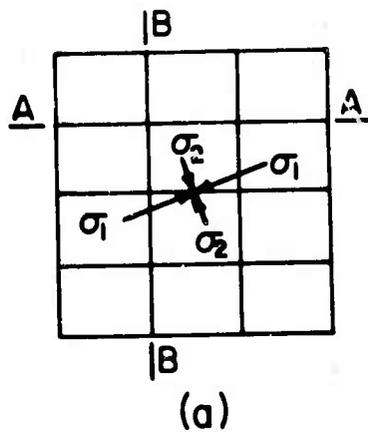
Figure 3: Strength of a Block Jointed System. (After Bray 12).
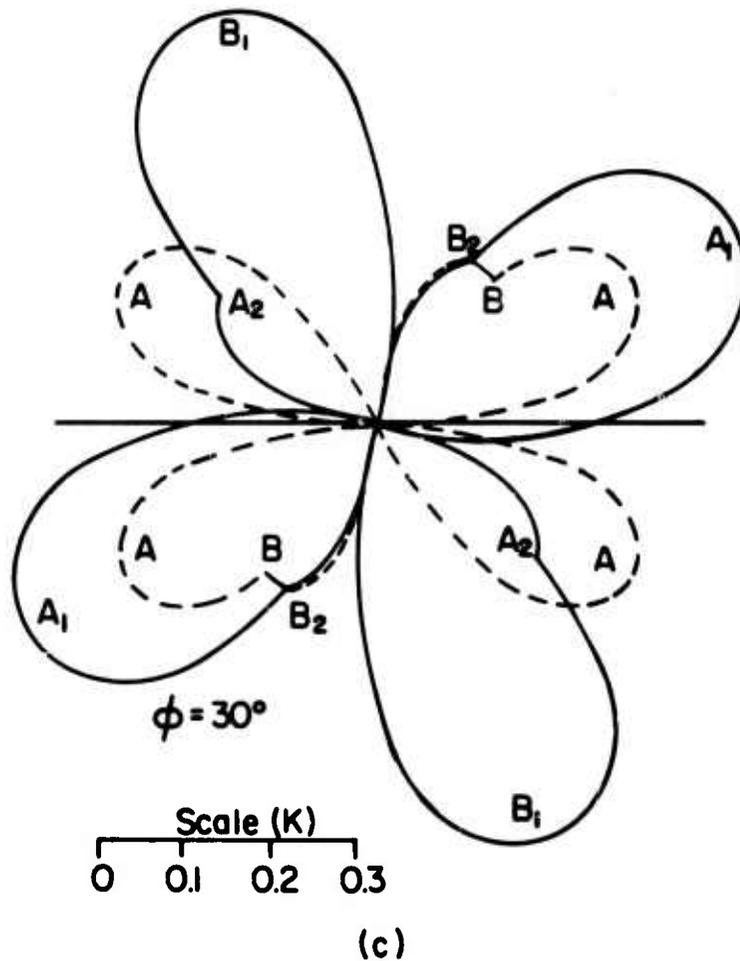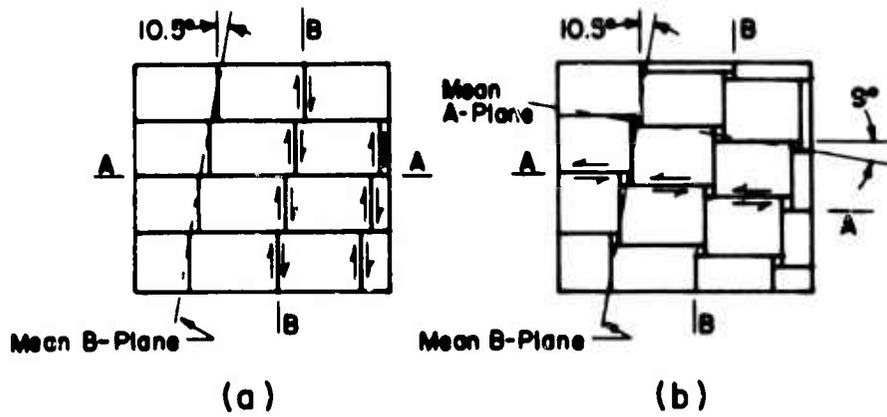
Figure 4: (a) Element of Rock Showing Staggered Vertical Joints Resulting from Slip of Horizontal Joints. (b) Additional Staggering of Horizontal Joints Resulting from a Subsequent Slip on Vertical Joints. (c) Failure Characteristics Corresponding to the Joint Systems Shown in (a) and (b).(After Bray 13)
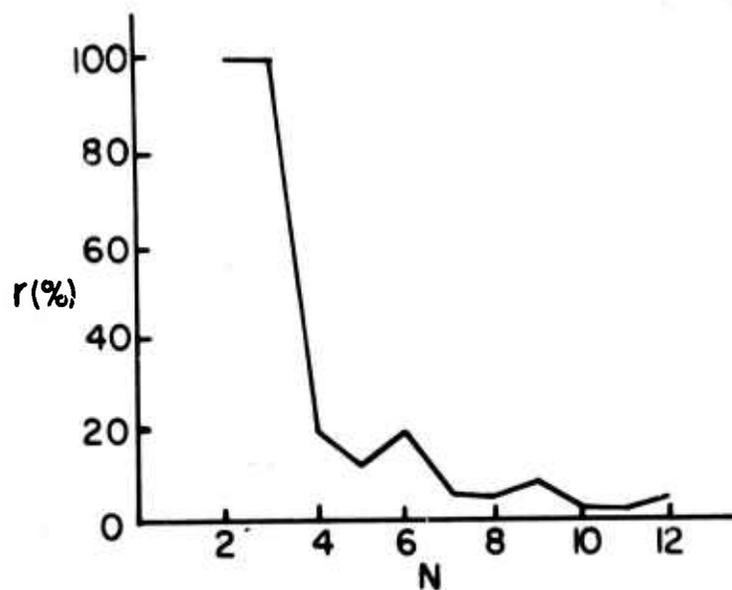
Figure 5: Variation of Anisotropy with Increasing Number of Differently Orientated Planes. (After Bray [13]).
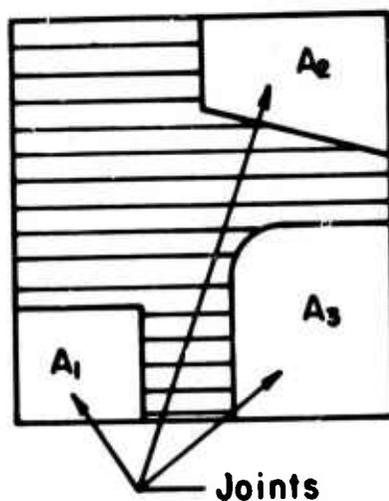
Figure 6: Two Dimensional Extent of a Joint.
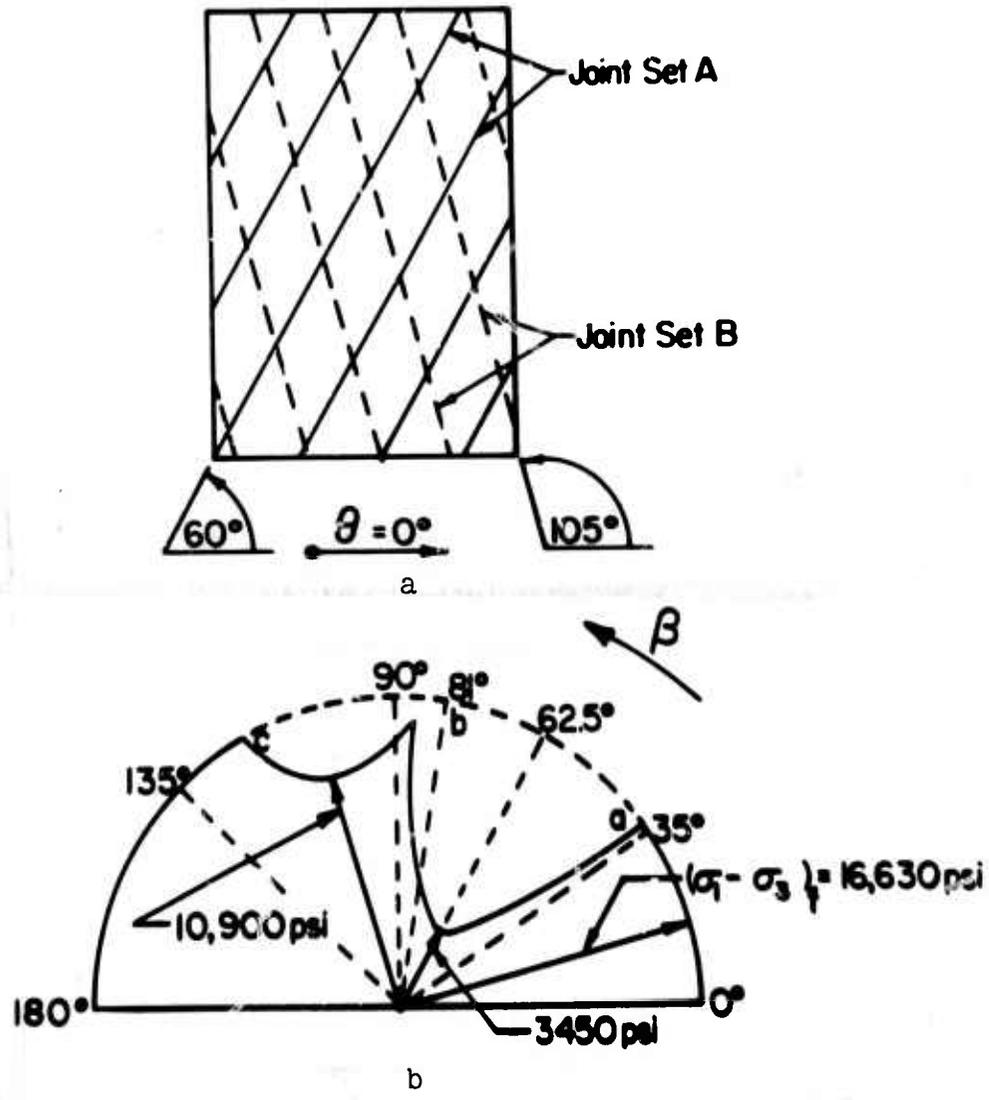
Figure 7: a) Joint Set in Rock, Continuous, Set A, Intermittent, Set B.
b) Variation of Principal Stress Difference with B.
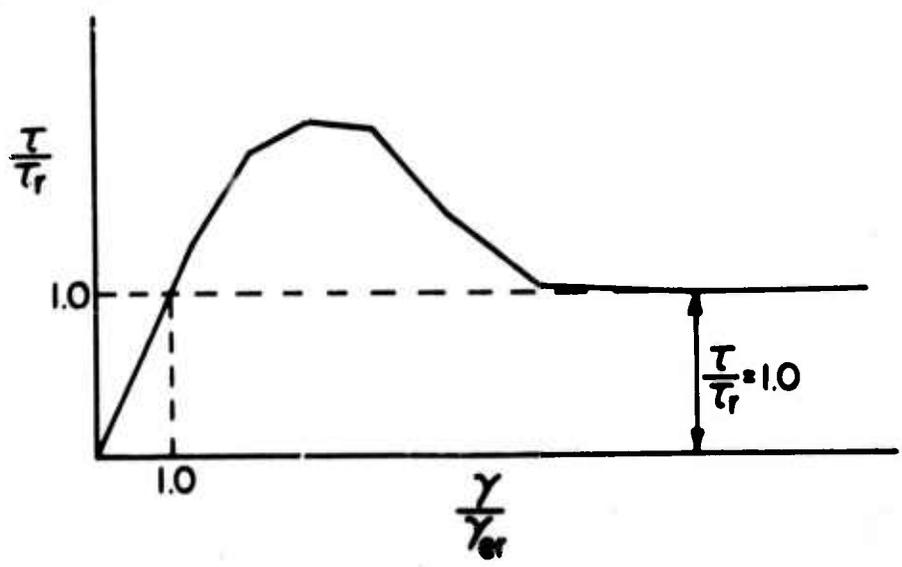
Figure 8: Typical Joint Characterization. (After Best [23]).
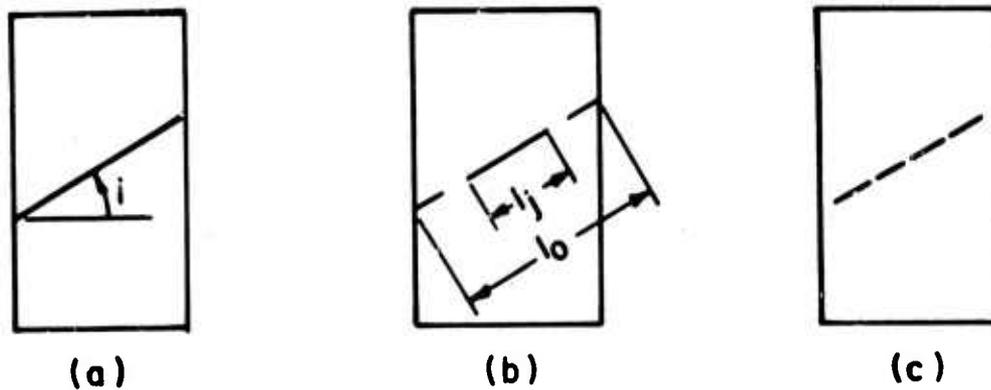
Figure 9: Examples of Hayashi's Uniaxial Compression Test Samples.
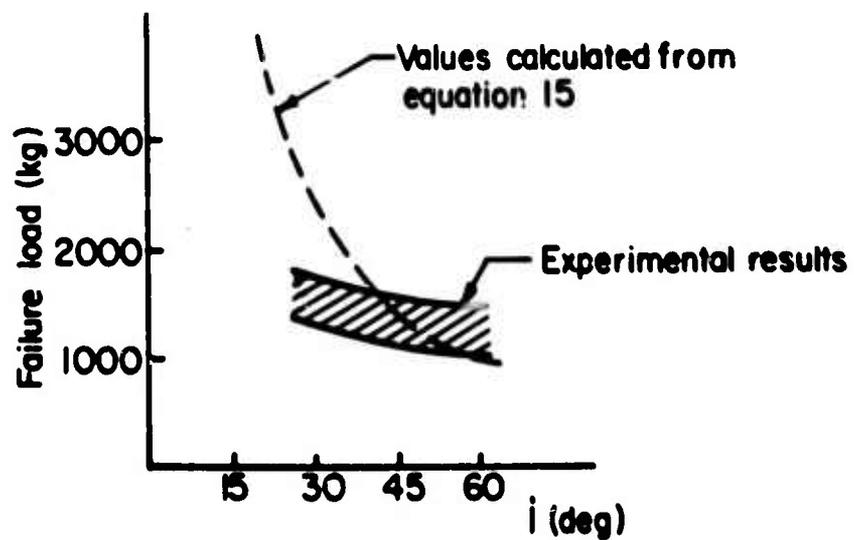
Figure 10: Comparison of Simple Theory with Hayashi's Uniaxial
Compression Test Results. (After Hayashi, 1965).

188
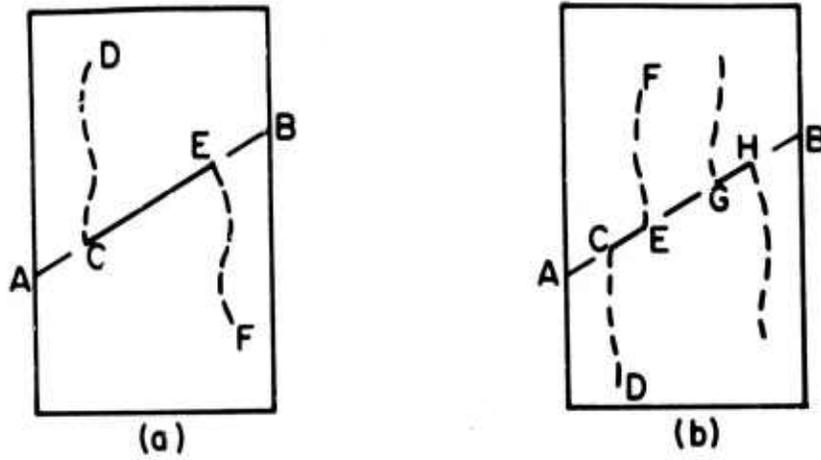
Figure 11: Possible Tensile Modes of Failure in Hayashi's Uniaxial
Compression Tests.
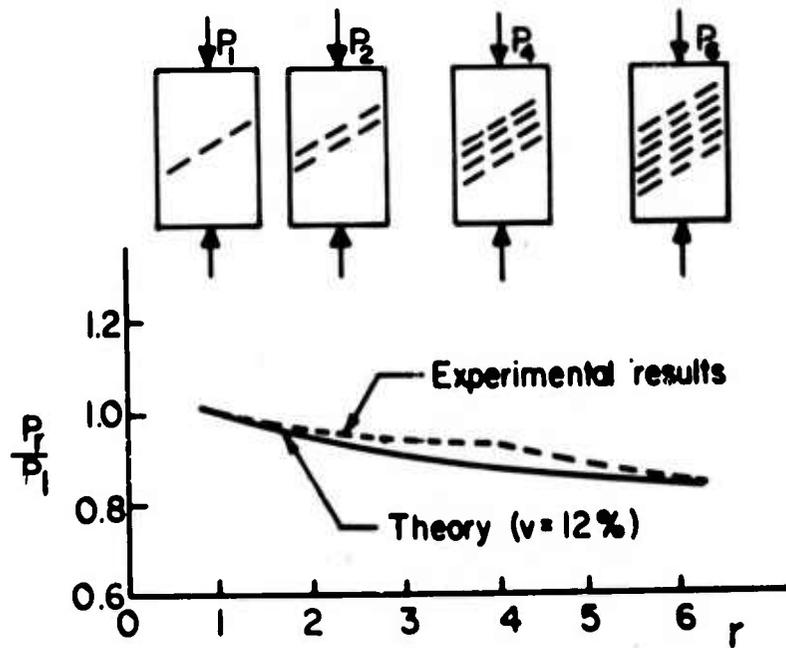
Figure 12: Decrease in Compressive Strength P_r with Number of Parallel
Rows of Joints, r. (After Hayashi, 1966a).

189
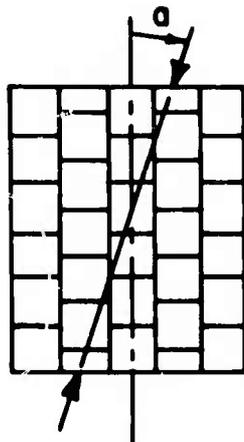
Figure 13:   Sirley;s "brick wall" System.

(a) Types of Failure   (b) Stability Quotients
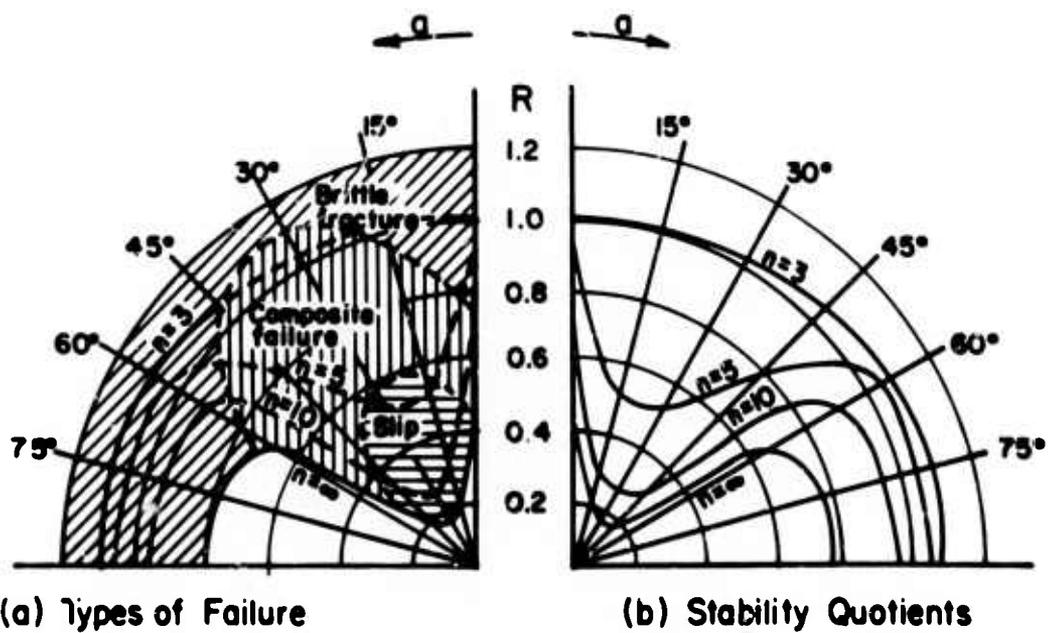
Figure 14:   Results of Müller and Pacher's Biaxial Compression Tests.
           (After Müller and Pacher, 1965).

The mechanical failure of block jointed model were studied using a servo-controlled loading system such that the progressive collapse of these models under uniaxial compressive loading could be studied in detail. The mechanism of collapse at these block jointed models were recorded photographically and indicate that several mechanisms are operative in this process. These include; fracture of individual blocks, rotation of individual blocks, collapse of columns of blocks by rotation or buckling, slip along joint planes and by shear deformation of individual blocks. No single simple theory of failure appears capable at this time of predicting the collapse loads of such systems.

The dilatant nature of the collapse of these block jointed models was studied under two different confinement pressures. Failure of the specimens was again controlled using a servo-controlled testing machine. These tests illustrate that the volumetric strain behavior of jointed specimens can be vastly different from that of comparable unjointed specimens.

The continuum characterization of a jointed rock mass is briefly reported in this report. The research results of this work have been reported in readily available journals so is only briefly reviewed here. The low shear stiffness of joints in general results in an anisotropic continuum characterization of the rock mass with a low shear stiffness. The practical significance of the anisotropic characterization, in that the pressure 'bulb' from any applied load on a boundary is distorted from that of the isotropic case, is discussed. The effect of joint spacing and thickness upon the reliability as a function of the number of dilatometer tests in a jointed rock mass is also discussed and presented in detail in one of the published papers.

Figure 15: Polar Diagram of Strength Against Joint Orientation Illustrating Transition Zone. (After John [44]).

(a)

(b)

(c)
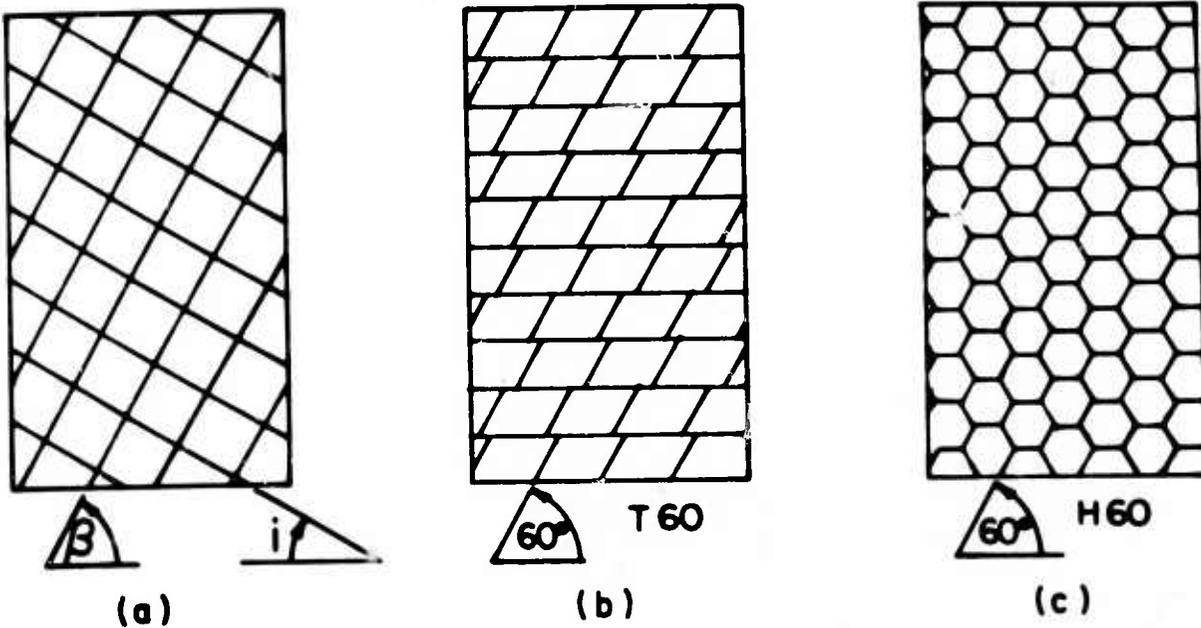
Figure 16: Illustration of Block Jointed Models Tested by Brown (28).
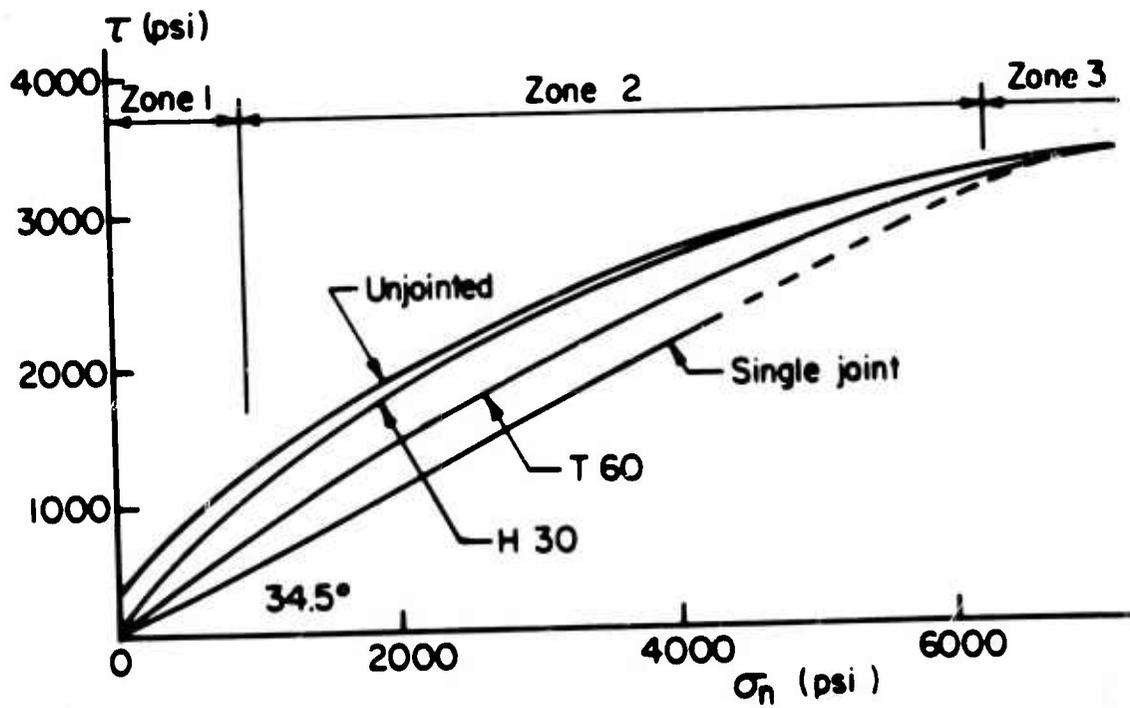
Figure 17: Summary of Results of Jointed Materials. (After Brown [28]).
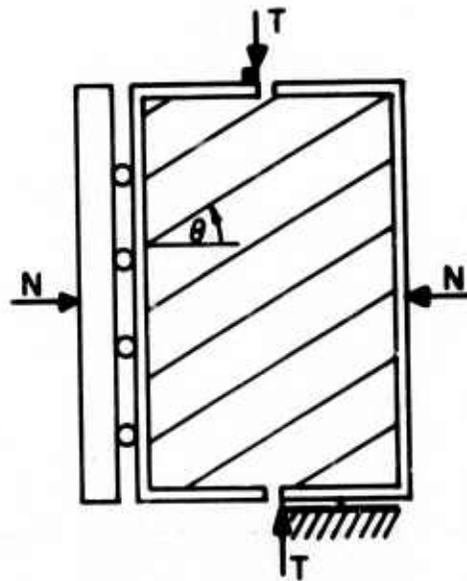
Figure 18: Direct Shear Experiments of Jointed Plaster. (After Hayashi [36]).

APPENDIX III

FATIGUE OF BLOCK JOINTED MODELS

SUMMARY

Present knowledge of the behaviour of rock masses under earthquake-indiced loadings is inadequate for engineering purposes. In a preliminary experimental study, highly idealised models of jointed rock were subjected to a series of uniaxial compression tests in which the applied loads were cycled between upper and lower limits at rates of 0.5, 1, or 2 cycles per second. The results obtained would indicate that discontinua such as jointed rock are susceptible to cyclic fatigue failure in both the pre-peak and post-peak regions. The time-dependent behaviour of rock associated with either quasi-static or cyclic fatigue loadings can be explained in terms of the residual strength locus. Catastrophic failure will occur when the accumulation of deformation is such that the post-peak section of this locus is intersected by the loading path. Failed rock supporting loads as in the walls of underground excavations is particularly susceptible to failure under cyclic fatigue.

INTRODUCTION

During earthquakes materials in the earth's crust are subjected to limited numbers of cycles of pulsating compressive stress. Analyses of the behaviour of rock structures under earthquake-induced loadings require a knowledge of both the nature of the disturbance and to response of rock to cyclic loading. Although the response of engineering materials such as metals, concrete and soils to cyclic loading has been well investigated in recent years, the corresponding properties of rock have received little attention. With the increasing use of underground construction in rock for military installations, urban transportation systems, liquid storage reservoirs, power plants, etc., it is essential that the oehaviour of rock under earthquake induced disturbances be investigated.

Haimson and Kim[1] have recently studied the mechanical behaviour of intact rock under cyclic fatigue. Their approach involved consideration of the role of the residual strength locus in determining limits for fatigue strain. This is considered to be an extremely useful approach and one that should be applied to the important practical case of jointed rock. It would appear reasonable to expect that because of the presence of discontinuities and the associated mobility of individual blocks, discontinua such as jointed rock might be more susceptible to repeated loading than the corresponding intact materials.

In this paper, the residual strength locus interpretation of time-dependent failure of rock is explained, some preliminary experimental results concerning the fatigue of idealised block-jointed systems are presented, and the practical

194

implications of these results discussed. It should be emphasised, however, that this paper is concerned with but one aspect of the total engineering problem of the seismic response of rock masses.

RESIDUAL STRENGTH LOCUS INTERPRETATION OF TIME-DEPENDENT FAILURE

Recent research into the mechanical behaviour of rock has involved the concept of the complete force-displacement curve. Using stiff or servo-controlled testing machines it is now possible to control rock failure and so obtain complete curves in a variety of experimental situations[2, 3]. In considering the behaviour of failed material in the post-peak region, it is necessary to think in terms of the fundamental quantities force and displacement rather than in terms of the derived quantities stress and strain. In the uniaxial compression test, for example, it is a simple matter to measure the total force applied to the specimen and the associated axial contraction. The relationship between these two quantities is a property of a certain volume of rock under the conditions of the test. It is difficult to scale these values to provide an estimate of stress and strain at any point within the volume of rock concerned because [4] the distribution of stress and strain within the specimen is far from uniform. In the post-peak region in particular, failure does not occur uniformly and the structure of the specimen continually changes. Thus it is impractical, if not impossible, to scale the results to true stress and true strain. It is interesting to note that recent attempts to apply numerical methods to the solution of problems of the mechanics of discontinua have also encountered some difficulty in presenting results in terms of stress and strain at a point.[5]

Displacement must be regarded as the independent variable in experimental studies of rock failure in the post-peak region. An attempt to maintain a constant loading rate results in violent failure at the peak of the complete force-displacement curve. A constantly increasing load is incompatible with the decrease in load-bearing capability of the specimen that occurs after the peak load has been reached. When a constant displacement rate is applied to the specimen, the dependent variable, force, rises to a maximum and then progressively decreases in the failure region. Rock failure can be controlled in almost any type of laboratory test using a closed-loop programmable testing system to control displacement[2].

The shape of the complete force-displacement curve obtained from any test on a given rock depends very much on test conditions. In this sense, the curve is not unique. Under quasi-static uniaxial compression, the shape of the curve varies with axial strain rate[6]. The shape of the post-peak curve can also vary with testing machine characteristics. With a closed-loop servo-controlled system such as that used by the authors, the curve obtained is a locus of points at which the energy available to the specimen is just sufficient to sustain the fracture mechanism. In other machines, the energy available to drive the propagating crack may be in excess of this equilibrium value in which case different curves may result.

Testing Technique

Quasi-static and cyclic loading uniaxial compression tests were carried out in a closed-loop servo-hydraulic testing system with a capacity of 4.45 MN. A block diagram of the closed-loop principle is shown in Figure 4. Details of the philosophy and techniques of use of servo-controlled testing systems in experimental rock mechanics have been given elsewhere[2, 3] and will not be repeated here.

Quasi-static force-axial displacement curves were obtained using axial displacement as the independent variable or feedback signal. Cyclic loading tests were carried out under load control with the compressive load being programmed to vary between two limits as a triangular function of time at rates of between 0.5 and 2 cycles per second. Seed and Chan[5] have shown that such loading is a reasonable first approximation to that resulting from earthquakes. Higher frequencies were not used because of limitations in the response time of the recorders used to monitor results. The use of a random function generator rather than a ramp generator could produce a more exact simulation of earthquake loading. If the practical situation were to be properly simulated, the specimen would have to be subjected to a triaxial state of stress with all components of applied load being cycled. Ground-water conditions would also have to be considered.

Boundary conditions are an important consideration in laboratory tests on brittle materials. It is common practice to apply compressive loads to specimens through comparatively rigid platens. This produces uniform displacement of the specimen ends but a non-uniform distribution of stress with the specimen[4]. In the present uniaxial compression tests on block-jointed models, an attempt was made to apply the axial force uniformly over the specimen ends. Loads were transmitted from the machine platens through two 0.12 cm thick sheets of copper to a number of ground steel cubes with 1.27 cm sides in contact with the specimen. The copper was sufficiently soft to accommodate any initial non-uniformity in the height of the specimen and subsequent small differential axial movements associated with failure. Calibration tests showed that this loading system did not undergo any detectable fatigue deformation under the force levels and numbers of cycles used in the tests.

Results

Mean peak loads obtained in quasi-static uniaxial compression tests carried out on the three specimen types at axial strain rates of approximately 10^{-5} sec^{-1} are given in Table 1.

Specimen Type	Number of Tests	Mean Peak Load, F_m (kN)	Corresponding Average Axial Stress (MNm^{-2})
SOLID	4	342	33.1
ST	4	184	17.8
H60	4	114	11.0

TABLE 1. Peak Load-Bearing Capability in Quasi-Static Tests

With these qualifications regarding uniqueness, it is possible for given test conditions to define a residual strength locus that represents the equilibrium relationship between force and displacement in the post-peak region. Stable force-displacement states of the rock exist at any point on or within this locus.

The time-dependent behaviour of the rock can be interpreted by considering the possible paths that specimens starting at various force-displacement states on or within the locus may follow. In Figure 1, the horizontal lines drawn from the points A, D, and H in the pre-peak, post-peak and unloaded regions respectively, represent the application of constant force, i.e. creep. The vertical lines represent a constant displacement constraint, i.e. relaxation. From A, time-dependent displacement can take place along AB until tertiary creep occurs and the residual strength locus is intersected. At D, however, an attempt to hold the axial force constant will lead to immediate failure. From H within the locus, time-dependent displacement can occur along HK, again until the locus is reached. Under a constant displacement constraint, there will be a time-dependent fall off in force in each case, but loci having the general shape of that shown in Figure 1 will not be intersected.

Arguments similar to these can be used to explain behaviour under cyclic fatigue. Figure 2 shows a situation in which displacement progressively accumulates when the applied force is cycled between the limits F_1 and F_2. The cycle moves from an initial position AB to a final position CD where the residual strength locus is intersected. Haimson and Kim[1] have shown this interpretation of fatigue failure to be valid for intact rock. The authors have attempted to extend this approach as part of a broader experimental study of the collapse of block-jointed rock systems[7,8].

FATIGUE OF BLOCK-JOINTED SYSTEMS

Specimen Preparation

Idealised models of block-jointed rock masses were prepared from a gypsum plaster. The three specimen types used were:

(a) SOLID - rectangular prisms of plaster used to simulate unjointed brittle rock (figure 3a);

(b) ST - prepared from 2.5 cm x 2.5 cm x 10.2 cm blocks of plaster to simulate a rock mass with continuous horizontal and discontinuous vertical jointing (figure 3b);

(c) H60 - prepared from 10.2 cm long hexagonal blocks with a cross-sectional area of 6.45 cm^2 to simulate a rock mass with discontinuous inclined jointing (figure 3c).

Details of the techniques used in preparing such specimens have been given elsewhere[7,8].

Representative results of the cyclic loading tests are shown in Figures 5-8. Specimen SOLID/8 (Figure 5) was first loaded to 270 kN (i.e. to 79% of F_m, the mean peak load sustained by specimens of its' type) and unloaded. The load was then cycled between 270 kN (0.79 F_m) and 9 kN (0.03 F_m) at a rate of 1 cycle per second. After 625 cycles catastrophic failure occurred. The residual failure locus obtained in a controlled test on another unjointed specimen is superimposed on the curve obtained for SOLID/8 in Figure 5. Although it can hardly be expected that the residual failure loci of different specimens of the same type will be coincident, Figure 5 clearly shows how a specimen subjected to cyclic loading from a point in the pre-peak region (c/f point A in Figure 1) will undergo increased displacement until failure occurs when the residual strength locus is intersected. Because such tests must necessarily be carried out under load control, the eventual failure will always be catastrophic rather than controlled.

Figure 6 shows the force-displacement behaviour of specimen H60/7. This specimen was loaded to 96.5 kN (0.85 F_m) under displacement control and then unloaded. Considerable cracking took place during this initial stage of loading. The load was then cycled between 78 kN (0.68 F_m) and 11 kN (0.11 F_m) at a rate of 1 cycle per second. Cyclic loading was discontinued after 100 cycles and the test resumed under displacement control. Cracking occurred throughout this stage of the test and it is apparent that the residual failure locus was soon reached. The irregular nature of the post-peak portion of this curve is typical of curves obtained for these block-jointed models. The plaster from which the specimens were prepared is extremely brittle. Consequently, fractures often propagate through individual blocks in an uncontrolled manner producing sharp local variations in the total load supported by the specimen.

At 50 kN (0.43 F_m), specimen H60/7 was unloaded and the load cycled between 21 kN (0.18 F_m) and 9 kN (0.07 F_m). Instability developed after 1140 cycles when the specimen was unloaded and the test completed under displacement control.

Figure 7 shows the force-displacement behaviour of specimen ST/4. The procedure used in this case was similar to that used for H60/7, the major difference being that the first sequence of cyclic loading was continued until instability developed. The results of this test further illustrate how the residual failure locus may be reached when the load is cycled from points in the pre-peak and post-peak ranges.

A more detailed set of results is presented in Figure 8 for specimen ST/5. This specimen was loaded to a point near the peak of its' force-displacement (F-Δ) curve, subjected to a few low speed loading cycles (now shown on the F-Δ curve in the interests of clarity) and unloaded when instability developed. At this stage the specimen was at point A on the F-Δ curve and contained a considerable number of fractures. The load was then cycled between 67 kN and 8.5 kN at a rate of 0.5 cycles per second. Instability developed after 3150 cycles. The failure locus for another specimen of this type, ST/2, is shown as a dashed line on the F-Δ plot. It is interesting to note that specimen ST/5 failed when this locus was intersected.

A plot of axial displacement against number of cycles (or time) is also shown in Figure 8. The axial displacement increased noticeably in the first 1500 cycles after which the rate of increase dropped to almost zero. From about 2500 cycles, displacement increased at an accelerating rate until uncontrolled failure finally occurred. These three stages of displacement development are analogous to primary, secondary and tertiary stages of creep. In those tests in which smaller numbers of cycles were required to produce failure (e.g. the first cyclic loading sequence for ST/4), these three stages were even more clearly defined. Haimson and Kim[1] observed similar behaviour in their cyclic fatigue tests on intact rock.

A third feature illustrated in Figure 8 is the progressive accumulation of damage to the specimen occurring during cyclic loading. The six photographs presented show how the density of cracking increased and existing cracks and joints progressively opened up as cyclic loading proceeded. The damage sustained during the primary and secondary "creep" stages was minimal, the major structural break-down occurring during the short tertiary stage of cyclic loading.

A number of other tests gave similar results to those described and need not be presented. It is important to note however, that a number of tests were stopped before failure under cyclic loading in the pre-peak range had occurred. In such cases specimens were subsequently loaded to failure under displacement control in order that individual peak loads, F_c, could be determined. Details of some of these cases are given in Table 2.

Specimen number	Maximum force reached in cycle	Number of cycles at which test stopped
SOLID/9	$0.40 \, F_c$ $0.79 \, F_c$	14,000 1,500
ST/6	$0.60 \, F_c$	13,500
H60/6	$0.77 \, F_c$	7,500

TABLE 2. Cases in which failure did not occur

DISCUSSION AND CONCLUSIONS

It is apparent that the models of jointed rock tested are susceptible to failure by cyclic fatigue, and that the conditions under which such failure is likely to occur can be described in terms of the residual strength locus interpretation of time-dependent failure. An extension of this concept would suggest that brittle rock may not have a fatigue limit in the sense that this term is applied to more ductile engineering materials. It can be argued that because the post-peak force-deflection curve for most rocks can be followed down to

almost zero force, it should be possible to intersect this curve and cause failure by cycling the load from almost any level (Figure 9). With more ductile materials, the residual strength locus would not be approached if the load were cycled to the levels shown in Figure 9. In these cases a real fatigue limit must exist. Such increased ductility can result when brittle rocks are subjected to confining pressure. The post-peak curves become flatter, and fatigue limits increase correspondingly[10]. In the in-situ case, of course, rock masses will generally be subjected to some confinement and this may help decrease susceptibility to cyclic fatigue failure.

The suggestion that rock masses may be susceptible to fatigue failure when loaded at quite low force levels is of academic rather than practical importance when cyclic loading begins in the pre-peak range. In such cases, the numbers of cycles required to produce failure would be far in excess of the few tens or hundreds of cycles resulting from earthquake or blast disturbances. However, the situation becomes more serious in the post-peak range. It is well established that around underground excavations, for example, rock performing a structural or load-bearing function may well be fractured and be in equilibrium with its surroundings at some point on the post-peak portion of the appropriate force-displacement curve. If rock in such a situation is subjected to cyclic loading in which the maximum applied force is equal to or greater than the equilibrium load, catastrophic failure of the structure will inevitably occur. This is the cyclic loading equivalent of the static loading condition given by line DE in Figure 1.

Although the experimental results available are too few to permit firm conclusions to be drawn, there is a suggestion that the jointed models are more susceptible to fatigue damage than the unjointed specimens. This would appear to be a reasonable result in view of the greater number of degrees of freedom available to blocks in the jointed models. Because individual blocks may be free to rotate the translate often irreversibly[5,8], mechanisms not involved in the failure of the unjointed material may contribute to the progressive accumulation of deformation and collapse of jointed media.[11] These mechanisms have parallels in other discontinua. Richart, Hall and Woods[11] have noted that in sands, for example, "the cumulative effects of minor rearrangements of soil particles or slips at the contact points are indicated by gradual increases in axial strain as the number of cycles increases".

The loading case considered in this paper, uniaxial compression, is the simplest one possible and so formed a useful starting point for a new area of investigation. More advanced studies should consider the important practical case of the shear behaviour of rock masses under cyclic load. Assuming that the phenomena observed for uniaxial compression also hold for shear, it is apparent that repeated small shocks could eventually lead to a major slip causing collapse of a rock structure such as an underground excavation or open pit. The need for further work in this area is obvious.

REFERENCES

1. B. C. Haimson and C. M. Kim, "Mechanical behaviour of rock under cyclic fatigue", Proc. 13th Symp. Rock Mech., Urbana, 1971 (in press).

2. J. A. Hudson, E. T. Brown and ' Fairhurst, "Optimizing the control of rock failure in servo-controlled laboratory tests", Rock Mechs., 3, 217-224 (1971).

3. J. A. Hudson, S. L. Crouch and C. Fairhurst, "Soft, stiff and servo-controlled testing machines - a review with reference to rock failure", Engg. Geol., 6 (1972).

4. C. Fairhurst, "Laboratory measurements of some physical properties of rock", Proc. Fourth Symp. Rock Mech., State Univ., 1961, 105-118.

5. B. C. Burman, "A numerical approach to the mechanics of discontinua", Ph.D. thesis, James Cook Univ. of North Queensland, 1971.

6. J. A. Hudson and E. T. Brown, "Studying time-dependent effects in failed rock", Proc. 14th Symp. Rock Mechs., Penn. State Univ., 1972 (in press).

7. E. T. Brown and D. H. Trollope, "Strength of a model of jointed rock", J. Soil Mechs. Foundns. Div., Am. Soc. Civ. Engrs., 96, SM2, 685-704 (1970).

8. E. T. Brown and J. A. Hudson, "Progressive collapse of simple block-jointed systems", Aust. Geomechs. J., 2 (1972) (in press).

9. H. B. Seed and C. K. Chan, "Clay strength under earthquake loading conditions", J. Soil Mechs. Foundns. Div., Am. Soc. Civ. Engrs., 92, SM2, 53-79 (1966).

10. N. T. Burdine, "Rock failure under dynamic loading conditions", Soc. Petr. Engrs. J., 1-8 (1963).

11. F. E. Richart, J. R. Hall and R. D. Woods, Vibrations of soils and foundations, Prentice Hall, Englewood-Cliffs, 1970.
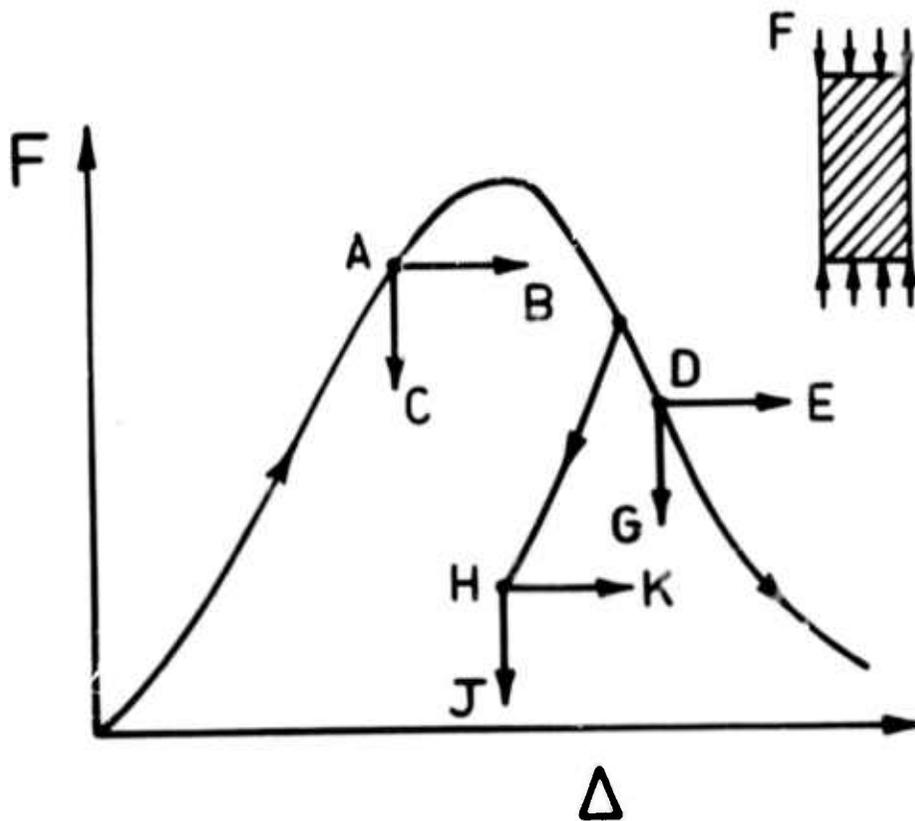
Figure 1: Constant Force and Constant Displacement Constraints.
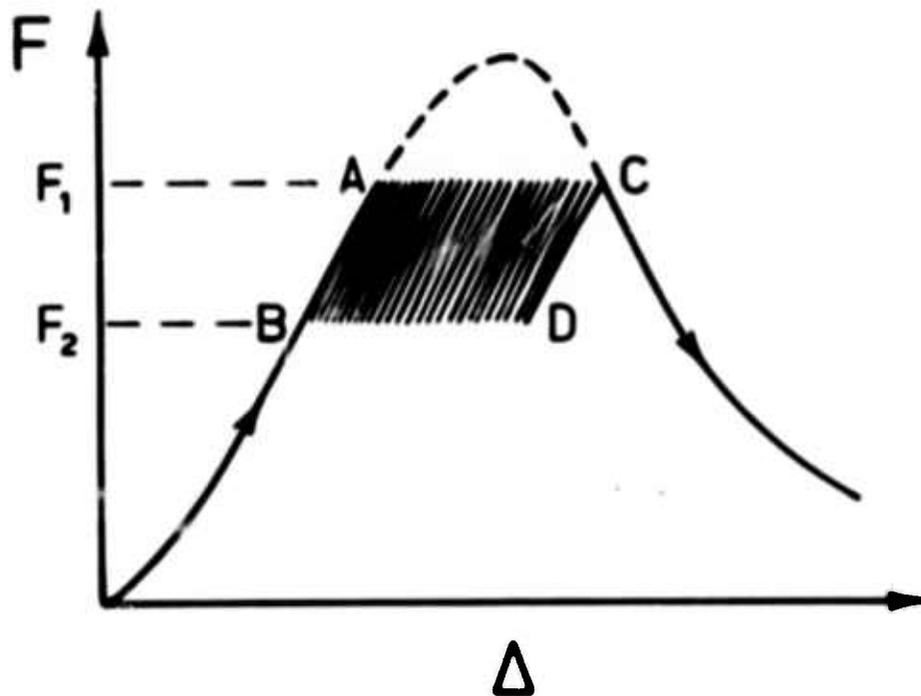
Figure 2: Accumulation of Displacement During Load Cycling can lead to Gross Failure.
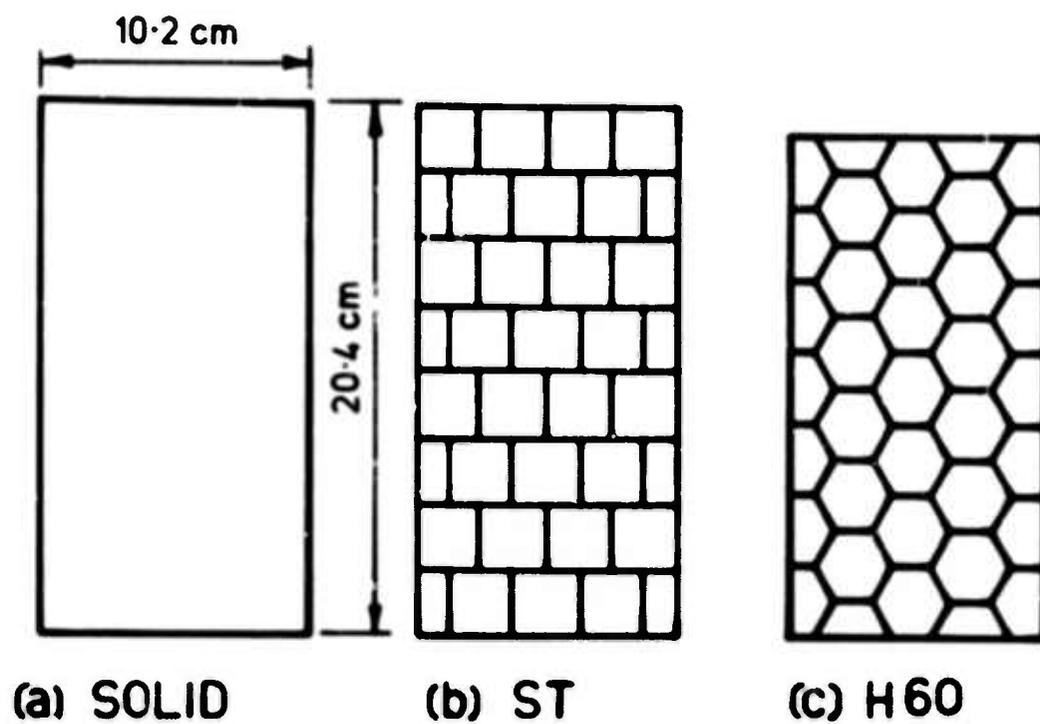
Figure 3: Specimen Types Tested.
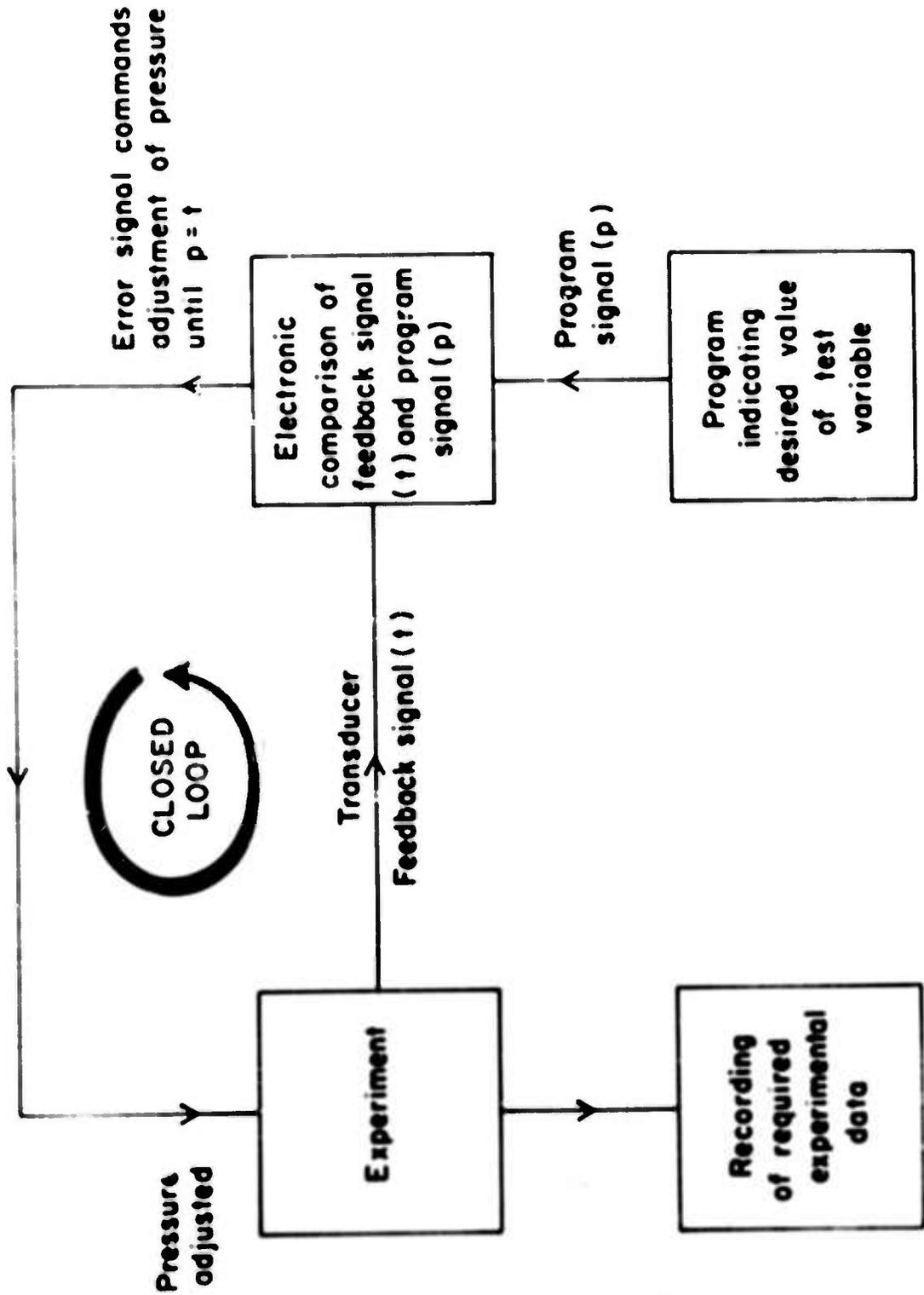
Figure 4: The Principle of Closed-Loop Control.
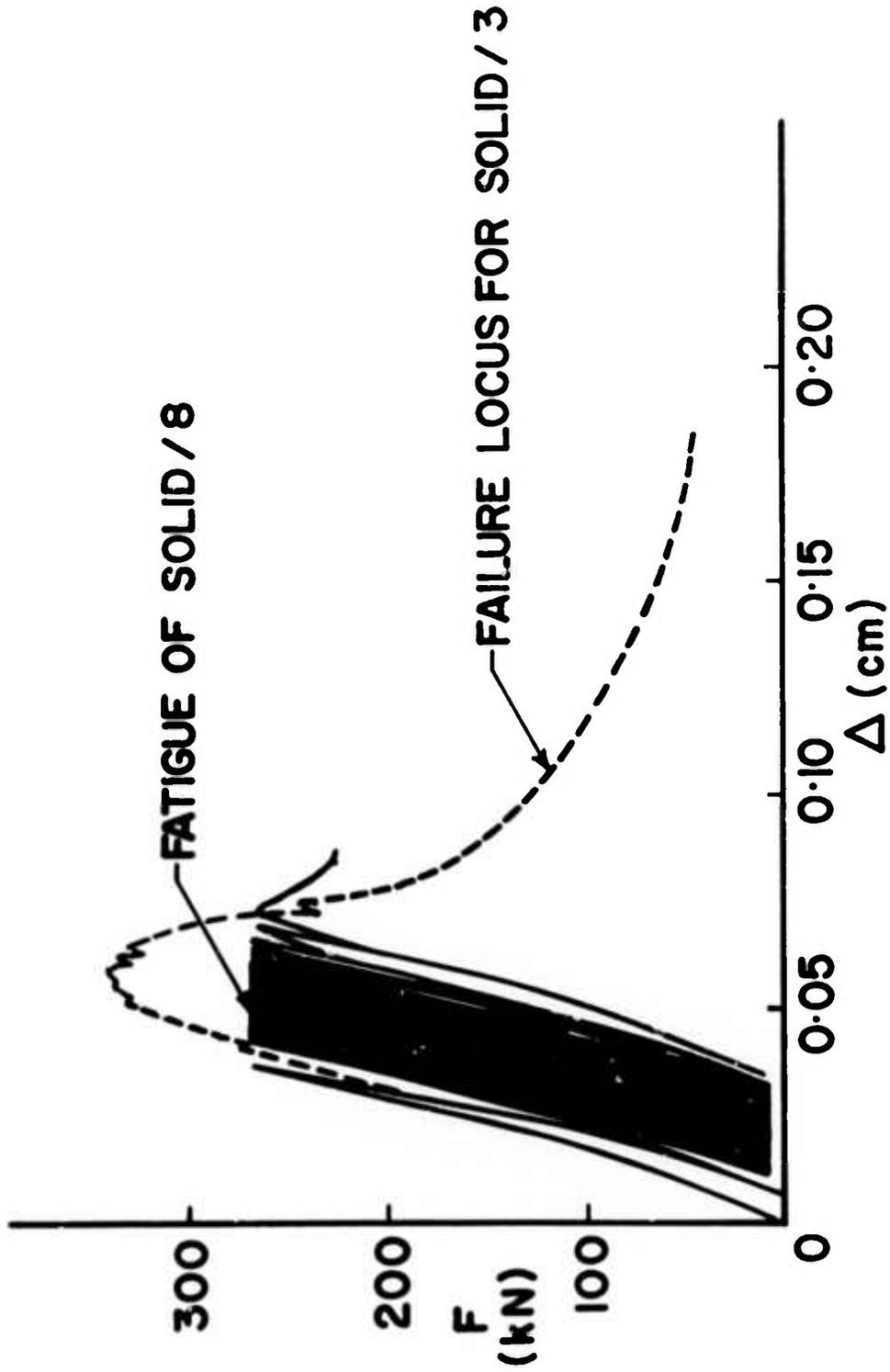
Figure 5: Force-Displacement Curve for Specimen SOLID/8.
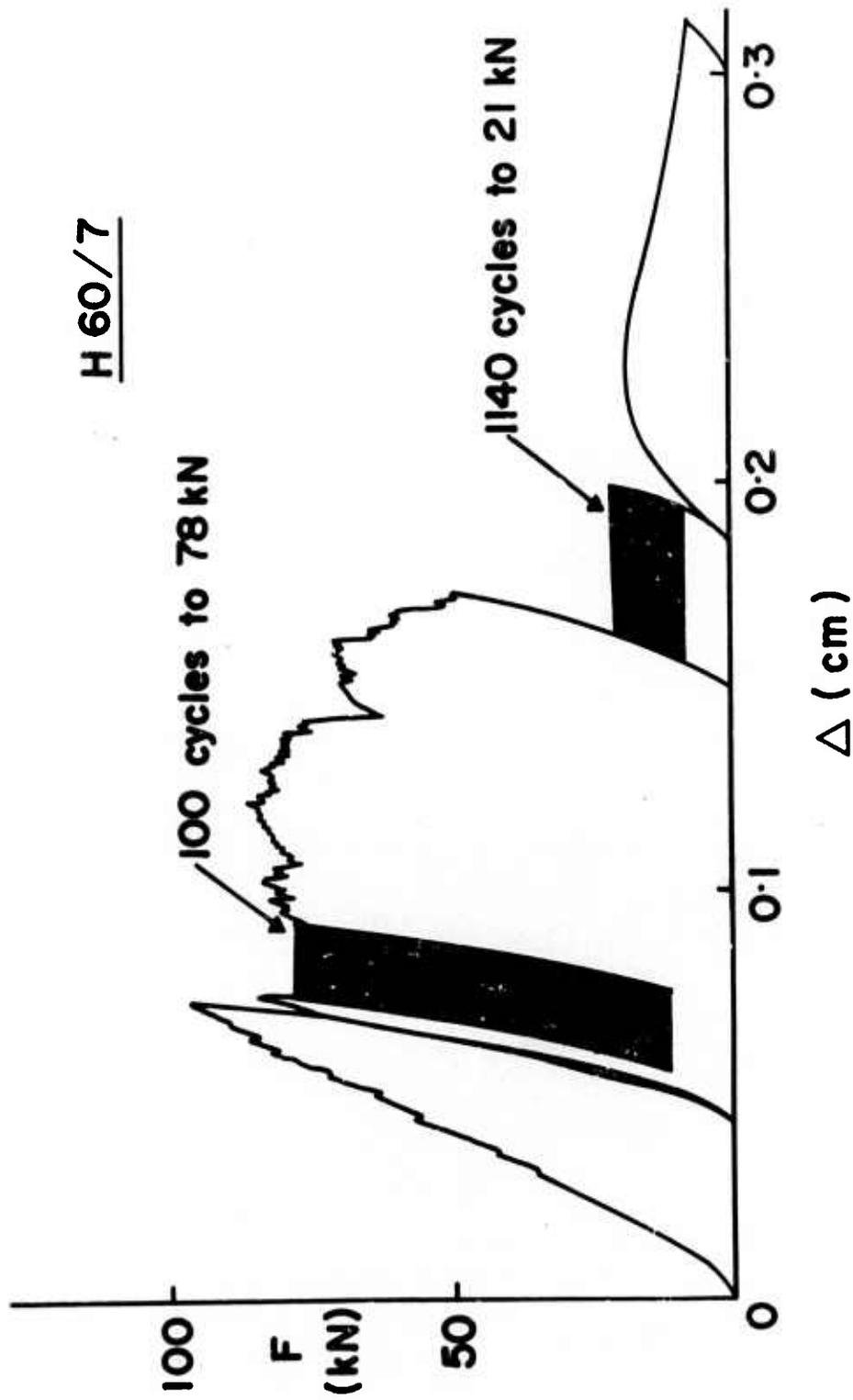
Figure 6: Force–Displacement Curve for Specimen H60/7.
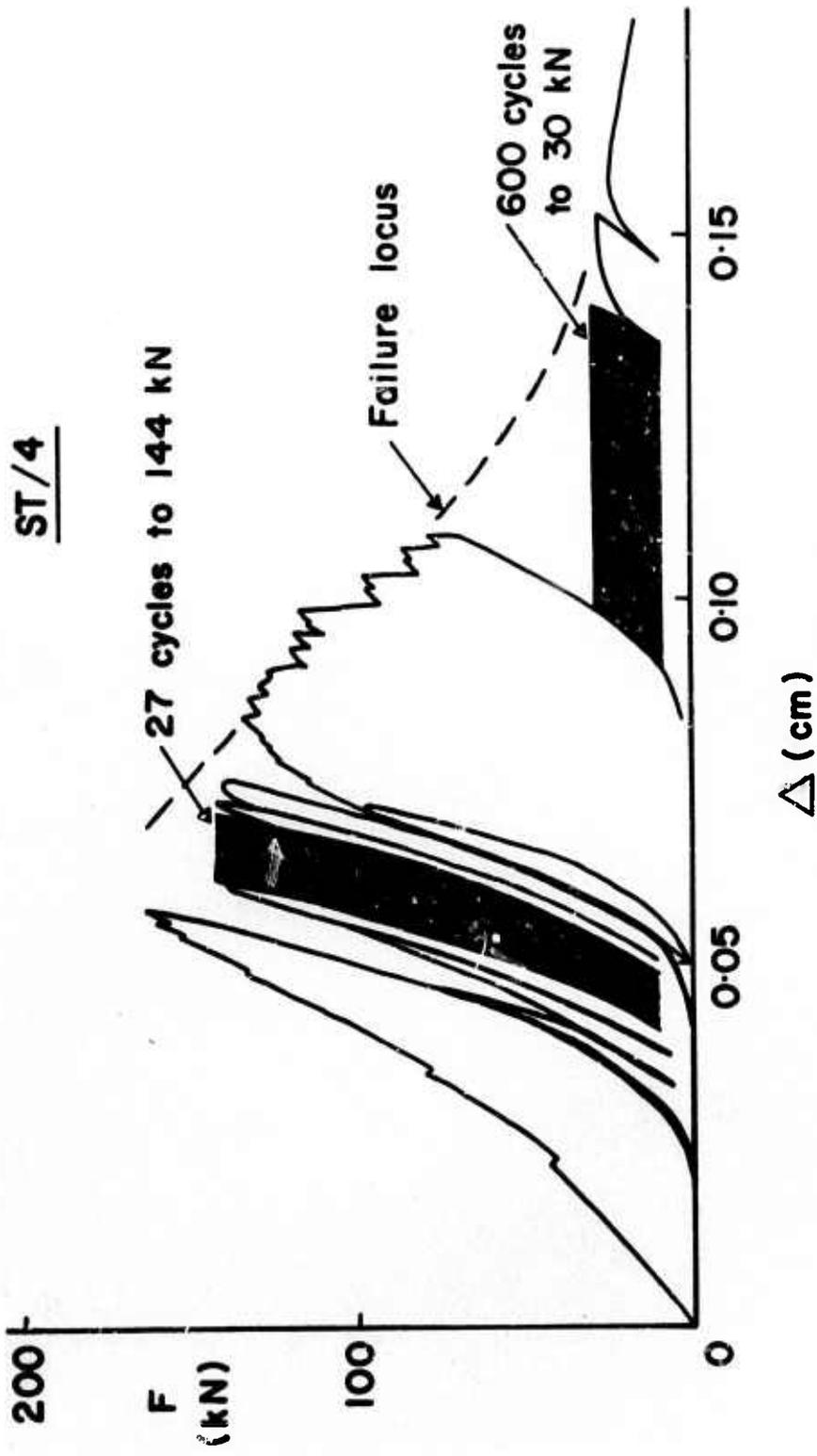
Figure 7: Force-Displacement Curve for Specimen ST/4.
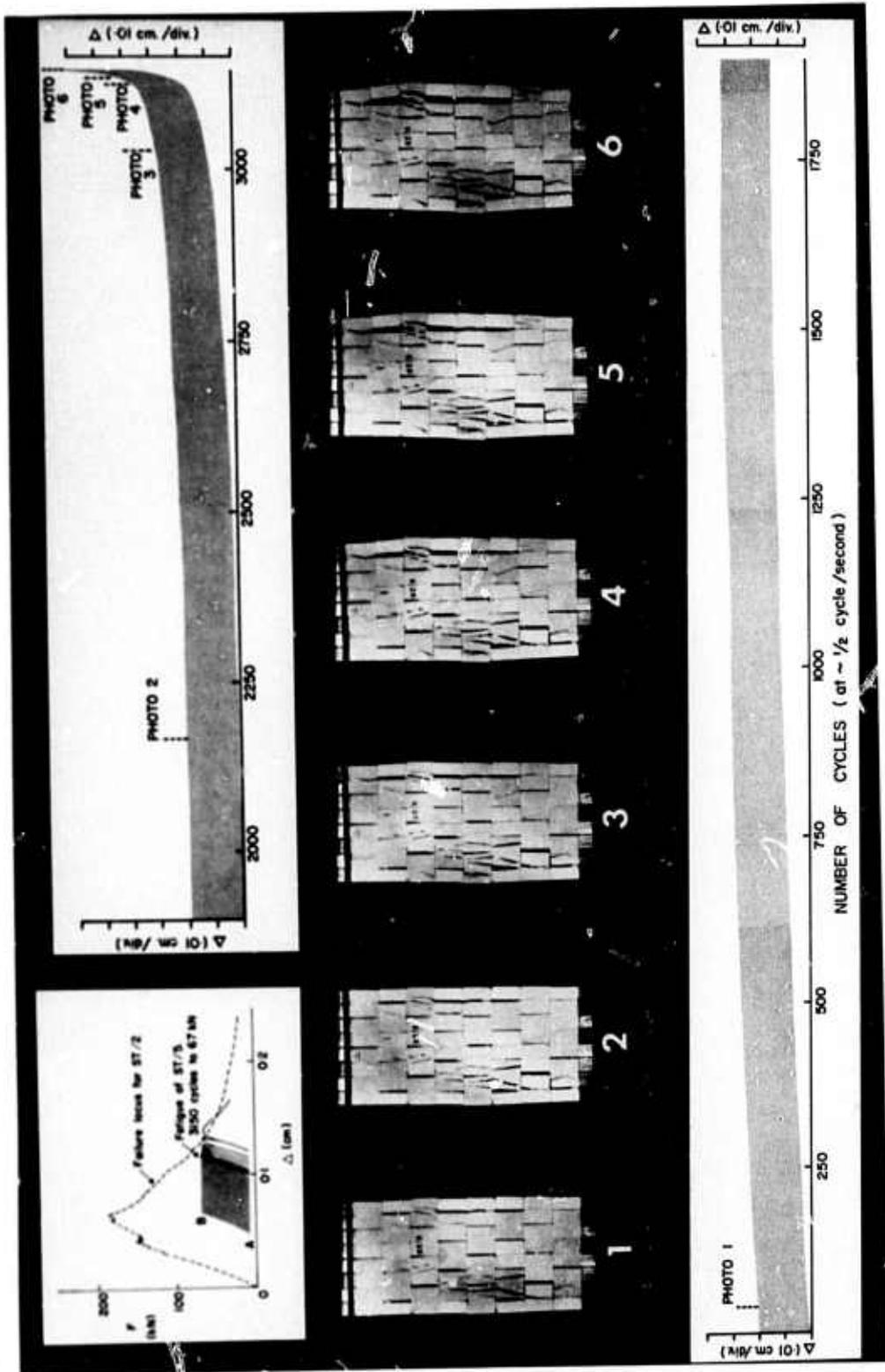
Figure 8: Behaviour of Specimen ST/5 under Cyclic Fatigue.
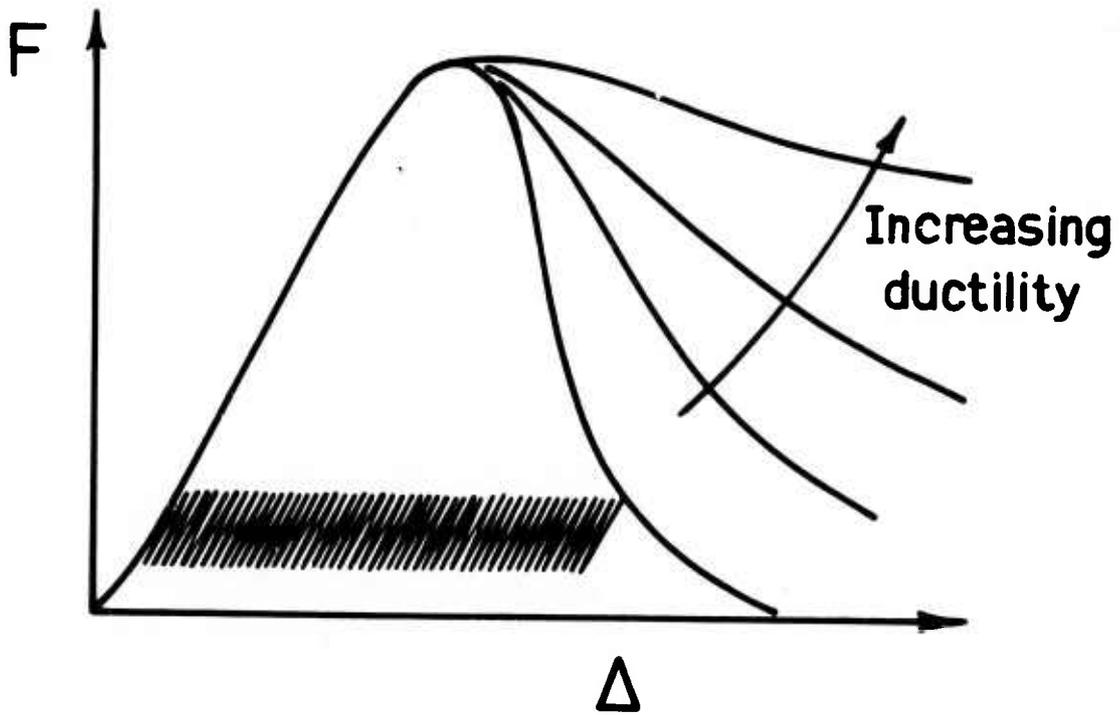
Figure 9: Susceptibility to Fatigue Failure at Low Force Levels Decreases with Increasing Ductility.